
Co-oxidation in Supercritical Water:
Methylphosphonic Acid-Ethanol and Ammonia-Ethanol Model Systems

by
Jason M. Ploeger

B.S. Chemical Engineering
B.S. Materials Science
University of California, Berkeley, 2000

M.S. Chemical Engineering Practice
Massachusetts Institute of Technology, 2005

Submitted to the Department of Chemical Engineering
in partial fulfillment of the requirements for the degree of

DOCTOR OF PHILOSOPHY IN CHEMICAL ENGINEERING

at the

MASSACHUSETTS INSTITUTE OF TECHNOLOGY

May, 2006

© Massachusetts Institute of Technology 2006
All Rights Reserved

Signature of Author:

Department of Chemical Engineering
May 12, 2006

Certified by:

Professor Jefferson W. Tester
Thesis Supervisor

Accepted by:

Professor William M. Deen
Professor of Chemical Engineering
Chairman, Committee for Graduate Students

Co-oxidation in Supercritical Water:
Methylphosphonic Acid-Ethanol and Ammonia-Ethanol Model Systems

by
Jason M. Ploeger

Submitted to the Department of Chemical Engineering on May 12, 2006 in partial fulfillment of the requirements for the degree of Doctor in Philosophy in Chemical Engineering

ABSTRACT

Supercritical water (SCW) is an effective solvent for the destruction of organic compounds by oxidation. Because both organics and oxygen have high solubility in water above its critical point ($T_c = 374\text{ }^\circ\text{C}$ (647 K), $P_c = 221\text{ bar}$), they can be reacted together in a single phase which avoids mass transfer limitations. At typical operating conditions ($T = 450\text{ to }650\text{ }^\circ\text{C}$, $P = 240\text{ to }300\text{ bar}$) for supercritical water oxidation (SCWO), H-C-N compounds are rapidly and completely oxidized to water, carbon dioxide, nitrogen, and nitrous oxide. The destruction of organic compounds in SCWO takes place primarily through free radical pathways rather than the ionic pathways that dominate in liquid water. This is because SCW acts as a nonpolar solvent with a dielectric constant ranging from 1.2 at $T = 650\text{ }^\circ\text{C}$ and $P = 250\text{ bar}$ to 2.5 at $T = 450\text{ }^\circ\text{C}$ and $P = 250\text{ bar}$ as compared to ambient water which has a dielectric constant equal to 80. The ion product of water, K_w , similarly drops to between 10^{-18} and 10^{-20} over this temperature range as compared to the ambient value of 10^{-14} .

Typically, SCWO has been studied by the analysis of either the oxidation of single model compounds to determine detailed kinetic mechanisms or by the oxidation of complex simulated waste streams to measure DRE levels. While kinetic rates and mechanisms are accurately determined by the analysis of pure compounds, this approach fails to characterize the co-oxidation effect: a phenomenon observed in mixed waste streams where refractory compounds oxidize more rapidly in the presence of labile compounds. The purpose of this research is to provide a quantitative mechanistic understanding of co-oxidation rate enhancement in supercritical water. This understanding is vital for the application of predictive elementary reaction rate models developed for individual model compounds to the analysis of mixed waste streams. By combining the two well-characterized, validated SCWO models for ethanol and MPA, mechanistic insight into the interaction of the two compounds in SCW is possible. This insight into the mechanism of co-oxidation could then be used to assist in the development and validation of an elementary reaction rate mechanism for ammonia.

The co-oxidative effect of ethanol on methylphosphonic acid (MPA, or $\text{PO}(\text{OH})_2\text{CH}_3$) was characterized for a range of MPA concentrations (0.1 to 1.0 mM) and ethanol concentrations (0 to 2.4 mM) for temperatures of 473 $^\circ\text{C}$ and 528 $^\circ\text{C}$, a pressure of 245 bar, and stoichiometric oxygen for the complete combustion of both organic compounds. Low concentrations of ethanol (0.1 and 0.3 mM) were found to have no statistically significant effect on MPA conversion for an initial MPA concentration of 1.0 mM, but higher concentrations of ethanol caused an increase in the conversion of MPA at $T = 473\text{ }^\circ\text{C}$, $P = 245\text{ bar}$, and $\tau = 9\text{ s}$ from $14\pm 2\%$ without ethanol present to $29\pm 2\%$ with 1.0 mM ethanol and $39\pm 2\%$ with 2.4 mM ethanol. The increase in MPA conversion was more pronounced at shorter residence times. Decreasing the initial concentration

of MPA at a constant initial ethanol concentration of 1.0 mM, $T = 473$ °C, $P = 245$ bar, and $\tau = 9$ s resulted in an increase in MPA conversion from $29 \pm 2\%$ at 1.0 mM MPA to $41 \pm 2\%$ at 0.1 mM MPA. At $T = 528$ °C and $P = 245$ bar, the initial concentration of MPA had a much greater effect on MPA conversion than the initial concentration of ethanol.

A supercritical water co-oxidation elementary reaction rate mechanism was constructed from submechanisms for MPA and ethanol with updated kinetic rate parameters for H_2O_2 and HO_2^\bullet chemistry. The co-oxidation mechanism accurately reproduces the experimentally observed conversion trend of the refractory MPA component as a function of initial concentration of the labile ethanol component. The increase in MPA conversion with increasing ethanol concentration is predicted to be caused by the increased concentration of hydroperoxy radicals (HO_2^\bullet) produced by ethanol oxidation. An analysis of the major organophosphorus reaction fluxes indicated that the co-oxidative effect would increase the conversion of MPA but not change the rate of formation of methane. An experiment using a model formaldehyde/methanol mixture as a co-oxidant was conducted to confirm this prediction.

The co-oxidative effect of ethanol on ammonia oxidation in supercritical water was studied for a range of temperatures (655-705 °C), initial ammonia (1 to 3 mM), ethanol (0 to 1.0 mM), and oxygen concentrations (0.7 to 5.0 mM), corresponding to fuel equivalence ratios ranging from 0.9 to 2.2. With a stoichiometric amount of oxygen available for complete oxidation, the addition of ethanol on an equivalent molar basis was found to increase ammonia conversion from 20% to 65% at initial concentrations of 1 mM for each reactant, $T = 700$ °C, $P = 246$ bar, and $\tau = 2.5$ s. Nitrous oxide was produced in much larger quantities for ammonia-ethanol co-oxidation than for ammonia oxidation. Based on fractional yields of nitrogen product, this amounted to 40 to 75% for co-oxidation with ethanol versus 4 to 13% without ethanol present.

A co-oxidation model was constructed from submechanisms for ammonia combustion at atmospheric pressure conditions and ethanol oxidation in supercritical water. The initial mechanism poorly reproduced experimental ammonia conversion data and was not able to consistently match nitrous oxide production as a function of temperature over a range from 655 to 700 °C. In order to improve model predictions, the low-pressure $\text{NH}_2 + \text{NO}_x$ submechanism was replaced with a submechanism that included the H_2NNO_x adduct species that are expected to be stabilized in the high-pressure supercritical water environment. Thermochemical and kinetic parameters for the adduct species were estimated with quantum chemical calculations using Gaussian 98 with the CBS-Q method. The explicit treatment of the H_2NNO_x adducts resulted in nitrous oxide yield predictions that correctly reproduced experimental trends.

Acknowledgments

I'd like to thank Jeff Tester, my advisor, for providing guidance through the long process of planning and executing this thesis. Conducting research at high temperatures and pressures is often a frustrating endeavor of finding and fixing clogs and leaks, occasionally at the same time, but Jeff has always been patient and quick to put the day-to-day worries in proper perspective. He always multiplies our time estimates by a factor of four so that when the project is finished in three times what we expected it still feels like success. I also must thank my thesis committee, who always challenged me and helped to find new avenues that I had not considered pursuing. In particular I would like to thank Bill Green for his patience in answering so many of my kinetic modeling questions.

I also want to thank the Tester Group, past and present, because none of this work can be done individually. Mike and Patty taught me everything I know about working with supercritical fluids, even though their philosophies on throwing things away or music may have differed. Brian and Heather accompanied me into the Tester Group, and I am glad I had their company on all of those bike and ski trips. A large portion of this thesis resulted from working with Russ, whether it was brainstorming on the kinetic models or cranking down on reactor fittings. I wish the best of luck to the current basement dwellers, that Chad, Rocco, Andy and Scott can get their reactors up and running, and in Chad's case without destroying any part of the building, and that Kurt and Russell find theses to work on, hopefully more quickly than I did. And as they would certainly tell you, my UROPs did most of the work reported in this thesis, in addition to constantly reminding me how old I am: Thank you, Laura, Adam, Steph, and Mike.

Finally, I want to thank my family and all of the friends I made here in Boston, in particular Kristin for putting up with my long, solipsistic complaints when everything was broken. In no particular order, the following people helped maintain my sanity during my stay at MIT: Jason, Marianne, Greg, Nick, Joe, Sanjoy, Theis, Roger, Oski, and the Boston Poker Tour.

Table of Contents

1	BACKGROUND AND MOTIVATION	10
1.1	SUPERCritical WATER OXIDATION.....	10
1.1.1	<i>Supercritical Water</i>	11
1.1.2	<i>Supercritical Water Oxidation Applications</i>	13
1.1.3	<i>SCWO Process Description</i>	16
1.1.4	<i>Previous Kinetics Research in SCWO</i>	20
1.1.5	<i>Co-oxidation in Supercritical Water</i>	26
1.2	MODEL COMPOUND SELECTION.....	27
1.2.1	<i>Ethanol</i>	27
1.2.2	<i>Methylphosphonic Acid (MPA)</i>	28
1.2.3	<i>Ammonia</i>	30
1.3	REFERENCES.....	33
2	OBJECTIVES AND APPROACH	43
3	EXPERIMENTAL EQUIPMENT AND PROCEDURES	46
3.1	DESCRIPTION OF THE BENCH SCALE SCWO SYSTEM.....	46
3.1.1	<i>Feed Preparation and Pressurization Stage</i>	46
3.1.2	<i>Preheating System</i>	51
3.1.3	<i>Reactor System</i>	53
3.1.4	<i>Letdown System and Sample Collection</i>	55
3.1.5	<i>Health and Safety</i>	56
3.1.6	<i>Reactor Operation and Data Collection</i>	58
3.2	BATCH CELL SCWO REACTOR.....	60
3.2.1	<i>Reactor Design</i>	61
3.2.2	<i>Reactor Operation and Data Collection</i>	63
3.3	ANALYTICAL METHODS AND ANALYSIS.....	64
3.3.1	<i>Product Analysis</i>	65
3.3.2	<i>Data and Error Analysis</i>	67
3.3.3	<i>Uncertainty Analysis</i>	72
3.4	REFERENCES.....	73
4	EXPERIMENTAL RESULTS FOR MPA-ETHANOL CO-OXIDATION	74
4.1	EXPERIMENTAL RESULTS.....	74
4.2	CONCLUSIONS.....	80
4.3	REFERENCES.....	80
5	ELEMENTARY REACTION RATE MODEL FOR MPA-ETHANOL CO-OXIDATION	81
5.1	BACKGROUND AND MOTIVATION.....	81
5.2	MODEL DEVELOPMENT.....	83
5.3	COMPARISON OF MODELING PREDICTIONS WITH EXPERIMENTAL DATA.....	84
5.4	THE REDUCED CO-OXIDATION MECHANISM.....	89
5.5	DESIGN OF AN EXPERIMENT TO VALIDATE THE MODEL.....	90
5.6	CONCLUSIONS.....	96
5.7	REFERENCES.....	97
6	EXPERIMENTAL RESULTS FOR AMMONIA OXIDATION	99
6.1	PLUG FLOW EXPERIMENTAL RESULTS.....	99
6.2	BATCH REACTOR EXPERIMENTAL RESULTS.....	108
6.3	CONCLUSIONS.....	111

6.4	REFERENCES	112
7	EXPERIMENTAL RESULTS FOR AMMONIA-ETHANOL CO-OXIDATION	113
7.1	EXPERIMENTAL RESULTS	113
7.2	CONCLUSIONS	120
7.3	REFERENCES	121
8	ELEMENTARY REACTION RATE MODEL FOR AMMONIA-ETHANOL CO-OXIDATION	122
8.1	BACKGROUND AND MOTIVATION.....	122
8.2	MODEL DEVELOPMENT	122
8.3	ANALYSIS OF MODEL PREDICTIONS	123
8.4	MODEL IMPROVEMENTS.....	127
8.5	UPDATED AMMONIA-ETHANOL MECHANISM.....	132
8.6	CONCLUSIONS	139
8.7	REFERENCES	140
9	CONCLUSIONS	142
10	RECOMMENDATIONS.....	147
11	APPENDIX.....	149

List of Figures

Figure 1-1: The effect of temperature on water density and dielectric strength at $P = 250$ bar from Haar et al. (1984)	12
Figure 1-2: The effect of temperature on ion dissociation product at $P = 250$ bar from Marshall and Franck (1981) and Bandura and Lvov (2000).....	13
Figure 1-3: Schematic of a typical SCWO process	17
Figure 1-4: Arrhenius plot of pseudo-first order oxidation rate constants for model compounds studied in our laboratory	23
Figure 1-5: Arrhenius plot of pseudo-first order hydrolysis rate constants for model compounds studied in our laboratory	23
Figure 1-6: Ball and stick model of ethanol.....	27
Figure 1-7: Ball and stick model of methylphosphonic acid (MPA).....	28
Figure 1-8: Organophosphorus nerve agents	29
Figure 1-9: Organophosphorus nerve agents hydrolysis intermediates.....	30
Figure 1-10: Ball and stick model of ammonia	30
Figure 3-1: Plug flow reactor system.....	47
Figure 3-2: Batch cell reactor schematic	62
Figure 4-1: Conversion of MPA as a function of residence time for five different values of $[\text{EtOH}]_0$. $T = 473 \pm 3$ °C, $P = 245 \pm 3$ bar, $[\text{MPA}]_0 = 0.95 \pm 0.05$ mM, $\Phi = 1.05 \pm 0.25$	77
Figure 4-2: Conversion of MPA as a function of residence time for four different values of $[\text{EtOH}]_0$. $T = 528 \pm 3$ °C, $P = 245 \pm 3$ bar, $[\text{MPA}]_0 = 1.0 \pm 0.1$ mM, $\Phi = 1.0 \pm 0.1$	78
Figure 4-3: Conversion of MPA as a function of residence time for three different values of $[\text{MPA}]_0$. $T = 528 \pm 3$ °C, $P = 245 \pm 3$ bar, $[\text{EtOH}]_0 = 1.00 \pm 0.06$ mM, $\Phi = 1.0 \pm 0.1$	79
Figure 4-4: Conversion of MPA as a function of $[\text{MPA}]_0$	79
Figure 5-1: MPA conversion as a function of initial ethanol concentration at $T = 473$ °C.	85
Figure 5-2: MPA conversion as a function of time for $T = 473$ °C.	86
Figure 5-3: MPA conversion as a function of initial MPA concentration at.....	87
Figure 5-4: Predicted $\text{OH}\cdot$ concentration profiles as a function of time for a varying initial ethanol concentration.....	88
Figure 5-5: Predicted $\text{HO}_2\cdot$ concentration profiles as a function of time for a varying initial ethanol concentration.....	88
Figure 5-6: Effect of uncertainty for the rate constant for the reaction $\text{H}_2\text{O}_2 + \text{OH} = \text{H}_2\text{O} + \text{HO}_2\cdot$	91
Figure 5-7: Major reaction pathways for MPA in the co-oxidation model.	92
Figure 5-8: Comparison of MPA conversion and CH_4 carbon fraction for two initial concentrations of formaldehyde to the MPA conversion and CH_4 carbon fraction for the oxidation of pure MPA.	96
Figure 6-1: Ammonia conversion as a function of residence time for three different temperatures.	101
Figure 6-2: Ammonia conversion as a function of residence time for two different initial ammonia concentrations..	102
Figure 6-3: Ammonia conversion as a function of time for three different fuel equivalence ratios..	103
Figure 6-4: Ammonia conversion as a function of time for four different pressures.	104

Figure 6-5: Parity plot for global rate law. Uncertainty in experimental NH ₃ conversion ranges from 1-3% at the 95% confidence level.....	105
Figure 6-6: Arrhenius plot for pseudo-first order rate constants from this study, Segond et al. (2002), and Webley et al. (1991). S/V ratios are in cm ⁻¹	106
Figure 6-7: Corrected temperature resulting from fitting Webley et al. (1991) data to global rate law from this study versus temperature reported by Webley et al.....	107
Figure 6-8: First-order plot of ln(1-X) as a function of residence time at T = 570 °C.....	110
Figure 6-9: Arrhenius plot for pseudo-first order rate constants from this study on two reactor systems.....	110
Figure 7-1: Ammonia conversion as a function of time for four different initial concentrations of ethanol.....	116
Figure 7-2: Ammonia conversion as a function of time for two different initial concentrations of ammonia.....	117
Figure 7-3: Ammonia conversion as a function of time for three different initial feed concentrations. T = 700±4 °C and P = 243±1 bar.	118
Figure 7-4: Nitrous oxide N fraction as a function of time for three different initial feed concentrations. T = 700±4 °C and P = 243±1 bar.	119
Figure 7-5: Ammonia conversion as a function of time for three different temperatures.....	120
Figure 7-6: Nitrous oxide yield as a function of time for three different temperatures.....	120
Figure 8-1: Comparison of experimental data to ammonia conversion profile predicted by initial ammonia-ethanol co-oxidation model.	124
Figure 8-2: Comparison of experimental data to ammonia conversion and nitrous oxide yield profiles predicted by initial ammonia-ethanol co-oxidation model.....	125
Figure 8-3: Major reaction pathways for initial ammonia-ethanol co-oxidation model. Molar flux through labelled reaction pathways can be found in Table 8-1.....	126
Figure 8-4: Dominant NH ₂ +NO ₂ adduct species and transition states.....	130
Figure 8-5: Dominant NH ₂ +NO adduct species and transition states.....	131
Figure 8-6: Comparison of experimental data to ammonia conversion and nitrous oxide yield profiles predicted by updated ammonia-ethanol co-oxidation model.....	133
Figure 8-7: Major reaction pathways and molar fluxes for NH ₂ +NO ₂ reaction network.....	135
Figure 8-8: Major reaction pathways and molar fluxes for NH ₂ +NO reaction network.....	136
Figure 8-9: Major reaction pathways for updated ammonia-ethanol co-oxidation model. Molar flux through labeled reaction pathways can be found in Table 8-2.....	137
Figure 8-10: Predicted HO ₂ • concentration profiles for three initial conditions.....	138
Figure 8-11: Predicted OH• concentration profiles for three initial conditions.....	139

List of Tables

Table 4-1: Summary of experimental data.....	76
Table 5-1: Rate parameter changes made to co-oxidation mechanism. Units are cm, mol, s, and cal.....	84
Table 5-2: Dominant reaction fluxes for co-oxidation of MPA and ethanol.....	93
Table 6-1: Summary of experimental data with uncertainties at the 95% confidence level.....	100
Table 6-2: Summary of batch cell experimental data with uncertainties at the 95% confidence level. $P = 246 \pm 7$ bar, $[\text{NH}_3]_0 = 3.4 \pm 0.1$ mM, $\Phi = 0.89 \pm 0.03$	109
Table 7-1: Summary of experimental data.....	114
Table 8-1: Average molar fluxes in 10^{-6} mol/L/s through the major reaction pathways shown in Figure 8-3 for $P = 246$ bar, $\Phi = 1$, $\tau = 0-6.5$ s. Predicted using the $\text{NH}_2 + \text{NO}_x$ submechanism in Dean and Bozzelli (2001).	126
Table 8-2: Average molar fluxes in 10^{-6} mol/L/s through the major reaction pathways shown in Figure 8-7 for $P = 246$ bar, $\Phi = 1$, $\tau = 0-6.5$ s. Predicted using the $\text{NH}_2 + \text{NO}_x$ submechanism developed in this paper.....	137
Table 11-1: H_2/O_2 SCWO submechanism. Units are in kcal, cm, mol, s.	149
Table 11-2: C2 SCWO submechanism. Units are in kcal, cm, mol, s.	149
Table 11-3: Organophosphorus SCWO submechanism. Units are in kcal, cm, mol, s.	156
Table 11-4: Ammonia SCWO submechanism. Units are in kcal, cm, mol, s.	159
Table 11-5: Thermodynamic values for SCWO mechanisms.	166

1 Background and Motivation

The oxidation kinetics of mixed binary organic feeds in supercritical water (SCW) were examined in this thesis. The motivation for this research is provided by the experimentally observed co-oxidation effect, whereby a refractory (stable) compound oxidizes more rapidly in the presence of a labile (reactive) compound. A mechanistic understanding of this co-oxidation enhancement is necessary to apply pure compound supercritical water oxidation (SCWO) studies to the destruction of real, mixed waste streams. To establish the background for this study, the properties of SCW, advantages of SCWO, and previous SCWO studies will be presented, followed by a discussion of model compound selection.

1.1 SUPERCRITICAL WATER OXIDATION

Supercritical water has similar properties to a nonpolar, dense gas, able to solvate organics, like benzene or methanol, and gases, like oxygen and nitrogen. By removing interphase mass transfer limitations, SCWO is an attractive method for the oxidation of organic compounds in aqueous waste streams. To improve the use of SCWO as a remediation method, basic research has focused on both fundamental science and engineering studies. To better predict and understand SCWO processes, fundamental research has been conducted on SCW physical property measurements, equation of state development, phase nucleation and equilibria, and the measurement and prediction of oxidation rates for model compounds. To improve the SCWO process, engineering studies have been conducted on heat transfer, salt deposition and clogging, and materials corrosion.

1.1.1 Supercritical Water

A supercritical fluid is defined as a substance that is above both its critical temperature and pressure. This critical point marks the termination of the liquid-vapor equilibrium line, on which the two phases co-exist. Traveling along the equilibrium line, as temperature and pressure increase, the liquid density decreases and the vapor density increases until the two are equal at the critical point. Above that point the fluid becomes a single, supercritical phase with properties in between those of the liquid and vapor.

As water passes through the region near the critical point ($T_c = 374\text{ }^\circ\text{C}$ and $P_c = 221\text{ bar}$), physical properties such as density, dielectric constant, dissociation constant, and viscosity undergo dramatic changes. Figure 1-1 illustrates these changes where density and dielectric constant are plotted as a function of temperature at a constant pressure of 250 bar (Haar et al. 1984). The density of supercritical water is about one-tenth that of ambient liquid water, resulting in greater spacing between water molecules and much less effective hydrogen bonding. As a result SCW has very little capacity to shield ions, as can be seen in the dielectric constant, which decreases from 80 at room temperature to 2.5 at $T = 450\text{ }^\circ\text{C}$ and 1.2 at $T = 650\text{ }^\circ\text{C}$, values typical of nonpolar hydrocarbon solvents such as hexane.

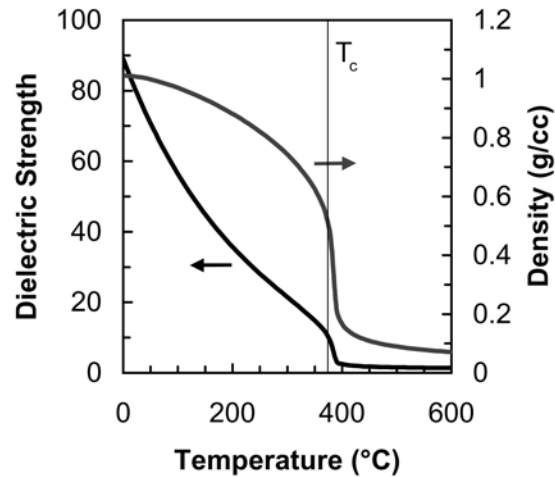


Figure 1-1: The effect of temperature on water density and dielectric strength at $P = 250$ bar from Haar et al. (1984)

The loss of hydrogen bonding also affects the ion-dissociation constant for supercritical water. Figure 1-2 shows the correlations of Marshall and Franck (1981) and Bandura and Lvov (2000) for the ion-dissociation constant of water ($K_w \equiv [a_{H^+}][a_{OH^-}]$) as a function of temperature at 250 bar. The K_w values of Bandura and Lvov are used for temperatures above the critical point because their study focused on lower water densities to ensure more accurate supercritical water values. As temperature increases through the subcritical, “hydrothermal” region, K_w increases from 10^{-14} at ambient conditions to a maximum of 10^{-11} at $T = 250$ °C. At neutral conditions, this corresponds to an increase in H^+ and OH^- activities $a_{H^+} = a_{OH^-}$ from 10^{-7} to 3×10^{-6} , and demonstrates the effectiveness of acid or base catalysis in hydrothermal water. However, above the critical point, K_w drops to between 10^{-18} and 10^{-20} as water loses the capacity to solvate ions.

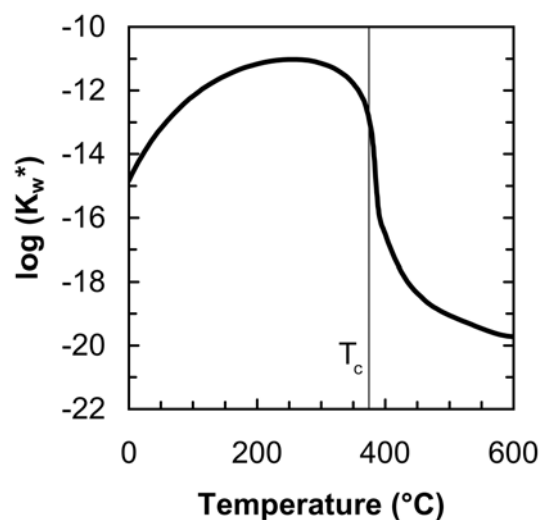


Figure 1-2: The effect of temperature on ion dissociation product at P = 250 bar from Marshall and Franck (1981) and Bandura and Lvov (2000)

Under these low-density, low-dielectric constant conditions, supercritical water is an excellent media for the oxidation of organic compounds. Most low molecular weight organic compounds and oxygen are both miscible in supercritical water, and due to higher diffusion constants and lower viscosities, mass transfer limitations are much lower than in liquid water. The lower solubility of ions and the lower activities of H^+ and OH^- cause reactions to proceed via free radical pathways rather than ionic pathways. At typical operating conditions, SCWO proceeds rapidly and completely with residence times of less than a minute required to achieve destruction efficiencies of 99.99% (Tester et al. 1993a).

1.1.2 Supercritical Water Oxidation Applications

SCWO is an attractive alternative to incineration for the remediation of aqueous organic wastes. At the lower operating temperatures of SCWO, typically between 400 and 700 °C, the dominant free radical pathways differ from those observed at higher temperature combustion conditions ($T > 1200$ °C). NO_x compounds are thermodynamically unstable at SCWO

conditions; the oxidation products of any nitrogen-containing organic compounds are N_2 and N_2O . In addition, the lower organic concentrations and lower temperatures of SCWO inhibit the formation of dioxins, polyaromatic hydrocarbons (PAH), and soot.

C-H-O compounds are oxidized to carbon dioxide and water in supercritical water. Heteroatoms such as chlorine, sulfur, and phosphorus react to form the corresponding acids HCl, H_2SO_4 , and H_3PO_4 , rather than gaseous products such as SO_x . These acids can cause corrosion at high concentrations, especially HCl, so are neutralized with NaOH and precipitated out as salts for separation and removal from the reactor.

SCWO is a useful remediation technique for aqueous waste streams that are too dilute for incineration, too concentrated for selective adsorption, or whose properties are such that selective adsorption or bioremediation techniques are not feasible, such as methyl tert-butyl ether (MTBE). At concentrations below 25 wt%, the energy required to incinerate an aqueous waste stream makes the process economically unfeasible (Tester et al. 1993a). For dilute streams, SCWO can achieve destruction and removal efficiency (DRE) levels of 99.99% or greater with residence times less than 60 s with a lower energy input due to the lower temperatures and the avoided water removal step. SCWO has been used for the destruction of highly toxic compounds such as chemical warfare agents and propellants (Shaw and Dahmen 2000). SCWO is preferable to incineration in these cases as well because the former process takes place in a contained system with a much lower risk of accidental release of dangerous chemicals.

SCWO applications are discussed in this section; detailed information can be found in the listed reviews. Freeman (1985), Modell (1989) and Thomason et al. (1990) contributed the initial reviews of SCWO technology. Later Tester et al. (1993a) reviewed the effectiveness of the technology for waste treatment, status of commercial development, process engineering

issues, and a summary of relevant research in the field. Engineering aspects of SCWO were reviewed by Gloyna and Li (1995). Savage et al. (1995) reviewed reactions in supercritical fluids in general, later focused on the reactions of organic compounds in SCW (1999), and most recently addressed issues of homogenous and heterogenous catalysis in SCW (2006). Tester and Cline (1999) discussed oxidation kinetics and corrosion in SCWO and detailed the research needed to better understand these processes. Ploeger et al. (2006a) reviewed the history of kinetic modeling in SCW and recommended a procedure for the development and validation of elementary reaction rate mechanisms. The use of SCWO technology for the destruction of toxic organic compounds was reviewed by Shaw and Dahmen (2000). Kritzer and Dinjus (2001) provided a review of current major issues and the state of reactor design research.

The effectiveness of SCWO to remediate a variety of dilute aqueous organic waste streams has been demonstrated by several studies. The first application of SCWO was in the destruction of polychlorinated biphenyls (PCB) and dichloro-diphenyl-trichloroethane (DDT) without the formation of dioxins by MODAR (Thomason and Modell 1984). SCWO has also been shown to be an effective treatment for human waste (Hong et al. 1987; Hong et al. 1988), municipal sludge (Shanableh and Gloyna 1991), a mixture of municipal sludge and distillery wastewater (Goto et al. 1998), pulp and paper sludge (Modell et al. 1992) and a mixture of primary clarifier sludge with bleach plant effluent (Cooper et al. 1997). The first full-scale SCWO sludge processing plant was built in Harlingen, TX, to process municipal and industrial wastes (Griffith and Raymond 2002). Additional SCWO pilot plants have been constructed in Sweden (Gidner and Stenmark 2001; Patterson et al. 2001) and Japan (Gidner et al. 2001) to destroy sewage sludges. Other waste streams for which SCWO has proven effective include

pharmaceutical and biopharmaceutical waste (Johnston et al. 1988), dinitrotoluene (DNT) process wastewater (Li et al. 1993), and polymer process effluents (Schmeider and Abeln 1999).

The Departments of Defense and Energy have targeted SCWO to destroy stockpiled chemical warfare agents, weapons, explosives, and propellants (Shaw and Dahmen 2000) in applications where the risk of accidental release makes incineration unacceptable. SCWO has been demonstrated an effective treatment for chemical warfare agents (Spritzer et al. 1995; Snow et al. 1996), propellants (Buelow 1990), smokes and dyes (Rice et al. 1994), and explosives (Harradine et al. 1993). SCWO was chosen to be part of the process to destroy VX, a chemical warfare agent (NRC 1998).

1.1.3 SCWO Process Description

Whether laboratory scale or plant scale, all SCWO processes contain key steps including pressurization, preheating, salt removal, and heat recovery. A typical SCWO flowchart is shown in Figure 1-3.

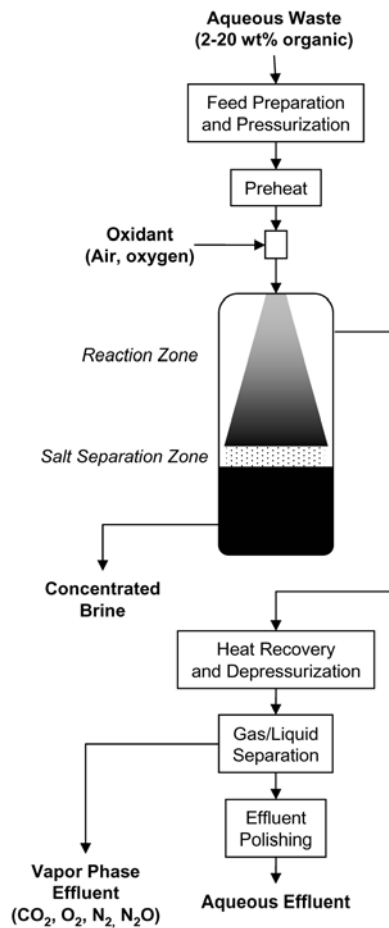


Figure 1-3: Schematic of a typical SCWO process

The first step in the SCWO process is the pretreatment and pressurization of the feed stream, typically to between 240 and 300 bar. Organic and oxidant streams are fed separately into the reactor. The organic stream may require pretreatment depending on the concentration and composition of the feed. Waste streams with a high solids content, such as sludges, may require maceration to reduce particle size and lengthen the lifetime of high-pressure pumps. The oxidant stream may consist of air, pure oxygen, or aqueous hydrogen peroxide that decomposes to form molecular oxygen during the preheating step. The choice of oxidant is usually determined by the scale of the process and economic factors. Laboratory scale processes often use hydrogen peroxide because high oxygen loadings can be obtained in a relatively safe manner

compared to high pressure compression of pure oxygen, while plant scale processes often use pure oxygen for economic considerations. The organic concentration of the feed stream determines the amount of heat generated from oxidation that is available to preheat the incoming feed stream once the reactor effluent exits the reactor. To achieve an optimal heating value, the organic waste stream may be diluted or an auxiliary fuel may be added prior to the entrance of the reactor. If the organic stream is relatively concentrated, the heat released by the reaction can be used for power generation or district heating. If the organics contain heteroatoms such as phosphorus, sulfur or chlorine, a caustic may be added to the feed stream to neutralize any acids formed in an attempt to mitigate corrosion.

Once the feed stream has been pressurized to the system operating pressure, it is preheated to between 300 and 400 °C by heat transfer from the reactor effluent via countercurrent heat exchange. The oxidant feed stream is usually also preheated before it mixes with the organic stream. At commercial feed concentrations and injection rates, when the feed streams are mixed, the heat generated from oxidation reactions can increase reactor temperatures to between 500 and 700 °C. At these conditions, complete destruction of most organics occurs in less than 60 s of residence time.

To prevent salt deposition and plugging, a salt separation method is typically employed in the SCWO reactor system. Salts formed from oxidation of heteroatom-containing organics are insoluble in supercritical water and fall out of solution in the SCWO reactor. Hodes et al. (2004b) and Marrone et al. (2004) reviewed the many different reactor designs that have been studied to prevent the precipitated salts from accumulating on the walls of the reactor and plugging the reactor. Most designs rely on a subcritical liquid water stream in which the salts can dissolve and be removed from the reactor. For example, in Figure 1-3, a temperature gradient in the

reactor causes the bottom of the tank to reach a subcritical temperature into which salts can form a concentrated brine.

After exiting the reactor, the effluent is quenched after contacting the inlet feed stream in the heat exchanger. The cooled effluent is depressurized to gas and liquid phase waste streams, which can be split using a gas-liquid separator. The vapor phase contains unreacted oxygen, carbon dioxide, nitrogen and nitrous oxide (if N-heteroatoms were present in the organic feed stream), all of which can be released into the atmosphere. The liquid effluent typically contains low concentrations of dissolved metals that can be removed to sufficiently low levels for discharge or use as potable water using effluent polishing methods such as ion exchange (Tester et al. 1993a).

In addition to the advantages of SCWO treatment, there are some drawbacks and challenges to the widespread application of SCWO technology. Kritzer and Dinjus (2001) highlight corrosion, salt plugging, and lack of experimental data for reliable cost estimation for scale-up as the three primary problems. A large capital investment is required at the industrial scale, since the high nickel alloys are required for reactor construction and high-pressure pumps required for feed delivery can be very expensive.

Corrosion can occur when high concentrations of halogen, sulfur, and phosphorus-containing organics are heated to SCW temperatures. Corrosion has been a major problem for the destruction of chemical warfare agents by SCWO (Shaw and Dahmen 2000). Many of the large chemical warfare agents hydrolyze in the preheater to form acids such as H_2SO_4 . At subcritical, hydrothermal conditions, these acids dissociate and corrode the preheater tubing. Several corrosion-resistant materials have been tested in SCWO reactor systems, including high-

nickel alloys like Inconel and Hastelloy, and titanium. Each material resists corrosion by certain acids, but no single alloy resists corrosion by all acids (Kritzer and Dinjus 2001).

Salt management remains another major design concern for SCWO technology. Salts formed by neutralizing acids in SCW precipitate into sticky deposits on reactor walls that are difficult to remove. Many reactor designs seek to prevent the initial formation of salt deposits on the walls, including the transpiring wall reactor, the reversible flow tubular reactor, and adsorption/reaction on a fluidized solid phase (Marrone et al. 2004). The transpiring wall reactor contains an inner porous tube through which colder water flows to form a protective film on the inner wall. Other research has sought to remove precipitated salts by mechanical methods such as brushing or scraping or by chemical methods such as reactor flushing or using additives. Further information on salt precipitation and removal can be found in the review by Marrone et al. (2004).

1.1.4 Previous Kinetics Research in SCWO

SCWO presents a wide variety of research challenges from fundamental studies of chemical and physical phenomena in SCW to engineering design research. Materials and corrosion research has focused on evaluating corrosion-resistant materials and improving fundamental understanding of corrosion mechanisms in SCWO (Kriksunov and Macdonald 1995; Kritzer et al. 1999; Tester and Cline 1999; Mitton et al. 2000; Mitton et al. 2001), and recently included reactor design studies to minimize corrosion (Fauvel et al. 2005; Lee et al. 2005). The behavior of salts in SCW has been studied extensively from fundamental studies of phase behavior and nucleation and growth kinetics to alternative reactor design studies (Armellini and Tester 1991; Armellini and Tester 1993; Armellini et al. 1994; McGuinness 1995;

Mueggenberg et al. 1995; La Roche et al. 1997; Tester et al. 1998; Hurst et al. 2002; Hodes et al. 2003; Hodes et al. 2004a).

The measurement and prediction of kinetics is also important for scale-up and reactor design for SCWO processes. Research in our group and others has focused on developing a fundamental understanding of SCWO kinetics including developing elementary reaction rate mechanisms while other groups have just measured DRE levels or determined global rate expressions.

Our group at MIT has characterized the hydrolysis, pyrolysis, and oxidation of model compounds in sub and supercritical water during the past 25 years. Model compounds were chosen either because they would be present or be formed as stable intermediates in the oxidation of larger compounds present in feed streams encountered in real SCWO processes. For each compound, the experimental space was well characterized by varying temperature, pressure or density, residence time, organic and oxidant concentrations. Multi-scale modeling tools are also employed to understand the model compound behavior on the reaction level. Macroscopic level models include global rate laws and macroscopic rate constants for major pathways regressed from experimental data. Predictive models have also been developed that simulate the SCWO process at the elementary reaction level. Elementary reaction rate mechanisms and rates at SCW conditions are developed from lower pressure ($P \leq 1$ bar) and higher temperature ($T > 1200$ °C) combustion mechanisms. Predictions are then compared to SCWO experimental data. *Ab initio* calculations have been used to calculate rate constants for elementary reactions by transition state theory.

Research in our group initially focused on small molecules expected to be refractory intermediates in the oxidation of larger compounds. The studied compounds included carbon

monoxide (Helling and Tester 1987; Holgate et al. 1992; Holgate and Tester 1994a), hydrogen (Holgate and Tester 1993; Holgate and Tester 1994a; Holgate and Tester 1994b), methane (Webley and Tester 1991), methanol (Webley and Tester 1989; Tester et al. 1993b; Phenix 1998), and ammonia (Helling and Tester 1988; Webley et al. 1991). More recently, studies have grown to include larger model compounds that would be expected in real waste streams. Some of these compounds hydrolyzed to a significant extent, including acetic acid (Meyer et al. 1995), glucose (Holgate et al. 1995), methylene chloride (Marrone et al. 1995; Marrone et al. 1998a; Marrone et al. 1998b; Salvatierra et al. 1999), thiodiglycol (Lachance et al. 1999), and methyl tert-butyl ether (Taylor et al. 2001; Taylor et al. 2002). For other large compounds the rate of oxidation dominated that of hydrolysis; those compounds include benzene (DiNaro et al. 2000a), ethanol (Helling and Tester 1988; Schanzenbacher et al. 2002), and methylphosphonic acid (Sullivan and Tester 2004). Elementary reaction rate mechanisms were developed to predict the oxidation of hydrogen, carbon monoxide, methane, benzene, and methylphosphonic acid to varying degrees of success (Webley and Tester 1991; Holgate and Tester 1994b; DiNaro et al. 2000; Sullivan et al. 2004a).

Apparent first order rate constants are often used to compare oxidation rates for different studies. Figure 1-4 and Figure 1-5 show the apparent first order rate constants for oxidation and hydrolysis, respectively, of the compounds studied in our laboratory at a constant pressure of 246 bar. It can be seen in Figure 1-4 that alcohols such as ethanol and tert-butanol are more labile while methane and ammonia are more refractory. Figure 1-5 shows that the rates of hydrolysis for both MTBE and methylene chloride decrease as temperature increases across the critical point. This non-Arrhenius behavior results from changes to the ion dissociation constant and dielectric constant of water across the critical point.

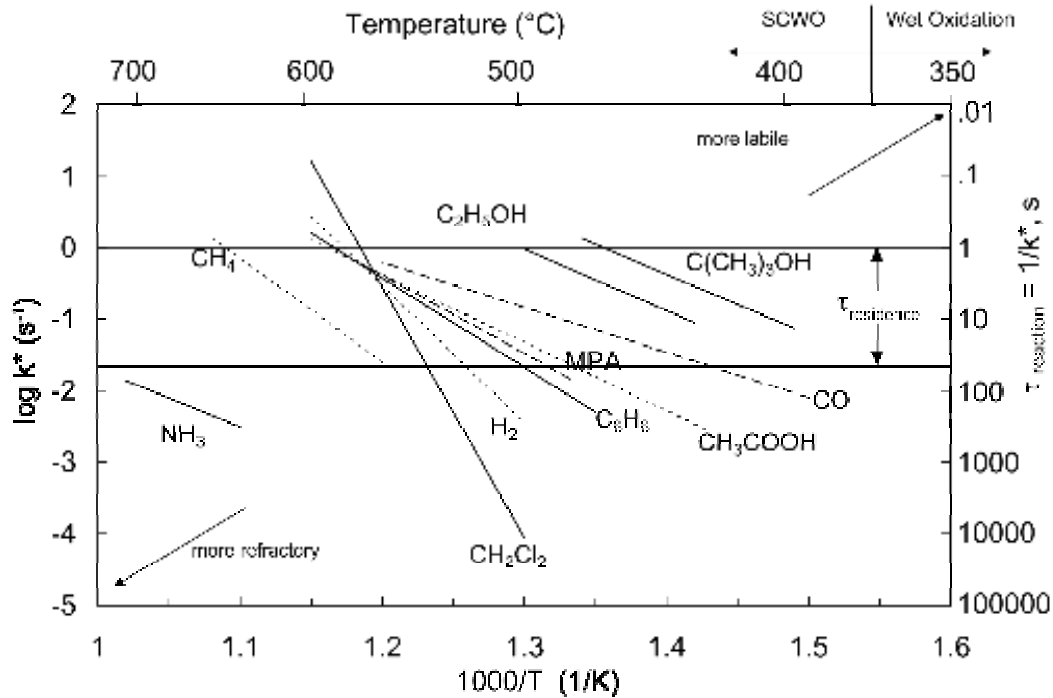


Figure 1-4: Arrhenius plot of apparent first order oxidation rate constants for model compounds studied in our laboratory

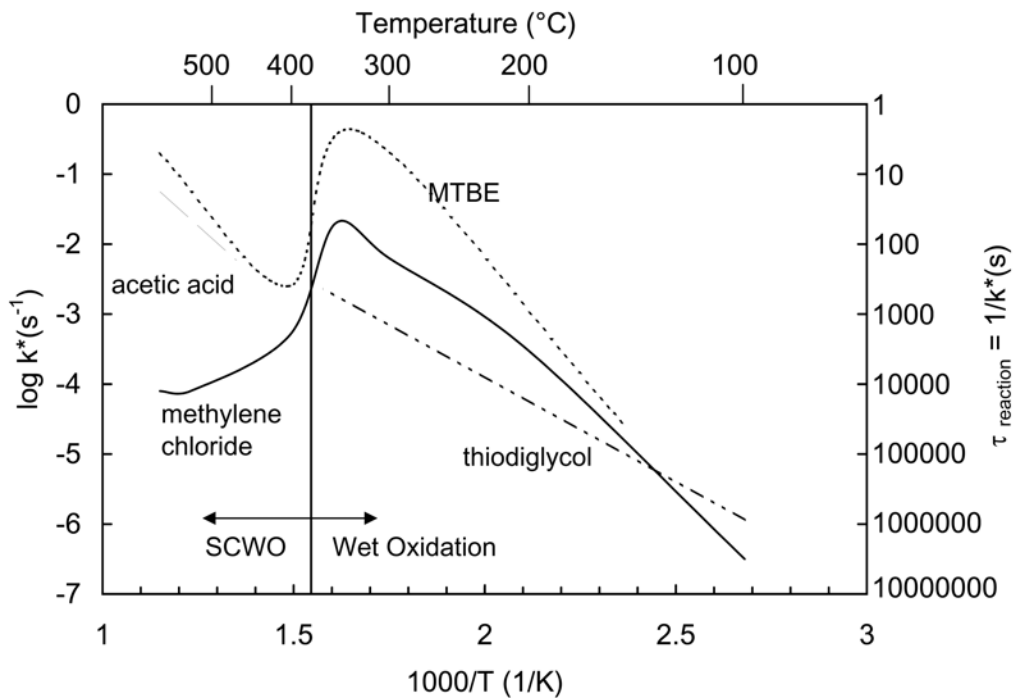


Figure 1-5: Arrhenius plot of apparent first order hydrolysis rate constants for model compounds studied in our laboratory

SCWO kinetics have been studied by several other groups as well. At the University of Michigan, Savage's group has studied the oxidation kinetics of several model compounds. The oxidation kinetics of phenol and substituted phenols were measured in the presence and absence of catalysts (Thornton and Savage 1992b; Thornton and Savage 1992a; Gopalan and Savage 1995; Martino and Savage 1997; Martino and Savage 1999b; Martino and Savage 1999a; Yu and Savage 1999; Yu and Savage 2000b; Yu and Savage 2000a). Savage and co-workers have also studied methane and methanol oxidation kinetics and developed elementary reaction rate models for these compounds and their mixtures (Brock and Savage 1995; Brock et al. 1996; Brock et al. 1998; Savage et al. 1998; Savage et al. 2000). Recent work in their group has focused on determining the effect of water concentration on SCWO reaction rates (Akiya and Savage 2000a; Akiya and Savage 2000b; Henrikson and Savage 2003; Henrikson and Savage 2004), and the H-C-N chemistry of methylamine oxidation (Benjamin and Savage 2004; Benjamin and Savage 2005b; Benjamin and Savage 2005a).

At the University of Texas, Professor Gloyna and coworkers have studied oxidation kinetics for a variety of waste compounds. Most of the studies measured the kinetics at high DRE levels with excess oxygen to determine the necessary conditions for complete destruction for reactor design applications. Model compounds studied include phenol and n-octanol (Li et al. 1997), pyridine (Crain et al. 1993), dinitrotoluene (Li et al. 1993), acetamide (Lee and Gloyna 1992), and acetic acid (Li et al. 1997). The Gloyna group has also studied the oxidation kinetics of sludges (Shanableh and Gloyna 1991; Blaney et al. 1995; Crain et al. 2000) and of organophosphorus compounds including dimethyl methylphosphonate (Turner 1993) and methylphosphonic acid (Bianchetta et al. 1999).

At Sandia National Laboratories, a research group led by Steve Rice has conducted many studies utilizing *in situ* Raman spectroscopy to measure oxidation rates of model compounds and the concentration profiles of their products and reaction intermediates. They have developed an understanding of such model compounds as methane (Steeper et al. 1996), methanol (Rice et al. 1996), isopropyl alcohol (Hunter et al. 1996), and ethanol (Rice and Croiset 2001), both on the experimental and elementary reaction model level. They have also studied the rate of hydrogen peroxide decomposition in supercritical water, which is one of the most important reactions in the generation of the free radical pool in SCWO (Croiset et al. 1997; Croiset and Rice 1998). Recently, they have studied the reforming of organic compounds in SCW (Taylor et al. 2003) and the stability and reactivity of nitrous oxide in SCW (Rice 2006).

At Los Alamos National Laboratory, Steve Buelow and coworkers have studied the oxidation kinetics of propellants and chlorinated hydrocarbons (Harradine et al. 1993; Foy et al. 1996). They have also studied the use of alternative oxidants, including nitrates, for the SCWO of compounds such as ammonia, EDTA, and acetic acid (Dell'Orco et al. 1995; Dell'Orco et al. 1997; Proesmans et al. 1997). In addition, they have studied the oxidation of ethanol and methanol using *in situ* Raman spectroscopy (Hack et al. 2005).

While at the University of Delaware, Professor Klein's group studied the oxidation and hydrolysis kinetics of several compounds. Oxidation studies focused on measuring the oxidation rates of alcohols and acetic acid and developing lumped reaction models for these compounds (Boock and Klein 1993; Iyer et al. 1998). Hydrolysis studies focused on nitriles (Iyer and Klein 1997; Izzo et al. 1999), urea (Schoppelrei et al. 1996), 1-nitrobutane (Iyer et al. 1996), nitroanilines (Wang et al. 1995), and substituted anisoles (Klein et al. 1992).

1.1.5 Co-oxidation in Supercritical Water

Typically, SCWO has been studied by the analysis of either the oxidation of single model compounds to determine detailed kinetic mechanisms or by the oxidation of complex mixtures formulated to simulate or duplicate actual waste streams to measure DRE levels. While kinetic rates and mechanisms are accurately determined by the analysis of pure compounds, this approach fails to characterize the co-oxidation enhancement effect: a phenomenon observed in mixed waste streams where refractory compounds oxidize more rapidly in the presence of labile compounds. Co-oxidation enhancement was observed experimentally during SCWO experiments in the early 1980s on sewage (Hong et al. 1987), but not enough was known to explain the effect on a mechanistic level. An attempt was made in our laboratory by Webley et al. (1991) to co-oxidize ammonia with methanol, but no increase in conversion was observed due to limitations on preheating and temperature measurement in the reactor. Cocero et al. (2000) co-oxidized ammonia, pyridine, acetonitrile, and aniline with isopropanol and measured the formation of trace (parts per million) products of such as NO_x , nitrates and nitrites. As the library of validated kinetic mechanisms has grown in number and detail, the challenge of understanding co-oxidation in two-compound organic feed streams on the mechanistic level has become tractable. Savage et al. (2000) was able to predict the increase of free radicals such as HO_2^\bullet and OH^\bullet via detailed chemical kinetic modeling for a mixed methanol/methane feed.

Anitescu and coworkers (2005) at Syracuse and O'Brien et al. (2005) at Clemson performed co-oxidation of polychlorinated biphenyls (PCBs) with methanol, but the oxidation mechanisms of such large molecules as PCBs are too complex to understand at this time, so the studies were limited to primarily experimental observations in which co-oxidation rate enhancement was measured and the reactor effluent characterized.

1.2 MODEL COMPOUND SELECTION

In order to develop an understanding of this co-oxidation enhancement at the mechanistic level, methylphosphonic acid (MPA) and ethanol were chosen as model refractory and labile compounds, respectively. The oxidation of even a simple, two-component mixed organic feed would more closely simulate the destruction of a real organophosphorus chemical warfare agent by supercritical water oxidation (SCWO) than the oxidation of pure MPA alone. More importantly, both compounds have been well-characterized at the mechanistic level (Rice and Croiset 2001; Sullivan et al. 2004a), which will make detailed analysis of the oxidation of the binary mixed feed possible.

In the second phase of this study, ammonia replaced MPA as the model refractory compound. Ammonia is not as well characterized at the mechanistic level in SCW as MPA, and the understanding of the co-oxidation phenomenon derived from the MPA-ethanol system will aid in the development of an ammonia-ethanol co-oxidation mechanism. The subsections that follow will provide more details on the properties of the model compounds chosen for this study.

1.2.1 Ethanol

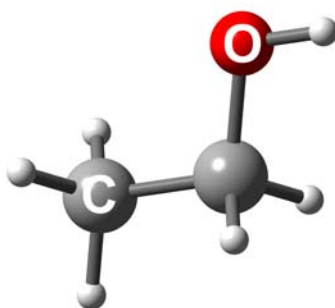


Figure 1-6: Ball and stick model of ethanol (C₂H₅OH)

Ethanol, illustrated in Figure 1-6, is common to both phases of the co-oxidation study as the model labile compound. As an alcohol, ethanol is a good model compound for the expected

hydrolysis intermediates of larger hydrocarbons that would be expected to form in the preheating section of real SCWO applications. Figure 1-4 shows that ethanol is one of the more labile compounds studied in this laboratory, and is expected to oxidize to more than 90% conversion at $T > 470$ °C for typical residence times achievable on our bench-scale tubular flow reactor ($\tau = 2$ to 10 s). This ensures that ethanol will rapidly oxidize and generate a large free radical pool at temperatures of interest for more refractory model compounds.

Ethanol was selected not only because it reacts rapidly but also because it has been well-characterized both experimentally and in elementary reaction rate models. In our group Helling (1988) and Schanzenbacher (2002) led experimental studies that detailed the oxidation and hydrolysis kinetics of ethanol in the tubular flow reactor system that will be used in this co-oxidation study. At Sandia National Laboratory, Rice and Croiset (2001) developed an elementary reaction rate mechanism for the SCWO of ethanol by adapting the ethanol combustion mechanism of Marinov (1999) to high pressures, and validated the mechanism with experimental data collected in their laboratory. The Rice and Croiset ethanol mechanism will be used to predict the effect that ethanol has on the free radical pool in SCW.

1.2.2 Methylphosphonic Acid (MPA)

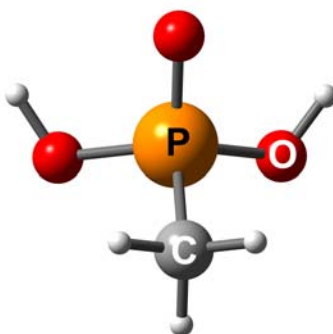


Figure 1-7: Ball and stick model of methylphosphonic acid (MPA, or $\text{PO}(\text{OH})_2\text{CH}_3$)

Methylphosphonic acid (MPA) is one of the major refractory intermediate compounds in the destruction of organophosphorus nerve agents, one of the two major classes of chemical warfare agents that the U.S. must destroy by 2007 as mandated by the 1997 Chemical Weapons Convention (CWC) (NRC 1999). Organophosphorus nerve agents include VX, Sarin and Soman, pictured in Figure 1-8, are acetylcholinesterase inhibitors that can cause death within ten minutes of exposure. These compounds are first neutralized with concentrated NaOH at elevated temperatures to cleave the P-F and P-S bonds, yielding compounds including ethylmethylphosphonic acid (EMPA) and MPA, shown in Figure 1-9. The P-C bond in these compounds remain because they are inert to acidic and basic hydrolysis (Cordeiro et al. 1986; Schowanek and Verstraete 1991). According to the CWC, EMPA and MPA are Schedule 2 precursors and must be destroyed because they could be used to reproduce the nerve agent. SCWO has been selected by the U.S. Army as the most likely method for completely mineralizing the phosphorus in EMPA and MPA to phosphoric acid (NRC 1998).

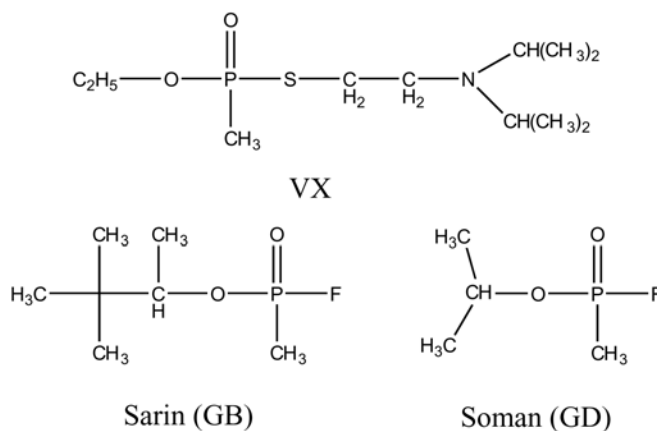


Figure 1-8: Organophosphorus nerve agents

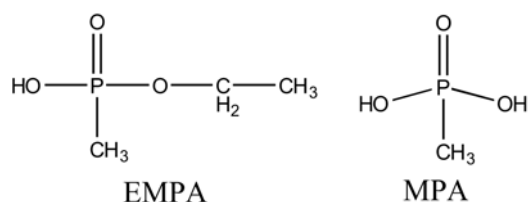


Figure 1-9: Organophosphorus nerve agents hydrolysis intermediates

Bianchetta and coworkers (1999) at the University of Texas studied the SCWO of MPA at high DRE levels, focusing on more practical treatment applications. Sullivan (Sullivan and Tester 2004) in our group at MIT conducted a study at moderate MPA conversions to regress a global rate law and macroscopic pathway analysis from the experimental data. Sullivan then used the understanding gained regarding the channel yields in the carbon-containing intermediate products, including methane, carbon monoxide, and carbon dioxide, to construct an elementary reaction rate mechanism for MPA oxidation in SCW (Sullivan et al. 2004a; Sullivan et al. 2004b). The mechanism has been validated with the Sullivan experimental data and will form the bulk of the MPA-ethanol elementary reaction rate mechanism.

1.2.3 Ammonia



Figure 1-10: Ball and stick model of ammonia (NH₃)

Ammonia, pictured in Figure 1-10, is the most refractory molecule for SCWO, typically requiring temperatures above 600 °C to observe measurable conversion at typical residence times of 60 s or less. Most nitrogen-containing waste streams, one of the most common being raw or partially treated sewage sludges, produce ammonia as an intermediate hydrolysate which in turn

must be oxidized to N_2 . Ammonia oxidation in SCW can show heterogeneous catalysis effects with observed rates often dependent on the surface-to-volume (S/V) ratio and the composition of the reactor wall material. These catalytic effects have been described as a linear combination of a homogenous and heterogeneous oxidation mechanism (Webley et al. 1991; Segond et al. 2002).

Ammonia co-oxidation has been restricted to studies of product distribution at long residence times and high DRE levels corresponding to conversion greater than 99.99%. Hong et al. (1987) reported roughly equal molar yields of nitrous oxide (N_2O) and nitrogen in the destruction of sewage, which consists of a complex mixture of refractory and labile compounds that includes ammonia and a wide variety of labile lignin-cellulosic and fatty acid hydrocarbons. In contrast, the experiments conducted as part of this study (Ploeger et al. 2006b) showed that the yield of nitrous oxide never exceeded 13% for the oxidation of pure ammonia. An attempt was made earlier in our laboratory by Webley et al. (1991) to co-oxidize ammonia with methanol, but no increase in conversion was observed. Later analysis has shown that limitations on preheating and mixing steps and inaccurate temperature measurements in the reactor may be the reason why no co-oxidation rate enhancement was observed. Cocero et al. (2000) co-oxidized ammonia, pyridine, acetonitrile, and aniline with isopropanol to near-complete destruction and measured trace (parts per million) nitrogen products (gas phase NO_x , or NO and NO_2 , and liquid phase nitrates and nitrites) in the effluent.

Efforts to model the oxidation of ammonia have not been as frequent as those for the oxidation of hydrocarbons. The most comprehensive study of ammonia combustion was conducted by Dean and Bozzelli (2000), which cites several rates at $P = 10$ atm, but the authors emphasize that their mechanism, while the best available, should not be considered complete.

Hughes and co-workers at Leeds University compiled a well-documented NO_x submechanism (2001) at typical combustion conditions of $P \leq 1$ atm. Interest in the thermal DeNO_x system by which NO_x is reduced by ammonia has spurred several studies of the reactions of ammonia and ammonia intermediates with nitrogen oxides, both at the mechanistic and *ab initio* level (Diau and Smith 1997; Mebel et al. 1995).

1.3 REFERENCES

- Akiya, N. and P. Savage (2000a). "Effect of water density on hydrogen peroxide dissociation in supercritical water. 1. Reaction equilibrium." *J. Phys. Chem. A* **104**(19): 4433-4440.
- Akiya, N. and P. Savage (2000b). "Effect of water density on hydrogen peroxide dissociation in supercritical water. 2. Reaction kinetics." *J. Phys. Chem. A* **104**(19): 4441-4448.
- Anitescu, G., V. Munteanu and L. L. Tavlarides (2005). "Co-oxidation effects of methanol and benzene on the decomposition of 4-chlorobiphenyl in supercritical water." *J. Supercrit. Fluid* **33**: 139-147.
- Armellini, F. J. and J. W. Tester (1991). "Experimental methods for studying salt nucleation and growth from supercritical water." *J. Supercrit. Fluids* **4**(4): 254.
- Armellini, F. J. and J. W. Tester (1993). "Solubility of sodium-chloride and sulfate in subcritical and supercritical water vapor from 450-500 degrees C and 100-250 bar." *Fluid Phase Equilib.* **84**: 123-142.
- Armellini, F. J., J. W. Tester and G. T. Hong (1994). "Precipitation of sodium-chloride and sodium-sulfate in water from sub- to supercritical conditions - 150 to 550-degrees-C, 100 to 300 bar." *J. Supercrit. Fluids* **7**(3): 147-158.
- Bandura, A. V. and S. N. Lvov (2000). The ionization constants of water over a wide range of temperatures and densities. Steam, water, and hydrothermal systems: Physics and chemistry meeting the needs of industry. P. R. Tremaine, P. G. Hill, D. E. Irish and P. V. Palakrishnan. Ottawa, NRC Press.
- Benjamin, K. M. and P. E. Savage (2004). "Hydrothermal reactions of methylamine." *Journal of Supercritical Fluids* **31**(3): 301-311.
- Benjamin, K. M. and P. E. Savage (2005a). "Detailed chemical kinetic modeling of methylamine in supercritical water." *Industrial & Engineering Chemistry Research* **44**(26): 9785-9793.
- Benjamin, K. M. and P. E. Savage (2005b). "Supercritical water oxidation of methylamine." *Industrial & Engineering Chemistry Research* **44**(14): 5318-5324.
- Bianchetta, S., L. Li and E. F. Gloyna (1999). "Supercritical water oxidation of methylphosphonic acid." *Ind. Eng. Chem. Res.* **38**: 2902-2910.
- Blaney, C., L. Li, E. F. Gloyna and S. U. Hossain (1995). Supercritical water oxidation of pulp and paper mill sludge as an alternative to incineration. Innovations in Supercritical Fluids. K. W. Hutchenson and N. R. Foster. Washington, D.C., American Chemical Society. **608**: 444-455.
- Boock, L. and M. T. Klein (1993). "Lumping strategy for modeling the oxidation of C1-C3 alcohols and acetic-acid in high-temperature water." *Ind. Eng. Chem. Res.* **32**(11): 2464-2473.
- Brock, E., Y. Oshima, P. Savage and J. Barker (1996). "Kinetics and mechanism of methanol oxidation in supercritical water." *J. Phys. Chem.* **100**: 15834-15842.

- Brock, E., P. Savage and J. Barker (1998). "A reduced mechanism for methanol oxidation in supercritical water." *Chem. Eng. Sci.* **53**(5): 857-867.
- Brock, E. E. and P. E. Savage (1995). "Detailed chemical kinetics model for supercritical water oxidation of C₁ compounds and H₂." *AIChE J.* **41**(8): 1874-1888.
- Buelow, S. J. (1990). Destruction of propellant components in supercritical water, Los Alamos National Laboratory.
- Cocero, M. J., E. Alonso, R. Torío, D. Vallelado and F. Fdz-Polanco (2000). "Supercritical Water Oxidation in a Pilot Plant of Nitrogenous Compounds: 2-Propanol Mixtures in the Temperature Range 500-750°C." *Ind. Eng. Chem. Res.* **39**: 3707-3716.
- Cooper, S. P., H. G. Folster, S. A. Gairns and E. G. Hauptmann (1997). "Treatment of lagoon sludge, primary clarifier sludge, and bleach plant effluent by supercritical water oxidation." *Pulp Pap. Can.* **98**(10): 37-41.
- Cordeiro, J. L., D. L. Pompliano and J. W. Frost (1986). "Degradation and detoxification of organophosphonates: Cleavage of the carbon to phosphorus bond." *J. Am. Chem. Soc.* **108**: 332-334.
- Crain, N., A. Shanableh and E. F. Gloyna (2000). "Supercritical water oxidation of sludges contaminated with toxic organic chemicals." *Water Sci Technol* **42**(7-8): 363-368.
- Crain, N., S. Tebbal, L. Li and E. F. Gloyna (1993). "Kinetics and reaction pathways of pyridine oxidation in supercritical water." *Ind. Eng. Chem. Res.* **32**(10): 2259-2268.
- Croiset, E. and S. F. Rice (1998). "Direct observation of H₂O₂ during alcohol oxidation by O₂ in supercritical water." *Ind. Eng. Chem. Res.* **37**(5): 1755-1760.
- Croiset, E., S. F. Rice and R. G. Hanush (1997). "Hydrogen peroxide decomposition in supercritical water." *AIChE J.* **43**(9): 2343-2352.
- Dean, A. M. and J. W. Bozzelli (2000). Combustion Chemistry of Nitrogen. Gas-Phase Combustion Chemistry. W. C. Gardiner Jr., Springer: 125-341.
- Dell'Orco, P., B. Foy, E. Wilmanns, L. Le, J. Ely, K. Patterson and S. Buelow (1995). Hydrothermal oxidation of organic compounds by nitrate and nitrite. Innovations in Supercritical Fluids. K. W. Hutchenson and N. R. Foster. Washington, D.C., American Chemical Society. **608**: 179-96.
- Dell'Orco, P. C., E. F. Gloyna and S. J. Buelow (1997). "Reactions of nitrate salts with ammonia in supercritical water." *Ind. Eng. Chem. Res.* **36**(7): 2547-2557.
- DiNaro, J., J. Howard, W. Green, J. W. Tester and J. Bozzelli (2000). "Elementary reaction mechanism for benzene oxidation in supercritical water." *J. Phys. Chem. A* **104**(45): 10576-10586.
- DiNaro, J., J. Tester, J. Howard and K. Swallow (2000a). "Experimental measurements of benzene oxidation in supercritical water." *AIChE J.* **46**(11): 2274-2284.
- Fauvel, E., C. Jousot-Dubien, V. Tanneur, S. Moussiere, P. Guichardon, G. Charbit and F. Charbit (2005). "A porous reactor for supercritical water oxidation: Experimental results on salty compounds and corrosive solvents oxidation." *Industrial & Engineering Chemistry Research* **44**(24): 8968-8971.

- Foy, B. R., K. Waldthausen, M. A. Sedillo and S. J. Buelow (1996). "Hydrothermal processing of chlorinated hydrocarbons in a titanium reactor." *Environ Sci Technol.* **30**(9): 2790-2799.
- Freeman, H. (1985). Supercritical Water Oxidation. Innovative Thermal Hazardous Organic Waste Treatment Processes: Pollution Technology Review No. 125. Park Ridge, NJ, Noyes Publications: 25-29.
- Gidner, A. and L. Stenmark (2001). Supercritical water oxidation of sewage sludge - state of the art. IBC Conference on Sewage Sludge and Disposal Options, Birmingham, UK.
- Gidner, A., L. Stenmark and K. Carlsson (2001). Treatment of different wastes by supercritical water oxidation. Twentieth IT3 Conference, Philadelphia.
- Gloyna, E. F. and L. Li (1995). "Supercritical water oxidation research and development update." *Environ. Progress* **14**(3): 182.
- Gopalan, S. and P. E. Savage (1995). Phenol oxidation in supercritical water: From global kinetics to a detailed mechanistic model. Innovations in Supercritical Fluids. K. W. Hutchenson and N. R. Foster. Washington, D.C., American Chemical Society. **608**: 217-231.
- Goto, M., T. Nada, A. Ogata, A. Kodama and T. Hirose (1998). "Supercritical water oxidation for the destruction of municipal excess sludge and alcohol distillery wastewater of molasses." *J. Supercrit. Fluids* **13**(1-3): 277-282.
- Griffith, J. W. and D. H. Raymond (2002). "The first commercial supercritical water oxidation sludge processing plant." *Waste Manage.* **22**(4): 453-459.
- Haar, L., J. S. Gallagher and G. S. Kell (1984). NBS/NRC Steam Tables. New York, Hemisphere Publishing Corp.
- Hack, W., D. A. Masten and S. J. Buelow (2005). "Methanol and ethanol decomposition in supercritical water." *Zeitschrift Fur Physikalische Chemie-International Journal of Research in Physical Chemistry & Chemical Physics* **219**(3): 367-378.
- Harradine, D. M., S. J. Buelow, P. Dell'Orco, R. B. Dyer, B. Foy, J. M. Robinson and J. A. Sanchez (1993). "Oxidation chemistry of energetic materials in supercritical water." *Hazard. Waste Hazard. Mater.* **10**(2): 233-246.
- Helling, R. K. and J. W. Tester (1987). "Oxidation kinetics of carbon monoxide in supercritical water." *Energy Fuels* **1**(5): 417-423.
- Helling, R. K. and J. W. Tester (1988). "Oxidation of simple compounds and mixtures in supercritical water - carbon monoxide, ammonia, and ethanol." *Environ Sci Technol.* **22**(11): 1319-1324.
- Henrikson, J. T. and P. Savage (2003). "Water-density effects on phenol oxidation in supercritical water." *AIChE J.* **49**(3): 718-726.
- Henrikson, J. T. and P. E. Savage (2004). "Potential explanations for the inhibition and acceleration of phenol SCWO by water." *Industrial & Engineering Chemistry Research* **43**(16): 4841-4847.

- Hodes, M., P. Griffith, K. A. Smith, W. S. Hurst, W. J. Bowers and K. Sako (2004a). "Salt solubility and deposition in high temperature and pressure aqueous solutions." *Aiche Journal* **50**(9): 2038-2049.
- Hodes, M., P. A. Marrone, G. T. Hong, K. A. Smith and J. W. Tester (2004b). "Salt precipitation and scale control in supercritical water oxidation - Part A: fundamentals and research." *Journal of Supercritical Fluids* **29**(3): 265-288.
- Hodes, M., K. A. Smith and P. Griffith (2003). "A natural convection model for the rate of salt deposition from near-supercritical, aqueous solutions." *Journal of Heat Transfer-Transactions of the Asme* **125**(6): 1027-1037.
- Holgate, H. R., J. C. Meyer and J. W. Tester (1995). "Glucose hydrolysis and oxidation in supercritical water." *AICHE J.* **41**(3): 637-648.
- Holgate, H. R. and J. W. Tester (1993). "Fundamental kinetics and mechanisms of hydrogen oxidation in supercritical water." *Combust. Sci. Technol.* **88**(5-6): 369-397.
- Holgate, H. R. and J. W. Tester (1994a). "Oxidation of hydrogen and carbon monoxide in sub- and supercritical water: reaction kinetics, pathways, and water-density effects. 1. Experimental results." *J. Phys. Chem.* **98**(3): 800-809.
- Holgate, H. R. and J. W. Tester (1994b). "Oxidation of hydrogen and carbon monoxide in sub- and supercritical water: reaction kinetics, pathways, and water-density effects. 2. Elementary reaction rate modeling." *J. Phys. Chem.* **98**(3): 810-822.
- Holgate, H. R., P. A. Webley, J. W. Tester and R. K. Helling (1992). "Carbon monoxide oxidation in supercritical water: the effects of heat transfer and the water-gas shift reaction on observed kinetics." *Energy Fuels* **6**(5): 586-597.
- Hong, G. T., P. K. Fowler, W. R. Killilea and K. C. Swallow (1987). Supercritical water oxidation: treatment of human waste and system configuration tradeoff study. Proceedings of 17th Intersociety Conference on Environmental Systems, Seattle, WA.
- Hong, G. T., W. R. Killilea and T. B. Thomason (1988). Supercritical water oxidation: space applications. ASCE Space '88 Proceedings, Albuquerque, NM.
- Hughes, K. J., A. S. Tomlin, E. Hampartsoumian, W. Nimmo, I. G. Zsély, M. Ujvári, T. Turányi, A. R. Clague and M. J. Pilling (2001). "An Investigation of Important Gas Phase Reactions of Nitrogen Species from the Simulation of Bulk Experimental Data in Combustion Systems." *Combust. Flame* **124**: 573-589.
- Hunter, T. B., S. F. Rice and R. G. Hanush (1996). "Raman spectroscopic measurement of oxidation in supercritical water .2. Conversion of isopropyl alcohol to acetone." *Ind. Eng. Chem. Res.* **35**(11): 3984-3990.
- Hurst, W. S., M. S. Hodes, W. J. Bowers, V. E. Bean, J. E. Maslar, P. Griffith and K. A. Smith (2002). "Optical flow cell and apparatus for solubility, salt deposition and Raman spectroscopic studies in aqueous solutions near the water critical point." *J. Supercrit. Fluids* **22**(2): 157-166.
- Iyer, S., P. Joshi and M. Klein (1998). "Automated model building and modeling of alcohol oxidation in high temperature water." *Environ. Progress* **17**(4): 221-233.

- Iyer, S., G. R. Nicol and M. T. Klein (1996). "Hydrothermal reactions of 1-nitrobutane in high-temperature water." *J. Supercrit. Fluids* **9**(1): 26-32.
- Iyer, S. D. and M. T. Klein (1997). "Effect of pressure on the rate of butyronitrile hydrolysis in high-temperature water." *J. Supercrit. Fluids* **10**(3): 191-200.
- Izzo, B., M. T. Klein, C. LaMarca and N. C. Scrivner (1999). "Hydrothermal reaction of saturated and unsaturated nitriles: Reactivity and reaction pathway analysis." *Ind. Eng. Chem. Res.* **38**(4): 1183-1191.
- Johnston, J. B., R. E. Hannah, V. L. Cunningham, B. P. Daggy, F. M. Sturm and R. M. Kelly (1988). "Destruction of pharmaceutical and biopharmaceutical wastes by the MODAR supercritical water oxidation process." *Biotechnology* **6**(12): 1423-1427.
- Klein, M. T., Y. G. Mentha and L. A. Torry (1992). "Decoupling substituent and solvent effects during hydrolysis of substituted anisoles in supercritical water." *Ind. Eng. Chem. Res.* **31**(1): 182-187.
- Kriksunov, L. B. and D. D. Macdonald (1995). "Corrosion in supercritical water oxidation systems: a phenomenological analysis." *J. Electrochem. Soc.* **142**(12): 4069-73.
- Kritzer, P., N. Boukis and E. Dinjus (1999). "Factors controlling corrosion in high-temperature aqueous solutions: a contribution to the dissociation and solubility data influencing corrosion processes." *J. Supercrit. Fluids* **15**(3): 205-227.
- Kritzer, P. and E. Dinjus (2001). "An assessment of supercritical water oxidation (SCWO) - Existing problems, possible solutions and new reactor concepts." *Chem. Eng. J.* **83**(3): 207-214.
- La Roche, H. L., M. Weber and C. Trepp (1997). "Design rules for the wallcooled hydrothermal burner (WHB)." *Chem. Eng. Technol.* **20**(3): 208-211.
- Lachance, R., J. Paschkewitz and J. W. Tester (1999). "Thiodiglycol hydrolysis and oxidation in sub- and supercritical water." *J. Supercrit. Fluids* **16**: 133-147.
- Lee, D. S. and E. F. Gloyna (1992). "Hydrolysis and oxidation of acetamide in supercritical water." *Environ Sci Technol.* **26**(8): 1587-1593.
- Lee, H. C., J. H. In, S. Y. Lee, J. H. Kim and C. H. Lee (2005). "An anti-corrosive reactor for the decomposition of halogenated hydrocarbons with supercritical water oxidation." *Journal of Supercritical Fluids* **36**(1): 59-69.
- Li, L., P. Chen and E. F. Gloyna (1997). "Pilot-plant validation of kinetic models for supercritical water oxidation." *Chem. Ox.* **4**: 219.
- Li, L., E. F. Gloyna and J. E. Sawicki (1993). "Treatability of DNT process waste-water by supercritical water oxidation." *Water Environ. Res.* **65**(3): 250-257.
- Marinov, N. M. (1999). "A detailed chemical kinetic model for high temperature ethanol oxidation." *Int. J. Chem. Kinet.* **31**(3): 183-220.
- Marrone, P. A., T. A. Arias, W. A. Peters and J. W. Tester (1998a). "Solvation effects on kinetics of methylene chloride reactions in sub and supercritical water: Theory, experiment, and ab initio calculations." *J. Phys. Chem. A.* **102**(35): 7013-7028.

- Marrone, P. A., P. M. Gschwend, K. C. Swallow, W. A. Peters and J. W. Tester (1998b). "Product distribution and reaction pathways for methylene chloride hydrolysis and oxidation under hydrothermal conditions." *J. Supercrit. Fluids* **12**(3): 239-254.
- Marrone, P. A., M. Hodes, K. A. Smith and J. W. Tester (2004). "Salt precipitation and scale control in supercritical water oxidation - part B: commercial/full-scale applications." *Journal of Supercritical Fluids* **29**(3): 289-312.
- Marrone, P. A., R. Lachance, J. DiNaro, B. D. Phenix, J. C. Meyer, J. W. Tester and W. A. Peters (1995). Methylene chloride oxidation and hydrolysis in supercritical water. Innovations in Supercritical Fluids. K. W. Hutchenson and N. R. Foster. Washington, D.C., American Chemical Society. **608**: 197-216.
- Marshall, W. L. and E. U. Franck (1981). "Ion product of water substance, 0-1000 °C, 1-10,000 bars. New international formulation and its background." *J. Phys. Chem. Ref. Data* **10**(2): 295.
- Martino, C. J. and P. Savage (1999a). "Oxidation and thermolysis of methoxy-, nitro-, and hydroxy-substituted phenols in supercritical water." *Ind. Eng. Chem. Res.* **38**(5): 1784-1791.
- Martino, C. J. and P. Savage (1999b). "Supercritical water oxidation kinetics and pathways for ethylphenols, hydroxyacetophenones, and other monosubstituted phenols." *Ind. Eng. Chem. Res.* **38**(5): 1775-1783.
- Martino, C. J. and P. E. Savage (1997). "Supercritical water oxidation kinetics, products, and pathways for CH₃- and CHO- substituted phenols." *Ind. Eng. Chem. Res.* **36**(5): 1391-1400.
- McGuinness, T. C. (1995). Supercritical water oxidation reactor apparatus and method. US Patent, 5,348,051.
- Meyer, J. C., P. A. Marrone and J. W. Tester (1995). "Acetic acid oxidation and hydrolysis in supercritical water." *AIChE J.* **41**(9): 2108-2121.
- Mitton, D. B., N. Eliaz, J. A. Cline and R. M. Latanision (2001). "An overview of the current understanding of corrosion in SCWO systems for the destruction of hazardous waste products." *Mater. Technol.* **16**(1): 44-53.
- Mitton, D. B., J. H. Yoon, J. A. Cline, H. S. Kim, N. Eliaz and R. M. Latanision (2000). "Corrosion behavior of nickel-based alloys in supercritical water oxidation systems." *Ind. Eng. Chem. Res.* **39**(12): 4689-4696.
- Modell, M. (1989). Supercritical water oxidation. Standard Handbook of Hazardous Waste Treatment and Disposal. H. M. Freeman. New York, McGraw Hill: 8.153-8.168.
- Modell, M., J. Larson and S. F. Sobczynski (1992). "Supercritical water oxidation of pulp mill sludges." *Tappi J.* **75**(6): 195-202.
- Mueggenberg, H. H., D. C. Rousar and M. F. Young (1995). SCWO reactor with wall conduits for boundary flow control. US Patent, 5,387,398.
- NRC (1998). Using Supercritical Water Oxidation to Treat Hydrolysate from VX Neutralization. Washington, D.C., Commission on Engineering and Technical Systems.

- NRC (1999). Review and Evaluation of Alternative Technologies for Demilitarization of Assembled Chemical Weapons. Washington, D.C., Commission on Engineering and Technical Systems.
- O'Brien, C. P., M. C. Theis and D. A. Bruce (2005). "Supercritical Water Oxidation of the PCB Congener 2-Chlorobiphenyl in Methanol Solutions: A Kinetic Analysis." *Environ. Sci. Technol.* **39**: 6839-6844.
- Patterson, D. A., L. Stenmark and F. Hogan (2001). Sixth European Biosolids and Organic Residuals Conference, Wakefield, UK.
- Phenix, B. (1998). Hydrothermal oxidation of simple organic compounds. Department of Chemical Engineering. Cambridge, MA, Massachusetts Institute of Technology.
- Ploeger, J. M., P. A. Bielenberg, J. L. DiNaro Blanchard, R. P. Lachance, J. D. Taylor, W. H. Green and J. W. Tester (2006a). "Modeling Oxidation and Hydrolysis Reactions in Supercritical Water - Free Radical Elementary Reaction Networks and Their Applications." *Comb. Sci. Tech.* **178**(1-3): 363-398.
- Ploeger, J. M., A. C. Madlinger and J. W. Tester (2006b). "Revised Global Kinetic Measurements of Ammonia Oxidation in Supercritical Water." *TBD submitted*.
- Proesmans, P. I., L. Luan and S. J. Buelow (1997). "Hydrothermal oxidation of organic wastes using ammonium nitrate." *Ind. Eng. Chem. Res.* **36**(5): 1559-1566.
- Rice, S. and E. Croiset (2001). "Oxidation of simple alcohols in supercritical water III. Formation of intermediates from ethanol." *Ind. Eng. Chem. Res.* **40**(1): 86-93.
- Rice, S. F. (2006). "Stability and reactivity of N₂O in supercritical water." *Combustion Science and Technology* **178**(1-3): 399-415.
- Rice, S. F., T. B. Hunter and Å. C. Rydén (1996). "Raman spectroscopic measurement of oxidation in supercritical water. 1. Conversion of methanol to formaldehyde." *Ind. Eng. Chem. Res.* **35**(7): 2161-2171.
- Rice, S. F., C. A. LaJeunesse, R. G. Hanush, J. D. Aiken and S. C. Johnston (1994). Supercritical water oxidation of colored smoke, dye, and pyrotechnic compositions, Sandia National Laboratory.
- Salvatierra, D., J. D. Taylor, P. A. Marrone and J. W. Tester (1999). "Kinetic study of hydrolysis of methylene chloride from 100 to 500 degrees C." *Ind. Eng. Chem. Res.* **38**(11): 4169-4174.
- Savage, P., J. Rovira, N. Stylski and C. Martino (2000). "Oxidation kinetics for methane/methanol mixtures in supercritical water." *J. Supercrit. Fluids* **17**: 155-170.
- Savage, P., J. Yu, N. Stylski and E. Brock (1998). "Kinetics and mechanism of methane oxidation in supercritical water." *J. Supercrit. Fluids* **12**: 141-153.
- Savage, P. E. (1999). "Organic chemical reactions in supercritical water." *Chem. Rev.* **99**(2): 603.
- Savage, P. E., J. B. Dunn and J. L. Yu (2006). "Recent advances in catalytic oxidation in supercritical water." *Combustion Science and Technology* **178**(1-3): 443-465.
- Savage, P. E., S. Gopalan, T. I. Mizan, C. J. Martino and E. E. Brock (1995). "Reactions at supercritical conditions: Applications and fundamentals." *AIChE J.* **41**(7): 1723-1778.

- Schanzenbacher, J., J. D. Taylor and J. W. Tester (2002). "Ethanol oxidation and hydrolysis rates in supercritical water." *J. Supercrit. Fluid* **22**(2): 139-147.
- Schmeider, H. and J. Abeln (1999). "Supercritical water oxidation: State of the art." *Chem Eng Technol.* **22**(11): 903.
- Schoppelrei, J. W., M. L. Kieke, X. Wang, M. T. Klein and T. B. Brill (1996). "Spectroscopy of hydrothermal reactions .4. Kinetics of urea and guanidinium nitrate at 200-300 degrees C in a diamond cell, infrared spectroscopy flow reactor." *Journal of Physical Chemistry* **100**(34): 14343-14351.
- Schowaneck, D. and W. Verstraete (1991). "Hydrolysis and free radical mediated degradation of phosphonates." *J. Environ. Qual.* **20**: 769-776.
- Segond, N., Y. Matsumura and K. Yamamoto (2002). "Determination of ammonia oxidation rate in sub- and supercritical water." *Ind. Eng. Chem. Res.* **41**(24): 6020-6027.
- Shanableh, A. and E. F. Gloyna (1991). "Supercritical water oxidation - wastewaters and sludges." *Water Sci Technol* **23**(1-3): 389-398.
- Shaw, R. W. and N. Dahmen (2000). Destruction of Toxic Organic Materials Using Supercritical Water Oxidation: Current State of the Technology. Supercritical Fluids. E. Kiran. Netherlands, Kluwer Academic Publishers.
- Snow, R. H., W. Sabato, K. Taylor, G. C. Sresty, K. Downey, D. Hazlebeck and D. Jensen (1996). "Demilitarization of chemical agents by hydrolysis and supercritical water oxidation." *Proceedings of ERDEC Scientific Conference on Chemical and Biological Defense Research*: 359.
- Spritzer, M. H., D. A. Hazlebeck and K. W. Downey (1995). "Supercritical water oxidation of chemical agents and solid propellants." *J. Energ. Mater.* **13**(3&4): 185-212.
- Steeper, R. R., S. F. Rice, I. M. Kennedy and J. D. Aiken (1996). "Kinetics measurements of methane oxidation in supercritical water." *J. Phys. Chem.* **100**(1): 184-9.
- Sullivan, P. A., J. M. Ploeger, W. H. Green and J. W. Tester (2004a). "Elementary reaction rate model for supercritical water oxidation of methylphosphonic acid." *Phys. Chem. Chem. Phys.* **6**(17): 4310-4320.
- Sullivan, P. A., R. Sumathi, W. Green and J. W. Tester (2004b). "Ab initio modeling of organophosphorus combustion chemistry." *Phys. Chem. Chem. Phys.* **6**(17): 4296-4309.
- Sullivan, P. A. and J. W. Tester (2004). "Methylphosphonic acid oxidation kinetics in supercritical water." *AIChE Journal* **50**(3): 673-683.
- Taylor, J. D., C. M. Herdman, B. C. Wu, K. Wally and S. F. Rice (2003). "Hydrogen production in a compact supercritical water reformer." *International Journal of Hydrogen Energy* **28**(11): 1171-1178.
- Taylor, J. D., F. A. Pacheco, J. I. Steinfeld and J. W. Tester (2002). "Multiscale reaction pathway analysis of methyl tert-butyl ether hydrolysis under hydrothermal conditions." *Ind. Eng. Chem. Res.* **41**(1): 1-8.

- Taylor, J. D., J. I. Steinfeld and J. W. Tester (2001). "Experimental measurement of the rate of methyl tert-butyl ether hydrolysis in sub- and supercritical water." *Ind. Eng. Chem. Res.* **40**(1): 67-74.
- Tester, J. W. and J. A. Cline (1999). "Hydrolysis and oxidation in sub- and supercritical water: Connecting process engineering science to molecular interactions." *Corrosion* **55**: 1088.
- Tester, J. W., H. R. Holgate, F. J. Armellini, P. A. Webley, W. R. Killilea, G. T. Hong and H. E. Barner (1993a). Supercritical water oxidation technology. Emerging Technologies in Hazardous Waste Management. W. D. Tedder and F. G. Pohland. Washington, D.C., American Chemical Society. **518**: 35-76.
- Tester, J. W., P. A. Marrone, M. M. DiPippo, K. Sako, M. T. Reagan, T. A. Arias and W. A. Peters (1998). "Chemical reactions and phase equilibria of model halocarbons and salts in sub- and supercritical water (200-300 bar, 100-600 degrees C)." *J. Supercrit. Fluids* **13**(1-3): 225-240.
- Tester, J. W., P. A. Webley and H. R. Holgate (1993b). "Revised global kinetic measurements of methanol oxidation in supercritical water." *Ind. Eng. Chem. Res.* **32**(1): 236-239.
- Thomason, T. B., G. T. Hong, K. C. Swallow and W. R. Killilea (1990). The MODAR Supercritical Water Oxidation Process. Innovative Hazardous Waste Treatment Technology Series, Volume 1: Thermal Processes. H. M. Freeman. Lancaster, PA, Technomic Publishing Co.: 31-42.
- Thomason, T. B. and M. Modell (1984). "Supercritical water destruction of aqueous wastes." *Hazardous Waste* **1**(1): 453-467.
- Thornton, T. D. and P. Savage (1992a). "Kinetics of phenol oxidation in supercritical water." *AIChE J* **38**(3): 321-327.
- Thornton, T. D. and P. Savage (1992b). "Phenol oxidation pathways in supercritical water." *Ind. Eng. Chem. Res.* **31**(11): 2451-2456.
- Turner, M. D. (1993). Supercritical water oxidation of dimethyl methylphosphonate and thiodiglycol, University of Texas at Austin: 208.
- Wang, X. G., L. U. Gron, M. T. Klein and T. B. Brill (1995). "The influence of high-temperature water on the reaction pathways of nitroanilines." *J. Supercrit. Fluid* **8**(3): 236-249.
- Webley, P. A. and J. W. Tester (1989). Fundamental kinetics of methanol oxidation in supercritical water. Supercritical Fluid Science and Technology. K. P. Johnston and J. M. L. Penninger. Washington, D.C., American Chemical Society. **406**: 259-275.
- Webley, P. A. and J. W. Tester (1991). "Fundamental kinetics of methane oxidation in supercritical water." *Energy and Fuels* **5**: 411-419.
- Webley, P. A., J. W. Tester and H. R. Holgate (1991). "Oxidation kinetics of ammonia and ammonia-methanol mixtures in supercritical water in the temperature range 530-700°C at 246 bar." *Ind. Eng. Chem. Res.* **30**(8): 1745-1754.
- Yu, J. and P. Savage (1999). "Catalytic oxidation of phenol over MnO₂ in supercritical water." *Ind. Eng. Chem. Res.* **38**(10): 3793-3801.

Yu, J. and P. Savage (2000a). "Kinetics of catalytic supercritical water oxidation of phenol over TiO₂." *Environ. Sci. Technol.* **34**(15): 3191-3198.

Yu, J. and P. Savage (2000b). "Phenol oxidation over CuO/Al₂O₃ in supercritical water." *Appl Catal B-Environ* **28**(3-4): 275-288.

2 Objectives and Approach

The purpose of this research is to provide a quantitative mechanistic understanding of co-oxidation rate enhancement in supercritical water. This understanding is vital for the application of predictive elementary reaction rate models developed for individual model compounds to the analysis of mixed waste streams. Co-oxidation enhancement has been observed in SCWO experiments dating back to the early 1980s on sewage (Hong, 1987), however, until recently, the state of SCWO elementary reaction rate modeling has not been sufficiently advanced to understand co-oxidation on a mechanism level. By combining the two well-characterized, validated SCWO models for ethanol and MPA, mechanistic insight into the interaction of the two compounds in SCW is possible. This insight into the mechanism of co-oxidation could then be used to assist in the development and validation of an elementary reaction rate mechanism for ammonia.

The approach to achieve these objectives consisted of five major elements:

- 1) *Experimentally measure the rate of MPA oxidation in a mixed MPA-ethanol feed to quantify the effect of ethanol on reaction kinetics.* These experiments were conducted on the plug flow reactor that was used for the pure MPA and pure ethanol SCWO studies conducted by Sullivan and Schanzenbacher, respectively. A full n-factorial experimental design was not feasible, so the effect of temperature, initial MPA concentration and initial ethanol concentration, on MPA oxidation rates were determined by systematic variation of these operating parameters. We focused on measuring MPA conversion because the intermediates of ethanol oxidation include methane, carbon monoxide, and carbon dioxide, the three primary carbon-containing intermediates of MPA oxidation. Experimental methods and results are presented in Chapter 4.

- 2) *Develop an elementary reaction rate model for MPA-ethanol co-oxidation in supercritical water and use insights gained from the model to design an experiment to verify modeling conclusions.* Previous modeling studies have suggested that the hydroperoxy ($\text{HO}_2\bullet$) radical is a key player in co-oxidation, but no experimental evidence has yet been offered. By examining the combined MPA-ethanol supercritical water co-oxidation mechanism, a testable hypothesis for the mechanism of co-oxidation was developed and experimentally verified. Modeling methods and results are presented in Chapter 5.
- 3) *Experimentally measure the rate of ammonia oxidation in supercritical water.* Although ammonia oxidation has previously been studied in our laboratory, improvements to reactant mixing, preheating, and temperature measurement brings the existing data into question. Before proceeding with the ammonia-ethanol co-oxidation experiments, a baseline for pure ammonia SCWO must be established using the improved plug flow reactor system. The effect of temperature, pressure or density, and initial ammonia and oxygen concentrations on the rate of ammonia oxidation and product distribution were examined. Experimental methods and results are presented in Chapter 6.
- 4) *Experimentally measure the rate of ammonia oxidation in a mixed ammonia-ethanol feed.* The effect of temperature and initial ammonia, ethanol, and oxygen concentrations on the rate of ammonia oxidation and product distribution were explored. The data were used in the development of an ammonia-ethanol co-oxidation model. Experimental methods and results are presented in Chapter 7.
- 5) *Develop an elementary reaction rate model for ammonia-ethanol co-oxidation in supercritical water.* Prior to this study, no verified ammonia SCWO elementary reaction

rate mechanism had been developed. Starting with the ethanol submechanism from the MPA-ethanol co-oxidation mechanism and high-temperature ammonia combustion mechanisms, the experimental results from the ammonia and ammonia-ethanol SCWO studies were used to guide the development of an ammonia-ethanol mechanism. Particular attention was devoted to accurately reproducing trends in product distribution. Analysis of the model identified the NO_x submechanism as the key set of reactions in the co-oxidation of ammonia. Low-pressure reactions of the amidogen (NH_2^\bullet) radical with NO and NO_2 were replaced with reactions forming the collision-stabilized adduct species H_2NNO and H_2NNO_2 . Estimation of rates in the NO_x submechanism by *ab initio* methods resulted in an improvement of product distribution predictions. Modeling methods and results are presented in Chapter 8.

3 Experimental Equipment and Procedures

This section details the construction and operation of the experimental apparatus and analytical equipment and methods used in this thesis. A bench-scale plug flow reactor was used for the MPA-ethanol, ammonia, and ammonia-ethanol SCWO studies, and a smaller batch cell was used for long residence time experiments for the ammonia SCWO study.

3.1 DESCRIPTION OF THE BENCH SCALE SCWO SYSTEM

Most experiments for this thesis were conducted using the bench-scale plug flow reactor that was previously modified by Phenix (1998) and DiNaro (1999). No significant modifications to the apparatus were made for the current work. The plug flow reactor system as shown in Figure 3-1 consisted of four major sections: the feed preparation and pressurization stage, the preheating system, the reactor stage, and the letdown and sample collection system.

3.1.1 Feed Preparation and Pressurization Stage

This section of the reactor system consisted of the feed tanks, feed solutions, and two HPLC pumps that were required for the accurate delivery of feed solutions to the reactor. Organic and oxygen saturators were also available to deliver aqueous solutions of gases, such as methane or oxygen, to the reactor system. In this section of the system, prepared aqueous solutions of organic (MPA, ammonia, and/or ethanol) and oxidant (hydrogen peroxide) were separately pressurized and delivered to the reactor using the HPLC pumps. All feed solutions were made from deionized water obtained from an in-house distilled water supply and a water purification system. The water purification system (ELGA LabWater, Model Purelab Ultra Scientific) delivered 18.2 M Ω -cm deionized water with a maximum TOC (total organic carbon)

level of 15 ppb using two purification packs in series to remove ionic and organic impurities from the house distilled water.

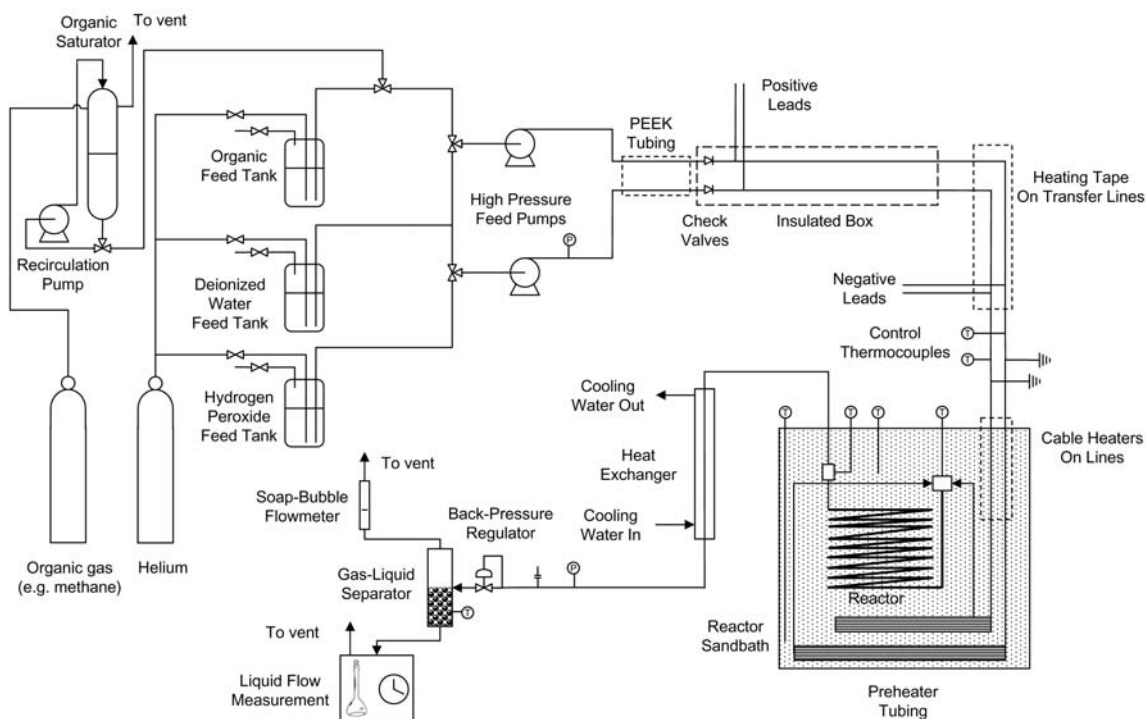


Figure 3-1: Schematic of the plug flow reactor system

The deionized water feed tank was a 30 L reservoir that was degassed with helium for ten minutes to remove all residual oxygen from the water and pressurized to a helium head pressure of 11 psig (1.76 bar). During heatup and cooldown phases, this tank fed deionized water through both HPLC pumps to the reactor. The water feed tank was connected by 340 SS tubing to three-way valves that were located before the pumps on both the organic and oxidant feed lines. These valves allowed for the pump feeds to be switched from the organic or oxidant solutions to the water feed tank without interrupting operation. During hydrolysis experiments, when the organic feed was reacted in the absence of oxygen, the water feed tank delivered water through the oxidant feed pump.

Most of the experiments performed used the organic feed tank, consisting of a 5 liter plastic-coated glass feed vessel with a conical bottom (Kontes, p/n 953901-5002), for holding aqueous solutions of MPA, ammonia, and/or ethanol. To prepare organic feed solutions, MPA (Aldrich Chemical Co., 98%, p/n 28,968-8) was used as received and the desired mass was measured using an analytical balance (Mettler Toledo, AG240). Ammonia (VWR Scientific Products, 28-30 wt%, p/n VW0580-3) and ethanol (Pharmco, 200 proof, anhydrous) were used as received with desired amounts measured using a volumetric buret. The MPA, ammonia, and/or ethanol were dissolved and/or diluted in a volumetric flask and the contents were transferred to the feed vessel where the solution was magnetically stirred. The feed solution was degassed with helium for ten minutes to remove any dissolved oxygen present in the solution. The tank was then sealed and pressurized with 11 psig (1.7 bar) of helium to provide adequate head pressure to deliver the solution to the HPLC organic feed pump via 1/8-in. (3.2-mm) O.D. Teflon tubing. Organic feed samples were withdrawn from the feed tank by a sampling line made of 1/8-in. (3.2-mm) O.D. Teflon tubing connected to the feed line with a three-way valve as it exited the feed tank.

For one set of experiments, methane was co-oxidized with a formaldehyde/methanol solution. To deliver methane to the reactor system, the organic saturator was used instead of the organic feed tank. The organic saturator was a 3-liter 304SS sample cylinder (Hoke, p/n 8HD3000) rated to 1800 psig. When in use, the organic saturator was first charged with deionized water, or an aqueous formaldehyde/methanol solution. Then, the gas lines were briefly flushed with the organic gas, in the case of this study, methane. The gas lines were then closed and the saturator was pressurized to a predetermined level. The Milton Roy positive

displacement recirculation pump was run overnight to ensure that the methane dissolved in the aqueous phase was in equilibrium with the methane in the vapor phase.

Hydrogen peroxide (H_2O_2) was used as the oxidant feed for all of the oxidation experiments conducted in this thesis. Using H_2O_2 allowed for higher reactor oxygen concentrations than were available with pure oxygen saturators. As first reported by Rice at Sandia National Laboratories (1998), H_2O_2 can be used as an oxygen source in a SCWO reactor because it decomposes in the preheating section via the following global reaction producing oxygen and water:



Phenix (1998) confirmed experimentally that H_2O_2 is converted completely to O_2 in the preheater before contacting the organic feed stream. Methanol conversions with a saturated O_2 feed and H_2O_2 feed were found to have identical oxidation kinetics. If H_2O_2 did not decompose completely to O_2 in the preheater, residual H_2O_2 could decompose to two $\text{OH}\cdot$ radicals in the reactor which could cause faster organic oxidation rates.

The hydrogen peroxide solutions were prepared by diluting a 30 wt% aqueous solution of A.C.S. grade H_2O_2 (Aldrich Chemical Co., p/n 21.676-3) with deionized water to the desired concentration. The hydrogen peroxide solution was transferred to the hydrogen peroxide feed tank, a 4 liter HDPE reservoir (Dionex, p/n 39164). The solution was degassed with helium for 10 minutes, after which the tank was sealed and pressurized with 11 psig (1.7 bar) of helium. The H_2O_2 feed solution was sampled via a Teflon tube sampling line with an on/off valve extended from the hydrogen peroxide feed tank. The concentration of the H_2O_2 feed solution was measured by performing the ceric ion titration method described in Section 3.3.1 on the hydrogen peroxide sample. The hydrogen peroxide feed tank was connected to the HPLC

oxidant feed pump via 1/8-in. (3.2-mm) O.D. Teflon tubing. All wetted parts preceding the oxidant feed pump were made of plastic (HDPE, ETFE, or PTFE) to minimize the rate of hydrogen peroxide decomposition, which is catalyzed by metals. Oxygen bubbles in the feed produced by hydrogen peroxide decomposition could cause the HPLC pump to cavitate and stall.

The organic and oxidant feed streams were pressurized to reactor pressure, typically 246 bar but ranging from 135 to 270 bar in this thesis, and delivered to the system via to independent digital HPLC pumps (Rainin, SD-200). Each pump had a 25 mL/min pump head which could increment flow at 0.001 mL/min and was rated for operation at 4,600 psig (318 bar) at maximum flow. Each pump had a pulse-dampening pressure module that maintained downstream pressure fluctuations to less than ± 2 bar at the normal operating pressure of 246 bar ($\pm 0.8\%$).

All feed tanks needed to be pressurized with sufficient head pressure to ensure that the feeds were delivered to the suction-side of the pump faster than the pump drew the solution on the intake stroke of the piston. Without the head pressure, air bubbles could form in the piston chamber and the pump would not be able to deliver the desired flow rate and possibly stall. A Tefzel ferrule (Upchurch, p/n P-300) and an 1/8-in. Delrin nut (Upchurch, p/n P-301) connected the 1/8-in. O.D. Teflon tubing from the organic and hydrogen peroxide feed tanks to each pump inlet. Each pump had a pressure transducer that displayed the pressure at the exit of the pump. For an additional measurement of the feed pressure, there was a pressure gauge on the oxidant feed line after the pump.

Although the flow rate of the HPLC pumps was set through the digital interface, it was observed that the actual flow rate differed up to $\pm 10\%$ from the setpoint. The actual flow rate delivered by the HPLC pumps was a function of pump setpoint, head pressure, and system

pressure, so care was taken that the head pressure remained constant at 11 psig. To simplify the process of setting the head pressure on each tank, all feed tanks were connected to the same helium source. The pumps were calibrated using the method developed by Phenix (1998), and those calibrations were used to calculate the flow rates for the design of experiments and data analysis.

3.1.2 Preheating System

The preheating system was designed to separately heat the organic and oxidant feed streams to the reaction temperature before the two streams were mixed at the reactor inlet. The preheating system is divided into two sections: a direct ohmic preheating section followed by a section of preheating coils positioned in the heated, fluidized sandbath that housed the reactor. Phenix (1998) installed the direct ohmic heating (DOH) system to replace the preheating sandbath in order to achieve higher temperatures with greater accuracy. All heated tubing in the preheating and reactor systems was made of high-nickel alloys, either Hastelloy 276 (HC-276) or Inconel 625, to provide better resistance to corrosion compared to stainless steels. All high pressure fittings in the reactor system were made of HC-276.

The DOH system was an adaptation of the preheating system used at Los Alamos National Laboratory, and operated by applying a voltage across a 9.5-m length of 1/16-in. (1.6-mm) O.D. x 0.01-in. (0.25-mm) wall HC-276 tubing for both organic and oxidant lines. Since the preheating tubing had a resistance of 11 Ω , up to 1300 W of power could be delivered to the fluid using the full 120 VAC. The voltage was applied by clamping the positive lead of a 120 VAC line to a 1/16-in. union (Swagelok, p/n 100-6) on the upstream end of each 9.5-m coil, and the negative lead to a 1/16-in. union on the downstream end. Connecting the leads to unions rather than the bare tubing allowed for a greater contact area, and in addition a back-up ground

was attached to a fitting immediately after the negative lead to direct the electricity to ground in the event that contact was lost between the negative lead and the union.

Prior to each DOH preheater and immediately upstream of the positive lead connection there was a short 10-cm length of high-pressure 1/8-in. (3.2-mm) O.D. x 0.04-in. (1.0-mm) I.D. PEEK tubing followed by a check valve (Nupro, p/n SS-53S4). The PEEK tubing electrically isolated the DOH system from the upstream section of the reactor system and the operator. In case of a loss of pressure upstream of the DOH system, the check valve prevented hot water from back-flowing through the PEEK tubing and destroying it.

Each length of 9.5-m DOH tubing was coiled and insulated, electrically and thermally, with two layers of high-temperature Nextel sleeving (Omega, p/n XC-116 and SXC-316). Electrical insulation was necessary to prevent contact between the organic and oxidant DOH lines and to avoid short circuiting within each line should successive coils come into contact with one another. The two DOH coils were housed in a 20 cm x 36 cm x 66 cm insulated box made of Kaowool board and fiber bond cement (Lynn Ceramics). Loose, bulk alumina-silicated ceramic fiber (Lynn Ceramics) was packed around the coils and completely filled the box to provide additional insulation. The last 0.5 m of the DOH coils were not located inside the insulated box due to geometric constraints, and were traced with Samox heat tape (Thermolyne, p/n BWH102060, 1 in. x 6 ft., 904 W) and wrapped in alumina-silicated ceramic fiber to minimize heat losses. Power to the heat tape was supplied by a Thermolyne Percentage Power Controller (Thermolyne, Type CN45500, 120 VAC, 15 A) with the control set to "HI".

The temperature of the DOH system was specified by 1/32-in. Type K thermocouples located immediately after the negative leads and the back-up grounds on each DOH line, and was controlled by varying the applied voltage. The thermocouples were placed such that the tips

extended into the fluid flow, and their output was routed to Omega PID temperature controllers (Omega, p/n CN9141A). Zero-voltage-switched, silicon controlled rectifier (SCR) power controllers (Omega, p/n CR71Z-230, 240 VAC, 30 A) regulated the percentage of complete sine waves delivered to the preheaters based on the signal from the PID controllers.

Between the DOH and reactor systems, a 30-cm length of tubing on each feed stream was heated by resistive cable heaters (Watlow, p/n 62H24A6X, 1/16-in. (1.6-mm) O.D. x 2 ft. (61 cm, 10 V, 240 W max) which were wrapped around the tubing. The power to the cable heaters was controlled by variable transformers (Powerstat, p/n 3PN117C, 0-120 V, 12 A) set to 30 V. The tubing and cable heaters were insulated with Zetex insulating wrap and alumina-silicate ceramic fiber to minimize heat losses.

The second part of the preheating section was contained within the reactor sandbath (Techne, FB-08). Once the organic and oxidant streams entered the sandbath, each stream passed through an additional 5.2-m coiled length of 1/16-in. (1.6-mm) O.D. x 0.01-in. (0.25 mm) wall HC-276 tubing, which ensured that the feeds entered the mixing tee prior to the reactor inlet at the desired reaction temperature.

3.1.3 Reactor System

The Techne FB-08 fluidized sandbath was selected to provide an isothermal environment for the reactor, since the bulk of the preheating load occurred in the DOH system. The sandbath operated at temperatures up to 700 °C, and was controlled by a Eurotherm PID controller (p/n 2408) which used a Type K thermocouple located in the sand to measure the bath temperature. The sandbath temperature was monitored by one 1/16-in. Type K thermocouple in the top of the sandbath and one in the bottom. When the bed was properly fluidized, the measured

temperatures were within 3 °C of each other, which is equal to the reproducibility of the thermocouples.

The organic and oxidant feed streams were mixed in a specially modified 1/8-in. HC-276 cross from High Pressure Equipment (p/n 60-24HF2). The feed streams entered the cross at an angle of 90° to each other. To increase the rate of mixing, the internal diameters of the two arms of the cross through which the feed streams entered were reduced from 1/16 in. (1.6 mm) to 0.01 in. (0.25 mm) by press fitting short lengths of 1/16-in. (1.6-mm) O.D. x 0.01-in. (0.25-mm) I.D. 316 SS tubing into the arms. With the mixing tee modified to increase the intensity of mixing, it also shortened mixing times as discussed in Phenix (1998). This also reduced the apparent induction time below the one to two seconds reported for previous oxidation data on this apparatus. A 1/16-in. Type K thermocouple was seated in a side port in the mixing cross with the thermocouple bead extending into the fluid to ensure accurate fluid temperature measurement. The fourth port of the cross connected to the reactor via an HC-276 1/8-in. to 1/4-in. adapter (High Pressure Equipment, p/n 60-21HF4HM2).

The reactor was constructed from a 1/4-in. (6.35-mm) O.D. x 0.067-in. (1.7-mm) I.D. x 4.71 m coiled length of Inconel 625 tubing with an internal volume of 10.71 cm³. The end of the reactor connected to an HC-276 tee (High Pressure Equipment, p/n 60-23HF2) by another HC-276 1/8-in. to 1/4-in. adapter. A 1/16-in. Type K thermocouple was seated in a side port in the mixing cross with the thermocouple bead extending into the fluid to measure the fluid temperature at the reactor outlet. The temperature at the reactor inlet and outlet were typically within 3 °C of each other at normal specified operating temperatures ranging from 450 to 700 °C.

The reactor outlet tee connected to a 26-cm. length of 1/4-in. (6.35-mm) O.D. x 1/16-in. (1.6-mm) I.D. HC-276 insulated tubing that led to the heat exchanger outside of the sandbath. This section of tubing, referred to as the riser, had an internal volume of 0.51 cm^3 . The temperature was measured at the end of the riser prior to the heat exchanger by a 1/32-in. Type K thermocouple. Since most of the riser was located outside of the sandbath, the riser was non-isothermal as evidenced by a measured temperature drop of 50 to 150 °C from the reactor outlet to the heat exchanger inlet. It is unknown at what point the reaction was quenched and what the volumetric flow rate was in the riser due to the strong dependence of density on temperature at SCW conditions.

Accurate measurement of the total reactor volume is essential for calculating the residence time in the reactor. The total reactor volume included the wetted volumes of reactor (10.71 cm^3), the fittings (0.28 cm^3), and the riser (0.51 cm^3). Due to a drop in temperature, the reaction probably was quenched partway through the riser. Fortunately, the riser volume only accounted for 4% of the total reactor volume, which when propagated to the residence time uncertainty, only resulted in a 3% uncertainty in the reactor residence time. To calculate the reactor residence time, the total reactor volume was estimated to be $11.23 \pm 0.60 \text{ cm}^3$, assuming that the reaction took place in only half of the riser volume.

3.1.4 Letdown System and Sample Collection

The objective of this section was to cool and depressurize the reactor effluent to ambient conditions to allow the measurement of gas and liquid flow rates and the collection of gas and liquid samples. After exiting the riser, the reactor effluent entered the inner tube of a shell-and-tube heat exchanger and was immediately quenched. The inner tube was a 3-m length of 1/4-in. (6.35-mm) O.D. x 0.065-in. (1.65-mm) wall HC-276 tubing and the outer wall shell was a 2.4-m

length of 1/2-in. (12.7-mm) O.D. x 0.035-in. (0.89-mm) wall copper tubing. The cooling source was the building cold water supply which was filtered through a 10 μm spiral-wound prefilter cartridge (VWR, p/n 26303-052).

After the heat exchanger, a pressure transducer (Dynisco, Model 832) measured the system pressure. The pressure read at this transducer was typically the same as that read by the pressure gauge located on the oxidant stream feed line within the reproducibility of the two instruments, except when clogging in the mixing cross resulted in a higher pressure in the oxidant feed line by up to 400 psi. After the pressure transducer, a spring-loaded, manual backpressure regulator (Tescom, p/n 26-3200) controlled system pressure. As the effluent passed through the backpressure regulator, it flashed to atmospheric pressure.

Downstream of the backpressure regulator, the effluent became liquid and vapor phases that were separated in gas-liquid separator constructed of 20 cm of 1/2-in. (12.7-mm) O.D. 316SS tubing packed with 4-mm borosilicate glass beads. The gas exited the top of the separator and passed through a sampling port and soap-bubble flowmeter before it was vented to the fume hood. Gas samples were drawn from the sampling port with a gas-tight syringe (Hamilton, p/n 1725), and the gas flow rate was measured with the soap-bubble flowmeter and a stopwatch. The liquid exited the bottom of the separator into a 1/8-in. (3.2-mm) O.D. 316SS sampling line in a vented box where samples could be collected and the flow rate could be measured using a Class A volumetric flask and a stopwatch.

3.1.5 Health and Safety

The operation of this high-pressure, high-temperature reactor system presents many potential hazards, including overpressurization of the reactor system, electric shock from the DOH system, inhalation of alumina from the sandbath, burns from the high-temperature fluid,

heated metal or sandbath, and exposure to toxic chemicals. This section details the procedures adopted to ensure operator safety.

The risk of overpressurization was minimized first by the digital HPLC pumps which would automatically shut down if the system pressure exceeded the maximum pump pressure of 4600 psig (318 bar). A rupture disk (High Pressure Equipment) downstream of the heat exchanger was set to burst at 4500 psig (311 bar) +6%, -3%. Finally, the reactor system was housed inside 3/8-in. (0.95-cm) to 1/2-in. (1.3-cm) thick Lexan mounted on a Unistrut frame to protect the operators should reactor contents or a piece of metal be forcibly ejected under pressure.

The primary safety concern regarding the DOH system was the conduction of electricity upstream or downstream from the DOH system to the operator via the conductive metal tubing. As previously mentioned, the DOH system was electrically isolated from the upstream system by the PEEK tubing, and downstream of the negative lead by a backup ground. All electrically conducting sections of the DOH system were well insulated to eliminate the possibility of any individuals accidentally contacting electrically live metal tubing, and the DOH system was contained within the Lexan-shielded Unistrut cage that remained closed during reactor operation. There were three readily accessible locations to cut power to the DOH system at any time, including the main circuit breaker.

The fluidized sandbath used chromatographic grade alumina (VWR, AX0611-1) that presented an inhalation hazard due to particulate size. To prevent inhalation, the fluidized sandbath was located within the Lexan cage which was connected to the fume hood air duct. The sandbath's air reclamation system recaptured most of the expelled sand, and the ventilation of the Lexan cage prevented the any sand from entering the laboratory. When it was necessary

to work in or near the fluidized sandbath, dust masks were worn to prevent inhalation of the alumina.

The heated sections of the reactor system could cause severe burns if physical contact was made with the hot metal. To prevent accidental burns, all heated sections of the reactor system were enclosed in insulation and located within the Lexan cage. In the case of leaks, hot process fluid was contained within the insulation or the Lexan cage.

The organic feed, the liquid effluent, and the vapor effluent presented an exposure risk, so the proper personal protective equipment of safety glasses, lab coat and nitrile gloves were worn at all times. The organic feed tank was housed in a fume hood, which would contain any potential leak from the tank. The vapor phase effluent vented to the same hood, as was the box that contained the liquid phase sampling port. Active ventilation prevented harmful vapors from accumulating in the laboratory.

3.1.6 Reactor Operation and Data Collection

Before performing an experiment on the plug flow reactor, the system was first pressurized and heated to the desired pressure and temperature. During this initial stage, deionized water from the water feed tank was fed through the system. The flow rate was set to 5 mL/min for each pump and the system was gradually pressurized using the backpressure regulator. Once the system was at the desired pressure, the sandbath was set to the desired temperature and the controllers for the cable heaters and heat tape were turned on. The cooling water was then turned on for the heat exchanger, and finally the DOH system was activated. The DOH controller was set to the reaction temperature in 100 °C increments to prevent overshoot, and the maximum temperature for the DOH was typically 550 °C to minimize the risk of tubing failure.

During the heatup stage, organic and oxidant feed solutions were prepared. Samples were taken from the feed tanks for analysis before the reactor feed was switched to organic and oxidant feeds to confirm that the correct reactant concentrations had been achieved. During the cooldown stage after the last experiment for the day, organic and oxidant samples were again analyzed to ensure that reactant concentrations had remained constant over the course of the day. Once the reactor system had reached the desired temperature, the pump flow rate was set to an appropriate level corresponding to the specified residence time and the pump feeds were switched from the water feed tank to the organic and oxidant feed tanks using the three-way valves on each feed line. After the feeds had been switched, about one hour was required to reach steady state conditions. Typically, the entire heatup stage needed two to three hours depending on the desired reaction temperature.

The typical length of an experiment at a single temperature, pressure, initial organic and oxidant concentration, and residence time, was one hour. During the hour, four to six liquid and gas flow rate measurements were made, and three to six liquid and gas effluent samples were taken for analysis. Gas samples were drawn from the septa-sealed sampling port above the gas/liquid separator using a gas-tight Teflon tipped syringe. The 200 μL sample was immediately injected into one of the gas chromatographs. Liquid samples were collected from the liquid sampling port at the bottom of the gas/liquid separator into 2 mL amber autosampler vials capped with PTFE/silicone caps for injection onto the ion or gas chromatograph. When analytical methods such as the ammonia ion-specific electrode required a larger sample, 50 mL of effluent was collected in a volumetric flask. The pressure measured just before the backpressure regulator was recorded every time the flow rates were measured. The temperatures measured at various thermocouples were logged to a computer, described in more detail below.

After recording at least three consistent measurements of the flow rates and concentrations for the gas and liquid phases, the HPLC pump setpoints were either adjusted to the next desired residence time or the reactor was shut down by turning off the heating elements. If the pump flow rates were changed, an hour was needed to achieve steady state at the new residence time. Typically, data were collected at two or three sets of conditions for each day of reactor operation.

Temperature measurements were recorded by logging thermocouple measurements every ten seconds using either the HOTMUX software from the DCC Corporation or the TracerDAQ software from Measurement Computing. The TracerDAQ software replaced the HOTMUX software when a new temperature logger was needed with USB connectivity. The software logged temperature measurements made by the thermocouples at the end of both DOH coils, the mixing cross at the reactor inlet, the tee at the reactor outlet, the tee at the end of the riser, and the top and bottom of the sandbath. For each day of experiments, the ambient temperature and pressure were recorded to calculate the aqueous solubility of the gas phase compounds in the liquid effluent.

3.2 BATCH CELL SCWO REACTOR

The batch cell reactor was used for lower-temperature ammonia SCWO experiments in which the residence time required to observe appreciable ammonia conversion was much greater than the 2 to 10 s that the plug flow reactor could deliver. The batch cell was identical to the reactor used by Taylor (2001) for the hydrolysis of MTBE, but the method of operation and downstream sample collection apparatus were changed in order to permit the oxidation of ammonia without limits on residence time.

3.2.1 Reactor Design

A schematic of the batch cell reactor is shown in Figure 3-2. The reactor was constructed of a 2-in. (5-cm) diameter solid HC-276 rod that was bored out to form a 1-in. (2.5-cm) I.D. cavity and then sealed with a 1/2-in. (1.3-cm) thick piece of HC-276. Four 1/8-in. (3.2-mm) taper seal HIP female ports were machined into the reactor to allow for temperature and pressure measurements as well as inlet and outlet flows. Four HC-276 thermocouple adapters (High Pressure Co., p/n 15-21AF1AM2-T) were placed in each port to allow 1/16-in. (1.6-mm) O.D. tubing to be inserted into the reactor. A 1/16-in. (1.6-mm) O.D. Type K thermocouple was inserted such that the tip extended into the center of the reactor cavity to ensure most accurate measurement of the fluid temperature. Pressure was monitored by pressure transducer (Dynisco, p/n G832-000-7.5M) connected to the reactor by 1/16-in. (1.6-mm) O.D. HC-276 tubing. Before the pressure transducer a pressure relief valve (Nupro p/n SS-4R3A-F) was set to open at 4000 psi (272 bar) in case of overpressurization. The inlet and outlet for the reactor was plumbed with 1/16-in. (1.6-mm) O.D. HC-276 tubing that extended into the center of the reactor cavity.

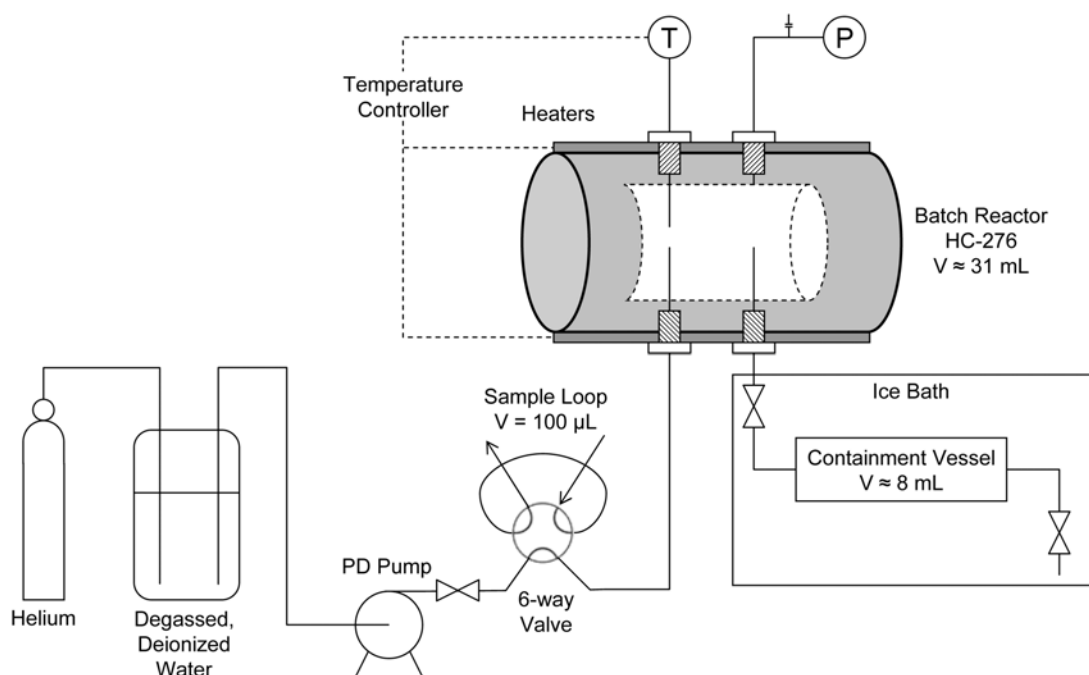


Figure 3-2: Batch cell reactor schematic

The reactor was heated by six strip heaters (Omega, p/n NSA-711) with a maximum power output of 125 W each (110 VAC) placed around the outside of the reactor and held in place by two steel straps. The reactor was then wrapped in two layers of Fiberfrax insulation (Durablanket-S) to minimize heat loss. Temperature was controlled by a PID controller (Omega, p/n CN9000A) based on the thermocouple measurement. The controller output (4-20 mA) was converted to on/off control (110 VAC) by a solid state relay (Omega, p/n SSR240DC45). The voltage was reduced manually with a potentiometer (Cole-Parmer, p/n P-02604-00) which was typically set from 30-40% of maximum output depending on the desired temperature.

The batch cell reactor was placed within an aluminum box inside a fume hood to both protect the operator from any hot process fluid or metal pieces that may be forcibly ejected in the unlikely event of catastrophic failure.

3.2.2 Reactor Operation and Data Collection

Prior to conducting a batch cell SCWO experiment, a 1-L glass bottle (Wheaton Scientific) was filled with deionized water from the ELGA system described in Section 3.1.1. The glass bottle was placed on a hot plate stirrer (VWR, p/n 58849-001) and boiled for one hour to drive off dissolved gases. The water was allowed to cool and the glass bottle was placed under a helium head pressure of 10 psig (1.7 bar). A 2-m length of 1/8-in. (3.2-mm) O.D. Teflon tubing carried the degassed water to the positive displacement pump (Eldex, Model B-100-S), which was set to the maximum flow rate setting to deliver approximately 7.5 mL/min against a system pressure of 3500 psig (242 bar).

The reactor was heated to the desired temperature with the inlet valve closed and the outlet valve open. Both valves were 316 SS needle valves (High Pressure, p/n 15-11-AF1), and the outlet valve was submerged in an ice bath to quench the reactor effluent and prevent the Grafoil packing from being destroyed (maximum rated temperature 343 °C). Once the reactor temperature stabilized at the desired reaction temperature, the outlet valve was closed and the inlet valve opened. Water was gradually pumped into the reactor, pausing to allow the temperature to return to the setpoint, until the reactor pressure reached an intermediate level that had previously been determined to lead to a final system pressure of 3550 psig (246 bar) after the injection of reactants described below.

Reactants were delivered to the reactor by a 100 μ L sampling loop connected to a Valco 6-way valve directly before the reactor. When the valve was in the “load” position, the pump delivered water directly to the reactor, and reactant could be injected through the sampling loop and to waste collection. When the valve was switched to the “inject” position, the pump delivered water through the sampling loop, pushing the 100 μ L of reactants from the loop into

the reactor. To ensure that the entire contents of the sampling loop were delivered to the reactor, each injection consisted of six strokes of the pump, which moved approximately 400 μL of water. To perform an oxidation experiment, first a solution of hydrogen peroxide was injected into the reactor. After five minutes had elapsed to allow the hydrogen peroxide to decompose to water and oxygen, a solution of ammonia was injected into the reactor. After the sixth stroke of the pump on the last injection, the inlet valve was closed and the stopwatch used to measure residence time was started. Several practice runs were conducted at each temperature by injecting water in the same manner as described above until an intermediate pressure was found such that the final system pressure would be 3550 psig (246 bar).

When the desired residence time was reached, the outlet valve was opened causing the reactor contents to rapidly evacuate and quench in the containment vessel, a 4-in. (10-cm) length of 1/2-in. (1.3-cm) O.D. 316SS tubing. The containment vessel was necessary to capture ammonia that remained in the gas phase. Before the experiment, the vessel was charged with 1 mL of 1 M sulfuric acid to drive the liquid-phase equilibrium toward the formation of the aqueous ammonium ion (NH_4^+). After venting the reactor contents, the reactor was twice charged with about 500 psig (34 bar) of deionized water and vented into the containment vessel to ensure that all of the reactor contents were well within the containment vessel. The vessel was then sealed, agitated to improve gas/liquid phase contact, and emptied into a volumetric flask for sampling. The reactor was flushed with deionized water and either heated back to reaction temperature for the next experiment or shut down and allowed to cool to room temperature.

3.3 ANALYTICAL METHODS AND ANALYSIS

Over the course of each experiment, from three to six gas and liquid samples were collected for analysis. The gas samples were immediately injected into the gas chromatographs,

while the liquid samples were collected and analyzed by ion chromatography, gas chromatography, and/or ion-specific electrode depending on the organic feed composition. Hydrogen peroxide feed concentrations were measured by ceric ion titration.

3.3.1 Product Analysis

An ion chromatograph (IC) was used to measure MPA and phosphoric acid concentrations in the feed effluent. The ion chromatograph was equipped with a Dionex IonPac AS11 anion column (p/n 044076), a Dionex IonPac AG11 guard column (p/n 044078), a Dionex IP25 Isocratic pump (p/n 054046), a Dionex Anion Self-Regenerating Suppressor ASRS-I (p/n 053946), a Dionex DS3 Detection Stabilizer (p/n 044130), and a Dionex ED40 electrochemical detector (p/n 046297) operated in conductivity mode with a 21 mM NaOH eluent flowing at a rate of 1 mL/min. The maximum concentration of MPA and phosphoric acid that could be measured accurately on the IC was 1200 ppm for each component, so samples were diluted as needed.

An HP 6890 Series gas chromatograph (GC) employing a flame ionization detector (FID) with helium carrier gas was used to measure the concentration of ethanol, acetaldehyde, and methanol in all liquid samples. A 30 m x 0.53 mm I.D. x 1 μ m film thickness DB-WAX column was used to separate the hydrocarbons.

An ammonium ion specific electrode (ThermoOrion p/n 9512) was used to measure the concentration of ammonia. The electrode measured the concentration of ammonia in an aqueous solution by detecting the amount of ammonia gas that diffused across a Teflon membrane stretched across the tip of the electrode. A sample of approximately 25 mL was placed in a 50 mL beaker on a magnetic stir plate and the tip of the electrode was placed in the sample at an angle to minimize the trapping of air bubbles on the membrane. To ensure that all of the

aqueous ammonia was in the ammonia (NH_3) state rather than the ammonium (NH_4^+) state, 0.5 mL of ionic strength adjustor (ThermoOrion, p/n 951211) was added to the sample, which increased the pH above 10. The voltage signal that the electrode delivered to a Orion benchtop meter (Model 720A) was linearly dependent on the logarithm of the ammonia concentration.

To analyze the gas effluent, four separate gas chromatographs were used. For oxygen, nitrogen, carbon monoxide, and carbon dioxide, an HP 6890 GC was used with a thermal conductivity detector (TCD) using helium as the carrier gas. Two columns were connected in series with an air actuated switching valve (HP Valving Option 404). The first column was a 5 ft. (1.5 m) x 1/8 in. (3.2 mm) 60-80 mesh Carboxen 1000 column which separates the carbon-containing gases CO , CO_2 and CH_4 and connects to an 8 ft. (2.4 m) x 1/8 in. (3.2 mm) 60/80 mesh Molsieve 5Å column which separates the O_2 and N_2 . N_2 , O_2 , and CO passed through both columns to the detector, but to prevent irreversible absorption of CO_2 on the Molsieve column, the switching valve reversed flow prior to CO_2 and CH_4 reaching the column. CO_2 and CH_4 flowed back through the Carboxen column to the detector.

An HP 5890 Series II GC with a TCD detector employed nitrogen as the carrier gas to analyze for helium and hydrogen. This GC also used the 60/80 mesh Carboxen 1000 and 60/80 mesh Molsieve 5Å for separation. Hydrogen was typically not observed in the gas phase effluent except in cases of the high temperature ($T = 700\text{ }^\circ\text{C}$) hydrolysis runs with ethanol present in the organic feed. Helium was delivered to the reactor in low quantities dissolved in both feed streams due to the 11 psig (1.76 bar) head pressure in both tanks.

A second HP 5890 Series II GC with an FID detector used a helium carrier gas to analyze for light hydrocarbons, such as methane, ethane and ethylene. The column was a bonded Astec PLOT column that can separate hydrocarbons up to C-10.

To detect nitrous oxide, a third HP 5890 Series II GC with an electron capture detector (ECD) and a DB-624 capillary column (J&W Scientific, p/n 1153432) was used with helium carrier gas and nitrogen makeup gas.

Hydrogen peroxide in the oxidant feed tank was measured by ceric ion titration. A H_2O_2 sample of known volume was titrated with Ce^{4+} , a strong oxidizer, in the presence of a ferroin ion indicator. When the hydrogen peroxide had been completely oxidized, the ceric ion oxidized the ferroin which changed the color of the solution from orange to blue. The titration was performed using a Hach digital titrator (Hach Co., p/n 16900-01) and Hach peroxide reagents (Hach Co., p/n 22928-00). In practice, approximately 30 mL of deionized water and 2 mL of 19.2 N H_2SO_4 were added to a 50 mL Erlenmeyer flask on a magnetic stir plate. A volume ranging from 100 to 500 μL , depending on the feed concentration, of H_2O_2 sample from the feed tank was added to the flask using a digital pipette. One drop of ferroin indicator was added, and the solution was then titrated with 0.5 N ceric ion solution using the digital titrator until the solution changed from orange to blue.

3.3.2 Data and Error Analysis

For each experiment on the plug flow reactor, the reactor temperature and pressure, ambient temperature and pressure, and the gas and liquid flow rates were recorded. For each experiment on the batch cell reactor, only the reactor temperature and pressure were recorded. The initial concentrations of organic and hydrogen peroxide were calculated from analytical measurements, as were the concentrations of products and unreacted organic in the liquid phase effluent, and O_2 , N_2 , CO , CO_2 , CH_4 , He , H_2 and C_2H_4 in the gas phase effluent. From these measurements, the residence time, the inlet and outlet reactor concentrations could be calculated, which would then be used to determine kinetic data such as conversion, carbon (or nitrogen)

yield, carbon (or nitrogen) fraction, pseudo-first order rate constants, and component mass balances. To understand the significance of those results, the uncertainty for each calculated value was also determined. The uncertainties in all measured quantities were calculated from the absolute error of the instrument and the precision error from multiple measurements of each quantity. The uncertainties in all calculated quantities were propagated from the uncertainties in the measured quantities using the differential method.

To calculate the initial reactant concentrations in the reactor inlet for the batch cell reactor, the initial reactant concentrations in the feed solution were multiplied by the dilution factor $V_{loop}/V_{reactor}$. For the plug flow reactor, concentrations were calculated from the volumetric flow rate of the organic and oxidant feed streams (F_{org} and F_{oxy}), the total measured flow rate (F_T), the ambient organic and H_2O_2 feed concentrations ($[Org]_{o,amb}$ and $[H_2O_2]_{o,amb}$), and the ambient and supercritical water densities (ρ_{amb} and ρ_{SCW}) using Eqns. 3-1 and 3-2 below.

$$[Org]_{o,in} = \frac{[Org]_{o,amb} F_{org} \rho_{SCW}}{F_T \rho_{amb}} \quad (\text{Eqn. 3-1})$$

$$[O_2]_{o,in} = \frac{[H_2O_2]_{o,amb} F_{oxy} \rho_{SCW}}{2F_T \rho_{amb}} \quad (\text{Eqn. 3-2})$$

Only the total flowrate F_T was measured, while the oxidant feed stream flow rate (F_{oxy}) was calculated from the oxidant pump calibration. The organic feed stream flow rate (F_{org}) was determined by subtracting F_{oxy} from F_T . There was a negligible difference in calculated flow rates if the organic pump calibration was used to calculate the organic feed stream flow rate and the oxidant feed stream flow rate was calculated by subtraction. The density of water at reactor and ambient conditions was calculated using steam tables (Haar, 1984). The outlet concentrations for liquid-phase products (LPP) were calculated using Eqn. 3-3 below, where $[LPP]_{amb}$ refers to the ambient outlet concentration of any liquid-phase product.

$$[\text{LPP}]_{out} = \frac{[\text{LPP}]_{amb} \rho_{SCW}}{\rho_{amb}} \quad (\text{Eqn. 3-3})$$

Reactor outlet concentrations of gas-phase products (GPP) were calculated from the concentrations of the product in both the gas and liquid phases. The concentration in the gas phase was determined by GC, and the concentration in the liquid phase was calculated assuming Henry's Law:

$$y_i \hat{\phi}_i(T, P, y_i) P = x_i H_{i, H_2O}(T, P) \quad (\text{Eqn. 3-4})$$

where y_i is the gas-phase mole fraction of component i , $\hat{\phi}_i$ is the gas-phase fugacity coefficient, P is the ambient pressure, T is the ambient temperature, x_i is the liquid-phase mole fraction, and H_{i, H_2O} is the Henry's Law constant. At atmospheric pressure, the fugacity coefficients were assumed to be unity, which is reasonable for light gases. Henry's Law constants were taken from the literature for O₂, (Benson 1979), CO (Rettich 1982), H₂, N₂, He, and CO₂ (Wilhelm 1977), CH₄ and C₂H₄ (Rettich 1981), and N₂O (Dean 1992). CO₂ and N₂O were the only gases that had a high enough solubility in the liquid phase that the molar flow rate of gas dissolved in the liquid was more than 1% of the flow rate in the gas phase. The concentration of a gas-phase product ($[\text{GPP}]_{out}$) could be calculated from Eqn. 3-5 using the mole fractions in the liquid and gas phase effluent, the gas and liquid phase flow rates (F_G and F_L), the liquid density (ρ_L) and the gas phase density from the ideal gas equation (ρ_G).

$$[\text{GPP}]_{out} = \frac{(x_{GPP} F_L \rho_{L, amb} + y_{GPP} F_G \rho_{G, amb}) \rho_{SCW}}{F_L \rho_{L, amb}} \quad (\text{Eqn. 3-5})$$

The reactor residence time of the batch cell reactor was calculated by stopwatch. For the plug flow reactor, the residence time was calculated by dividing the total reactor volume (V_{rxtr}) by the volumetric flow rate at reactor conditions.

$$\tau = \frac{V_{rxr} \rho_{SCW}}{F_L \rho_{amb}} \quad (\text{Eqn. 3-6})$$

As discussed in Section 3.1.3, there is a finite uncertainty in the reactor volume due to the unknown extent of reaction in the riser, which is incorporated into the error in residence time along with precision errors in the measurements of temperature, pressure, and liquid flow rate. The uncertainty due to mixing times was not included, instead a minimum residence time of 2 s was set for the plug flow apparatus to ensure that the mixing time would not be greater or equal to the total residence time.

The conversion of a given organic compound (X_{org}) was calculated from the inlet and outlet reactor concentrations.

$$X_{org} = \frac{[\text{Org}]_{in} - [\text{Org}]_{out}}{[\text{Org}]_{in}} \quad (\text{Eqn. 3-7})$$

The fuel equivalence ratio (Φ) indicates whether the organic compounds are oxidizing in fuel-rich or fuel-lean conditions, and is defined as:

$$\Phi \equiv \sum_{org} \frac{S_{org} [\text{Org}]_{in}}{[\text{O}_2]_{in}} \quad (\text{Eqn. 3-8})$$

where S_{org} is the stoichiometric ratio of oxygen to fuel required for each compound. Values of Φ greater than one indicate fuel-rich conditions and values less than one indicate fuel-lean.

Reaction products are typically reported in terms of carbon fraction or carbon yield:

$$\text{Product}_i \text{ carbon fraction} \equiv \frac{\text{Moles of carbon in Product}_i}{\text{Total moles carbon fed}} \quad (\text{Eqn. 3-9})$$

$$\text{Product}_i \text{ carbon yield} \equiv \frac{\text{Moles of carbon in Product}_i}{\text{Total moles carbon reacted}} \quad (\text{Eqn. 3-10})$$

The carbon fraction normalizes the product to the total amount of organic fed into the reactor, and was used in closing a mass balance. The carbon yield was used in determining the relative

rates of different macroscopic reaction pathways. These parameters can also be calculated for nitrogen or phosphorus to determine the fate of those atoms in the SCWO reaction network.

Component mass balances were calculated by summing the fractions calculated in Eqn. 3-9 and were calculated for carbon, phosphorus, and nitrogen when applicable. Balance values were used to ensure that all products were being measured and typically equaled $100 \pm 5\%$. Poor balance values indicated possible problems with analytical measurements or undetected products.

Pseudo-first order rate constants (k^*) were calculated to compare oxidation rates at different conditions, assuming that the global rate law was first order in organic and zeroth order in oxygen.

$$-\frac{d[\text{Org}]}{dt} = k^* [\text{Org}] \quad (\text{Eqn. 3-11})$$

$$k^* = -\frac{\ln\left(\frac{[\text{Org}]_{out}}{[\text{Org}]_{in}}\right)}{\tau} = -\frac{\ln(1-X)}{\tau} \quad (\text{Eqn. 3-12})$$

For the batch cell reactor, it was assumed that the first five seconds of residence time included a significant mixing time. To correct for the mixing time, all reaction parameters were calculated using a short (5-60 s) residence time experiment as a reference point, rather than the initial organic concentration. The pseudo-first order rate constant was calculated by Eqn. 3-13 where the subscript “short” refers to the short residence time reference point.

$$k^* = -\frac{\ln\left(\frac{[\text{Org}]_{out}}{[\text{Org}]_{short}}\right)}{\tau - \tau_{short}} \quad (\text{Eqn. 3-13})$$

3.3.3 Uncertainty Analysis

The uncertainties in all derived quantities were propagated from the uncertainties in all measured variables, such as flow rates, temperatures, pressures, and analytical signals. The uncertainty in the measured variables derived from two sources: precision error and reproducibility error. The precision error resulted from the variance in the repeated measurement of the same quantity. The reproducibility error was the rated error in the measurement device, which was ± 3 °C in the case of the thermocouples. For most measurements, the precision error dominated the reproducibility error, but for temperature and pressure measurements, the reproducibility error typically dominated.

Precision errors were represented by 95% confidence intervals, assuming that the error on all measured values was represented by a student's t-distribution. For example, the confidence interval for the measured variable x would be calculated by Eqn. 3-14.

$$\bar{x} \pm \frac{s \times t_{1-CL}((n_{obs} - 1) \text{ degrees of freedom})}{\sqrt{n_{obs}}} \quad (\text{Eqn. 3-14})$$

where \bar{x} is the mean, s is the standard deviation, n_{obs} is the number of observations and $t_{1-CL}((n_{obs} - 1) \text{ degrees of freedom})$ is the t-value at the stated confidence interval for the given number of measurements.

To estimate the uncertainty in the reactor temperature and pressure, the absolute error had to be included in the calculation. The reactor temperature was calculated from 400-600 temperature measurements logged over the course of the experiment, which resulted in a precision error less than ± 1 °C by using Eqn. 3-14. Since the uncertainty inherent to the Type K thermocouples was ± 3 °C, the reported uncertainty was calculated by using Eqn. 3-15.

$$\text{Uncertainty} = \sqrt{CI^2 + \sigma_{reproducibility}^2} \quad (\text{Eqn. 3-15})$$

Where CI is the confidence interval calculated in Eqn. 3-15 and $\sigma_{reproducibility}$ is the reproducibility error for the instrument.

The confidence intervals for all measured quantities were then propagated through to the derived quantities using standard differential techniques. For quantities that were calculated using calibration curves, the uncertainties in the calibration parameters were included at the 95% confidence level.

3.4 REFERENCES

- DiNaro, J. L. (1999). Oxidation of benzene in supercritical water: experimental measurements and development of an elementary reaction mechanism. Department of Chemical Engineering, Massachusetts Institute of Technology, Cambridge, MA.
- Phenix, B. (1998). Hydrothermal oxidation of simple organic compounds. Department of Chemical Engineering, Massachusetts Institute of Technology, Cambridge, MA.
- Rice, S. F. and R. R. Steeper (1998). "Oxidation rates of common organic compounds in supercritical water." *Journal of Hazardous Materials* **59**(2-3): 261-278.
- Taylor, J. D. (2001). Hydrothermal Chemistry of Methylene Chloride and MTBE: Experimental Kinetics and Reaction Pathways. Chemical Engineering, Massachusetts Institute of Technology, Cambridge, MA.

4 Experimental Results for MPA-Ethanol Co-oxidation

This chapter details the experimental findings of the co-oxidation of MPA with ethanol. Ethanol was chosen as a model compound for the labile oxygenated hydrocarbons also produced by the caustic hydrolysis of chemical warfare agents because it has been well characterized by Schanzenbacher et al. (2002), Rice and Croiset (2001), and Marinov (1999). In the temperature range from 470 to 530 °C, MPA conversions at the residence times of interest (3-10 s) range from 10 to 50%, but ethanol conversions range from 90 to 100%. Over these temperatures, the rapid and complete oxidation of ethanol is expected to cause an acceleration of the rate of MPA oxidation, which will be easy to measure due to the low conversion of pure MPA in this region. Most importantly, both compounds have been well-characterized by experimental and modeling studies in our laboratory, which enables a quantitative analysis of the co-oxidation effect.

4.1 EXPERIMENTAL RESULTS

Experimental data were taken at two temperatures ($T = 473$ and 528 °C) for organic feedstreams with initial concentrations ranging from $[MPA]_0 = 0.1$ to 1.0 mM and $[EtOH]_0 = 0$ to 2.4 mM. The concentrations of organics in the feedstream are low enough to ensure that heat released by the reactants will not cause an increase in the temperature of the reactor contents. The inlet and outlet temperature measurements confirmed that the reactor operates isothermally. Oxygen was sufficient for the stoichiometric oxidation of both MPA and ethanol to CO_2 , H_2O , and H_3PO_4 . The fuel equivalence ratio, Φ , is defined as

$$\Phi \equiv \frac{S_{MPA} [MPA]_0 + S_{EtOH} [EtOH]_0}{[O_2]_0} \quad (\text{Eqn. 4-1})$$

where S is the stoichiometric ratio for each model compound ($S_{MPA} = 2$, $S_{EtOH} = 3$). For all co-oxidation experiments conducted Φ ranged from 0.8 to 1.3.

The oxygen requirement of the additional ethanol forces the initial oxygen concentration to be higher for an MPA-ethanol co-oxidation experiment than for an MPA oxidation experiment with the same $[\text{MPA}]_0$. In order to separate the effect of the increase in oxygen concentration from the co-oxidation effect of adding ethanol to the organic feedstream, three experiments were conducted at $T = 473\text{ }^\circ\text{C}$, $P = 246\text{ bar}$, $\tau = 9\text{ s}$, and $[\text{MPA}]_0 = 0.1\text{ mM}$. The first experiment measured the conversion of MPA ($X_{\text{MPA}} = 14 \pm 2\%$) for a feed with no ethanol and $[\text{O}_2]_0 = 0.2\text{ mM}$ ($\Phi = 1$). The second experiment was conducted with $[\text{EtOH}]_0 = 1.0\text{ mM}$ and $[\text{O}_2]_0 = 3.2\text{ mM}$ ($\Phi = 1$), under which conditions the conversion increased to $X_{\text{MPA}} = 41 \pm 2\%$. Finally, at these $[\text{MPA}]_0$ and $[\text{O}_2]_0$ conditions, a third experiment was conducted with no ethanol ($\Phi = 0.07$) which yielded a $X_{\text{MPA}} = 23 \pm 2\%$. The large decrease from the second to third experiment confirms that the presence of ethanol accounts for the bulk of the increase in MPA conversion. After confirming that ethanol does co-oxidize MPA, the effect of initial concentration of both ethanol and MPA on MPA conversion was explored. For $T = 473$ and 530°C , $P = 246\text{ bar}$, and $\Phi = 1$, $[\text{EtOH}]_0$ was varied while $[\text{MPA}]_0$ was held constant at 1 mM , and $[\text{MPA}]_0$ was varied while $[\text{EtOH}]_0$ was held constant at 1 mM . The data are summarized in Table 4-1 below. The measured phosphorus mass balance closed within experimental error of $100 \pm 5\%$ for all but three runs, showing that the observed phosphoric acid in the effluent accounts for essentially all of the reacted MPA. At $T = 473\text{ }^\circ\text{C}$, ethanol conversion was at least 95% for all experiments, and at $T = 530\text{ }^\circ\text{C}$, ethanol conversion was greater than 99.9% .

Table 4-1: Summary of experimental data

T (°C)	P (bar)	$[MPA]_0$ (mM)	$[EtOH]_0$ (mM)	Φ	τ (s)	X_{MPA} (%)	P_{bal} (%)
474±3	247±1	0.97±0.02	1.02±0.07	1.3±0.1	9.0±0.5	29±2	101±2
473±3	244±1	0.95±0.01	1.00±0.05	1.3±0.1	5.9±0.3	19±2	102±2
474±3	246±1	0.96±0.02	0.10±0.00	1.1±0.0	8.9±0.5	14±2	101±2
473±3	246±1	0.95±0.02	0.10±0.00	1.1±0.0	5.9±0.4	8±3	103±3
473±3	249±1	0.10±0.00	1.02±0.03	hydrolysis	9.2±0.5	5±3	99±3
474±3	243±1	0.09±0.00	0.95±0.02	1.1±0.0	8.8±0.5	41±2	109±2
474±3	244±1	0.09±0.00	0.00±0.00	0.07±0.00	8.8±0.5	23±2	103±2
473±3	244±1	0.32±0.01	0.95±0.02	1.1±0.0	8.8±0.5	37±2	97±2
474±3	244±1	0.90±0.01	0.34±0.01	1.1±0.0	8.8±0.5	18±2	101±2
474±3	242±1	0.92±0.01	2.39±0.17	0.8±0.0	8.8±0.5	39±2	102±2
474±3	245±1	0.93±0.02	2.43±0.17	0.8±0.0	5.9±0.4	36±2	103±3
472±3	244±1	0.92±0.02	0.00±0.00	1.1±0.0	4.9±0.3	9±3	102±3
473±3	247±1	0.94±0.01	0.00±0.00	1.0±0.0	6.0±0.4	11±2	102±2
473±3	246±1	0.93±0.01	0.00±0.00	1.1±0.0	8.9±0.5	14±2	102±2
527±3	242±1	1.12±0.02	0.95±0.05	1.0±0.0	8.9±0.5	73±2	104±4
527±3	243±1	1.13±0.01	0.96±0.05	1.0±0.0	6.0±0.4	60±2	107±4
525±3	244±1	1.14±0.01	0.97±0.05	1.0±0.0	4.0±0.2	51±2	103±3
528±3	244±1	1.08±0.02	0.09±0.01	1.1±0.0	9.0±0.5	69±2	115±4
529±3	242±1	1.06±0.01	0.09±0.01	1.1±0.0	6.0±0.3	52±3	112±4
528±3	247±1	1.09±0.01	0.10±0.01	1.1±0.0	4.1±0.2	39±3	109±4
530±3	244±1	0.97±0.01	0.38±0.02	1.0±0.0	9.2±0.5	71±2	100±3
530±3	244±1	0.99±0.01	0.39±0.02	1.1±0.0	6.1±0.4	58±2	99±3
529±3	242±1	0.09±0.00	1.03±0.02	1.0±0.0	8.9±0.5	96±0	106±4
528±3	242±1	0.09±0.00	1.04±0.02	1.0±0.0	6.0±0.4	86±1	108±4
528±3	242±1	0.28±0.00	1.05±0.02	1.1±0.0	9.0±0.5	82±1	106±3
526±3	243±1	0.29±0.01	1.06±0.02	1.1±0.0	6.0±0.4	71±2	104±3
527±3 ^a	245±1	0.98±0.02	0.00±0.00	1.0±0.0	4.0±0.2	33±2	102±2
527±3 ^a	246±1	0.99±0.05	0.00±0.00	1.0±0.1	3.0±0.2	27±4	102±4
527±3 ^a	244±1	1.00±0.04	0.00±0.00	1.0±0.1	3.9±0.2	38±3	101±4
527±3 ^a	246±1	1.00±0.03	0.00±0.00	1.0±0.1	4.0±0.2	37±2	101±2
527±3 ^a	245±1	1.00±0.03	0.00±0.00	1.0±0.1	4.0±0.2	37±2	101±3
527±3 ^a	245±1	0.98±0.02	0.00±0.00	1.0±0.0	4.0±0.2	33±2	102±2
527±3 ^a	245±1	1.00±0.03	0.00±0.00	1.1±0.1	4.7±0.3	40±2	101±3
527±3 ^a	243±1	0.99±0.03	0.00±0.00	1.0±0.1	6.0±0.4	48±2	102±3
527±3 ^a	245±2	1.00±0.02	0.00±0.00	1.1±0.0	6.1±0.4	48±2	101±2
527±3 ^a	246±1	1.00±0.03	0.00±0.00	1.0±0.1	6.1±0.4	51±2	102±3
527±3 ^a	248±1	1.00±0.03	0.00±0.00	1.0±0.1	6.2±0.4	50±2	101±3

^a Data from Sullivan and Tester (2004c)

The plot in Figure 4-1 of MPA conversion versus τ for varying $[EtOH]_0$ with $T = 473$ °C, $P = 246$ bar, $[MPA]_0 = 1$ mM, and $\Phi = 1$ reveals two notable features. The first is that low

concentrations of ethanol have no measurable effect on MPA conversion. For $[\text{EtOH}]_0 = 0.1$ and 0.3 mM, the MPA conversion is still within the 95% confidence interval of the data taken with no ethanol present. The second feature is that higher concentrations of ethanol cause a dramatic increase in MPA conversion, which is roughly doubled and tripled at $[\text{EtOH}]_0 = 1.0$ and 2.4 mM, respectively. Ethanol can increase the rate of MPA oxidation at $T = 473$ °C, but there appears to be a threshold below which there is no appreciable co-oxidative effect. At $T = 528$ °C, the effect of ethanol concentration is not as pronounced. Figure 4-2 shows that at $T = 528$ °C and $P = 245$ bar, MPA conversions with $[\text{EtOH}]_0 = 0.1$ mM are equal to MPA conversions with no ethanol present. A clear increase of 10-15% in MPA conversion can be seen for $[\text{EtOH}]_0 = 0.4$ and 1.0 mM. But for all concentrations of initial ethanol, at a residence time of 9 s the MPA conversion data converge to the same value within experimental uncertainty.

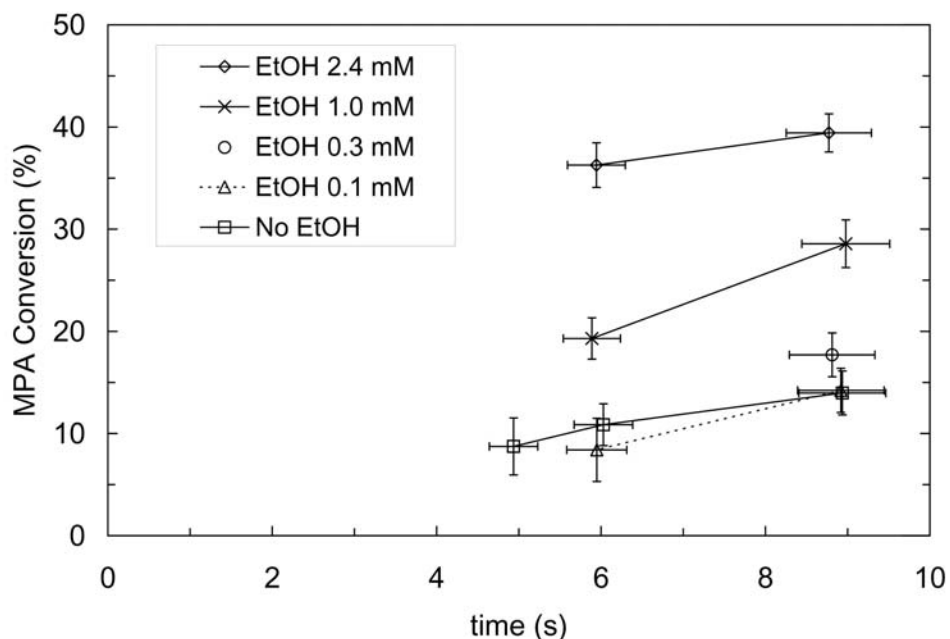


Figure 4-1: Conversion of MPA as a function of residence time for five different values of $[\text{EtOH}]_0$. $T = 473 \pm 3$ °C, $P = 245 \pm 3$ bar, $[\text{MPA}]_0 = 0.95 \pm 0.05$ mM, $\Phi = 1.05 \pm 0.25$.

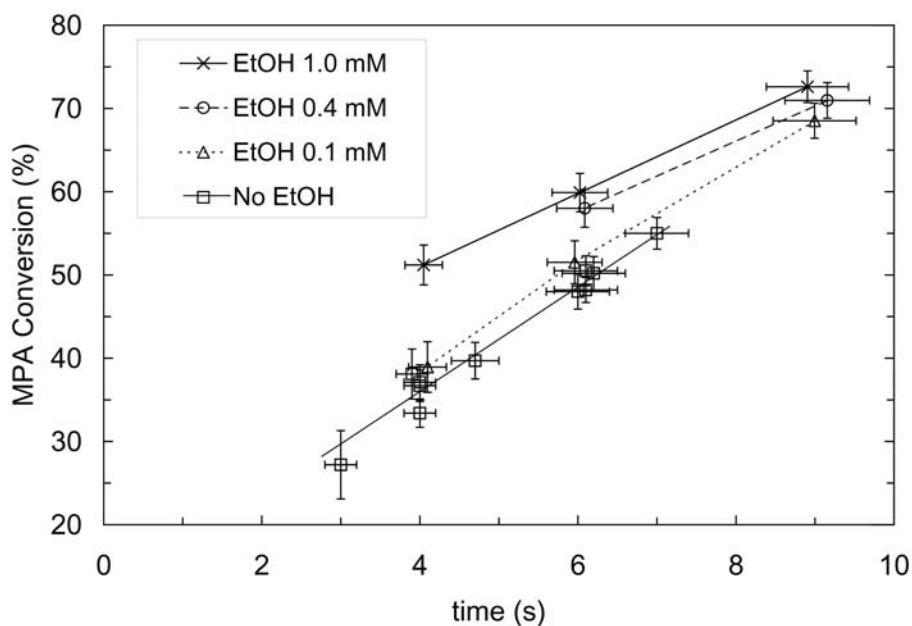


Figure 4-2: Conversion of MPA as a function of residence time for four different values of $[\text{EtOH}]_0$. $T = 528 \pm 3$ °C, $P = 245 \pm 3$ bar, $[\text{MPA}]_0 = 1.0 \pm 0.1$ mM, $\Phi = 1.0 \pm 0.1$.

A much greater increase in MPA conversion is observed when the initial concentration of MPA is decreased while the initial concentration of ethanol is held constant at 1 mM. MPA conversion versus residence time for three different values of $[\text{MPA}]_0$ with $T = 528$ °C and $P = 246$ bar is plotted in Figure 4-3, and shows a large increase in conversion as $[\text{MPA}]_0$ decreases. The MPA must be consuming the free radical pool generated by ethanol to a significant degree, so that for higher values of $[\text{MPA}]_0$ a lower concentration of free radicals is formed and therefore MPA conversion decreases. In Figure 4-4, a plot of MPA conversion versus $[\text{MPA}]_0$ for $T = 473$ °C, $P = 246$ bar, $\tau = 9$ s, $[\text{EtOH}]_0 = 1$ mM, and $\Phi = 1$ shows that increasing the concentration of MPA decreases the co-oxidation enhancement at a lower temperature as well.

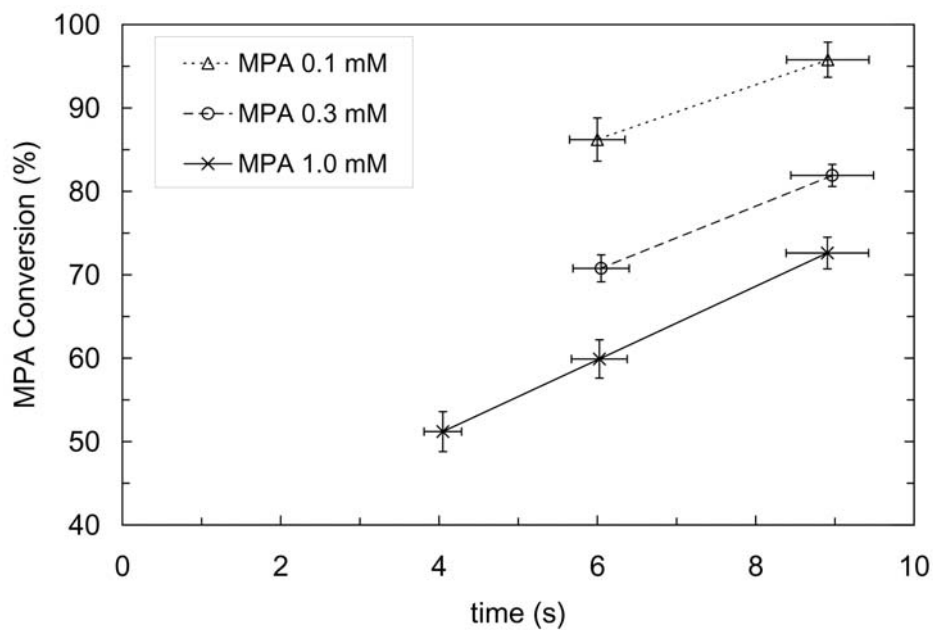


Figure 4-3: Conversion of MPA as a function of residence time for three different values of $[\text{MPA}]_0$. $T = 528 \pm 3$ °C, $P = 245 \pm 3$ bar, $[\text{EtOH}]_0 = 1.00 \pm 0.06$ mM, $\Phi = 1.0 \pm 0.1$.

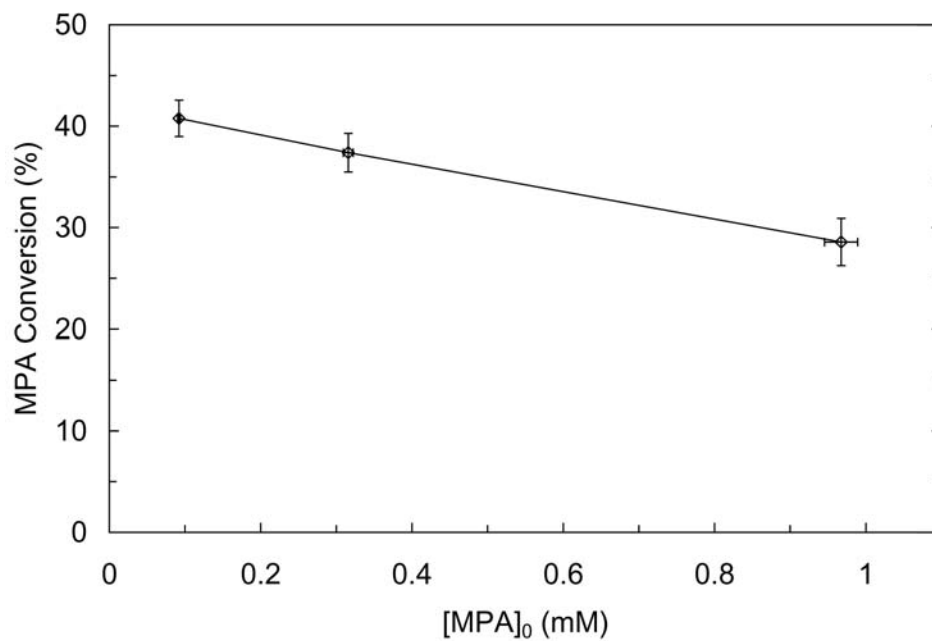


Figure 4-4: Conversion of MPA as a function of $[\text{MPA}]_0$. $T = 473 \pm 3$ °C, $P = 245 \pm 3$ bar, $[\text{EtOH}]_0 = 0.97 \pm 0.04$ mM, $\Phi = 1.2 \pm 0.1$, $\tau = 9.0 \pm 0.5$ s.

4.2 CONCLUSIONS

An experimental study of MPA-ethanol co-oxidation in supercritical water was completed that explored the effect of initial concentrations of MPA and ethanol on conversion at two temperatures and constant pressure and fuel equivalence ratio over a range of residence times. MPA conversion was found to increase with decreasing $[MPA]_0$ and increasing $[EtOH]_0$. At $T = 528$ °C, MPA conversions measured at $[EtOH]_0 = 0.1$ mM were identical to those measured without ethanol present, and at $T = 473$ °C, concentrations of ethanol at $[EtOH]_0 = 0.3$ mM and 0.1 mM were found to have no measurable effect on MPA conversion. These findings indicate that co-oxidation enhancement is only significant when the molar concentration of labile compound is at least on the same order of magnitude as the concentration of refractory compound. At both temperatures the co-oxidation effect is more pronounced at shorter residence times. The effect of $[MPA]_0$ on MPA conversion at both $T = 473$ and 528 °C indicates that MPA consumes a significant portion of the free radical pool generated by ethanol oxidation in supercritical water.

4.3 REFERENCES

- Marinov, N. M. (1999). "A detailed chemical kinetic model for high temperature ethanol oxidation." *Int. J. Chem. Kinet.* **31**(3): 183-220.
- Rice, S. and E. Croiset (2001). "Oxidation of simple alcohols in supercritical water III. Formation of intermediates from ethanol." *Ind. Eng. Chem. Res.* **40**(1): 86-93.
- Schanzenbacher, J., J. D. Taylor and J. W. Tester (2002). "Ethanol oxidation and hydrolysis rates in supercritical water." *J. Supercrit. Fluid* **22**(2): 139-147.
- Sullivan, P. A. and J. W. Tester (2004c). "Methylphosphonic acid oxidation kinetics in supercritical water." *AIChE Journal* **50**(3): 673-683.

5 Elementary Reaction Rate Model for MPA-Ethanol Co-oxidation

In this chapter we will provide mechanistic insight into the experimental co-oxidation effect detailed in Chapter 4 and design an experiment to validate these modeling conclusions. In practice, the MPA-ethanol system simulates the mixed organic feeds encountered in the SCWO of organophosphorus nerve agents. From a modeling perspective, the MPA-ethanol system offers two well-characterized elementary reaction models for both MPA (Sullivan et al. 2004) and ethanol (Rice and Croiset 2001) that can be combined to gain an understanding of the co-oxidation effect on the reaction level.

5.1 BACKGROUND AND MOTIVATION

To gain a mechanistic insight into the dominant pathways for SCWO kinetics, elementary reaction rate models have been developed by adapting high-temperature ($T > 1200$ °C), low-pressure ($P = 0.001$ to 1 bar) combustion mechanisms to lower-temperature, high-pressure SCW conditions. Combustion models are primarily modified by extrapolating pressure-dependent rate constants to SCW conditions and by including collision-stabilized intermediates like hydroperoxy (HO_2^*) species that are not present in significant concentrations at combustion conditions. For SCW conditions, radical concentrations cannot be directly measured, in contrast to normal combustion conditions, where direct measurement of radicals is possible. Elementary reaction rate models can be used to estimate the concentrations of key radical species and infer the dominant pathways for SCWO.

Several assumptions must be made to develop and solve the SCWO models which generally contain hundreds of reactions and dozens of species. Reaction rates at combustion conditions are assumed to be similar to those at SCW conditions. Water is treated only as a

reactant and third-body collider; any solvation effects are ignored. Ideal gas conditions are assumed as well because fugacity coefficients in SCW approach one and the compressibility factor (Z) is approximately 0.9 (Haar et al. 1984). SCWO models have been developed for model compounds such as hydrogen, carbon monoxide, ammonia, methane, methanol, ethanol, and benzene. Though the models had varying degrees of success in predicting measured concentration profiles, they have been useful in identifying and validating important reaction pathways and intermediate species.

One of the biggest challenges to using SCWO models for predicting the oxidation mechanisms of more complex, mixed waste streams is the co-oxidation effect. This is the process by which the oxidation of a labile, reactive species accelerates the rate of oxidation of a refractory, stable species. The phenomenon has been observed experimentally dating back to experiments in the 1980s on the SCWO of sewage (Hong et al. 1987), but mechanistic understanding has been elusive. Many experimental studies of co-oxidation have focused on refractory model compounds such as polychlorinated biphenyls (PCBs) which are so complex that they have yet to be adequately modeled at the elementary reaction level (Anitescu et al. 2005). Savage and coworkers modeled the co-oxidation of methane and methanol and concluded that the co-oxidation effect was due in large part to the increase in concentration of the HO_2^\bullet (Savage et al. 2000). The most convincing experimental evidence of this conclusion would be found in the channel yields of the refractory species (Ploeger et al. 2006a). However, because the methanol mechanism is completely contained within the methane mechanism, it is difficult to develop conclusive experimental tests using the methane-methanol system.

5.2 MODEL DEVELOPMENT

The MPA-ethanol mechanism was constructed from an MPA submechanism developed in our group by Sullivan (2003) and an ethanol submechanism developed at Sandia by Rice and Croiset (2001). The organophosphorous and C1 reaction rate constants and thermochemical data were taken from the Sullivan mechanism and were augmented with C2 reaction rate parameters from the ethanol SCWO submechanism. Rice and Croiset added CH_3CO_3 chemistry from Kaiser (1986) to the Marinov (1999) ethanol oxidation mechanism. The Rice and Croiset mechanism has been validated with experimental SCWO data.

Two changes were made to the co-oxidation mechanism. The $\text{H}_2\text{O}_2 + \text{OH}^\bullet = \text{H}_2\text{O} + \text{HO}_2^\bullet$ reaction rate constant from the Baulch et al. (1994) literature review replaced the Hippler et al. 1995 value (1995) used by Sullivan. This modification had very little effect on the predicted MPA conversions for pure MPA oxidation and resulted in a more accurate prediction for MPA conversions under co-oxidation conditions. This modification will be discussed in greater detail later in the paper. Second, the HOCO^\bullet radical was treated explicitly using reaction rate constants from the Senosiain et al. *ab initio* study (2003) and thermochemical parameters from Janoschek et al. (2002). Although the updated parameters had a negligible effect on the predicted concentration profiles for MPA, CO, CO_2 , CH_4 , OH^\bullet , and HO_2^\bullet , we considered it preferable to treat the HOCO^\bullet adduct explicitly. The two changes are summarized in Table 5-1.

Table 5-1: Rate parameter changes made to co-oxidation mechanism. Units are cm, mol, s, and cal.

Rxn #	Reaction	A	n	Ea	Ref
8	$\text{H}_2\text{O}_2 + \text{OH} = \text{H}_2\text{O} + \text{HO}_2$	7.83E+12	0	1331	a
302	$\text{CO} + \text{OH} (+\text{M}) = \text{HOCO} (+\text{M})$	1.20E+07	1.8	-236	b
	Low pressure limit:	7.24E+25	-3.85	1550	
	TROE centering: 0.6 1E-15 1E+15				
303	$\text{OH} + \text{CO} (+\text{M}) = \text{H} + \text{CO}_2 (+\text{M})$	9.54E+04	2	-1484	b
	High pressure limit:	3.80E-138	51.93	-75965	
	TROE centering: 0.6 1E-15 1E+15				

a) Baulch et al. (1994), b) Senosiain et al. (2003).

5.3 COMPARISON OF MODELING PREDICTIONS WITH EXPERIMENTAL DATA

The combined MPA-ethanol mechanism was first tested to determine if the mechanism predicts an increase in MPA conversion in a mixed MPA-ethanol feed. We compared the predicted trends in MPA conversion as a function of initial MPA and ethanol concentration to the experimental data taken on our laboratory-scale plug flow reactor (Ploeger et al. 2006b) in Figure 5-1. The predicted increase in MPA conversion as ethanol concentration increases is greater than what is observed experimentally, but the overall trend is correct.

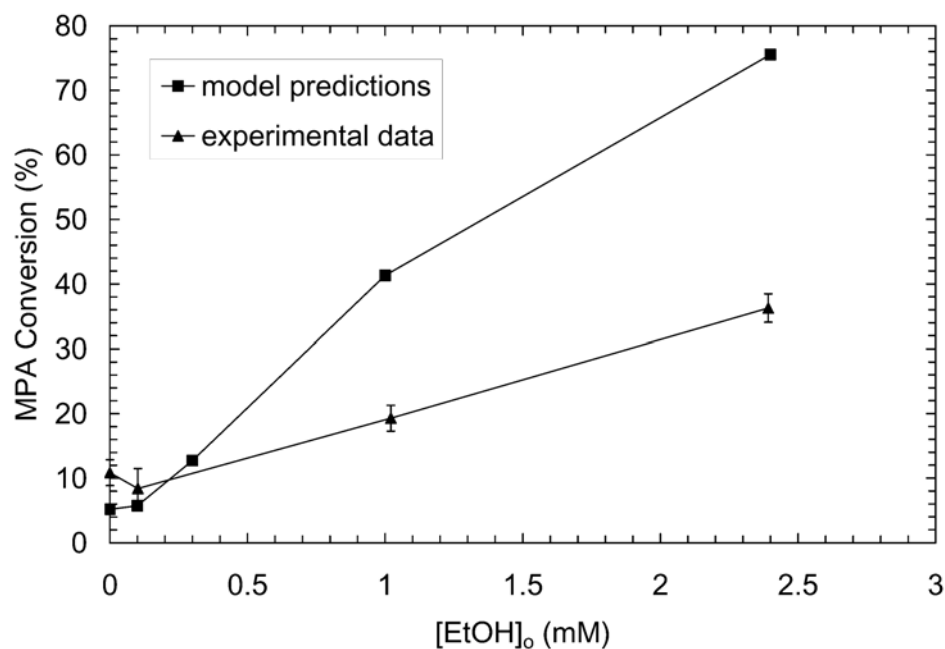


Figure 5-1: MPA conversion as a function of initial ethanol concentration at $T = 473$ °C, $P = 246$ bar, $[MPA]_0 = 1$ mM, $\Phi = 1$, $\tau = 6$ s.

Also consistent with experimental observation is the prediction that the addition of 0.1 mM ethanol to 1.0 mM MPA causes only a negligible increase in MPA conversion at $T = 473$ °C, $P = 246$ bar, and $\Phi = 1$, which can be seen in Figure 5-2. Contrary to the perception that co-oxidation functions like a homogenous catalyst, small additions of an ethanol co-oxidant do not generate significantly more free radicals than MPA. Analysis of the molar fluxes through free radical reactions indicates that for the first few seconds of reaction, ethanol dominates OH^\bullet consumption, leaving behind very little to react with MPA. It is only after the ethanol is mostly consumed that the additional OH^\bullet radicals are available to consume MPA. For short time scales ($t < 5$ s), MPA conversion for the pure oxidation case is predicted to be $\sim 1\%$ greater than MPA conversion for the dilute ethanol co-oxidation case, but this small difference is impossible to resolve given our standard experimental error of $\pm 2\text{-}3\%$ for measured conversion.

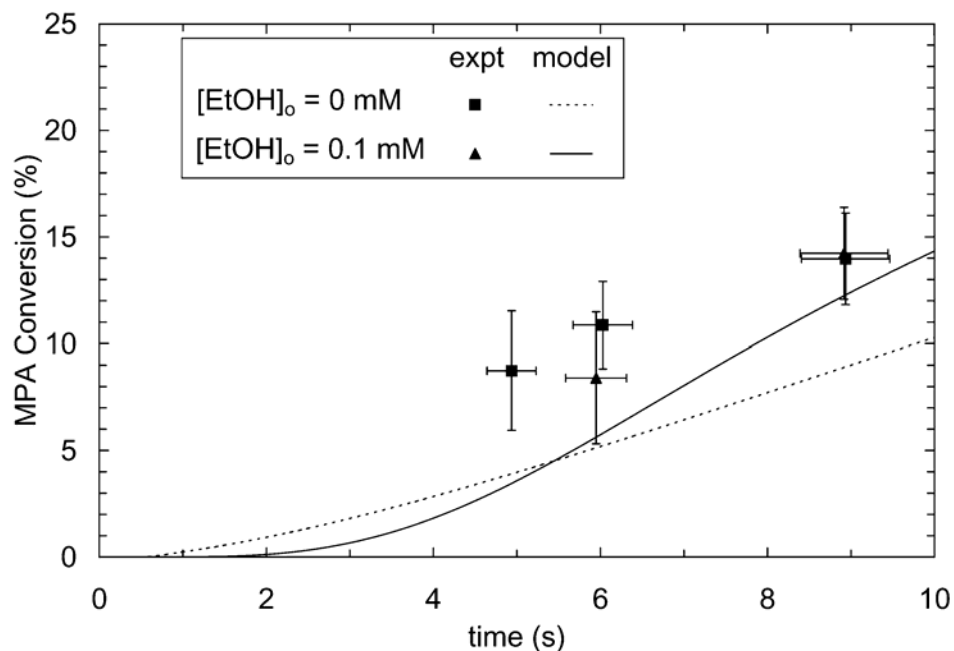


Figure 5-2: MPA conversion as a function of time for $T = 473$ °C, $P = 246$ bar, $[MPA]_0 = 1$ mM, and $\Phi = 1$.

The model fails to predict the observed increase in MPA conversion with decreasing initial MPA concentration, as shown in Figure 5-3. The model predicts a slight decrease (6%) in conversion as $[MPA]_0$ is lowered from 1.0 mM to 0.1 mM for $T = 473$ °C, $P = 246$ bar, $[EtOH]_0 = 1$ mM, $\Phi = 1$ and $\tau = 9$ s. This is because the MPA SCWO model predicts that MPA oxidation is greater than first order in $[MPA]$, where an increase in $[MPA]_0$ would cause an increase in MPA conversion. Experimentally, MPA oxidation has been observed to be first order in $[MPA]$, where we would expect conversion to be independent of $[MPA]_0$ (Sullivan and Tester 2004). It is presumed that in actuality a lower $[MPA]_0$ in the mixed feed consumes less of the overall free radical pool, resulting in higher concentrations of OH^\bullet and HO_2^\bullet and a more rapid rate of MPA oxidation compared to an organic feed with an equal $[EtOH]_0$ and a higher $[MPA]_0$. In the model, the lower $[MPA]_0$ mixed feed generates a lower $[HO_2^\bullet]$ which leads to a lower MPA

conversion. Despite the shortcomings with respect to treating $[\text{MPA}]_0$, the model does agree with the trends observed for varying $[\text{EtOH}]_0$ with a constant $[\text{MPA}]_0$.

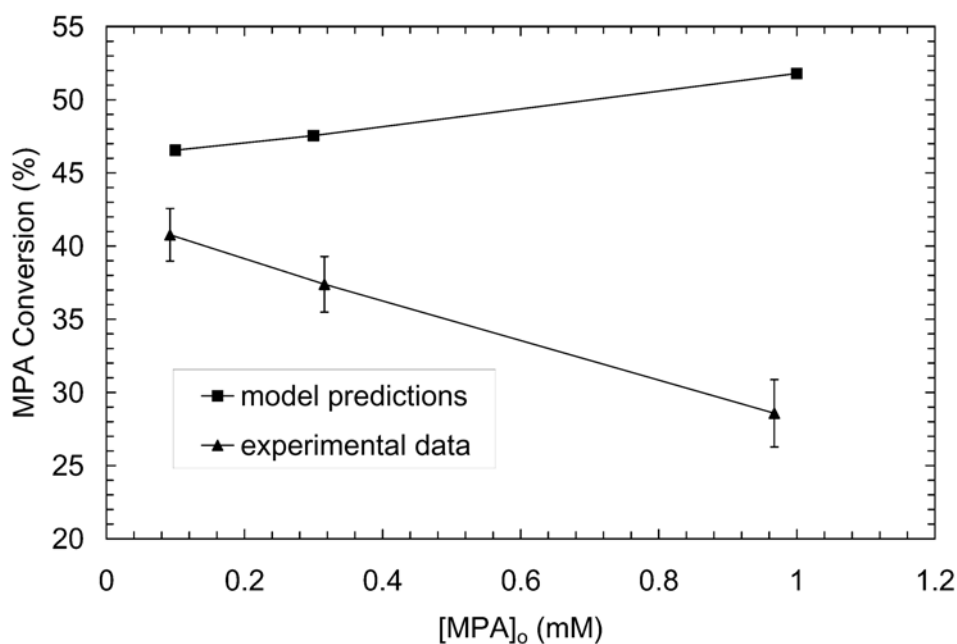
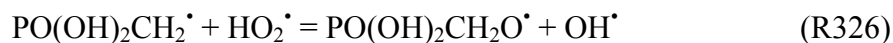


Figure 5-3: MPA conversion as a function of initial MPA concentration at $T = 473\text{ }^{\circ}\text{C}$, $P = 246\text{ bar}$, $[\text{EtOH}]_0 = 1\text{ mM}$, $\Phi = 1$, $\tau = 9\text{ s}$.

The effect of $[\text{EtOH}]_0$ on the free radical pool as predicted by the co-oxidation model is shown in Figure 5-4 and Figure 5-5. The increases in $[\text{HO}_2^{\bullet}]$ are much greater than the increases in $[\text{OH}^{\bullet}]$. The shape of the $[\text{OH}^{\bullet}]$ profile is different for pure MPA oxidation because most of the OH^{\bullet} is generated by the reaction



which rapidly achieves a steady state concentration of OH^{\bullet} . The increase in peak $[\text{OH}^{\bullet}]$ from no ethanol to 2.4 mM $[\text{EtOH}]_0$ is only about a factor of 2, but the increase in peak $[\text{HO}_2^{\bullet}]$ is about a factor of 16. Savage (2000) also attributed increased methane conversion when co-oxidized with methanol to the increase in predicted HO_2^{\bullet} concentration using his C1 SCWO mechanism.

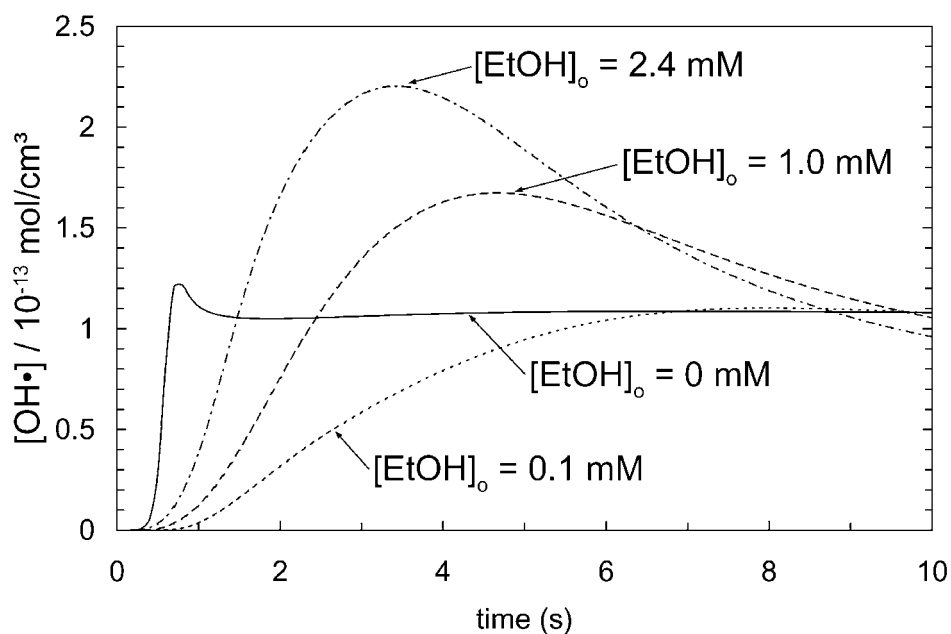


Figure 5-4: Predicted $\text{OH}\cdot$ concentration profiles as a function of time for a varying initial ethanol concentration at $T = 473 \text{ }^\circ\text{C}$, $P = 246 \text{ bar}$, $[\text{MPA}]_0 = 1 \text{ mM}$, $\Phi = 1$.

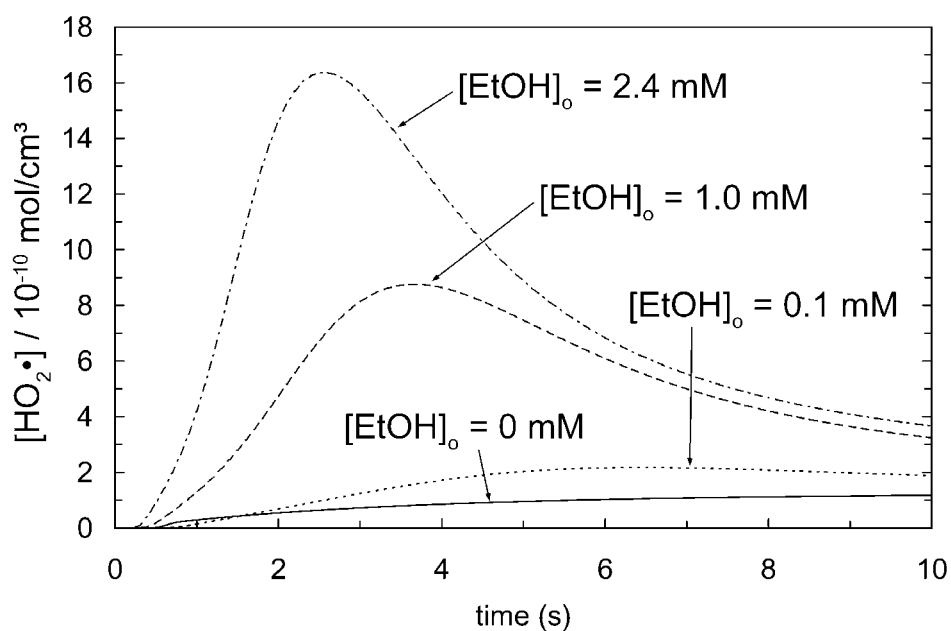


Figure 5-5: Predicted $\text{HO}_2\cdot$ concentration profiles as a function of time for a varying initial ethanol concentration at $T = 473 \text{ }^\circ\text{C}$, $P = 246 \text{ bar}$, $[\text{MPA}]_0 = 1 \text{ mM}$, $\Phi = 1$.

5.4 THE REDUCED CO-OXIDATION MECHANISM

To understand how co-oxidation effects the concentration of HO_2^\bullet , the radical-producing reactions in the ethanol SCWO submechanism can be simplified as follows:



where RH_2 and R represent stable species such as ethanol ($\text{CH}_3\text{CH}_2\text{OH}$) and acetaldehyde (CH_3CHO) and RH^\bullet represents free radical species such as $\text{CH}_3\text{CHOH}^\bullet$. Although free radical intermediates can also dissociate via,



note that the hydrogen atom rapidly reacts with O_2 to form HO_2^\bullet so rapidly that it can be treated as equivalent to reaction RC above.

Although the six-reaction mechanism obviously lacks many key steps such as the breaking of the C-C bond or any peroxy reactions, it serves as a useful tool to understand the generation of the free radical pool. The oxidation of a hydrocarbon species first consumes a radical in reaction RA (OH^\bullet) or RB (HO_2^\bullet), then forms HO_2^\bullet in reaction RC. HO_2^\bullet radicals then undergo a self reaction to form H_2O_2 via reaction RD, which decomposes into 2 OH^\bullet . When the cycle is initiated by reaction RA it is chain-propagating, and when initiated by reaction RB it is chain-branching. Typically reaction RA dominates over reaction RB, but for alcohols and aldehydes the flux through reaction RB is significant and results in the production of a large free

radical pool. As the OH^\bullet concentration increases, it begins to attack the H_2O_2 via reaction RF, which is a chain terminating reaction since most of the H_2O_2 is produced from 2HO_2^\bullet . As a consequence, it is the relative rates of reactions RE and RF that determine the overall size of the free radical pool and therefore the magnitude of the co-oxidation effect.

5.5 DESIGN OF AN EXPERIMENT TO VALIDATE THE MODEL

While the understanding reached above is valuable, given the uncertainties in rate parameter values, it is inappropriate to focus modeling validation efforts on matching experimental conversion data. Even with the uncertainty in only a single rate included, large uncertainties in predicted MPA conversion can result. In general, the MPA conversion predictions are highly sensitive to uncertainties in the rates of the hydrogen peroxide consumption reactions



Replacing the Hippler rate (Hippler et al. 1995) for reaction RF with the parameters recommended by Baulch et al. in the 1994 review (Baulch et al. 1994) mitigates the overprediction of MPA conversion substantially. The Baulch review is recommended for a temperature range (23-723 °C) that spans our temperature of interest, but the Hippler study was conducted at a temperature range (657-1407 °C) much greater than used in our study. The Baulch rate is faster than the Hippler rate by a factor of 2.2 at $T = 473$ °C, which reduces the size of the free radical pool. Reaction RF is the primary chain terminating route for MPA-ethanol co-oxidation, but does not act as a chain terminator in pure MPA oxidation. The rate of MPA oxidation is much less sensitive to reaction RF for pure oxidation than for co-oxidation with ethanol because the concentrations of hydrogen peroxide are much lower in the pure MPA

oxidation environment, so changing the rate used by Sullivan would not have a significant impact on the results of that study. Figure 5-6 illustrates that the uncertainty in the rate of reaction RF can translate to an uncertainty of $\pm 16\%$ in predicted MPA conversion.

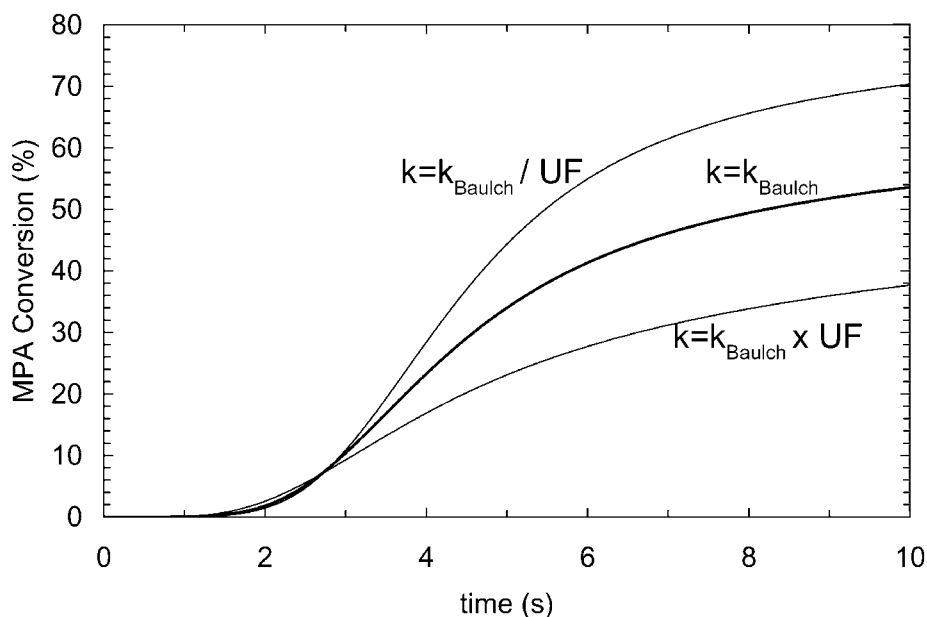


Figure 5-6: Effect of uncertainty for the rate constant for the reaction $\text{H}_2\text{O}_2 + \text{OH} = \text{H}_2\text{O} + \text{HO}_2$. The center line represents the MPA conversion profile for the Baulch 1994 rate at $T = 473 \text{ }^\circ\text{C}$, $P = 246 \text{ bar}$, $[\text{MPA}]_0 = [\text{EtOH}]_0 = 1 \text{ mM}$, $\Phi = 1$. Uncertainty factor (UF) = 3.1.

With these limitations, it is typically more reliable to use product distributions (Ploeger et al. 2006a) to validate model predictions and derive mechanistic insights. In order to identify any possible experiments to validate the co-oxidation mechanism, we compared the major reaction fluxes for MPA at $T = 473 \text{ }^\circ\text{C}$, $P = 246 \text{ bar}$, and $\Phi = 1$ for four different initial ethanol concentrations: 0, 0.1, 1.0, and 2.4 mM in Table 5-2. Major reaction pathways are also illustrated in Figure 5-7.

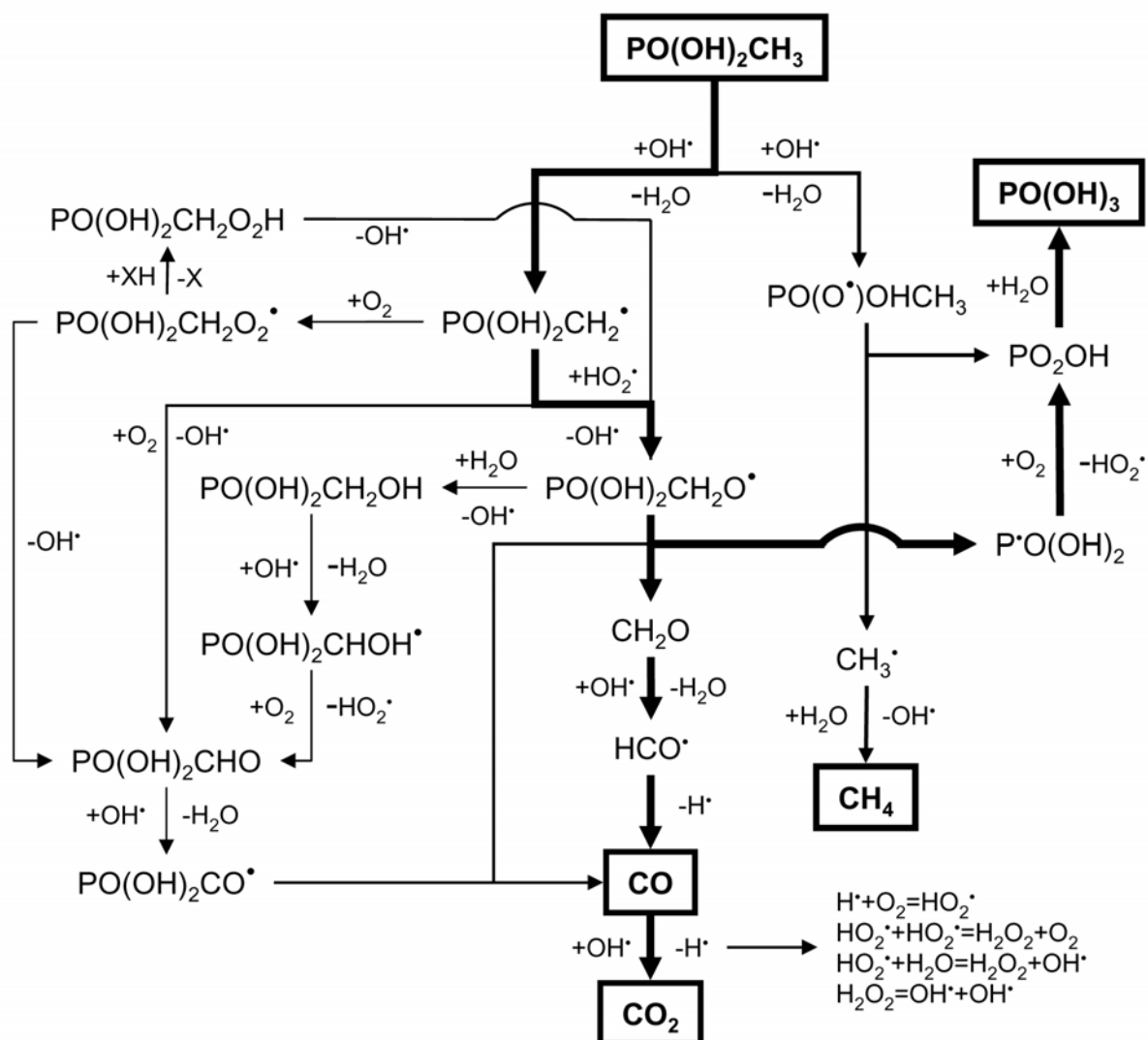


Figure 5-7: Major reaction pathways for MPA in the co-oxidation model. Bold arrows indicate dominant pathways and boxes indicate stable products and intermediates CO, CO₂, CH₄, and H₃PO₄.

Table 5-2: Dominant reaction fluxes for co-oxidation of MPA and ethanol

Rxn #	Reaction	[C ₂ H ₅ OH] ₀ (mM)			
		0	0.1	1.0	2.4
309	PO(OH) ₂ CH ₃ + OH [•] = PO(OH) ₂ CH ₂ [•] + H ₂ O	7.9	13.8	73.9	119.0
310	PO(OH) ₂ CH ₃ + OH [•] = PO(O [•])OHCH ₃ + H ₂ O	1.8	1.3	1.5	1.0
389	PO(O [•])OHCH ₃ = PO ₂ OH + CH ₃ [•]	1.8	1.3	1.5	1.0
-321	PO(OH) ₂ CH ₂ [•] + H ₂ O ₂ = PO(OH) ₂ CH ₃ [•] + HO ₂ [•]	0	0.7	17.9	35.7
326	PO(OH) ₂ CH ₂ [•] + HO ₂ [•] = P [•] O(OH) ₂ CH ₂ O + [•] OH	6.5	10.8	38.9	43.5
323	PO(OH) ₂ CH ₂ [•] + O ₂ = PO(OH) ₂ CH ₂ OO [•]	1.3	2.2	16.7	39.3
366	PO(OH) ₂ CH ₂ OO [•] + H ₂ O ₂ = PO(OH) ₂ CH ₂ OOH + HO ₂ [•]	0.1	0.5	7.7	22.4
365	PO(OH) ₂ CH ₂ OO [•] + HO ₂ [•] = PO(OH) ₂ CH ₂ OOH + O ₂	0.7	1.2	6.7	12.1
372	PO(OH) ₂ CH ₂ OO [•] + CH ₂ O = PO(OH) ₂ CH ₂ OOH + HCO [•]	0.1	0.2	1.7	4.0
384	PO(OH) ₂ CH ₂ OOH = PO(OH) ₂ CH ₂ O [•] + OH [•]	1.1	2.0	16.2	38.7
328	PO(OH) ₂ CH ₂ O [•] = P [•] O(OH) ₂ + CH ₂ O	7.2	11.9	51.6	76.9
-336	PO(OH) ₂ CH ₂ O [•] + H ₂ O = PO(OH) ₂ CH ₂ OH + OH [•]	0.7	1.2	4.3	6.1
341	PO(OH) ₂ CH ₂ OH + OH [•] = PO(OH) ₂ CHOH [•] + H ₂ O	0.3	0.4	2.4	3.8
340	PO(OH) ₂ CH ₂ OH + HO ₂ [•] = PO(OH) ₂ CHOH [•] + H ₂ O ₂	0	0.1	0.9	2.0
347/ 348	P [•] O(OH) ₂ CHOH + O ₂ = PO(OH) ₂ CHO + HO ₂ [•]	0.3	0.5	3.4	5.7
197	PO(OH) ₂ CHO + OH [•] = PO(OH) ₂ CO [•] + H ₂ O	0.3	0.4	2.1	3.3
196	PO(OH) ₂ CHO + HO ₂ [•] = PO(OH) ₂ CO [•] + H ₂ O ₂	0	0.1	1.2	2.5
361	PO(OH) ₂ CO [•] = P [•] O(OH) ₂ + CO	0.3	0.5	3.3	5.9
395	P [•] O(OH) ₂ + O ₂ = PO ₂ OH + HO ₂ [•]	7.6	12.4	54.9	82.8
-390	PO ₂ OH + H ₂ O = PO(OH) ₃	9.4	13.7	56.4	83.8

Average predicted molar flux through major pathways from $\tau = 0-10$ s (10^{-6} mol/L/s) for a set initial concentration of MPA mixed with four initial concentrations of ethanol. $T = 473$ °C, $P = 246$ bar, $[MPA]_0 = 1$ mM, $\Phi = 1$.

The SCWO of MPA is initiated by hydrogen abstraction by OH^\bullet , attacking either the hydroxyl or the methyl group. Both intermediate species can react with water to re-form MPA. As can be seen in the table, the hydroxyl-attack pathway yielding $\text{PO}(\text{O}^\bullet)\text{OHCH}_3$ is relatively unchanged by the presence of ethanol. $\text{PO}(\text{O}^\bullet)\text{OHCH}_3$ unimolecularly decomposes to form PO_2OH , which reacts with water to form phosphoric acid [$\text{PO}(\text{OH})_3$], and CH_3^\bullet , which abstracts a hydrogen from water to form methane. The pathway through $\text{PO}(\text{OH})_2\text{CH}_2^\bullet$ is greatly enhanced by ethanol co-oxidation because the rate limiting step is the reaction of $\text{PO}(\text{OH})_2\text{CH}_2^\bullet$ with HO_2^\bullet . The increased concentration of oxygen required for the stoichiometric oxidation of the added ethanol results in an increased flux through the peroxy species $\text{PO}(\text{OH})_2\text{CH}_2\text{OO}^\bullet$ as well. Both $\text{PO}(\text{OH})_2\text{CH}_2^\bullet$ and $\text{PO}(\text{OH})_2\text{CH}_2\text{OO}^\bullet$ react to form $\text{PO}(\text{OH})_2\text{CH}_2\text{O}^\bullet$, which either decomposes to form the phosphoric acid precursor $\text{P}^\bullet\text{O}(\text{OH})_2$ and CH_2O , or reacts with water to form $\text{PO}(\text{OH})_2\text{CH}_2\text{OH}$, which eventually decomposes to form $\text{P}^\bullet\text{O}(\text{OH})_2$ and CO . CH_2O will oxidize to CO and CO_2 at $T = 473^\circ\text{C}$, but at such a low temperature CH_4 is not expected to react.

Because CH_4 is relatively inert at these conditions, it can be used as a tracer to measure the flux through the unimolecular decomposition of $\text{PO}(\text{O}^\bullet)\text{OHCH}_3$. The formation of CH_4 from MPA requires the participation of only one OH^\bullet , but the production of CO/CO_2 from MPA requires one OH^\bullet and either one HO_2^\bullet or one H_2O_2 . If, as we hypothesize, the co-oxidation effect acts via a very large increase in HO_2^\bullet but only a small increase in OH^\bullet , then MPA when co-oxidized with ethanol will undergo an increased flux only through the CO/CO_2 -forming $\text{PO}(\text{OH})_2\text{CH}_2^\bullet$ pathway. We expect to observe a large increase in MPA conversion and no change in CH_4 carbon fraction.

Ethanol generates methane as an intermediate, so it cannot be used as a co-oxidant for this experimental test. Since oxygenated hydrocarbon co-oxidants tend to function in the same

fashion, by generating HO_2^\bullet and chain-branching reactions that produce H_2O_2 , a mixture of CH_2O and CH_3OH (37% w/w formaldehyde in a 10% aqueous methanol solution, Aldrich PS-2031) was chosen as a co-oxidant. Both are predicted to generate large concentrations of HO_2^\bullet but have only a small effect on OH^\bullet concentrations, similarly to ethanol, but neither formaldehyde nor methanol generate a methane intermediate.

The only source of methane in the MPA- $\text{CH}_2\text{O}/\text{CH}_3\text{OH}$ co-oxidation experiment is from MPA. The stability of methane in the co-oxidative environment was tested by reacting a methane-formaldehyde-methanol organic stream with excess oxygen at $T = 473^\circ\text{C}$ and $P = 246$ bar. The conversion of methane was $0 \pm 3\%$ at $\tau = 9$ s, the longest residence time achievable on the plug-flow reactor. This finding confirmed our assumption that methane could be used as a stable tracer

MPA at an initial concentration of 1 mM was co-oxidized with the formaldehyde/methanol mixture at $[\text{CH}_2\text{O}]_0 = 2$ mM and 10 mM at $T = 473^\circ\text{C}$, $P = 246$ bar, and $\Phi = 1$. The MPA conversion and CH_4 carbon fraction at $\tau = 6$ s for the two co-oxidation cases were compared to the MPA conversion and CH_4 carbon fraction at $\tau = 6$ s for the oxidation of pure 1 mM $[\text{MPA}]_0$ at $T = 473^\circ\text{C}$, $P = 246$ bar, $\Phi = 1$. Figure 5-8 shows the percentage change compared to the pure MPA oxidation case for the two initial concentrations of formaldehyde, where we see a large increase in overall MPA conversion but only a small increase in methane formation. This difference is reasonable since methane formation is only a function of OH^\bullet concentration, but overall MPA conversion is a function of both OH^\bullet and HO_2^\bullet concentrations. Again we confirm that the co-oxidation effect is dominated by HO_2^\bullet formation.

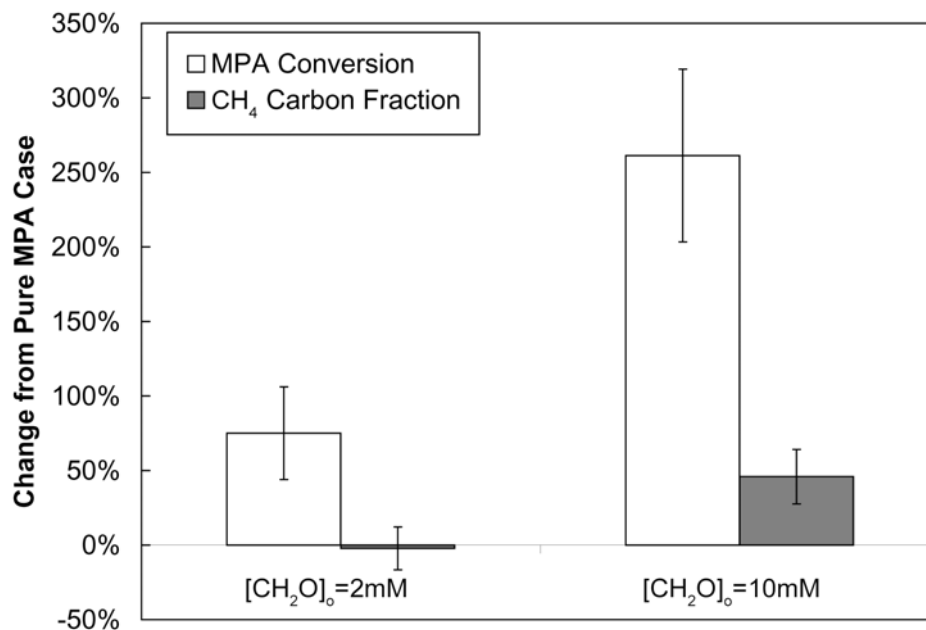


Figure 5-8: Comparison of MPA conversion and CH₄ carbon fraction for two initial concentrations of formaldehyde to the MPA conversion and CH₄ carbon fraction for the oxidation of pure MPA.

All experiments were run at $T = 473$ °C, $P = 246$ bar, $[MPA]_0 = 1$ mM, $\Phi = 1$.

5.6 CONCLUSIONS

An MPA-ethanol SCW co-oxidation mechanism was built from submechanisms for MPA developed by Sullivan and for ethanol developed by Rice and Croiset. It was found that ethanol and most other labile hydrocarbons generate a free radical pool by a simple cycle of hydrogen abstraction to form a reactive hydrocarbon radical, and then the reaction of that radical with oxygen to form the hydroperoxy radical HO_2^\bullet and another stable hydrocarbon. The dominant method of chain branching occurs when HO_2^\bullet abstracts a hydrogen off of a stable hydrocarbon, typically an alcohol or aldehyde, and forms H_2O_2 which decomposes to form $2 OH^\bullet$. The co-oxidation model overpredicts the increase in MPA conversion when ethanol is added, but the predicted MPA conversion values are highly sensitive to key rate parameters involving the radical precursor H_2O_2 . The model predicts that the introduction of 2.4 mM ethanol to 1.0 mM MPA causes a 16-fold increase in HO_2^\bullet concentration, but only a 2-fold increase in OH^\bullet

concentration. In order to validate this prediction experimentally, we used product distributions rather than MPA conversions. Methane was chosen as a tracer for OH^\bullet concentration since it is only formed from MPA when it reacts with OH^\bullet . An experiment was designed using formaldehyde and methanol as a co-oxidant which showed that the increase in MPA conversion was much greater than the increase in methane carbon fraction, which indicates that the increase in HO_2^\bullet concentration was much greater than the increase in OH^\bullet concentration, thus confirming the co-oxidation model predictions.

5.7 REFERENCES

- Anitescu, G., V. Munteanu and L. L. Tavlarides (2005). "Co-oxidation effects of methanol and benzene on the decomposition of 4-chlorobiphenyl in supercritical water." *J. Supercrit. Fluid* 33: 139-147.
- Baulch, D., C. J. Cobos, R. A. Cox, P. Frank, G. Hayman, T. Just, J. A. Kerr, T. Murrels, M. Pilling, J. Troe, R. W. Walker and J. Warnatz (1994). "Evaluated kinetic data for combustion modeling supplement-I." *J. Phys. Chem. Ref. Data* 23(6): 847-1033.
- Haar, L., J. S. Gallagher and G. S. Kell (1984). *NBS/NRC Steam Tables*. New York, Hemisphere Publishing Corp.
- Hippler, H., H. Neunaber and J. Troe (1995). "Shock wave studies of the reactions $\text{HO} + \text{H}_2\text{O}_2 \Rightarrow \text{H}_2\text{O} + \text{HO}_2$ and $\text{HO} + \text{HO}_2 \Rightarrow \text{H}_2\text{O} + \text{O}_2$ between 930 and 1680K." *J. Chem. Phys.* 103(9): 3510-3516.
- Hong, G. T., P. K. Fowler, W. R. Killilea and K. C. Swallow (1987). *Supercritical water oxidation: treatment of human waste and system configuration tradeoff study*. Proceedings of 17th Intersociety Conference on Environmental Systems, Seattle, WA.
- Janoschek, R. and M. J. Rossi (2002). "Thermochemical Properties of Free Radicals from G3MP2B3 Calculations." *Int. J. Chem. Kinet.* 34: 550-560.
- Kaiser, E., C. Westbrook and W. Pitz (1986). "Acetaldehyde oxidation in the negative temperature coefficient regime: Experimental and modeling results." *Int. J. of Chem. Kinet.* 18(6): 655-688.
- Marinov, N. M. (1999). "A detailed chemical kinetic model for high temperature ethanol oxidation." *Int. J. Chem. Kinet.* 31(3): 183-220.
- Ploeger, J. M., P. A. Bielenberg, J. L. DiNaro Blanchard, R. P. Lachance, J. D. Taylor, W. H. Green and J. W. Tester (2006a). "Modeling Oxidation and Hydrolysis Reactions in Supercritical Water - Free Radical Elementary Reaction Networks and Their Applications." *Comb. Sci. Tech.* 178(1-3): 363-398.

- Ploeger, J. M., P. A. Bielenberg, R. P. Lachance and J. W. Tester (2006b). "Co-oxidation of Methylphosphonic Acid and Ethanol in Supercritical Water: I. Experimental Results." *J. Supercrit. Fluids* accepted.
- Rice, S. and E. Croiset (2001). "Oxidation of simple alcohols in supercritical water III. Formation of intermediates from ethanol." *Ind. Eng. Chem. Res.* 40(1): 86-93.
- Savage, P., J. Rovira, N. Stylski and C. Martino (2000). "Oxidation kinetics for methane/methanol mixtures in supercritical water." *J. Supercrit. Fluids* 17: 155-170.
- Senosiain, J. P., C. B. Musgrave and D. M. Golden (2003). "Temperature and pressure dependence of the reaction of OH and CO: Master equation modeling on a high-level potential energy surface." *Int. J Chem. Kinet.* 35(9): 464-474.
- Sullivan, P. A. (2003). *Oxidation Kinetics of Methylphosphonic Acid in Supercritical Water: Experimental Measurements and Model Development*. Chemical Engineering, Massachusetts Institute of Technology, Cambridge.
- Sullivan, P. A., J. M. Ploeger, W. H. Green and J. W. Tester (2004). "Elementary reaction rate model for supercritical water oxidation of methylphosphonic acid." *Phys. Chem. Chem. Phys.* 6(17): 4310-4320.
- Sullivan, P. A. and J. W. Tester (2004). "Methylphosphonic acid oxidation kinetics in supercritical water." *AIChE Journal* 50(3): 673-683.

6 Experimental Results for Ammonia Oxidation

Before embarking on a study of ammonia-ethanol co-oxidation, we needed reliable data on the SCWO of pure ammonia. Measurements of ammonia oxidation rates in supercritical water were first reported by our group over 14 years ago (Webley et al. 1991). Since then we have made several improvements to our experimental apparatus upgrading the preheating sections to reduce heat losses, improving mixing of reactants and oxygen and improving temperature measurement methods. Based on these improvements and earlier validation runs with methanol (Tester et al. 1993; Vogel et al. 2005), we believed that systematic uncertainties were present in our earlier temperature data causing the global rate expressions for oxidation to be incorrect. The objectives of this chapter are to document our new results and to present revised global rate parameters.

6.1 PLUG FLOW EXPERIMENTAL RESULTS

Ammonia oxidation experiments were conducted over temperatures ranging from 655 to 705 °C, and pressures from 135 to 270 bar. Initial ammonia concentration ranged from 0.8 to 2.7 mM. The fuel equivalence ratio, defined as

$$\Phi \equiv \frac{S[\text{NH}_3]_0}{[\text{O}_2]_0} \quad (\text{Eqn. 6-1})$$

where $S = 0.75$, the stoichiometric ratio of O_2 to NH_3 , ranged from 0.22 to 1.93. Reactor residence times ranged from 2 to 9 s.

Results are summarized in Table 6-1. Uncertainties cited represent the precision error at the 95% confidence interval. With the exception of two experiments where evidence of corrosion was observed, the nitrogen balance was closed within experimental error of $100 \pm 3\%$.

This ensures that we are measuring all of the ammonia oxidation products. Nitrous oxide (N₂O) accounts for 4 to 13% of the oxidized ammonia, with N₂ making the balance.

Table 6-1: Summary of experimental data with uncertainties at the 95% confidence level. N₂O is defined as the moles of nitrogen as N₂O in the reactor effluent divided by the moles of nitrogen as ammonia consumed in the reactor.

T (°C)	P (bar)	$[\text{NH}_3]_0$ (mM)	Φ	τ (s)	X_{NH_3} (%)	N bal (%)	N ₂ O yield (%)
698±3	241±1	0.82±0.02	0.75±0.03	4.6±0.3	40±2	101±3	^a
698±3	245±1	0.84±0.03	0.75±0.04	2.6±0.2	25±4	97±4	^a
681±3	241±1	0.94±0.03	0.87±0.03	6.6±0.4	20±3	104±3	^a
681±3	241±2	0.94±0.02	0.87±0.03	4.6±0.3	17±3	102±3	^a
680±3	242±1	0.94±0.02	0.87±0.03	3.1±0.2	16±2	97±2	^a
680±3	242±1	0.96±0.02	0.95±0.03	6.4±0.4	21±2	100±2	4±0
679±3	242±1	0.96±0.02	0.96±0.03	4.5±0.3	13±2	102±2	5±0
677±3	242±1	0.97±0.02	0.97±0.03	2.5±0.1	11±2	98±2	4±0
658±3	244±1	0.87±0.02	0.89±0.04	6.5±0.4	15±3	101±3	^a
656±3	244±1	0.87±0.02	0.88±0.04	4.6±0.3	13±3	99±3	^a
655±3	244±1	0.88±0.02	0.90±0.04	2.5±0.1	7±3	100±3	^a
698±3	242±1	0.94±0.01	0.92±0.03	2.5±0.1	20±2	101±2	5±0
698±3	244±1	0.93±0.02	0.89±0.03	4.5±0.3	33±2	102±2	4±0
702±3	243±1	0.93±0.02	0.96±0.05	8.9±0.5	58±1	104±3	4±0
704±3	242±1	1.05±0.02	0.22±0.01	6.4±0.4	100±0 ^b	111±4	8±0
703±3	243±1	1.06±0.02	0.22±0.01	3.4±0.2	86±1 ^b	110±3	10±1
704±3	242±1	0.99±0.02	1.91±0.06	6.4±0.4	31±2	101±3	5±0
701±3	243±1	1.01±0.02	1.93±0.06	4.0±0.2	21±2	102±2	6±0
701±3	242±1	2.63±0.06	0.89±0.04	6.5±0.4	56±1	103±3	7±0
699±3	248±1	2.72±0.04	0.91±0.03	3.0±0.2	38±1	99±2	8±0
699±3	203±1	1.14±0.02	1.00±0.04	5.2±0.3	45±2	99±2	6±0
697±3	203±1	1.17±0.03	1.04±0.04	2.8±0.2	29±2	98±2	7±1
698±4	269±1	0.94±0.02	1.01±0.04	4.5±0.3	43±1	99±2	8±1
697±3	270±1	0.94±0.02	0.99±0.04	7.1±0.4	53±1	102±2	7±0
695±3	245±1	1.96±0.06	1.03±0.05	4.4±0.3	29±3	103±6	8±1
690±3	245±1	1.96±0.06	1.02±0.05	3.6±0.2	22±3	105±4	10±1
696±3	243±1	1.01±0.03	0.73±0.03	6.5±0.4	61±2	104±4	6±0
697±3	242±1	1.01±0.03	0.73±0.03	4.5±0.3	42±3	107±4	7±0
697±3	243±1	1.02±0.02	0.73±0.02	3.5±0.2	38±2	104±3	7±0
695±3	135±1	1.03±0.03	1.01±0.04	3.1±0.2	28±2	105±2	10±1
690±3	136±1	1.04±0.02	1.01±0.03	2.1±0.1	16±2	105±4	13±1

(a) data not available; (b) corrosion products observed in effluent.

Hydrolysis experiments in the absence of added oxygen were conducted at 700 °C by mixing a helium-sparged ammonia stream at $[\text{NH}_3]_0 = 1 \text{ mM}$ with a helium-sparged 18.2 M Ω -cm deionized water stream. At a residence time of 6.5 s, ammonia conversion was equal to $4.1 \pm 2.2\%$, which confirmed that hydrolysis or pyrolysis in the preheaters can be neglected for the conditions of interest.

Figure 6-1 shows the effect of temperature on ammonia conversion. The maximum temperature 700 °C for the experiments was restricted by the sandbath maximum rated temperature, and the minimum temperature 655 °C was the lowest temperature for which a measurable conversion of ammonia was possible over the reported residence times of 2 to 9 s achievable on the plug flow reactor system.

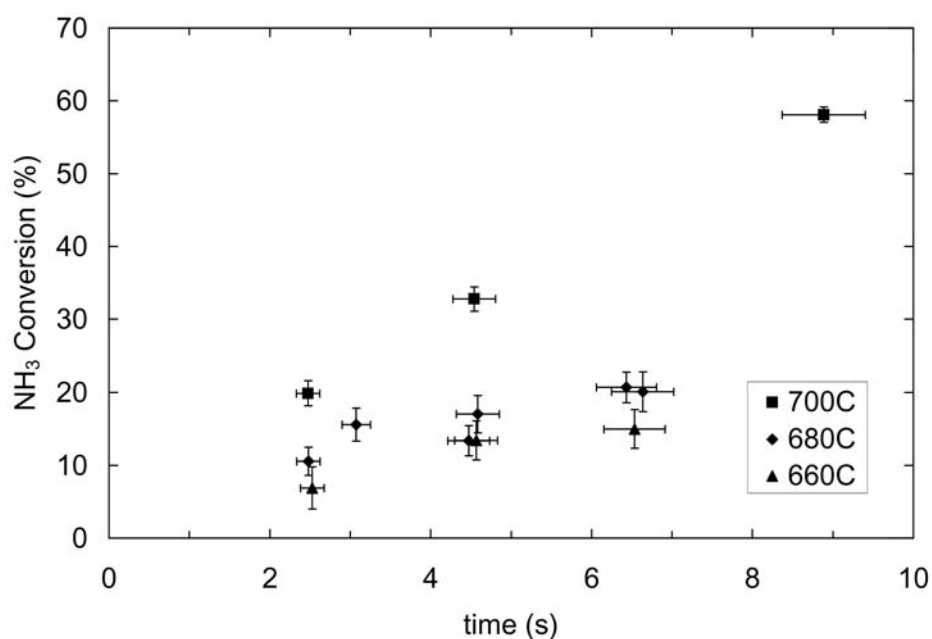


Figure 6-1: Ammonia conversion as a function of residence time for three different temperatures. $P = 243 \pm 2 \text{ bar}$, $[\text{NH}_3]_0 = 0.92 \pm 0.05 \text{ mM}$, $\Phi = 0.92 \pm 0.05$.

To illustrate the effect of initial ammonia concentration on the rate of oxidation, ammonia conversion was plotted as a function of time for two different initial ammonia concentrations at $T = 696 \pm 6 \text{ °C}$ and $P = 245 \pm 3 \text{ bar}$ in Figure 6-2. We can conclude that ammonia conversion has

little if any dependence on initial ammonia concentration, which is consistent with first-order oxidation kinetics.

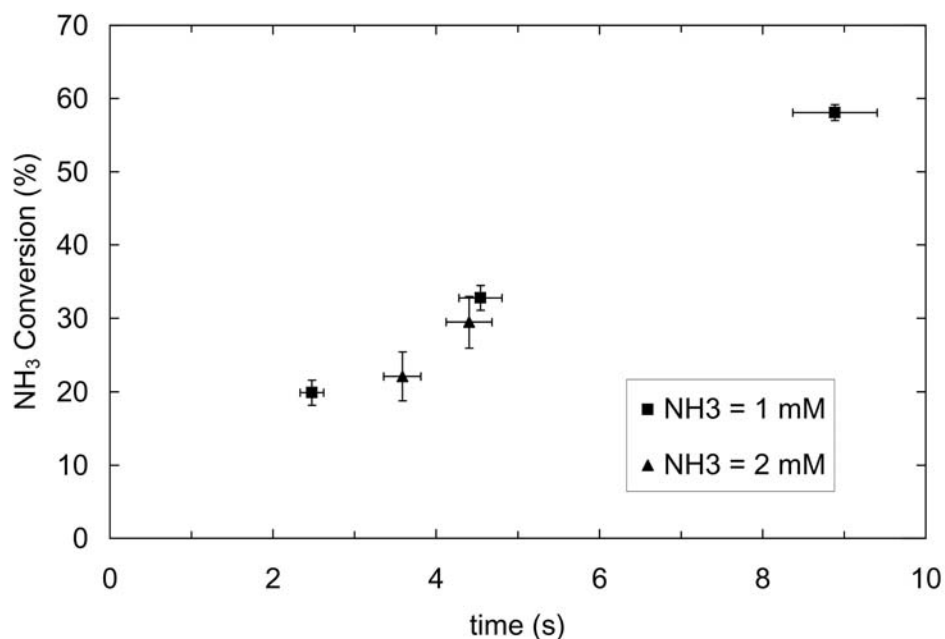


Figure 6-2: Ammonia conversion as a function of residence time for two different initial ammonia concentrations. $T = 696 \pm 6$ °C, $P = 245 \pm 3$ bar, $\Phi = 0.96 \pm 0.07$.

The effect of oxygen concentration is complicated by an observed tendency towards increased corrosion at the high temperatures required to detect measurable ammonia conversion. At $T = 703$ °C, $P = 243$ bar, $[\text{NH}_3]_0 = 1$ mM, $\tau = 6.5$ s, and 350% excess oxygen ($\Phi = 0.22$), corrosion products were observed in the effluent, which took on a pale yellow color due to dissolved metals leached from the reactor walls. Chromium was measured in the effluent at a concentration of 4.2 ppm. The ammonia conversion was measured to be $99.9 \pm 0.0\%$, much higher than any other conversions measured. This rapid destruction of ammonia is attributed to the oxidation of ammonia by the Cr(VI) oxyanion (Dell'Orco et al. 1997). When the residence time was shortened to $\tau = 4.5$ s, chromium concentrations dropped to 0.5 ppm and ammonia conversion dropped to $86.4 \pm 0.6\%$.

At lower oxygen concentrations, no chromium was observed in the outlet at a detection limit of 0.1 ppm. Ammonia conversion as a function of time for three different values of Φ is presented in Figure 6-3. Although ammonia oxidation was not limited by oxygen concentration in the fuel-excess experiment, Figure 6-3 shows a clear dependence of the rate of ammonia oxidation on oxygen concentration.

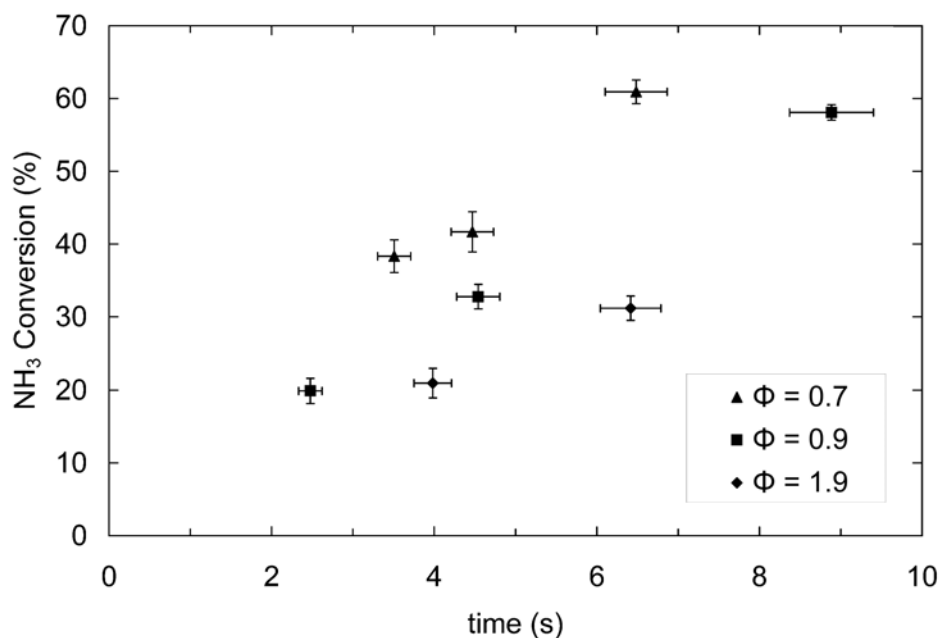


Figure 6-3: Ammonia conversion as a function of time for three different fuel equivalence ratios. $T = 700 \pm 4$ °C, $P = 243 \pm 1$ bar, $[\text{NH}_3]_0 = 0.97 \pm 0.05$ mM.

Previous studies have found no dependence of ammonia conversion on system pressure (Segond et al. 2002), which is equivalent to there being no dependence of ammonia conversion on water concentration. Figure 6-4 plots ammonia conversion versus residence time for four different pressures/densities. The data clearly support the previous findings that the concentration of water has no effect on ammonia oxidation.

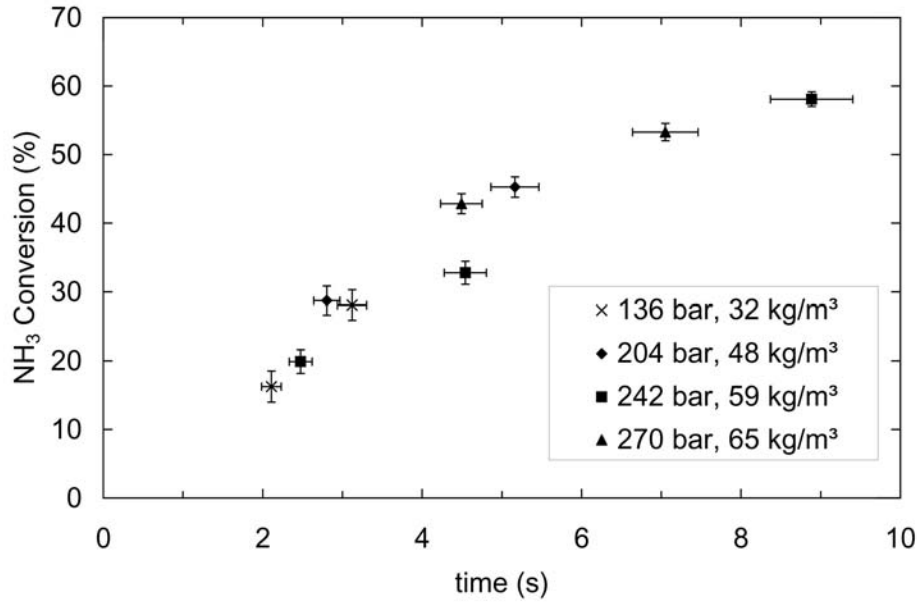


Figure 6-4: Ammonia conversion as a function of time for four different pressures. The calculated fluid density is also listed for each corresponding pressure. $T = 696 \pm 6$ °C, $[\text{NH}_3]_0 = 1.05 \pm 0.12$ mM, $\Phi = 0.96 \pm 0.08$.

The data were fit to a five-parameter empirical global rate law

$$k = A \times \exp\left(\frac{-E_a}{RT}\right) \times [\text{NH}_3]^a \times [\text{O}_2]^b \times [\text{H}_2\text{O}]^c \quad (\text{Eqn. 6-2})$$

The parameters were regressed using the Marquardt method from a published algorithm (Constantinides and Mostoufi 1999) in MATLAB. The c parameter for water dependence was not found to be statistically different from 0, which is consistent with experimental observations that ammonia conversion is independent of water density. The a parameter for ammonia dependence was not found to be statistically different from 1, which is also consistent with experimental observation of first order behavior. The regression was performed again holding a and c constant at 1 and 0, respectively, resulting in the following global rate law

$$k = 10^{19.0 \pm 4.5} \times \exp\left(\frac{-83 \pm 19}{RT}\right) \times [\text{NH}_3] \times [\text{O}_2]^{0.44 \pm 0.30} \quad (\text{Eqn. 6-3})$$

in units of kcal, L, mol, and s. The parity plot for this global rate law is presented in Figure 5 below.

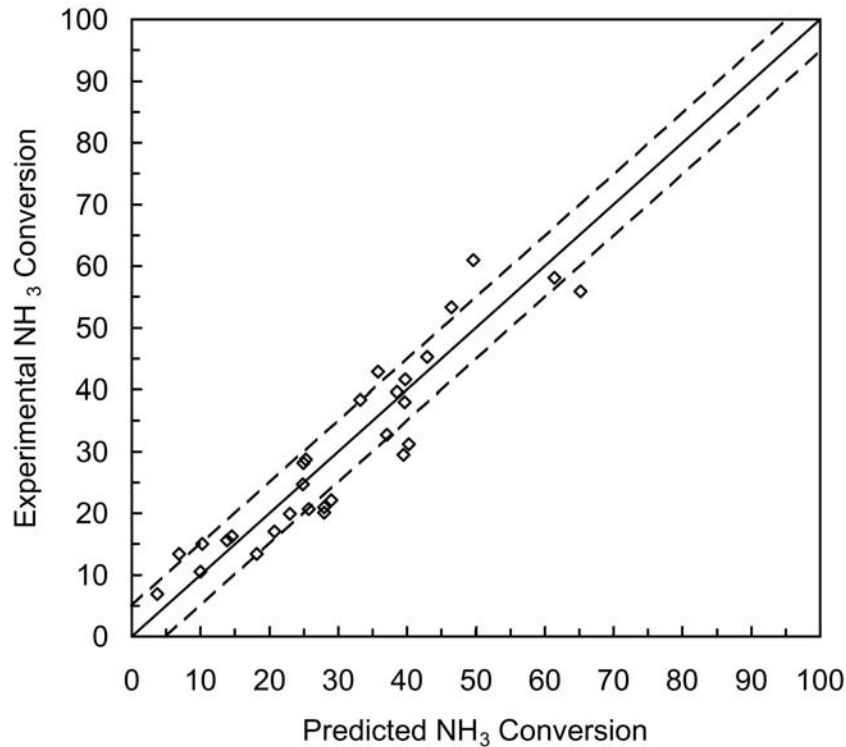


Figure 6-5: Parity plot for global rate law. Uncertainty in experimental NH₃ conversion ranges from 1-3% at the 95% confidence level.

To compare data from different studies, each data point is fit to an assumed first-order rate constant with no oxygen or water dependence. These pseudo first-order rate constants are calculated by Eqn. 6-4:

$$k^* = \frac{-\ln(1-X_{\text{NH}_3})}{\tau} \quad (\text{Eqn. 6-4})$$

The pseudo-first order rate constants for this study are plotted with the earlier study in our group by Webley (1989) as well as the 2002 study by Segond et al. in Figure 6-6. The rates for our study are slower than the Segond data for comparable surface-to-volume (S/V) ratios, but Segond employed a reactor constructed from 316 stainless steel. Stainless steel may have a

greater catalytic activity for ammonia oxidation, a faster rate of chromium leaching that would lead to the homogenous catalysis of ammonia oxidation, or a combination of the two. The rates reported by Webley are significantly slower than those measured in this study using the same Inconel 625 reactor wall material. The difference in observed oxidation rates is attributed to insufficient preheating, heat losses, and errors in the measured fluid temperature in the Webley study.

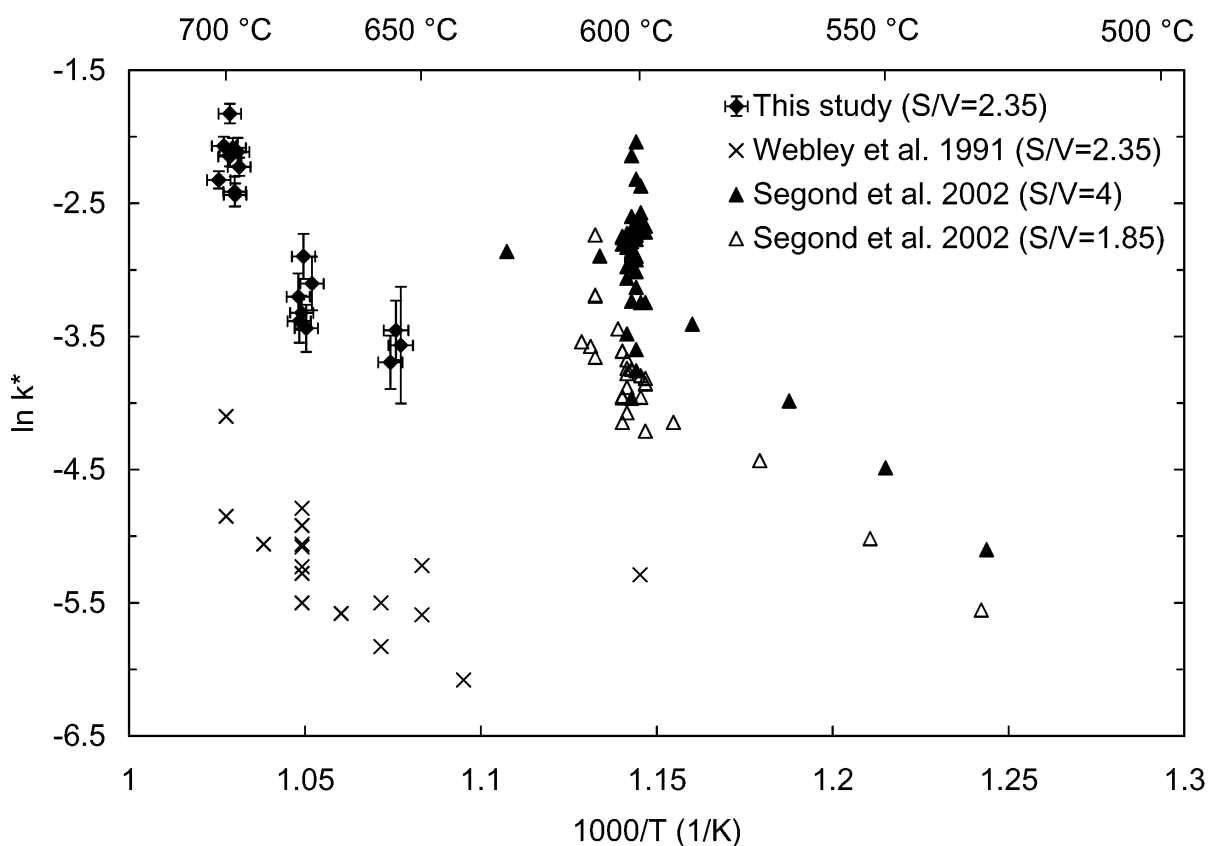


Figure 6-6: Arrhenius plot for pseudo-first order rate constants from this study, Segond et al. (2002), and Webley et al. (1991). S/V ratios are in cm^{-1} .

To estimate the magnitude of the temperature correction for the Webley experiments, the old data were fit to the new global rate law (Eqn. 6-3). Given the initial concentrations of ammonia and oxygen, residence times, and pressures reported by Webley, the temperature was solved such that the global rate law would predict the same conversion measured by Webley.

These “corrected” temperatures are plotted against the temperatures reported by Webley in Figure 6-7. With the exception of the reported temperature of 600 °C, all reported temperatures are 10 to 58 °C greater than the corrected temperature. The ammonia converted reported by Webley at 600 °C was $3.4 \pm 1.6\%$, which propagates to an error of ± 10 °C in the corrected temperature. The seemingly inconsistent underestimation of temperature by Webley is also attributed to additional error in extrapolating the global rate law so far from the temperature region for which it was fit. The rest of the data shows a trend of increasing temperature correction with increasing reported temperature, which is consistent with the theory of insufficient preheating. The average temperature correction is 30 °C, which is also consistent with the temperature correction of 26 °C calculated for methanol oxidation in the same reactor system used by Webley (Tester et al. 1993; Vogel et al. 2005).

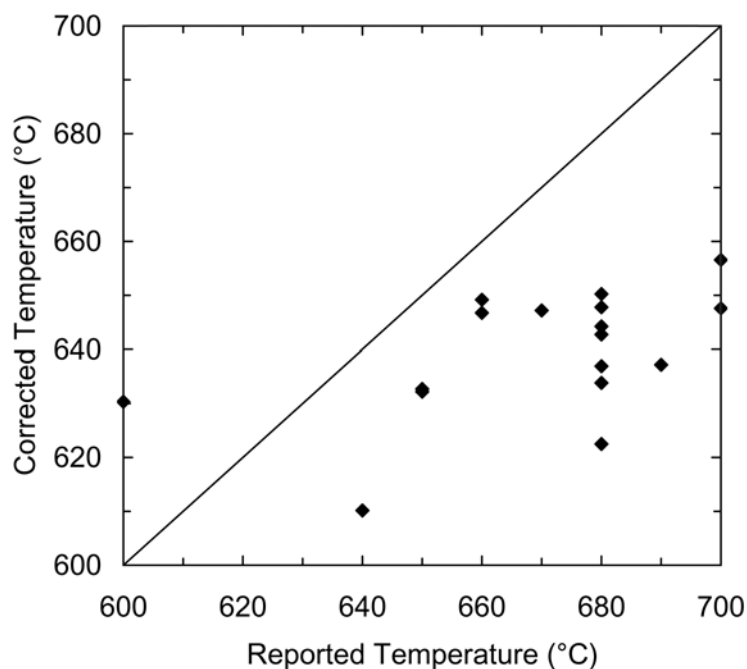


Figure 6-7: Corrected temperature resulting from fitting Webley et al. (1991) data to global rate law from this study versus temperature reported by Webley et al.

6.2 BATCH REACTOR EXPERIMENTAL RESULTS

The minimum temperature at which we could measure appreciable ammonia conversion after residence times achievable in the plug flow reactor was 655 °C. Restricted by a maximum reactor temperature of 700 °C, it was decided that the batch cell reactor described in Chapter 3 should be utilized to expand the temperature range of ammonia oxidation data. The study was led by Stephanie Lee and Adam Madlinger, two undergraduate laboratory assistants in our group.

In the initial stage of the study temperature was varied from 500 °C to 620 °C at a pressure of 3550±100 psig (246±7 bar), initial ammonia concentration of 3.4±0.1 mM, and fuel equivalence ratio of 0.89±0.03. At each temperature, one experiment was conducted at a short residence time (5-60 s) at which very low conversion of ammonia was expected. Then up to 6 experiments were conducted at longer residence times and the outlet concentration of ammonia for each experiment was compared to the outlet concentration of ammonia for the short-time experiment to calculate the ammonia conversion. The residence time reported was the difference between the two measured residence times. Using a short-time experiment as a reference point corrected for mixing effects, which were assumed to be consistent across experiments and no longer than 5 s.

$$X_{NH_3} = \frac{[NH_3]_{ref} - [NH_3]_{exp}}{[NH_3]_{ref}} \quad (\text{Eqn. 6-5})$$

$$\tau = \tau_{exp} - \tau_{ref} \quad (\text{Eqn. 6-6})$$

Table 6-2: Summary of batch cell experimental data with uncertainties at the 95% confidence level. $P = 246 \pm 7$ bar, $[\text{NH}_3]_0 = 3.4 \pm 0.1$ mM, $\Phi = 0.89 \pm 0.03$.

T (°C)	τ (s)	X	k^* (10^{-5}s^{-1})
620±3	290±5	22.4±0.6	87.4±8.3
620±3	590±5	37.4±1.1	79.3±4.1
620±3	890±5	46.7±1.3	70.7±2.7
620±3	1490±5	70.9±2.0	82.8±1.6
600±3	540±5	20.0±0.6	41.2±4.5
600±3	540±5	21.1±0.6	43.8±4.5
600±3	840±5	36.6±1.0	54.2±2.9
600±3	1132.5±5	51.3±1.5	63.5±2.1
600±3	1140±5	41.4±1.2	46.9±2.1
600±3	1440±5	54.7±1.5	55.0±1.7
600±3	1920±5	69.5±2.0	61.8±1.3
585±3	595±5	28.6±0.8	36.3±4.0
585±3	1195±5	38.7±1.1	38.9±2.0
585±3	1795±5	50.3±1.4	56.7±1.3
585±3	2395±5	58.1±1.6	41.0±1.0
570±3	1140±5	24.1±0.7	26.3±2.1
570±3	1740±5	36.7±1.0	24.8±1.4
570±3	2640±5	47.8±1.4	24.2±0.9
570±3	3540±5	58.4±1.7	24.6±0.7
540±3	5340±5	43.2±1.2	10.6±0.5
540±3	8940±5	62.6±1.8	11.0±0.3
500±3	5340±5	24.6±0.7	5.3±0.5

Ammonia oxidation in the batch reactor obeyed first-order dependence on ammonia consistent with observations on the plug flow reactor. A plot of $\ln(1-X)$, where X is the ammonia conversion, as a function of residence time is expected to be linear if the oxidation kinetics are first order, and this is confirmed in Figure 6-8 for data taken at 570 °C.

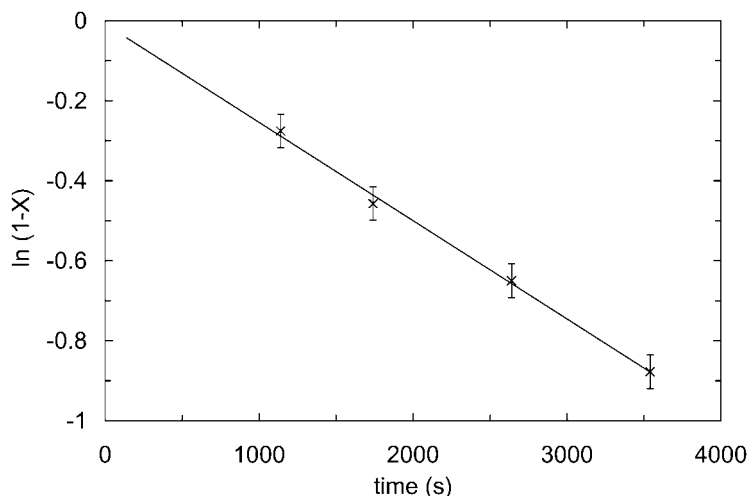


Figure 6-8: First-order plot of $\ln(1-X)$ as a function of residence time at $T = 570\text{ }^\circ\text{C}$.

The pseudo-first order rate constants for each experiment were calculated by Eqn. 6-7 and are plotted with the rate constants from the plug-flow reactor study (Section 6.1) in Figure 6-9.

$$k^* = \frac{-\ln\left(\frac{[\text{NH}_3]_{out}}{[\text{NH}_3]_{out,ref}}\right)}{\tau - \tau_{ref}} \quad (\text{Eqn. 6-7})$$

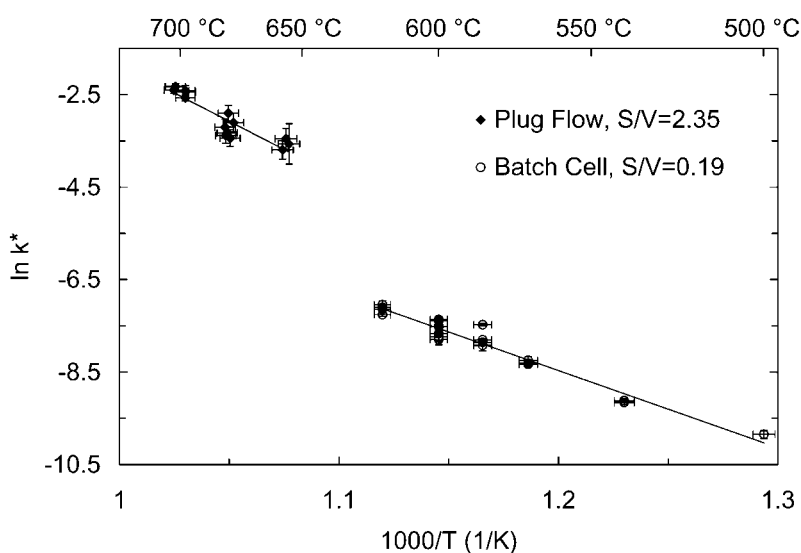


Figure 6-9: Arrhenius plot for pseudo-first order rate constants from this study on two reactor systems

The rate of oxidation in the batch cell is slower than the rate observed in the plug flow reactor because of the lower surface-to-volume ratio of the batch cell ($S/V = 0.19 \text{ cm}^{-1}$). The data also show Arrhenius behavior, and can be fit to the following global rate law in units of kcal, mol, s, and L.

$$k = 10^{5.0 \pm 0.8} \times \exp\left(\frac{-33.2 \pm 3.3}{RT}\right) \times [NH_3] \quad (\text{Eqn. 6-6})$$

Future work on the batch-cell SCWO of ammonia will continue with the goal of publishing a paper based on the results. Because a gas-sampling method had not been developed to capture the very small quantities of gas evolved during the oxidation of ammonia, only the ammonia conversion could be measured. Experiments will be conducted with a small initial charge of helium gas to increase the total amount of gas sample to a volume that can be accurately measured and analyzed by GC. In this way we hope to close the nitrogen balance and determine the nitrous oxide yields. The effect of fuel equivalence ratio on the rate of oxidation will also be explored. Finally, a batch reactor will be designed with a large high pressure fitting port through which metal particles can be introduced to the reactor to alter the S/V ratio to determine its effect on ammonia oxidation.

6.3 CONCLUSIONS

The oxidation of ammonia in supercritical water was studied in two reactor systems, the plug flow and batch cell. Global rate laws for each reactor system were fit that were first-order in ammonia. The plug flow data served to update the study by Webley (1991) in our group, which was conducted on a reactor system with poor preheating and temperature measurement. Applying the global rate law for this study to the Webley data, the actual temperature was estimated to be 30 °C lower than the reported temperature. This is consistent with the Tester et

al. (1993) study that estimated the temperatures reported in the methanol oxidation study on the same reactor system to be overestimated by 26 °C. The plug flow data were also used as a baseline in the ammonia-ethanol experimental study detailed in Chapter 7. The rate of ammonia oxidation was found to be significantly slower in the batch reactor than in the plug flow reactor, which was attributed to the lower S/V ratio of the batch cell. Ongoing work on the batch cell seeks to determine effect of S/V ratio by developing a batch reactor that can be charged with a known amount of metal particles.

6.4 REFERENCES

- Constantinides, A. and N. Mostoufi (1999). *Numerical Methods for Chemical Engineers with Matlab Applications*. Upper Saddle River, NJ, Prentice Hall PTR.
- Dell'Orco, P. C., E. F. Gloyne and S. J. Buelow (1997). "Reactions of nitrate salts with ammonia in supercritical water." *Ind. Eng. Chem. Res.* 36(7): 2547-2557.
- Segond, N., Y. Matsumura and K. Yamamoto (2002). "Determination of ammonia oxidation rate in sub- and supercritical water." *Ind. Eng. Chem. Res.* 41(24): 6020-6027.
- Tester, J. W., P. A. Webley and H. R. Holgate (1993). "Revised global kinetic measurements of methanol oxidation in supercritical water." *Ind. Eng. Chem. Res.* 32(1): 236-239.
- Vogel, F., J. L. DiNaro Blanchard, P. A. Marrone, S. F. Rice, P. A. Webley, W. A. Peters, K. A. Smith and J. W. Tester (2005). "Critical review of kinetic data for the oxidation of methanol in supercritical water." *J. Supercrit. Fluid* 34: 249-286.
- Webley, P. A., J. W. Tester and H. R. Holgate (1991). "Oxidation kinetics of ammonia and ammonia-methanol mixtures in supercritical water in the temperature range 530-700°C at 246 bar." *Ind. Eng. Chem. Res.* 30(8): 1745-1754.

7 Experimental Results for Ammonia-Ethanol Co-oxidation

The objective of this chapter is to determine the effect of co-oxidation with ethanol on ammonia SCWO kinetics, focusing on measuring ammonia conversion and product distribution as a function of temperature and reactant concentration. This data will be used in Chapter 8 to guide the development of an elementary reaction rate mechanism for ammonia-ethanol co-oxidation.

7.1 EXPERIMENTAL RESULTS

Experimental data were taken over a temperature range from 655 to 705 °C at a pressure of 246 bar, initial ammonia concentrations ranging from 1 to 3 mM, and initial ethanol concentrations ranging from 0 to 1 mM. Introducing ethanol to the ammonia feed requires an addition of oxygen to maintain stoichiometric oxygen for both ammonia and ethanol. The fuel equivalence ratio is defined as

$$\Phi \equiv \frac{S_{NH_3} [NH_3]_o + S_{EtOH} [EtOH]_o}{[O_2]_o} \quad (\text{Eqn. 7-1})$$

where S_i is the stoichiometric ratio of oxygen to fuel required for each compound ($S_{NH_3} = 0.75$ and $S_{EtOH} = 3$). Co-oxidation experiments were conducted at stoichiometric oxygen ($\Phi = 1.00 \pm 0.05$) except for two fuel-rich experiments ($\Phi = 2.2 \pm 0.1$) and one pyrolysis/hydrolysis experiment with no added oxygen ($T = 700$ °C, $P = 246$ bar, $[NH_3]_o = [EtOH]_o = 1$ mM, $[O_2]_o \approx 0$ mM, $\tau = 6.5$ s). The ammonia conversion in the pyrolysis experiment was $4 \pm 2\%$, which permits the assumption that ammonia does not significantly pyrolyze or hydrolyze in the preheaters.

Table 7-1: Summary of experimental data

Run #	T (°C)	P (bar)	$[\text{NH}_3]_0$ (mM)	$[\text{EtOH}]_0$ (mM)	Φ	τ (s)	X_{NH_3} (%)	N balance (%)	N_2O yield (%)
1	701±3	241±1	1.03±0.02	0.96±0.04	0.95±0.03	6.4±0.4	75±1	97±3	29±2
2	701±3	245±1	1.06±0.03	0.99±0.05	0.98±0.04	4.5±0.3	72±1	90±3	30±2
3	698±3	246±1	1.08±0.03	1.00±0.05	0.99±0.04	2.5±0.2	64±2	90±2	38±2
4	701±3	241±1	1.04±0.02	0.97±0.04	0.96±0.03	5.4±0.3	71±1	92±4	31±2
5	699±3	242±1	1.05±0.02	0.98±0.04	0.98±0.03	3.5±0.2	70±1	93±2	42±2
6	681±3	242±1	0.94±0.03	0.97±0.02	0.94±0.03	6.4±0.4	67±1	100±3	51±3
7	680±3	242±1	0.94±0.03	0.97±0.02	0.95±0.03	4.5±0.3	66±1	99±3	55±3
8	655±3	244±1	0.97±0.02	0.97±0.03	0.97±0.03	6.6±0.4	52±1	109±2	68±2
9	652±3	243±1	0.98±0.02	0.98±0.03	0.97±0.03	4.6±0.3	49±1	107±2	71±3
10	703±3	241±1	0.97±0.02	0.95±0.03	2.18±0.09	6.4±0.4	16±2	97±4	7±2
11	701±3	242±1	0.96±0.02	0.96±0.04	2.18±0.09	4.0±0.2	15±3	97±3	14±1
12	703±3	242±1	0.95±0.03	0.09±0.00	0.93±0.04	6.4±0.4	63±2	109±3	18±1
13	703±3	244±1	0.96±0.03	0.09±0.00	0.93±0.04	4.5±0.3	54±2	108±3	20±1
14	702±3	243±1	0.96±0.02	0.09±0.00	0.94±0.03	3.4±0.2	46±2	107±2	25±1
15	705±3	243±1	3.00±0.05	0.98±0.02	1.05±0.04	6.4±0.4	72±1	104±2	34±2
16	704±3	244±1	3.02±0.05	0.99±0.01	1.05±0.04	4.5±0.3	67±1	103±2	35±2
17	704±3	244±1	3.01±0.05	0.99±0.02	1.04±0.04	3.4±0.2	62±1	100±2	33±1
18	698±4	243±1	1.04±0.03	0.48±0.01	0.99±0.04	6.4±0.4	69±2	112±4	44±2
19	694±3	246±1	1.06±0.04	0.49±0.02	0.99±0.04	2.5±0.2	53±2	110±3	58±3
20	681±3	243±1	0.96±0.02	1.00±0.03	0.99±0.04	4.5±0.3	65±1	113±3	64±4
21	677±3	244±1	0.97±0.02	1.01±0.03	1.00±0.04	2.6±0.2	58±1	113±4	73±5
22	681±3	241±1	0.94±0.03	0.00±0.00	0.87±0.03	6.6±0.4	20±3	104±3	^a
23	681±3	241±2	0.94±0.02	0.00±0.00	0.87±0.03	4.6±0.3	17±3	102±3	^a
24	680±3	242±1	0.94±0.02	0.00±0.00	0.87±0.03	3.1±0.2	16±2	97±2	^a
25	680±3	242±1	0.96±0.02	0.00±0.00	0.95±0.03	6.4±0.4	21±2	100±2	4±0
26	679±3	242±1	0.96±0.02	0.00±0.00	0.96±0.03	4.5±0.3	13±2	102±2	5±0
27	677±3	242±1	0.97±0.02	0.00±0.00	0.97±0.03	2.5±0.1	11±2	98±2	4±0
28	658±3	244±1	0.87±0.02	0.00±0.00	0.89±0.04	6.5±0.4	15±3	101±3	^a
29	656±3	244±1	0.87±0.02	0.00±0.00	0.88±0.04	4.6±0.3	13±3	99±3	^a
30	655±3	244±1	0.88±0.02	0.00±0.00	0.90±0.04	2.5±0.1	7±3	100±3	^a
31	698±3	242±1	0.94±0.01	0.00±0.00	0.92±0.03	2.5±0.1	20±2	101±2	5±0
32	698±3	244±1	0.93±0.02	0.00±0.00	0.89±0.03	4.5±0.3	33±2	102±2	4±0
33	702±3	243±1	0.93±0.02	0.00±0.00	0.96±0.05	8.9±0.5	58±1	104±3	4±0
34	696±3	243±1	1.01±0.03	0.00±0.00	0.73±0.03	6.5±0.4	61±2	104±4	6±0
35	697±3	242±1	1.01±0.03	0.00±0.00	0.73±0.03	4.5±0.3	42±3	107±4	7±0
36	697±3	243±1	1.02±0.02	0.00±0.00	0.73±0.02	3.5±0.2	38±2	104±3	7±0

(a) data not available.

 Φ = Fuel equivalence ratio (see Eqn. 7-1) X_{NH_3} = Conversion of ammonia τ = Residence time, assuming plug flow conditions

Experimental results are summarized in Table 7-1. The nitrogen balance for ammonia-ethanol co-oxidation runs closed within experimental error of $100\pm 10\%$, which is a larger error than the pure ammonia oxidation data ($100\pm 3\%$). The increased error is attributed to errors in measuring nitrous oxide in the reactor effluent, since N_2O yields were much higher in the co-oxidation runs. The high solubility of N_2O in water multiplies the error in measuring N_2O in the gas phase because the molar flow rate of N_2O in the liquid effluent is calculated using a Henry's Law approximation, whereby it is assumed that the concentration in the liquid phase is linearly proportional to partial pressure in the gas phase (Dean 1992). No carbon products other than carbon dioxide were observed in the reactor effluent for co-oxidation experiments, which supports the assumption that at such high temperatures ethanol oxidation would be rapid and complete.

The effect of initial ethanol concentration on ammonia conversion is shown in Figure 7-1. Increases in ammonia conversion are quite dramatic for the addition of ethanol at equal initial molar concentrations as ammonia. Note that for initial ethanol concentrations of 0.5 mM and 1.0 mM the conversion at 6.5 s is not much greater than the conversion at 2.5 s; this indicates that the co-oxidation enhancement is primarily occurring in the first two seconds of exposure to reaction conditions. Due to comparable times required for achieving sufficient mixing of reactants and oxygen, we cannot unequivocally conclude that this is a purely kinetic effect. To underscore the effect that ethanol has on the rate of ammonia oxidation, at $T = 699\pm 5$ °C, $P = 243\pm 3$ bar, $[NH_3]_0 = 1.00\pm 0.08$ mM, $\Phi = 0.95\pm 0.05$, and $\tau = 2.5\pm 0.2$ s, the addition of 0.5 mM ethanol results in a $164\pm 25\%$ increase in ammonia conversion and the addition of 1.0 mM ethanol results in a $224\pm 29\%$ increase.

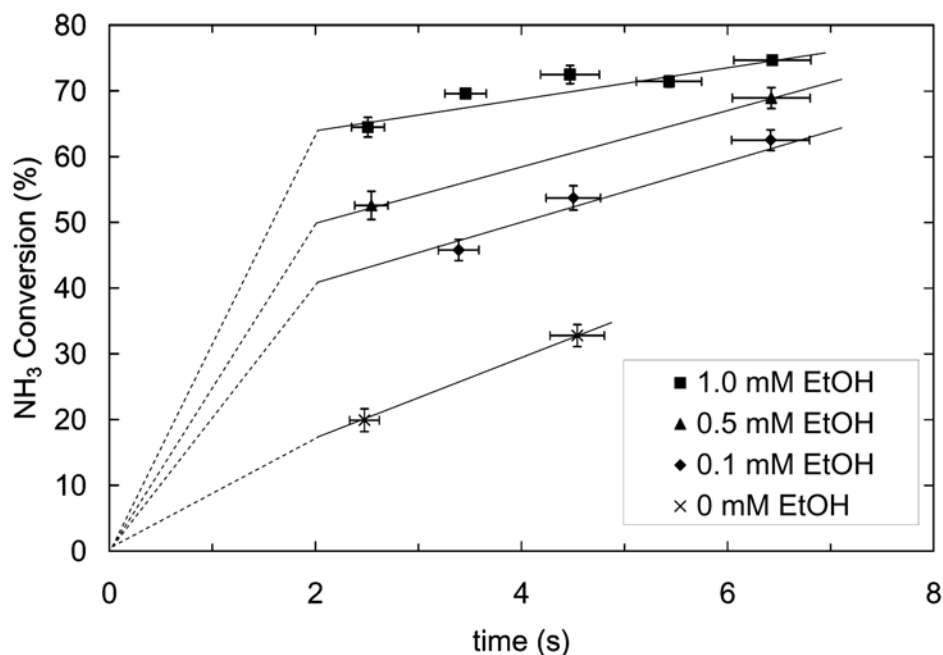


Figure 7-1: Ammonia conversion as a function of time for four different initial concentrations of ethanol.

$T = 699 \pm 5$ °C, $P = 243 \pm 3$ bar, $[\text{NH}_3]_0 = 1.00 \pm 0.08$ mM, and $\Phi = 0.95 \pm 0.05$.

Initial ammonia concentration has a much smaller effect on ammonia conversion, as illustrated in Figure 7-2. When the initial ammonia concentration is tripled with all other parameters held constant, the conversion decreases by less than 10%, which shows that ammonia has a small impact on the free radical pool generated by ethanol.

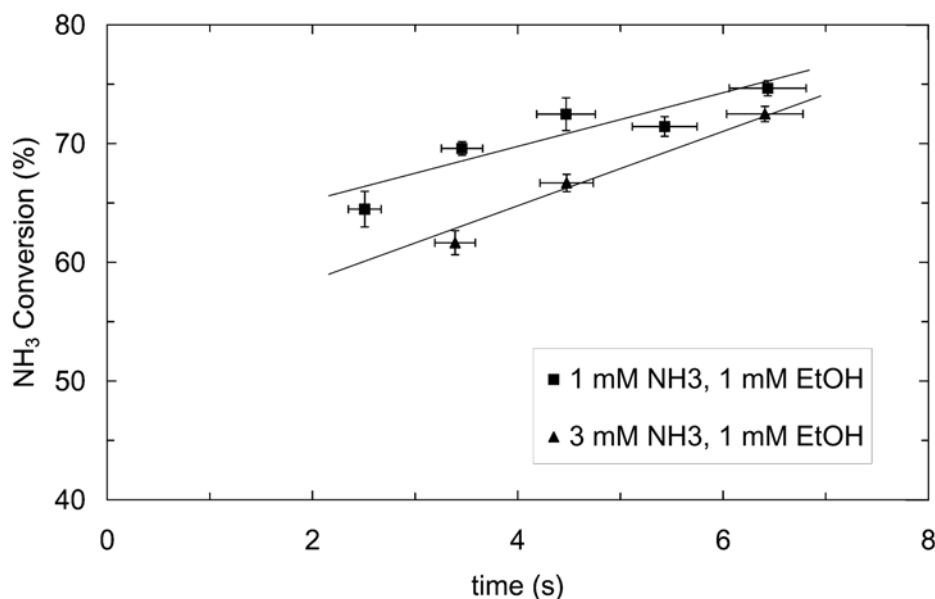


Figure 7-2: Ammonia conversion as a function of time for two different initial concentrations of ammonia.

$T = 701 \pm 4$ °C, $P = 243 \pm 3$ bar, $[\text{EtOH}]_0 = 0.97 \pm 0.02$ mM, and $\Phi = 1.00 \pm 0.05$.

Separating the effect of adding ethanol from the effect of adding oxygen for the stoichiometric oxidation of both ammonia and ethanol is complicated by the tendency towards reactor corrosion under conditions of excess oxygen and high temperatures. The only co-oxidation experiments which could be repeated without ethanol at the same ammonia and oxygen concentrations were Runs 12-14, which corresponded to an initial ethanol concentration of 0.1 mM. Figure 7-3 compares the ammonia conversion data for three experiments at $T = 700$ °C and $P = 246$ bar: $[\text{NH}_3]_0 = 1$ mM and $[\text{O}_2]_0 = 0.75$ mM ($\Phi = 1$), $[\text{NH}_3]_0 = 1$ mM and $[\text{O}_2]_0 = 1.05$ mM, ($\Phi = 0.73$), and $[\text{NH}_3]_0 = [\text{EtOH}]_0 = 1$ mM, $[\text{O}_2]_0 = 1.05$ mM ($\Phi = 1$). The co-oxidation enhancement of ethanol is approximately the same (~10%) as the enhancement gained when oxygen is added, which is consistent with what was seen for low concentrations of ethanol added to methylphosphonic acid (MPA) (Ploeger et al. 2006b).

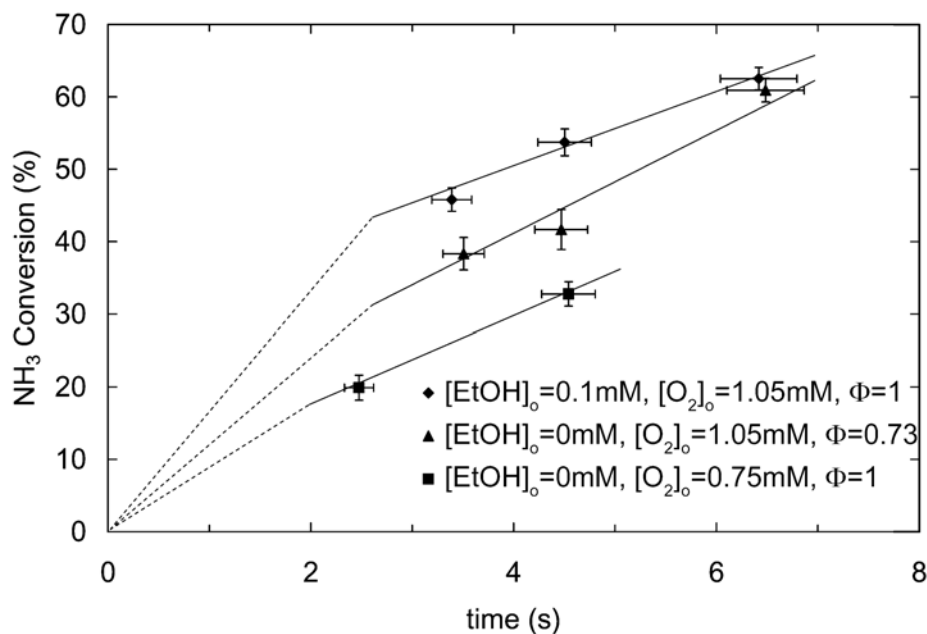


Figure 7-3: Ammonia conversion as a function of time for three different initial feed concentrations. $T = 700 \pm 4$ °C and $P = 243 \pm 1$ bar.

For the same three experiments, the effect of ethanol addition on product distribution is much more dramatic. Figure 7-4 shows the nitrous oxide fraction, defined as moles of nitrogen as N_2O in the effluent divided by moles of nitrogen as NH_3 in the feed, as a function of residence time for the same conditions as Figure 7-3. Adding oxygen has a small impact on N_2O formation, but the addition of ethanol causes the N_2O fraction to more than triple. The N_2O fraction remains constant over time for the ethanol co-oxidation data, which corroborates our theory that most of the co-oxidation enhancement is happening in the first two seconds of residence time. From 3.5 to 6.5 s, ammonia continues to oxidize, but it predominantly oxidizes to N_2 . Over time, this causes the N_2O yield, defined as moles of nitrogen as N_2O in the effluent divided by moles of nitrogen as NH_3 consumed in the reactor, to decrease as N_2O is diluted by additional N_2 .

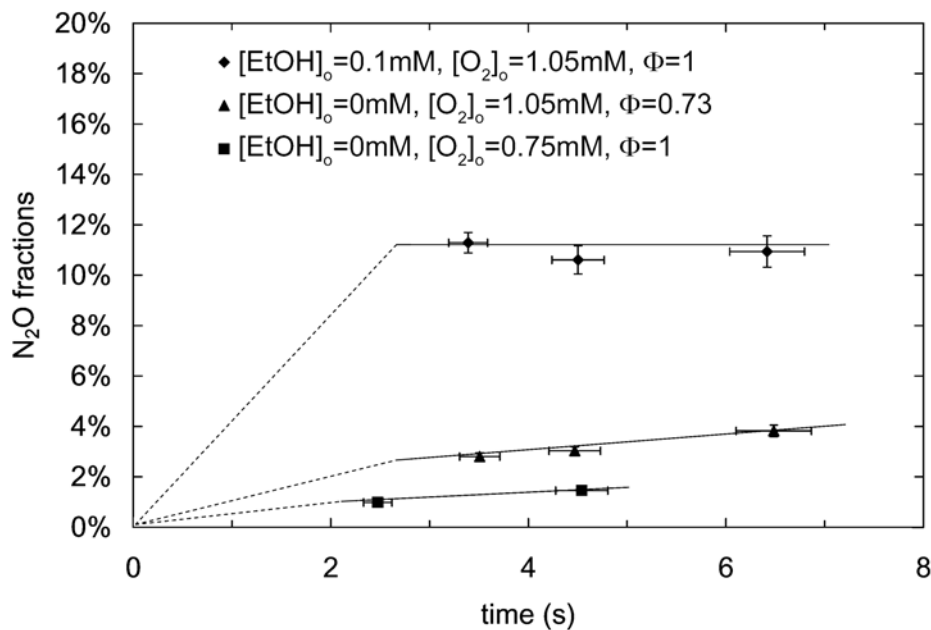


Figure 7-4: Nitrous oxide N fraction as a function of time for three different initial feed concentrations. $T = 700 \pm 4$ °C and $P = 243 \pm 1$ bar.

The effect of temperature on both ammonia conversion and N₂O yield was explored at $P = 246$ bar, $[\text{NH}_3]_0 = [\text{EtOH}]_0 = 1$ mM, and $\Phi = 1$. Figure 7-5 shows that conversion ranges from 50% at $T = 655$ °C to 65-75% at $T = 700$ °C, and at all three temperatures most of the co-oxidation enhancement occurs in the first two seconds. Figure 7-6 shows that for equimolar mixtures of ammonia and ethanol, very high N₂O yields are possible, up to 73% at $T = 680$ °C. As temperature increases, N₂O yield decreases to 30-40% at $T = 700$ °C. Previous studies have shown that matching product distributions is the most reliable method for validating elementary reaction rate mechanisms (Ploeger et al. 2006a), so the N₂O yield data will be key to the development of an ammonia-ethanol co-oxidation model.

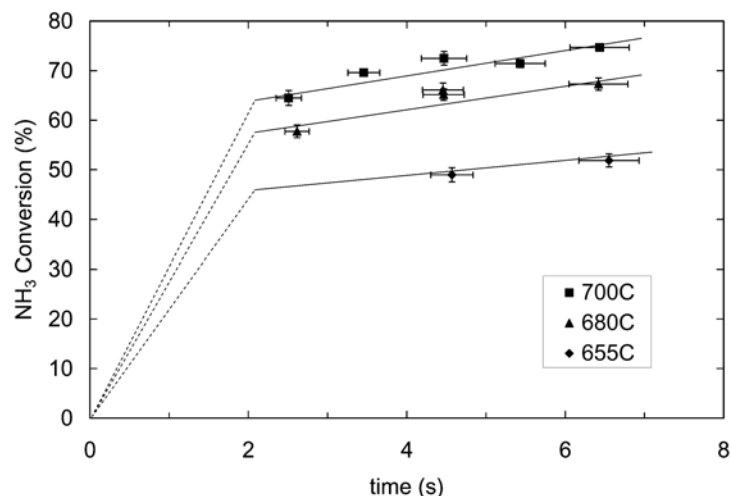


Figure 7-5: Ammonia conversion as a function of time for three different temperatures.
 $P = 243 \pm 3$ bar, $[\text{NH}_3]_0 = 1.00 \pm 0.08$ mM, $[\text{EtOH}]_0 = 0.97 \pm 0.04$ mM, and $\Phi = 0.97 \pm 0.03$.

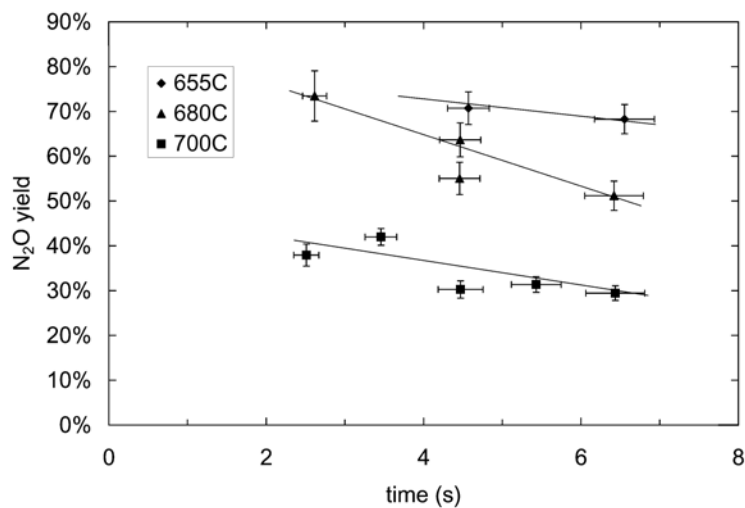


Figure 7-6: Nitrous oxide yield as a function of time for three different temperatures.
 $P = 243 \pm 3$ bar, $[\text{NH}_3]_0 = 1.00 \pm 0.08$ mM, $[\text{EtOH}]_0 = 0.97 \pm 0.04$ mM, and $\Phi = 0.97 \pm 0.03$.

7.2 CONCLUSIONS

Co-oxidation of ammonia with ethanol in supercritical water indicates that ethanol had a dramatic effect on both the rate of ammonia oxidation and the product distribution. For example, at a 2.5 s residence time and stoichiometric oxygen conditions, ammonia conversion increased from 20% to 65% when a molar equivalent of ethanol was added to the organic feed at $T =$

700°C, $P = 246$ bar, and $[\text{NH}_3]_0 = 1$ mM. Nitrous oxide yields for co-oxidation experiments ranged from 40% at $T = 700$ °C to over 70% at $T = 655$ °C and 680 °C, compared to yields between 4 and 13% for pure ammonia oxidation under similar conditions. The co-oxidation enhancement primarily occurred during the first 2 s of residence time, after which ammonia destruction proceeded more slowly and predominantly to form N_2 . These experimental observations will be used to guide the development of an elementary reaction rate mechanism for the co-oxidation of ammonia and ethanol in supercritical water in Chapter 8.

7.3 REFERENCES

- Dean, J. A. (1992). Lange's Handbook of Chemistry, McGraw-Hill, Inc.
- Ploeger, J. M., P. A. Bielenberg, J. L. DiNaro Blanchard, R. P. Lachance, J. D. Taylor, W. H. Green and J. W. Tester (2006a). "Modeling Oxidation and Hydrolysis Reactions in Supercritical Water - Free Radical Elementary Reaction Networks and Their Applications." Comb. Sci. Tech. 178(1-3): 363-398.
- Ploeger, J. M., P. A. Bielenberg, R. P. Lachance and J. W. Tester (2006b). "Co-oxidation of Methylphosphonic Acid and Ethanol in Supercritical Water: I. Experimental Results." J. Supercrit. Fluids accepted.

8 Elementary Reaction Rate Model for Ammonia-Ethanol Co-oxidation

In Chapter 7 we reported our experimental findings on the co-oxidation of ammonia and ethanol in supercritical water, detailing the effect of temperature and initial reactant concentrations on ammonia conversion and product distribution between nitrogen and nitrous oxide (N_2O). Here we use the experimental data as a guide for the development and validation of an ammonia-ethanol supercritical water co-oxidation model.

8.1 BACKGROUND AND MOTIVATION

Efforts to model the oxidation of ammonia are rare in comparison to modeling studies of hydrocarbon oxidation. The most comprehensive study of ammonia combustion was conducted by Dean and Bozzelli (2000), which cites several rates at $P = 10$ atm, but the authors emphasize that their mechanism, should not be considered complete or fully validated. Hughes and co-workers at Leeds University compiled a well-documented NO_x submechanism (2001) at typical combustion conditions of $P \leq 1$ atm, where NO_x refers to nitric oxide, NO , and nitrogen dioxide, NO_2 . Interest in the Thermal De NO_x system by which NO_x is reduced to N_2 by ammonia has spurred several studies of the reactions of ammonia and ammonia intermediates with nitrogen oxides, both at the mechanism and *ab initio* level.

8.2 MODEL DEVELOPMENT

A model for ammonia-ethanol co-oxidation was constructed using the MPA-ethanol co-oxidation mechanism developed in our group (Ploeger et al. 2006b) as a framework. An ammonia submechanism was added to our ethanol submechanism using rates from the Dean and Bozzelli ammonia combustion model (2000) and Hughes et al. NO_x submechanism (2001). Rates for the NO_3^\bullet radical species were added from Glarborg (1995), and rates for the reaction of

nitrogen oxides with carbon monoxide were added from Allen (1997). The high-pressure limited rate for the decomposition of N_2O was taken from Rörhig (1996).

8.3 ANALYSIS OF MODEL PREDICTIONS

The ammonia-ethanol co-oxidation mechanism does an adequate job of modeling the oxidation of pure ammonia in supercritical water. Figure 8-1 compares the predicted ammonia conversion profile to experimental data as a function of time at $T = 700$ °C, $P = 246$ bar, $[NH_3]_0 = 1$ mM and $\Phi = 1$. We see that the model underpredicts the conversion of ammonia significantly, with a predicted pseudo-first order rate constant approximately four times slower than the experimental value. Some of this must be attributed to the lack of heterogeneous oxidation rates in the mechanism since ammonia oxidation is known to have a significant surface-catalyzed component, but the degree of the underprediction suggests that some pathways for ammonia SCWO may be missing from the model. The model predicts that for pure ammonia oxidation the only products will be nitrogen and nitrous oxide with a N_2O yield between 1 and 2%, which agrees with the observed experimental values ranging from 4 to 5% at those conditions.

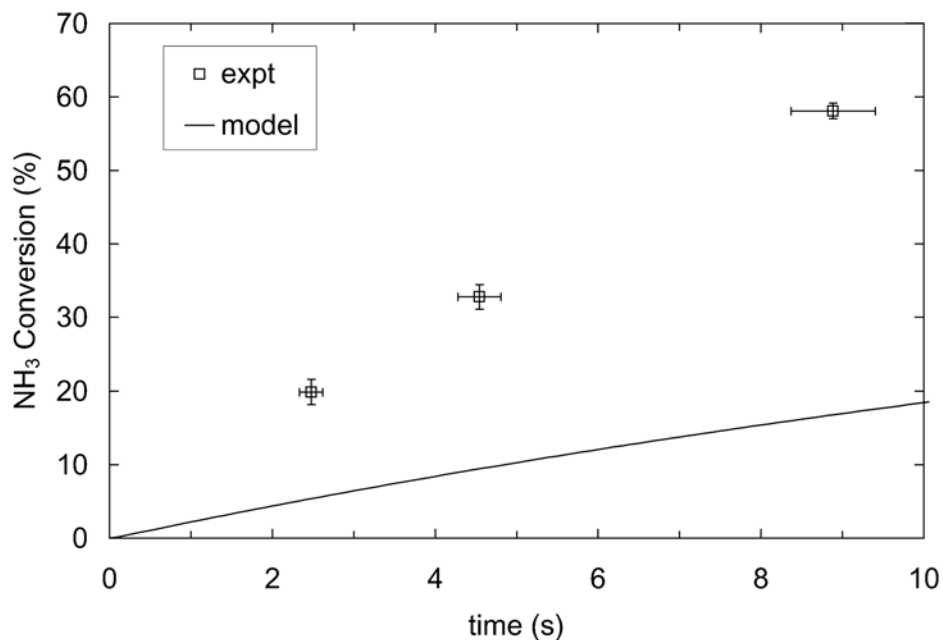


Figure 8-1: Comparison of experimental data to ammonia conversion profile predicted by initial ammonia-ethanol co-oxidation model.

$T = 700\text{ }^{\circ}\text{C}$, $P = 246\text{ bar}$, $[\text{NH}_3]_0 = 1\text{ mM}$, $\Phi = 1$.

Model predictions of ammonia conversions and N_2O yields for ammonia-ethanol co-oxidation are poor as shown in Figure 8-2. Although the predicted ammonia conversion profiles are closer to the experimental data, for three different temperatures the trend in ammonia conversion is in the wrong direction as compared to experimental observation. Furthermore, the predicted N_2O yield profiles are constant with respect to temperature at 20%, well below the experimentally observed values. Correcting these two inconsistencies were targeted in our efforts to improve the ammonia-ethanol co-oxidation model.

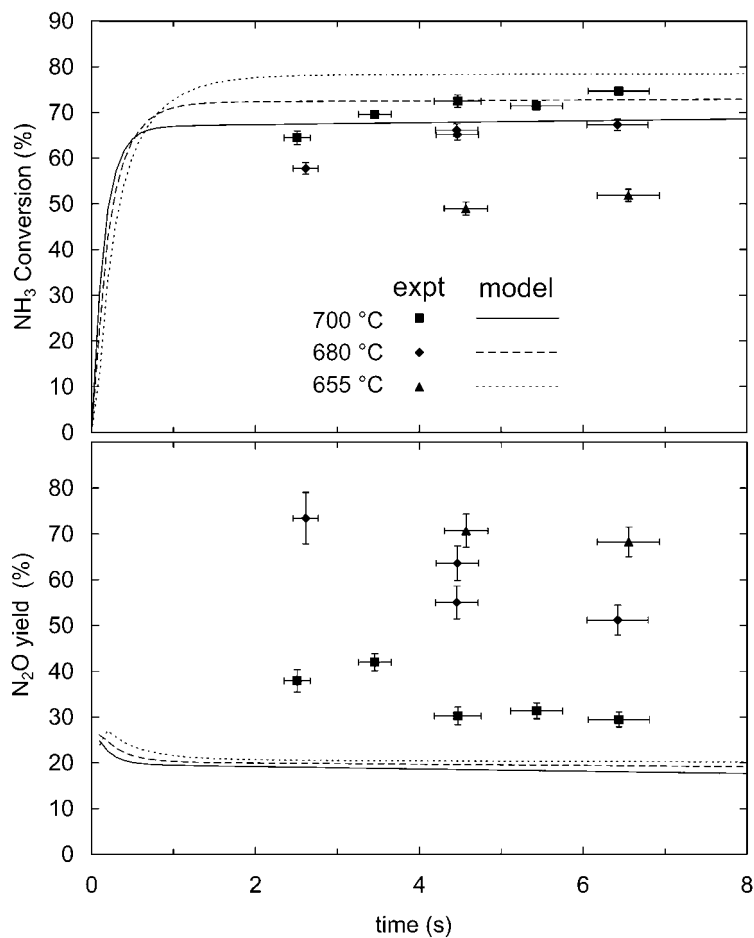


Figure 8-2: Comparison of experimental data to ammonia conversion and nitrous oxide yield profiles predicted by initial ammonia-ethanol co-oxidation model.

$P = 246 \text{ bar}$, $[\text{NH}_3]_0 = [\text{EtOH}]_0 = 1 \text{ mM}$, $\Phi = 1$.

The dominant pathways in the initial ammonia-ethanol mechanism are illustrated in

Figure 8-3.

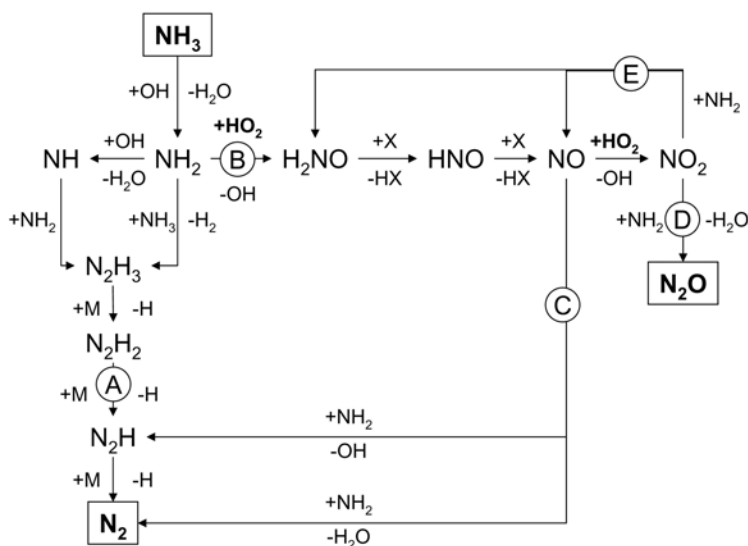


Figure 8-3: Major reaction pathways for initial ammonia-ethanol co-oxidation model.
Molar flux through labelled reaction pathways can be found in Table 8-1.

Table 8-1: Average molar fluxes in 10^{-6} mol/L/s through the major reaction pathways shown in Figure 8-3 for $P = 246$ bar, $\Phi = 1$, $\tau = 0-6.5$ s. Predicted using the $\text{NH}_2 + \text{NO}_x$ submechanism in Dean and Bozzelli (2001).

	Description	$T = 700$ °C [NH_3] ₀ = 1 mM [EtOH] ₀ = 1 mM	$T = 655$ °C [NH_3] ₀ = 1 mM [EtOH] ₀ = 1 mM	$T = 700$ °C [NH_3] ₀ = 1 mM [EtOH] ₀ = 0 mM
A	$\text{NH}_2 + \text{NH}_x \rightarrow \text{N}_2$	1.0	0.1	6.0
B	$\text{NH}_2 \rightarrow \text{NO}_x$	48.4	61.3	4.0
C	$\text{NH}_2 + \text{NO} \rightarrow \text{N}_2$	41.4	47.9	3.7
D	$\text{NH}_2 + \text{NO}_2 \rightarrow \text{N}_2\text{O}$	7.0	13.4	0.3
E	$\text{NH}_2 + \text{NO}_2 \rightarrow \text{H}_2\text{NO} + \text{NO}$	30.8	58.9	1.3

Ammonia oxidation is initiated by the hydrogen abstraction reaction

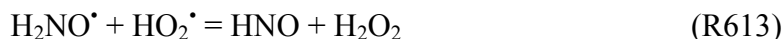


The NH_2^\bullet radical can undergo another hydrogen abstraction step to form NH^\bullet . These NH_x species can react to form a nitrogen-nitrogen bond, the dominant reactions being

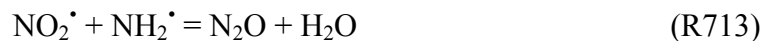
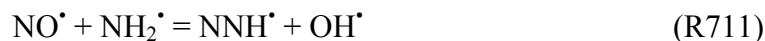


The $\text{N}_2\text{H}_3^\bullet$ radical loses three hydrogen atoms by hydrogen abstraction or decomposition to yield N_2 .

The other major pathway for NH_2^\bullet radicals is the NO_x -forming submechanism,



At the relatively low temperatures of SCWO, NO_x species are unstable; they are reduced by the NH_2^\bullet radical in the following reactions:



Because the HO_2^\bullet radical only participates in the NO_x -forming submechanism, we would expect those pathways to be favored in ammonia-ethanol co-oxidation. As can be seen in Table 8-1, the model also predicts the dominance of the NO_x submechanism under co-oxidation conditions. This is also supported by the experimental observation that N_2O , which is only produced from the NO_x submechanism, is produced in much higher concentrations when ammonia is co-oxidized with ethanol.

8.4 MODEL IMPROVEMENTS

In order to improve the model predictions for ammonia conversion and N_2O yield as a function of temperature, we focused on the $\text{NO}_x + \text{NH}_2^\bullet$ reactions. The relative rates of R712

and R713 have a particularly strong effect on both on the N₂O yield trend and the NH₃ conversion trend, because the former is chain propagating while the latter is chain terminating.

Previous experimental studies measuring NO_x + NH₂[•] rates, including the Park and Lin (1996; 1997) rates used by Dean and Bozzelli, were conducted at pressures below 0.01 bar. These low-pressure rates are suitable for combustion models, but are not expected to be accurate for oxidation at 250 bar. The NO_x + NH₂[•] reactions are expected to proceed through H₂NNO_x intermediate adduct species, which are more likely to be collision-stabilized at high pressures. These adducts can then undergo rearrangement, decomposition, and hydrogen abstraction. The H₂NNO_x adduct species have been the subject of *ab initio* studies to better understand the Thermal DeNO_x process, but the results have not yet been applied to SCWO conditions, which occur at lower temperatures, higher pressures and more dilute reactant concentrations. The explicit treatment of these adduct species will result in a more accurate prediction of ammonia-ethanol co-oxidation than using the low-pressure rates given in reactions R710-R713.

The reaction surface for the H₂NNO₂ adduct and rearrangement products was calculated using quantum chemical methods utilizing Gaussian 98 software with the CBS-Q method (Ochterski et al. 1996) and initial geometries from Mebel et al. (1995). The reaction surface for the H₂NNO adduct and rearrangement products was calculated using the same method and initial geometries from Diau and Smith (1997). Rates for the reaction and rearrangement of H₂NNO_x adducts were estimated using transition state theory with the Wigner correction to account for tunneling.

$$\frac{k_{corrected}}{k_{TST}} = 1 + \frac{1}{24} \left(\frac{hc\nu}{k_B T} \right) \quad (\text{Eqn. 8-1})$$

Radical recombination rates were set to 10¹³ M⁻¹s⁻¹ while the corresponding decomposition rates were calculated from the thermochemical parameters assuming microscopic reversibility.

The activation energy for each hydrogen abstraction rate was estimated using the method of Blowers and Masel (2000) which correlates the activation energy to the enthalpy of reaction with the following equation,

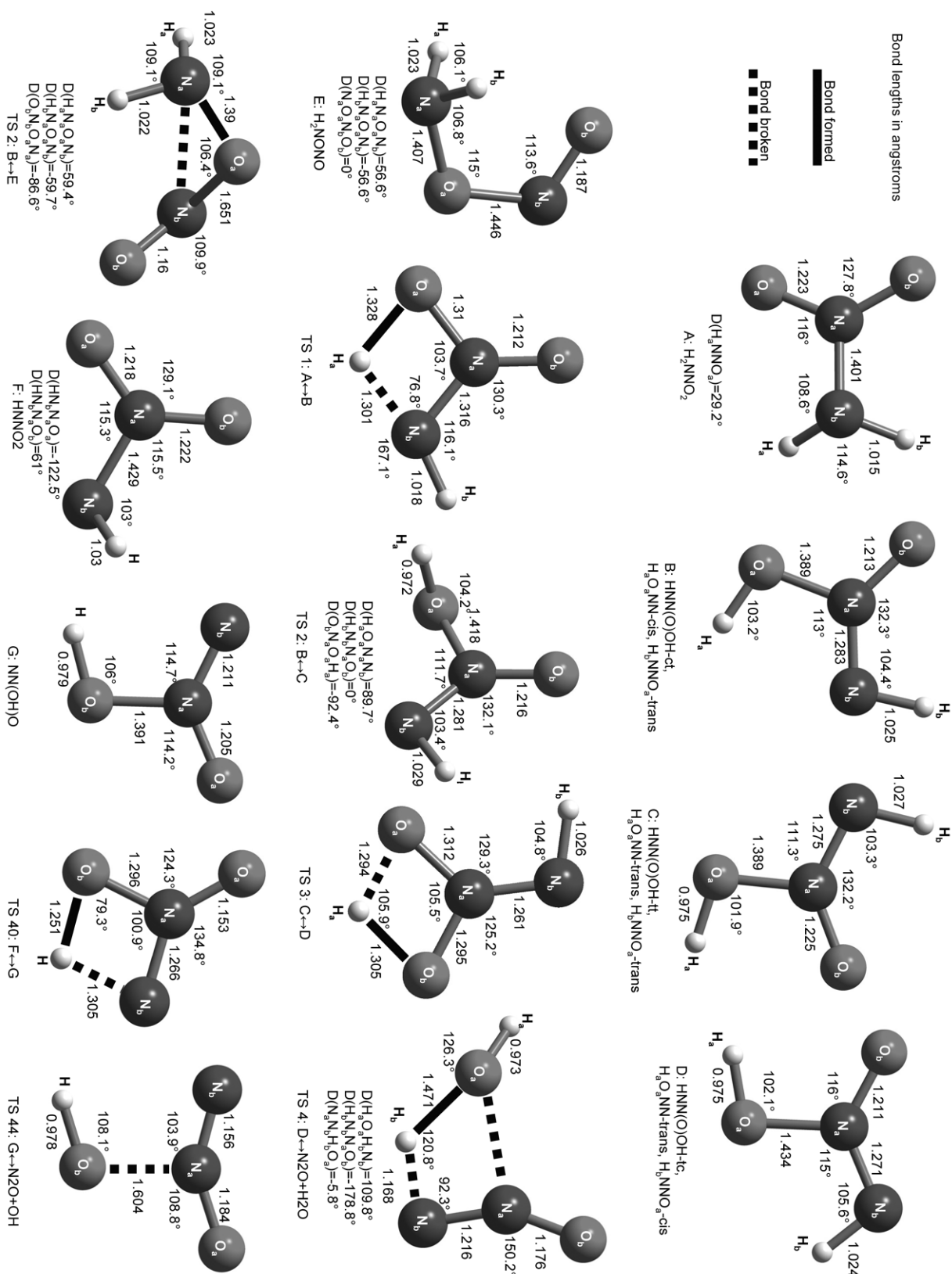
$$E_A = \begin{cases} 0, & \text{for } \Delta H_{rxn} < -4E_a^0 \\ \left(\frac{w_B + w_F + \Delta H_{rxn}}{2} \right) (V_p - w_B - w_F + \Delta H_{rxn})^2, & \text{for } -4E_a^0 < \Delta H_{rxn} < 4E_a^0 \\ \Delta H_{rxn}, & \text{for } \Delta H_{rxn} > 4E_a^0 \end{cases}, \text{ for } -4E_a^0 < \Delta H_{rxn} < 4E_a^0 \text{ (Eqn. 8-2)}$$

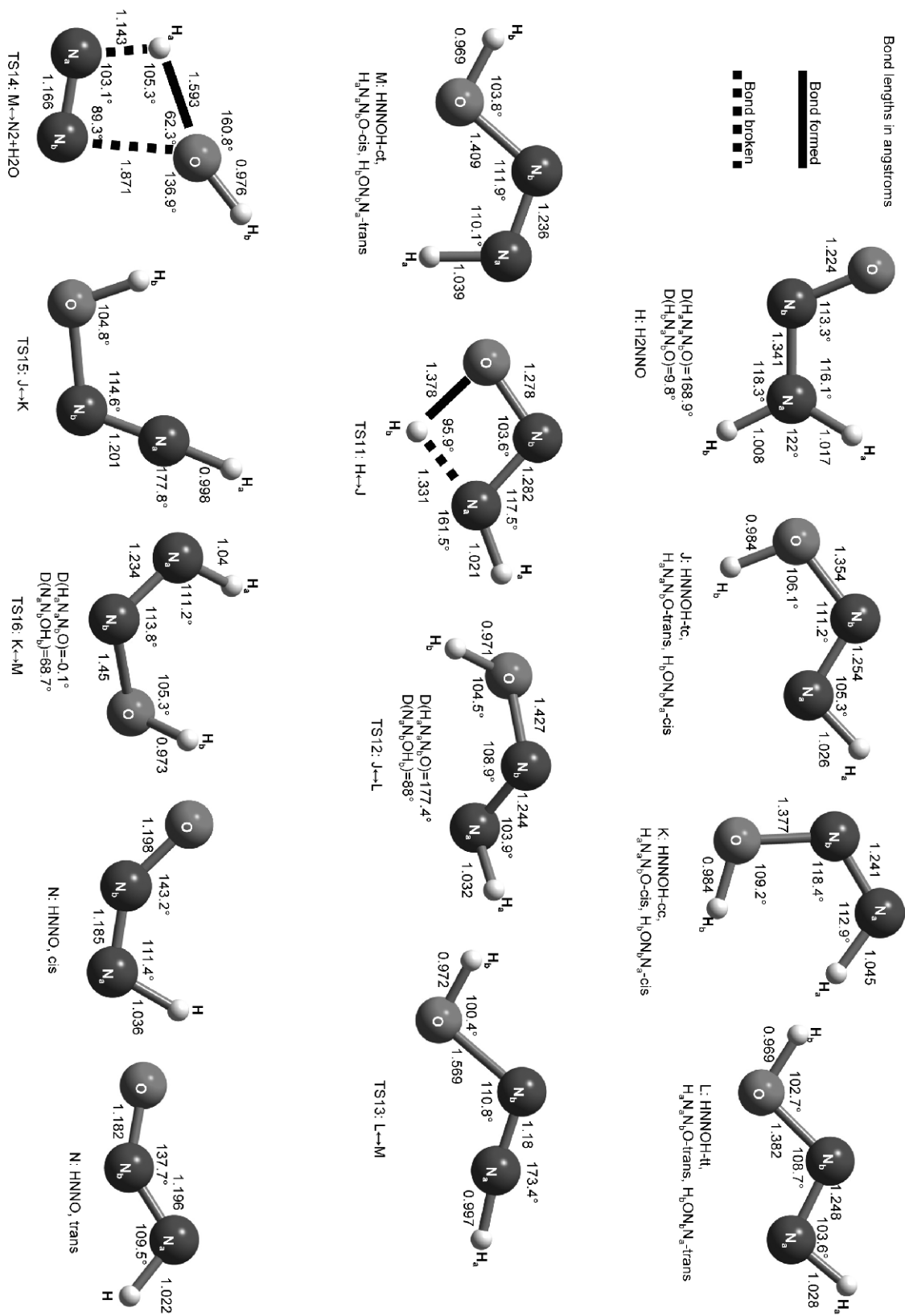
where w_B and w_F are the bond dissociation energies of the hydrogen bonds that are broken and formed, respectively. E_a^0 is an adjustable parameter which is set to 10 kcal/mol to provide the best fit for 151 independent hydrogen transfer reactions. V_p is defined as

$$V_p = (w_B + w_F) \frac{w_B + w_F + 2E_a^0}{w_B + w_F - 2E_a^0} \quad \text{(Eqn. 8-3)}$$

The prefactors for all hydrogen abstraction rates were set to a collision rate of $10^{13} \text{ M}^{-1} \text{ s}^{-1}$. The process was repeated for each H_2NNO_x species with OH^\bullet , HO_2^\bullet , O_2 , and NO_2^\bullet . Thermodynamic and kinetic parameters for the HNNO_2 species were calculated by the CBS-Q method using the initial geometries from the Mebel et al. study of the $\text{NO}_2^\bullet + \text{NH}^\bullet$ reaction surface (1994).

Thermochemical parameters for all stable structures and transition states were calculated and compared to literature values, when available. Heats of formation (ΔH_f^0) were calculated by the standard atomization method of Nicolaides et al. (1996) Ideal gas state entropies (S^0) and heat capacities (C_p^0) were calculated using the rigid rotor harmonic oscillator approximation, with harmonic vibrational frequencies scaled by the empirically derived factor of 0.91844. A summary of thermochemical parameters used in this study can be found in the Appendix.

Figure 8-4: Dominant NH_2+NO_2 adduct species and transition states

Figure 8-5: Dominant NH_2+NO adduct species and transition states

8.5 UPDATED AMMONIA-ETHANOL MECHANISM

The introduction of H_2NNO_x adduct species and reactions improved model predictions for ammonia-ethanol co-oxidation, as can be seen in Figure 8-6. The ammonia conversion profiles over the entire temperature range are within $\pm 1\%$ of each other, which is well within experimental error and so predicted ammonia conversion must be considered constant with respect to temperature. Although the model did not reproduce the experimentally observed trend, the prediction is strongly dependent on the rate of reaction



which is 10^{13} $\text{cm}^3/\text{mol}/\text{s}$ in the updated mechanism. For rates of reaction R455 less than 2×10^{12} $\text{cm}^3/\text{mol}/\text{s}$, more reaction flux traveled through the chain terminating, N_2O -forming pathways and the predicted ammonia conversion profiles increased with increasing temperature. We do not feel that these predictions should be used as justification for arbitrarily setting the rate of R455 to fit the predictions to the experimental data, rather we suggest that future modeling efforts focus on accurate estimation of rates for reaction R455.

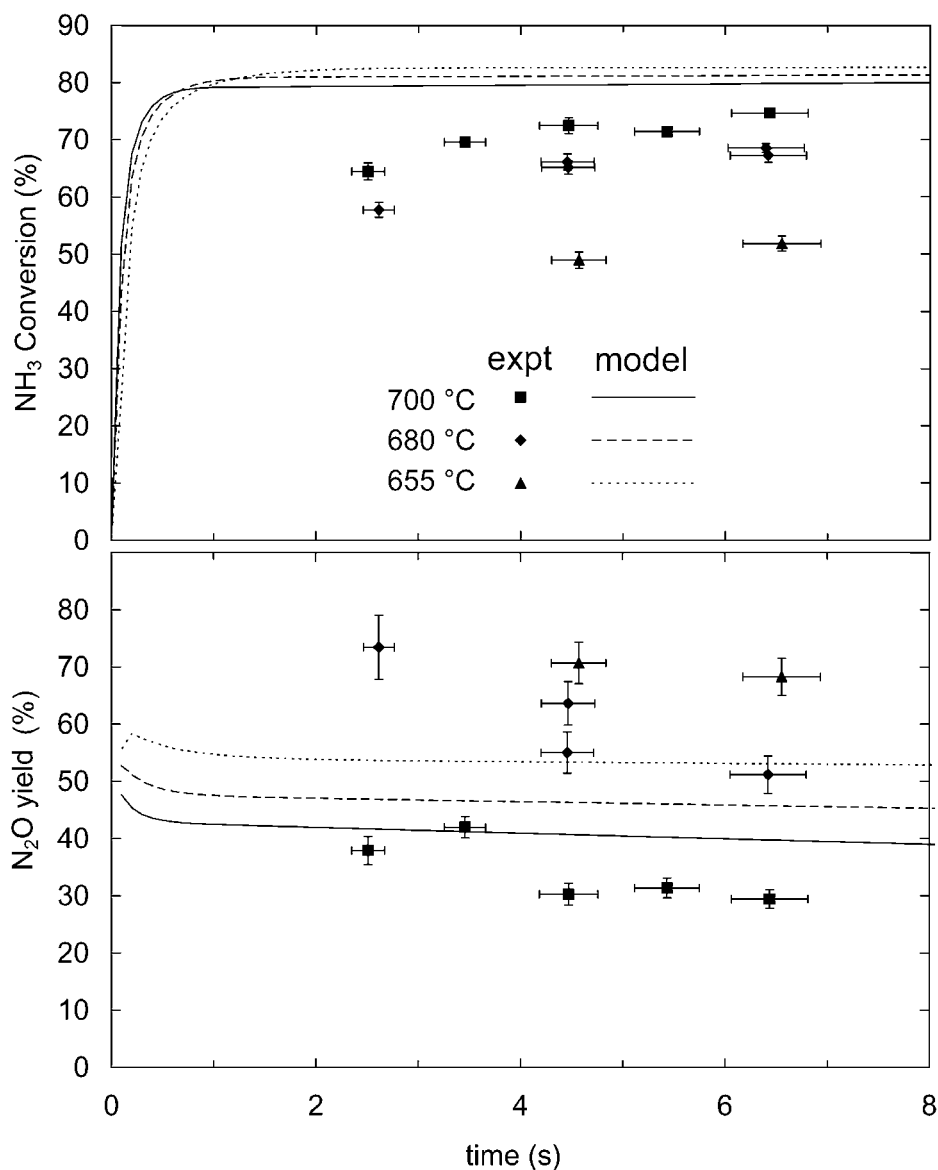


Figure 8-6: Comparison of experimental data to ammonia conversion and nitrous oxide yield profiles predicted by updated ammonia-ethanol co-oxidation model.

$P = 246 \text{ bar}$, $[\text{NH}_3]_0 = [\text{EtOH}]_0 = 1 \text{ mM}$, $\Phi = 1$.

The modified co-oxidation model shows marked improvement in predicting N_2O yields, as can be seen in Figure 8-6. The predicted N_2O yields are much closer to experimentally observed values and reproduce the experimental trend of decreasing yield with increasing temperature. Since matching experimental channel yields is a more reliable method of validating elementary reaction rate mechanisms (Ploeger et al. 2006a), we interpret the improved N_2O yield

predictions as confirmation that the updated ammonia-ethanol mechanism more accurately models the co-oxidation reaction.

The major change to the low-pressure NH_2+NO_x submechanism is in the H_2NNO_2 chemistry. As can be seen in Figure 8-7, the updated NH_2+NO_2 submechanism still has N_2O , H_2NO , and NO as the dominant products, but the branching ratio has changed. As temperature decreases, the net flux shifts from H_2NONO to H_2NNO_2 because the heat of reaction to form the latter is 20 kcal/mol lower. The decomposition reaction



is significantly slower at 655 °C than at 700 °C, which results in a higher net flux to form H_2NNO_2 at lower temperatures. The decomposition reaction for H_2NONO does not have as great a temperature dependence, so the branching ratio favors the N_2O -forming H_2NNO_2 adduct at lower temperatures. In addition, a pathway has been added that derives a significant fraction of N_2O from the hydrogen abstraction of H_2NNO_2 and subsequent rearrangement of the HNNO_2 species to form N_2O and OH^\bullet .

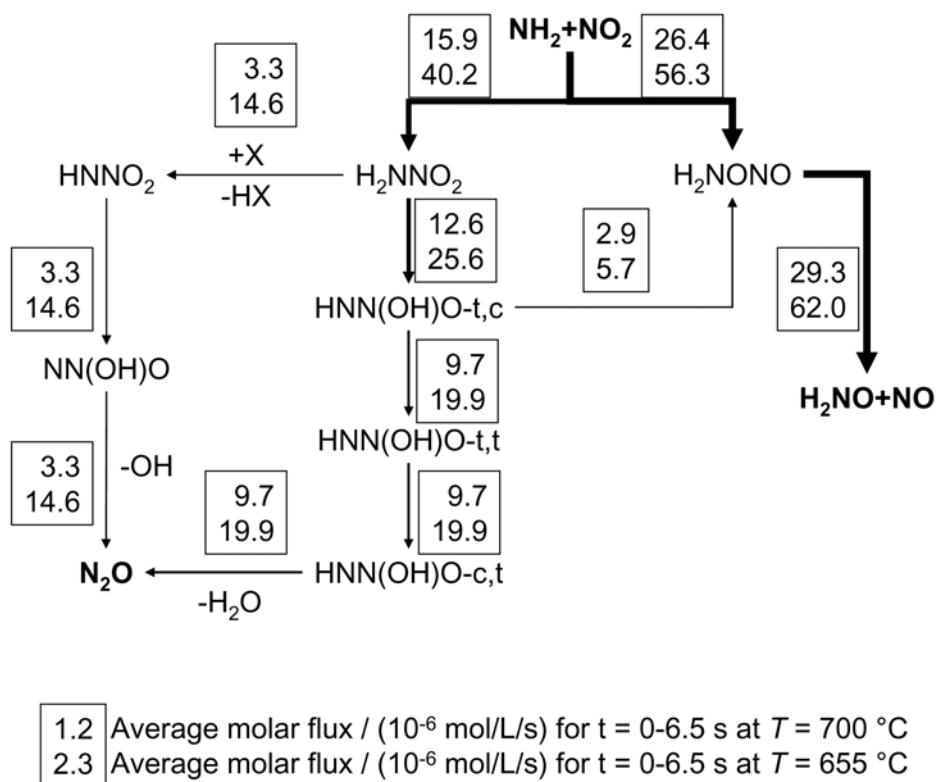


Figure 8-7: Major reaction pathways and molar fluxes for NH_2+NO_2 reaction network.
 $P = 246$ bar, $[\text{NH}_3]_0 = [\text{EtOH}]_0 = 1$ mM, $\Phi = 1$.

The H_2NNO adduct submechanism had a lesser impact on the model predictions. Figure 8-8 shows the updated NH_2+NO submechanism, where the primary pathways forming $\text{NNH}^\bullet+\text{OH}^\bullet$ and $\text{N}_2+\text{H}_2\text{O}$ are unchanged. The hydrogen abstraction pathways to form N_2O are insignificant at the conditions of interest in this study.

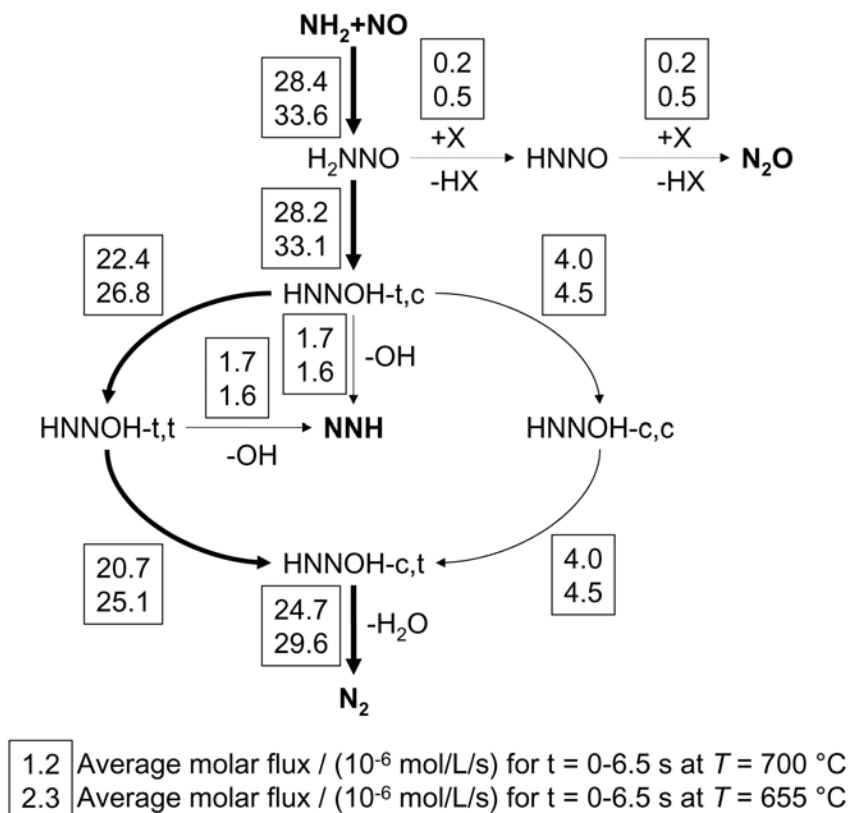


Figure 8-8: Major reaction pathways and molar fluxes for $\text{NH}_2 + \text{NO}$ reaction network.
 $P = 246\text{ bar}$, $[\text{NH}_3]_0 = [\text{EtOH}]_0 = 1\text{ mM}$, $\Phi = 1$.

The major pathways for the updated ammonia-ethanol mechanism are shown in Figure 8-9, and the net reaction fluxes are listed in Table 8-2. The dominance of the NO_x submechanism under co-oxidation conditions is similar to the findings in the original model, but the branching ratios have shifted to favor increased N_2O formation, particularly at lower temperatures.

the peak concentration of HO_2^\bullet radicals by three orders of magnitude. For co-oxidation of 1 mM ethanol and 1 mM ammonia, at $T = 700^\circ\text{C}$, the HO_2^\bullet concentration decreases more rapidly than at $T = 655^\circ\text{C}$ due to the faster rate of the recombination reaction,



The average concentration of HO_2^\bullet is higher at $T = 655^\circ\text{C}$ than at $T = 700^\circ\text{C}$ for this reason, which results in a greater shift towards N_2O formation and roughly equal ammonia conversion.

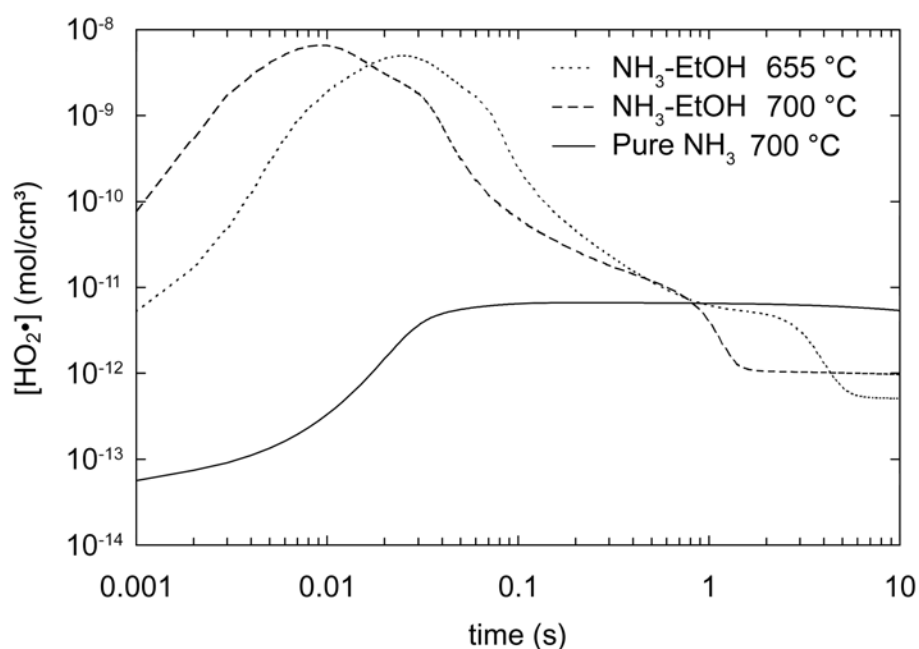


Figure 8-10: Predicted HO_2^\bullet concentration profiles for three initial conditions: $T = 655^\circ\text{C}$, $[\text{NH}_3]_0 = [\text{EtOH}]_0 = 1\text{ mM}$; $T = 700^\circ\text{C}$, $[\text{NH}_3]_0 = [\text{EtOH}]_0 = 1\text{ mM}$; and $T = 700^\circ\text{C}$, $[\text{NH}_3]_0 = 1\text{ mM}$. $P = 246\text{ bar}$ and $\Phi = 1$ for all three simulations.

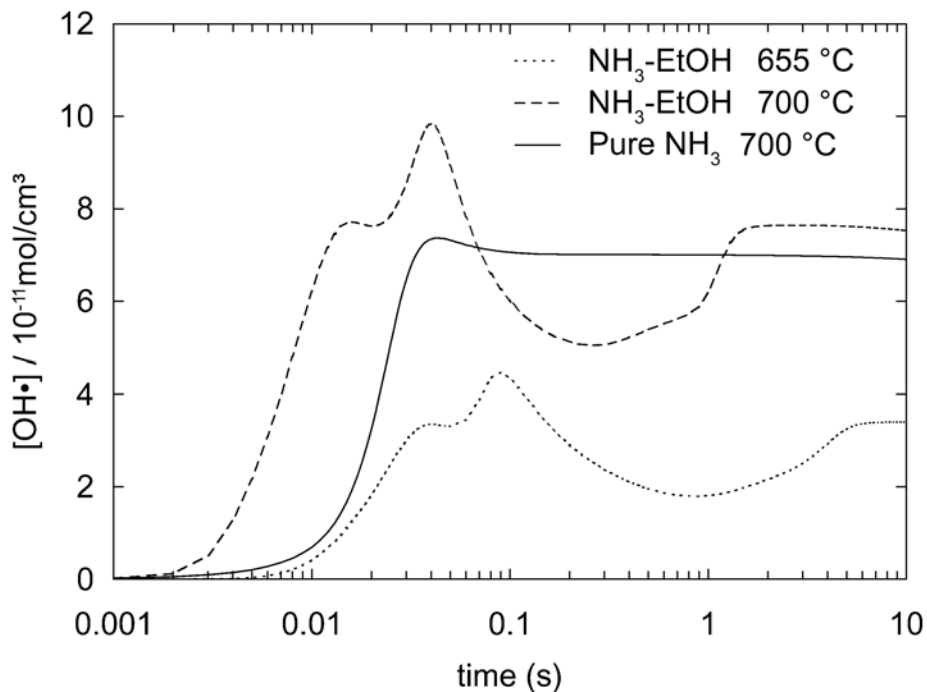


Figure 8-11: Predicted OH• concentration profiles for three initial conditions: $T = 655$ °C, $[\text{NH}_3]_0 = [\text{EtOH}]_0 = 1$ mM; $T = 700$ °C, $[\text{NH}_3]_0 = [\text{EtOH}]_0 = 1$ mM; and $T = 700$ °C, $[\text{NH}_3]_0 = 1$ mM. $P = 246$ bar and $\Phi = 1$ for all three simulations.

8.6 CONCLUSIONS

An ammonia-ethanol supercritical water co-oxidation model was constructed using submechanisms and rates from Dean and Bozzelli (2000), Hughes et al. (2001), Glarborg et al. (1995), Allen et al. (1997), Röhrig et al. (1996), and Ploeger et al. (2006b). The initial mechanism poorly reproduced the ammonia conversion and nitrous oxide trends as a function of temperature. This was attributed to the use of a low-pressure $\text{NH}_2 + \text{NO}_x$ submechanism which did not account for the stabilization of H_2NNO_x adduct species. Thermochemical and kinetic parameters for the $\text{NH}_2 + \text{NO}_2$ reaction were estimated quantum chemically using the CBS-Q method with initial geometries from the work of Mebel et al. (1995). Parameters for the $\text{NH}_2 + \text{NO}$ reaction were calculated using the same method and initial geometries from Diau and Smith (1997). The explicit treatment of the H_2NNO_x adduct species resulted in nitrous oxide

yield predictions that correctly reproduced experimental trends. The identification of the NO_x submechanism as an area needing improvement in the co-oxidation model demonstrates the value of co-oxidation as another means of interrogating an SCWO mechanism in addition to varying the experimental variables of temperature, pressure, and reactant concentrations. If only pure ammonia oxidation data were used to verify the model, the NO_x submechanism would not have been identified as inadequate.

The inability of the modified co-oxidation model to correctly reproduce the experimentally observed ammonia conversion trend as a function of temperature shows that the ammonia-ethanol co-oxidation model requires further improvement. The rates of the radical recombination reactions that form the H_2NNO_x adducts impart a strong effect on the ammonia conversion trends, and a detailed analysis using an *ab initio* method such as QRRK would provide a more accurate estimation for those rates. In addition, ammonia-ethanol co-oxidation experiments in reactors with different surface to volume ratios are needed to determine the importance of heterogeneous oxidation rates in the co-oxidation model.

8.7 REFERENCES

- Allen, M. T., Y. R.A. and F. L. Dryer (1997). "High Pressure Studies of Moist Carbon Monoxide / Nitrous Oxide Kinetics." *Combustion and Flame* 109: 449-470.
- Blowers, P. and R. Masel (2000). "Engineering Approximations for Activation Energies in Hydrogen Transfer Reactions." *AIChE J* 46(10): 2041-2052.
- Dean, A. M. and J. W. Bozzelli (2000). *Combustion Chemistry of Nitrogen. Gas-Phase Combustion Chemistry*. W. C. Gardiner Jr., Springer: 125-341.
- Diau, E. G. W. and S. C. Smith (1997). "Theoretical investigation of the potential energy surface for the $\text{NH}_2 + \text{NO}$ reaction via density functional theory and *ab initio* molecular electronic structure theory." *J. Chem. Phys.* 106(22): 9236-9251.
- Glarborg, P., K. Dam-Johansen and J. A. Miller (1995). "The Reaction of Ammonia with Nitrogen Dioxide in a Flow Reactor: Implications for the $\text{NH}_2 + \text{NO}_2$ Reaction." *Int. J. Chem. Kinet.* 27: 1207-1220.

- Hughes, K. J., A. S. Tomlin, E. Hampartsoumian, W. Nimmo, I. G. Zsély, M. Ujvári, T. Turányi, A. R. Clague and M. J. Pilling (2001). "An Investigation of Important Gas Phase Reactions of Nitrogen Species from the Simulation of Bulk Experimental Data in Combustion Systems." *Combust. Flame* 124: 573-589.
- Mebel, A. M., C. C. Hsu, M. C. Lin and K. Morokuma (1995). "An ab initio molecular orbital study of potential energy surface of the NH_2+NO_2 reaction." *J. Chem. Phys.* 103(13): 5640-5649.
- Mebel, A. M., K. Morokuma and M. C. Lin (1994). "Ab initio molecular orbital study of potential energy surface for the $\text{NH} + \text{NO}_2$ reaction." *J. Chem. Phys.* 101(5): 3916-3922.
- Nicolaides, A., A. Rauk, M. N. Glukhovtsev and L. Radom (1996). "Heats of formation from G2, G2(MP2), and G2(MP2,SVP) total energies." *J. Phys. Chem.* 100(44): 17460-17464.
- Ochterski, J. W., G. A. Petersson and J. A. Montgomery (1996). "A complete basis set model chemistry .5. Extensions to six or more heavy atoms." *J. Chem. Phys.* 104(7): 2598-2619.
- Park, J. and M. C. Lin (1996). "Direct Determination of Product Branching for the $\text{NH}_2 + \text{NO}$ Reaction at Temperatures between 302 and 1060 K." *J. Phys. Chem.* 100: 3317-3319.
- Park, J. and M. C. Lin (1997). "A Mass Spectrometric Study of the $\text{NH}_2 + \text{NO}_2$ Reaction." *J. Phys. Chem. A* 101: 2643-2647.
- Ploeger, J. M., P. A. Bielenberg, J. L. DiNaro Blanchard, R. P. Lachance, J. D. Taylor, W. H. Green and J. W. Tester (2006a). "Modeling Oxidation and Hydrolysis Reactions in Supercritical Water - Free Radical Elementary Reaction Networks and Their Applications." *Comb. Sci. Tech.* 178(1-3): 363-398.
- Ploeger, J. M., W. H. Green and J. W. Tester (2006b). "Co-oxidation of Methylphosphonic Acid and Ethanol in Supercritical Water: II. Elementary Reaction Rate Model." *J. Supercrit. Fluids* accepted.
- Röhrig, M., E. L. Petersen, D. F. Davidson and R. K. Hanson (1996). "The Pressure Dependence of the Thermal Decomposition of N_2O ." *Int. J. Chem. Kinet.* 28: 599-608.

9 Conclusions

Co-oxidative rate enhancement, which is known to occur during the oxidation of real, mixed waste streams in supercritical water, was well-characterized for two model systems. The first phase of the thesis studied the co-oxidation of a model refractory compound, methylphosphonic acid (MPA), with a model labile compound, ethanol, using a combined experimental and modeling approach to determine the effect that the labile co-oxidant had on the free radical pool. The co-oxidative rate enhancement was found to be caused primarily by an increase in the concentration of hydroperoxy (HO_2^*) radicals. The second phase involved another model system with ammonia as the refractory compound and ethanol. The understanding of co-oxidation gained in the first phase was used to develop and improve an elementary reaction rate model for ammonia-ethanol co-oxidation in supercritical water.

MPA-Ethanol Co-oxidation Experiments

Experimental data were taken at two temperatures ($T = 473\text{ }^\circ\text{C}$ and $528\text{ }^\circ\text{C}$) for organic feedstreams with initial concentrations ranging from $[\text{MPA}]_0 = 0.1$ to 1.0 mM and $[\text{EtOH}]_0 = 0$ to 2.4 mM . MPA conversion was found to increase with decreasing $[\text{MPA}]_0$ and increasing $[\text{EtOH}]_0$. At $T = 528\text{ }^\circ\text{C}$, MPA conversions measured at $[\text{EtOH}]_0 = 0.1\text{ mM}$ were identical to those measured without ethanol present, and at $T = 473\text{ }^\circ\text{C}$, concentrations of ethanol at $[\text{EtOH}]_0 = 0.3\text{ mM}$ and 0.1 mM were found to have no measurable effect on MPA conversion. These findings indicated that co-oxidation enhancement is only significant when the molar concentration of labile compound was at least on the same order of magnitude as the concentration of refractory compound. At both temperatures studied, the co-oxidation effect was more pronounced at shorter residence times. The effect of $[\text{MPA}]_0$ on MPA conversion at both T

= 473 °C and 528 °C indicated that MPA consumed a significant portion of the free radical pool generated by ethanol oxidation in supercritical water.

MPA-Ethanol Co-oxidation Model

An MPA-ethanol mechanism was constructed from an MPA submechanism developed in our group by Sullivan and an ethanol submechanism developed earlier at Sandia National Laboratories by Rice and Croiset. It was found that ethanol and most other labile hydrocarbons generate a free radical pool by a simple cycle of hydrogen abstraction to form a reactive hydrocarbon radical, followed by the reaction of that radical with oxygen to form the hydroperoxy radical (HO_2^\bullet) and another stable hydrocarbon. The dominant method of chain branching occurred when HO_2^\bullet abstracted a hydrogen off of a stable hydrocarbon, typically an alcohol or aldehyde, and formed H_2O_2 which decomposes to form 2OH^\bullet . These reactions can be summarized as a six-reaction mechanism which highlights the similarities of labile oxygenated hydrocarbons as they generate a free radical pool.

The co-oxidation model overpredicted the increase in MPA conversion when ethanol was added, but the predicted MPA conversion values were highly sensitive to key rate parameters involving the radical precursor H_2O_2 . The model predicted that the introduction of 2.4 mM ethanol to 1.0 mM MPA caused a 16-fold increase in HO_2^\bullet concentration, but only a 2-fold increase in OH^\bullet concentration. In order to validate this prediction experimentally, we used product distributions rather than MPA conversions. Methane was chosen as a tracer for OH^\bullet concentration since it was only formed from MPA when it reacts with OH^\bullet . An experiment was designed using formaldehyde and methanol as a co-oxidant which showed that the increase in MPA conversion was much greater than the increase in methane carbon fraction, which indicated

that the increase in HO_2^\bullet concentration was much greater than the increase in OH^\bullet concentration, thus confirming the co-oxidation model predictions. The change in the composition of the free radical pool that occurs during co-oxidation will alter the oxidation mechanism of the refractory compound, favoring pathways that include reactions with the HO_2^\bullet radical.

Ammonia Experiments

The oxidation of ammonia in supercritical water was studied in two reactor systems, the plug flow and batch cell. Global rate laws for each reactor system were fit that were first-order in ammonia. The plug flow data served to update the study by Webley (1991) in our group, which was conducted on a reactor system with poor preheating and temperature measurement. By applying the global rate law for this study to the original Webley data, the actual temperature was estimated to be 30 °C lower than the reported temperature. This is consistent with the 26 °C temperature correction that Tester et al. (1993) estimated for the temperatures reported in the methanol oxidation study on the same reactor system that Webley used. The plug flow data were also used as a baseline in the ammonia-ethanol experimental study detailed in Chapter 7. The rate of ammonia oxidation was found to be significantly slower in the batch reactor than in the plug flow reactor, which was attributed to the lower S/V ratio of the batch cell. Ongoing work utilizing the batch cell seeks to determine effect of S/V ratio by developing a batch reactor that can be charged with a known quantity of metal particles.

Ammonia-Ethanol Co-oxidation Experiments

Experimental data were taken over a temperature range from 655 to 705 °C at a pressure of 246 bar, initial ammonia concentrations ranging from 1 to 3 mM, and initial ethanol

concentrations ranging from 0 to 1 mM. Co-oxidation of ammonia with ethanol in supercritical water indicated that ethanol had a dramatic effect on both the rate of ammonia oxidation and the product distribution. For example, at a 2.5 s residence time and stoichiometric oxygen conditions, ammonia conversion increased from 20% to 65% when a molar equivalent of ethanol was added to the organic feed at $T = 700^\circ\text{C}$, $P = 246$ bar, and $[\text{NH}_3]_0 = 1$ mM. Nitrous oxide yields for co-oxidation experiments ranged from 40% at $T = 700^\circ\text{C}$ to over 70% at $T = 655^\circ\text{C}$ and 680°C , compared to yields between 4 and 13% for pure ammonia oxidation under similar conditions. The co-oxidative rate enhancement primarily occurred during the first 2 s of residence time, after which ammonia destruction proceeded more slowly and predominantly to form N_2 , which suggests that after a brief initial co-oxidation period, ethanol has no effect on ammonia oxidation after 2 s.

Ammonia-Ethanol Co-oxidation Model

An ammonia-ethanol supercritical water co-oxidation model was constructed using submechanisms and rates from Dean and Bozzelli (2000), Hughes et al. (2001), Glarborg et al. (1995), Allen et al. (1997), and Röhrig et al. (1996) with the ethanol submechanism developed in Chapter 5. The initial mechanism poorly reproduced the ammonia conversion and nitrous oxide trends as a function of temperature detailed in Chapter 7. This was attributed to the use of a low-pressure NH_2+NO_x submechanism which did not account for the stabilization of H_2NNO_x adduct species. Thermochemical and kinetic parameters for the NH_2+NO_2 reaction were estimated quantum chemically using the CBS-Q method with initial geometries from the work of Mebel et al. (1995). Parameters for the NH_2+NO reaction were calculated using the same method and initial geometries from Diau and Smith (1997). The explicit treatment of the H_2NNO_x adduct

species resulted in nitrous oxide yield predictions that correctly reproduced experimental trends. The identification of the NO_x submechanism as an area needing improvement in the co-oxidation model demonstrated the value of co-oxidation as another means of interrogating an SCWO mechanism in addition to varying the experimental variables of temperature, pressure, and reactant concentrations. If solely pure ammonia oxidation data were used to verify the model, the NO_x submechanism would not have been identified as inadequate.

10 Recommendations

A mechanistic understanding of co-oxidation was developed for two model systems that stressed the effect of increasing HO_2^\bullet concentration on the rate of oxidation and product distribution. However, for both the ammonia-ethanol and MPA-ethanol systems, the rate enhancement effect was overestimated, and in the case of ammonia-ethanol, the correct trend in ammonia conversion as a function of temperature could not be reproduced. Furthermore, the predicted rate of pure ammonia oxidation in supercritical water was underestimated by a factor of four. The following recommendations would help to improve the accuracy of the co-oxidation models developed in this thesis.

- 1) **Perform a more detailed *ab initio* study of NH_2+NO_2 adduct formation.** As determined in Chapter 8, the explicit treatment of NH_2+NO_2 adducts was key to improving the product distribution model predictions for ammonia-ethanol co-oxidation. The rate of formation for H_2NNO_2 and H_2NONO were both estimated to be about equal to the collision rate ($10^{13} \text{ cm}^3/\text{mol s}$) as a first-order approximation. The predicted ammonia conversion profiles were also strongly dependent on the rate of NH_2+NO_2 adduct formation, particularly the H_2NONO species. A more rigorous estimation method, such as QRRK, would lead to more accurate model predictions for both product distribution and ammonia conversion. Estimated rates for the hydrogen abstraction of H_2NNO_x adducts showed that some hydrogen abstraction pathways could be significant routes to form N_2O . These rates could be more accurately estimated using transition state theory, and could improve the accuracy of N_2O yield predictions.
- 2) **Construct a variable-S/V ratio batch reactor.** The oxidation of ammonia has a significant heterogeneous, wall-catalyzed component. Due to the difficulties of building,

installing, and operating reactors with different surface-to-volume (S/V) ratios, most studies on the effect of S/V ratio on the rate of ammonia oxidation have been limited to two or three different values of S/V, typically varying by less than a factor of 3. A batch reactor with a 1/2 to 1 in. O.D. high pressure port would allow the packing of the reactor with metal beads to achieve a wide range of S/V ratios of up to 2 orders of magnitude with much less difficulty. In addition to testing the hypothesis that the rate of ammonia oxidation is a linear function of S/V ratio, a reactor with variable S/V ratio could determine if there is a heterogeneous component of co-oxidative rate enhancement. It has been hypothesized that overpredicted oxidation rates could be explained by a missing wall-catalyzed radical termination reaction. If that is the case, co-oxidative rate enhancement would decrease as S/V increases.

3) Explore more mixed-feed systems across a range of temperatures and

concentrations. Co-oxidation was studied near both extremes of the typical SCWO temperature range. Other well-characterized compounds such as benzene and methane could serve as model refractory compounds. The use of an isotopic labeled organic compound where carbon atoms have been replaced by C-13 or C-14 isotopes could be used to trace the co-oxidative effect on product distribution for both the labile and refractory compound. This would permit the measurement of CO and CO₂ yields for both the refractory and labile model compounds, in the typical case when both contain carbon. More data on product distribution would assist in model development and improve the quantitative understanding of co-oxidative enhancement.

11 Appendix

Table 11-1: H₂/O₂ SCWO submechanism. Units are in kcal, cm, mol, s.

#	Reaction	A	n	E _a	Ref.
1	H ₂ +O=OH+H	5.12E+04	2.7	6278	a
2	H ₂ O+H=H ₂ +OH	4.52E+08	1.6	18423	a
3	O ₂ +H=HO ₂	2.07E+18	-1.7	890	a
4	O ₂ +H=OH+O	9.76E+13	0	14845	a
5	H ₂ O ₂ +H=HO ₂ +H ₂	1.69E+12	0	3755	a
6	H ₂ O ₂ +H=OH+H ₂ O	1.02E+13	0	3578	a
7	H ₂ O ₂ +O=OH+HO ₂	6.62E+11	0	3975	a
8	H ₂ O ₂ +OH=H ₂ O+HO ₂	7.83E+12	0	1331	b
9	OH+OH=H ₂ O ₂	2.96E+28	-5.3	2980	a
10	H+H+M=H ₂ +M Enhancement factor: O ₂ 0.4/CO 0.75/CO ₂ 1.5/H ₂ O 6.5/CH ₄ 3.0	1.87E+18	-1	0	a
11	H+H+H ₂ =H ₂ +H ₂	9.79E+16	-0.6	0	a
12	H+O+M=OH+M Enhancement factor: O ₂ 0.4/CO 0.75/CO ₂ 1.5/H ₂ O 6.5/CH ₄ 3.0	1.18E+19	-1	0	a
13	H+OH+M=H ₂ O+M Enhancement factor: O ₂ 0.4/CO 0.75/CO ₂ 1.5/H ₂ O 6.5/CH ₄ 3.0	5.53E+22	-2	0	a
14	H+HO ₂ =H ₂ +O ₂	4.28E+13	0	1410	a
15	H+HO ₂ =OH+OH	1.69E+14	0	875	a
16	H+HO ₂ =H ₂ O+O	3.01E+13	0	1721	a
17	O+O+M=O ₂ +M Enhancement factor: O ₂ 0.4/CO 0.75/CO ₂ 1.5/H ₂ O 6.5/CH ₄ 3.0	5.40E+13	0	-1788	a
18	O+HO ₂ =O ₂ +OH	3.19E+13	0	0	a
19	OH+OH=O+H ₂ O	1.51E+09	1.1	100	a
20	OH+HO ₂ =H ₂ O+O ₂	1.91E+16	-1	0	a
21	HO ₂ +HO ₂ =H ₂ O ₂ +O ₂	4.22E+14	0	11984	a
22	Duplicate	1.32E+11	0	-1630	

a) Sullivan et al. (2004a); b) Baulch et al. (1994)

Table 11-2: C₂ SCWO submechanism. Units are in kcal, cm, mol, s.

#	Reaction	A	n	E _a	Ref.
23	CH ₄ +O ₂ =CH ₃ +HO ₂	3.97E+13	0	56892	a
24	CH ₄ +H=CH ₃ +H ₂	1.32E+04	3	8038	a
25	CH ₄ +CH ₂ =CH ₃ +CH ₃	4.30E+12	0	10038	a
26	CH ₄ +CH ₂ (S)=CH ₃ +CH ₃	7.00E+13	0	0	a
27	CH ₄ +O=CH ₃ +OH	7.23E+08	1.6	8485	a
28	CH ₄ +OH=CH ₃ +H ₂ O	1.57E+07	1.8	2782	a
29	CH ₄ +HO ₂ =CH ₃ +H ₂ O ₂	9.03E+12	0	24720	a
30	CH ₄ +CH ₃ OO=CH ₃ OOH+CH ₃	1.81E+11	0	18481	a
31	O ₂ +CH ₃ =CH ₂ O+OH	3.31E+11	0	8944	a
32	O ₂ +CH ₃ =CH ₃ O+O	1.32E+14	0	31398	a
33	CH ₃ +O ₂ (+M)=CH ₃ OO(+M)	7.83E+08	1.2	0	a

#	Reaction	A	n	E _a	Ref.
	Low pressure limit:	1.55E+26	-3.3	0	
	TROE centering: 0.336 239 100000				
	Enhancement factor: O ₂ 0.4/CO 0.75/CO ₂ 1.5/H ₂ O 6.5/CH ₄ 3.0				
34	H+CH ₃ (+M)=CH ₄ (+M)	2.11E+14	0	0	a
	Low pressure limit:	1.76E+24	-1.8	0	
	TROE centering: 0.37 3320 61				
	Enhancement factor: O ₂ 0.4/CO 0.75/CO ₂ 1.5/H ₂ O 6.5/CH ₄ 3.0				
35	H ₂ +CH ₂ (S)=CH ₃ +H	7.23E+13	0	0	a
36	CH ₃ +O=CH ₂ O+H	8.43E+13	0	0	a
37	CH ₃ +O=CH ₃ O	7.97E+16	-2.1	625	a
38	CH ₃ +OH(+M)=CH ₃ OH(+M)	2.79E+18	-1.4	1330	a
	Low pressure limit:	4.00E+36	-5.92	3140	
	TROE centering: 0.412 195 5900 6390				
39	CH ₂ (S)+H ₂ O(+M)=CH ₃ OH(+M)	4.80E+18	-1.2	1145	a
	Low pressure limit:	1.88E+38	-6.36	5040	
	TROE centering: 0.603 208 3920 10200				
40	CH ₃ +HO ₂ =CH ₃ O+OH	1.80E+13	0	0	a
41	CH ₃ +HO ₂ =CH ₂ O+H ₂ O	1.11E+05	1.9	-2460	a
42	CH ₃ +HCO=CH ₄ +CO	1.20E+14	0	0	a
43	CH ₂ O+CH ₃ =CH ₄ +HCO	7.83E-08	6.1	1970	a
44	CH ₃ +CH ₃ O=CH ₄ +CH ₂ O	2.41E+13	0	0	a
45	CH ₃ +CH ₂ OH=CH ₄ +CH ₂ O	2.41E+12	0	0	a
46	CH ₃ +CH ₃ OO=CH ₃ O+CH ₃ O	2.41E+13	0	0	a
47	CH ₃ OH+CH ₃ =CH ₄ +CH ₂ OH	3.19E+01	3.2	7172	a
48	CH ₃ OH+CH ₃ =CH ₄ +CH ₃ O	1.44E+01	3.1	6935	a
49	CH ₂ +H=CH ₃	2.16E+13	0.3	0	a
50	O ₂ +CH ₃ O=CH ₂ O+HO ₂	2.17E+10	0	1750	a
51	O ₂ +CH ₂ OH=CH ₂ O+HO ₂	1.57E+15	-1	0	a
52	Duplicate	7.23E+13	0	3578	a
53	H+CH ₃ O=CH ₂ O+H ₂	1.81E+13	0	0	a
54	H+CH ₂ OH=CH ₂ O+H ₂	3.08E+13	0	0	a
55	OH+CH ₃ O=CH ₂ O+H ₂ O	1.81E+13	0	0	a
56	OH+CH ₂ OH=CH ₂ O+H ₂ O	2.41E+13	0	0	a
57	CH ₃ OOH=CH ₃ O+OH	6.00E+14	0	42330	a
58	O+CH ₃ O=CH ₂ O+OH	1.81E+12	0	0	a
59	O+CH ₂ OH=CH ₂ O+OH	9.03E+13	0	0	a
60	CH ₃ O+HO ₂ =CH ₂ O+H ₂ O ₂	3.01E+11	0	0	a
61	CH ₂ OH+HO ₂ =CH ₂ O+H ₂ O ₂	1.21E+13	0	0	a
62	2CH ₃ O=CH ₂ O+CH ₃ OH	6.03E+13	0	0	a
63	CH ₃ O+CH ₂ OH=CH ₃ OH+CH ₂ O	2.41E+13	0	0	a
64	CH ₂ OH+CH ₂ OH=CH ₃ OH+CH ₂ O	4.82E+12	0	0	a
65	CH ₃ O+CH ₃ OH=CH ₃ OH+CH ₂ OH	3.01E+11	0	4074	a
66	CH ₃ O+CH ₂ =CH ₃ +CH ₂ O	1.81E+13	0	0	a
67	CH ₃ O+CH ₂ (S)=CH ₃ +CH ₂ O	1.81E+13	0	0	a
68	CH ₂ +CH ₂ OH=CH ₃ +CH ₂ O	1.21E+12	0	0	a
69	CH ₃ O+CH ₂ O=CH ₃ OH+HCO	1.02E+11	0	2981	a
70	CH ₂ OH+CH ₂ O=CH ₃ OH+HCO	5.49E+03	2.8	5862	a
71	CH ₃ O+HCO=CH ₃ OH+CO	9.04E+13	0	0	a
72	CH ₂ OH+HCO=CH ₃ OH+CO	1.21E+14	0	0	a

#	Reaction	A	n	E _a	Ref.
73	CH ₂ OH+HCO=CH ₂ O+CH ₂ O	1.81E+14	0	0	a
74	CH ₃ O+CO=CH ₃ +CO ₂	6.81E-18	9.2	-2840	a
75	CH ₃ O+CH ₃ OO=CH ₂ O+CH ₃ OOH	3.01E+11	0	0	a
76	CH ₂ OH+CH ₃ OO=CH ₂ O+CH ₃ O+OH	1.21E+13	0	0	a
77	CH ₃ O(+M)=CH ₂ O+H(+M)	6.80E+13	0	26171	a
	Low pressure limit:	5.17E+23	-2.4	24307	
	TROE centering: 8.02 1260 1020 454				
	Enhancement factor: O ₂ 0.4/CO 0.75/CO ₂ 1.5/H ₂ O 6.5/CH ₄ 3.0				
78	CH ₂ OH(+M)=CH ₂ O+H(+M)	7.00E+14	0	29637	a
	Low pressure limit:	1.26E+16	0	30000	
	Enhancement factor: O ₂ 0.4/CO 0.75/CO ₂ 1.5/H ₂ O 6.5/CH ₄ 3.0				
79	CH ₃ OH+H=CH ₂ OH+H ₂	1.44E+13	0	6095	a
80	CH ₃ OH+H=CH ₃ O+H ₂	3.60E+12	0	6095	a
81	CH ₃ OH+O=CH ₂ OH+OH	3.88E+05	2.5	3080	a
82	CH ₃ OH+O=CH ₃ O+OH	1.00E+13	0	4684	a
83	CH ₃ OH+OH=CH ₂ OH+H ₂ O	7.10E+06	1.8	-596	a
84	CH ₃ OH+OH=CH ₃ O+H ₂ O	1.00E+06	2.1	497	a
85	CH ₃ OH+O ₂ =CH ₂ OH+HO ₂	2.05E+13	0	44900	a
86	CH ₃ OH+HO ₂ =CH ₂ OH+H ₂ O ₂	3.98E+13	0	19400	a
87	CH ₃ OH+CH ₂ =CH ₂ OH+CH ₃	3.19E+01	3.2	7172	a
88	CH ₃ OH+CH ₂ =CH ₃ O+CH ₃	1.44E+01	3.1	6935	a
89	CH ₃ OH+CH ₂ (S)=CH ₂ OH+CH ₃	1.51E+12	0	0	a
90	CH ₃ OH+CH ₃ OO=CH ₂ OH+CH ₃ OOH	1.81E+11	0	13712	a
91	CH ₃ OH(+M)=CH ₂ OH+H(+M)	2.69E+16	-0.1	98940	a
	Low pressure limit:	2.34E+40	-6.33	103100	
	TROE centering: 0.773 693 5330 100000				
92	H+CH ₃ O(+M)=CH ₃ OH(+M)	2.43E+12	0.5	50	a
	Low pressure limit:	4.66E+41	-7.44	14080	
	TROE centering: 0.7 100 90000 10000				
	Enhancement factor: O ₂ 0.4/CO 0.75/CO ₂ 1.5/H ₂ O 6.5/CH ₄ 3.0				
93	CH ₃ OO+H ₂ =CH ₃ OOH+H	3.01E+13	0	26032	a
94	CH ₃ OO+H=CH ₃ O+OH	9.64E+13	0	0	a
95	CH ₃ OO+O=CH ₃ O+O ₂	3.61E+13	0	0	a
96	CH ₃ OO+OH=CH ₃ OH+O ₂	6.03E+13	0	0	a
97	CH ₃ OO+HO ₂ =CH ₃ OOH+O ₂	2.29E+11	0	-1550	a
98	CH ₃ OO+H ₂ O ₂ =CH ₃ OOH+HO ₂	2.41E+12	0	9936	a
99	CH ₂ O+CH ₃ OO=CH ₃ OOH+HCO	1.99E+12	0	11665	a
100	CH ₃ OO+HCO=CH ₃ OOH+CO	3.01E+13	0	0	a
101	CH ₂ +CH ₃ OO=CH ₂ O+CH ₃ O	1.81E+13	0	0	a
102	CH ₃ OOH+H=CH ₃ O+H ₂ O	7.27E+10	0	1860	a
103	CH ₃ OOH+OH=CH ₃ OO+H ₂ O	7.23E+11	0	-258	a
104	CH ₃ OOH=CH ₂ O+H ₂ O	3.09E-02	4.5	39758	a
105	H+CH ₂ (S)=CH ₂ +H	2.00E+14	0	0	a
106	CH ₂ +O=CO+H+H	7.20E+13	0	0	a
107	CH ₂ +O=CO+H ₂	4.80E+13	0	0	a
108	O+CH ₂ =H+HCO	8.00E+13	0	0	a
109	CH ₂ (S)+O=H ₂ +CO	1.50E+13	0	0	a
110	CH ₂ (S)+O=CO+H+H	1.50E+13	0	0	a
111	CH ₂ +OH=CH ₂ O+H	1.81E+13	0	0	a

#	Reaction	A	n	E _a	Ref.
112	OH+CH ₂ (S)=H+CH ₂ O	3.00E+13	0	0	a
113	O ₂ +CH ₂ =CO ₂ +H ₂	5.43E+12	0	1491	a
114	O ₂ +CH ₂ =CO ₂ +H+H	5.43E+12	0	1491	a
115	O ₂ +CH ₂ =CO+OH+H	8.15E+12	0	1491	a
116	O ₂ +CH ₂ =CO+H ₂ O	1.48E+12	0	1491	a
117	O ₂ +CH ₂ =CH ₂ O+O	4.20E+12	0	1491	a
118	CH ₂ +O ₂ =HCO+OH	4.30E+10	0	-500	a
119	O ₂ +CH ₂ (S)=CO+OH+H	3.13E+13	0	0	a
120	CH ₂ (S)+O ₂ =CO+H ₂ O	1.20E+13	0	0	a
121	HO ₂ +CH ₂ =OH+CH ₂ O	2.00E+13	0	0	a
122	HO ₂ +CH ₂ (S)=OH+CH ₂ O	3.02E+13	0	0	a
123	CH ₂ (S)+H ₂ O ₂ =CH ₃ +HO ₂	3.01E+13	0	0	a
124	CO ₂ +CH ₂ =CH ₂ O+CO	2.35E+10	0	0	a
125	CH ₂ (S)+CO ₂ =CO+CH ₂ O	1.40E+13	0	0	a
126	CH ₂ (S)+CH ₂ O=CH ₃ +HCO	1.20E+12	0	0	a
127	CH ₂ +HCO=CH ₃ +CO	1.81E+13	0	0	a
128	CH ₂ (S)+HCO=CH ₃ +CO	1.81E+13	0	0	a
129	CH ₂ (S)+M=CH ₂ +M	1.51E+13	0	0	a
	Enhancement factor: O ₂ 0.4/CO 0.75/CO ₂ 1.5/H ₂ O 6.5/CH ₄ 3.0				
130	CH ₂ O+H=HCO+H ₂	1.26E+08	1.6	2165	a
131	CH ₂ O+O=HCO+OH	4.16E+11	0.6	2763	a
132	CH ₂ O+OH=HCO+H ₂ O	3.43E+09	1.2	-447	a
133	O ₂ +CH ₂ O=HCO+HO ₂	6.02E+13	0	40657	a
134	CH ₂ O+HO ₂ =H ₂ O ₂ +HCO	3.01E+12	0	13076	a
135	H+HCO(+M)=CH ₂ O(+M)	1.09E+12	0.5	-260	a
	Low pressure limit:	2.47E+24	-2.57	425	
	TROE centering: 0.782 271 2760 6570				
	Enhancement factor: H ₂ 2.0/CO 1.5/CO ₂ 2.0/H ₂ O 6.0/CH ₄ 2.0				
136	H ₂ +CO(+M)=CH ₂ O(+M)	4.30E+07	1.5	79600	a
	Low pressure limit:	5.07E+27	-3.42	84350	
	TROE centering: 0.932 197 1540 10300				
	Enhancement factor: H ₂ 2.0/CO 1.5/CO ₂ 2.0/H ₂ O 6.0/CH ₄ 2.0				
137	H+HCO=CO+H ₂	9.03E+13	0	0	a
138	O+HCO=CO+OH	3.01E+13	0	0	a
139	O+HCO=CO ₂ +H	3.01E+13	0	0	a
140	O ₂ +HCO=HO ₂ +CO	3.01E+12	0	0	a
141	OH+HCO=H ₂ O+CO	1.02E+14	0	0	a
142	HCO+HCO=CH ₂ O+CO	3.01E+13	0	0	a
143	HCO=H+CO	4.50E+13	0	21500	a
144	O ₂ +CO=CO ₂ +O	1.26E+13	0	47060	a
145	O+CO(+M)=CO ₂ (+M)	1.80E+10	0	2385	a
	Low pressure limit:	6.02E+14	0	3000	
	Enhancement factor: H ₂ 2.0/CO 1.5/CO ₂ 3.5/H ₂ O 6.0/O ₂ 6.0/CH ₄ 2.0				
146	CO+HO ₂ =CO ₂ +OH	1.51E+14	0	23666	a
147	C ₂ H ₅ OH(+M)=CH ₂ OH+CH ₃ (+M)	5.94E+23	-1.7	91163	c
	Low pressure limit:	2.88E+85	-18.9	109910	
	TROE centering: 0.5 200 890 4600				
	Enhancement factor: H ₂ 2.0/CO 2.0/CO ₂ 3.0/H ₂ O 5.0				
148	C ₂ H ₅ OH(+M)=C ₂ H ₅ +OH(+M)	1.25E+23	-1.5	96005	c

#	Reaction	A	n	E _a	Ref.
	Low pressure limit:	3.25E+85	-18.8	114930	
	TROE centering: 0.5 300 900 5000				
	Enhancement factor: H ₂ 2.0/CO 2.0/CO ₂ 3.0/H ₂ O 5.0				
149	C ₂ H ₅ OH(+M)=C ₂ H ₄ +H ₂ O(+M)	2.79E+13	0.1	66136	c
	Low pressure limit:	2.57E+83	-18.8	86452	
	TROE centering: 0.7 350 800 3800				
	Enhancement factor: H ₂ O 5.0				
150	C ₂ H ₅ OH(+M)=CH ₃ CHO+H ₂ (+M)	7.24E+11	0.1	91007	c
	Low pressure limit:	4.46E+87	-19.4	115590	
	TROE centering: 0.9 900 1100 3500				
	Enhancement factor: H ₂ O 5.0				
151	C ₂ H ₅ OH+OH=C ₂ H ₄ OH+H ₂ O	1.74E+11	0.3	600	c
152	C ₂ H ₅ OH+OH=CH ₃ CHOH+H ₂ O	4.64E+11	0.1	0	c
153	C ₂ H ₅ OH+OH=CH ₃ CH ₂ O+H ₂ O	7.46E+11	0.3	1634	c
154	C ₂ H ₅ OH+H=C ₂ H ₄ OH+H ₂	1.23E+07	1.8	5098	c
155	C ₂ H ₅ OH+H=CH ₃ CHOH+H ₂	2.58E+07	1.6	2827	c
156	C ₂ H ₅ OH+H=CH ₃ CH ₂ O+H ₂	1.50E+07	1.6	3038	c
157	C ₂ H ₅ OH+O=C ₂ H ₄ OH+OH	9.41E+07	1.7	5459	c
158	C ₂ H ₅ OH+O=CH ₃ CHOH+OH	1.88E+07	1.9	1824	c
159	C ₂ H ₅ OH+O=CH ₃ CH ₂ O+OH	1.58E+07	2	4448	c
160	C ₂ H ₅ OH+CH ₃ =C ₂ H ₄ OH+CH ₄	2.19E+02	3.2	9622	c
161	C ₂ H ₅ OH+CH ₃ =CH ₃ CHOH+CH ₄	7.28E+02	3	7948	c
162	C ₂ H ₅ OH+CH ₃ =CH ₃ CH ₂ O+CH ₄	1.45E+02	3	7649	c
163	C ₂ H ₅ OH+HO ₂ =C ₂ H ₄ OH+H ₂ O ₂	1.23E+04	2.5	15750	c
164	C ₂ H ₅ OH+HO ₂ =CH ₃ CHOH+H ₂ O ₂	8.20E+03	2.5	10750	c
165	C ₂ H ₅ OH+HO ₂ =CH ₃ CH ₂ O+H ₂ O ₂	2.50E+12	0	24000	c
166	CH ₃ CH ₂ O+M=CH ₃ CHO+H+M	1.16E+35	-5.9	25274	c
167	CH ₃ CH ₂ O+M=CH ₃ +CH ₂ O+M	1.35E+38	-7	23800	c
168	CH ₃ CH ₂ O+CO=C ₂ H ₅ +CO ₂	4.68E+02	3.2	5380	c
169	CH ₃ CH ₂ O+O ₂ =CH ₃ CHO+HO ₂	4.00E+10	0	1100	c
170	CH ₃ CH ₂ O+H=CH ₃ +CH ₂ OH	3.00E+13	0	0	c
171	CH ₃ CH ₂ O+H=C ₂ H ₄ +H ₂ O	3.00E+13	0	0	c
172	CH ₃ CH ₂ O+OH=CH ₃ CHO+H ₂ O	1.00E+13	0	0	c
173	CH ₃ CHOH+O ₂ =CH ₃ CHO+HO ₂	4.82E+14	0	5017	c
174	Duplicate	8.43E+15	-1.2	0	c
175	CH ₃ CHOH+O=CH ₃ CHO+OH	1.00E+14	0	0	c
176	CH ₃ CHOH+H=CH ₃ +CH ₂ OH	3.00E+13	0	0	c
177	CH ₃ CHOH+H=C ₂ H ₄ +H ₂ O	3.00E+13	0	0	c
178	CH ₃ CHOH+HO ₂ =CH ₃ CHO+OH+OH	4.00E+13	0	0	c
179	CH ₃ CHOH+OH=CH ₃ CHO+H ₂ O	5.00E+12	0	0	c
180	CH ₃ CHOH+M=CH ₃ CHO+H+M	1.00E+14	0	25000	c
181	CH ₃ CHO+OH=CH ₃ CO+H ₂ O	3.00E+12	-0.1	-979	c
182	CH ₃ CHO+OH=CH ₂ CHO+H ₂ O	1.11E+11	0.5	403	c
183	CH ₃ CHO+O=CH ₃ CO+OH	1.77E+18	-1.9	2975	c
184	CH ₃ CHO+O=CH ₂ CHO+OH	3.72E+13	-0.2	3556	c
185	CH ₃ CHO+H=CH ₃ CO+H ₂	4.66E+13	-0.3	2988	c
186	CH ₃ CHO+H=CH ₂ CHO+H ₂	1.85E+12	0.4	5359	c
187	CH ₃ CHO+CH ₃ =CH ₃ CO+CH ₄	3.90E-07	5.8	2200	c
188	CH ₃ CHO+CH ₃ =CH ₂ CHO+CH ₄	2.45E+01	3.1	5727	c

#	Reaction	A	n	E _a	Ref.
189	CH ₃ CHO+HO ₂ =CH ₃ CO+H ₂ O ₂	2.40E+19	-2.2	14030	c
190	CH ₃ CHO+HO ₂ =CH ₂ CHO+H ₂ O ₂	2.32E+11	0.4	14864	c
191	CH ₃ CHO+O ₂ =CH ₃ CO+HO ₂	1.00E+14	0	42200	c
192	CH ₂ CHO+H=CH ₃ +HCO	5.00E+13	0	0	c
193	CH ₂ CHO+H=CH ₂ CO+H ₂	2.00E+13	0	0	c
194	CH ₂ CHO+O=CH ₂ O+HCO	1.00E+14	0	0	c
195	CH ₂ CHO+OH=CH ₂ CO+H ₂ O	3.00E+13	0	0	c
196	CH ₂ CHO+O ₂ =CH ₂ O+CO+OH	3.00E+10	0	0	c
197	CH ₂ CHO+CH ₃ =C ₂ H ₅ +CO+H	4.90E+14	-0.5	0	c
198	CH ₂ CHO+HO ₂ =CH ₂ O+HCO+OH	7.00E+12	0	0	c
199	CH ₂ CHO+HO ₂ =CH ₃ CHO+O ₂	3.00E+12	0	0	c
200	CH ₂ CHO=CH ₃ +CO	1.17E+43	-9.8	43756	c
201	CH ₂ CHO=CH ₂ CO+H	1.81E+43	-9.6	45868	c
202	C ₂ H ₆ +CH ₃ =C ₂ H ₅ +CH ₄	5.50E-01	4	8300	c
203	C ₂ H ₆ +H=C ₂ H ₅ +H ₂	5.40E+02	3.5	5210	c
204	C ₂ H ₆ +O=C ₂ H ₅ +OH	3.00E+07	2	5115	c
205	C ₂ H ₆ +OH=C ₂ H ₅ +H ₂ O	7.23E+06	2	864	c
206	C ₂ H ₅ +H=C ₂ H ₄ +H ₂	1.25E+14	0	8000	c
207	C ₂ H ₅ +H=CH ₃ +CH ₃	3.00E+13	0	0	c
208	C ₂ H ₅ +H=C ₂ H ₆	3.00E+13	0	0	c
209	C ₂ H ₅ +OH=C ₂ H ₄ +H ₂ O	4.00E+13	0	0	c
210	C ₂ H ₅ +O=CH ₃ +CH ₂ O	1.00E+14	0	0	c
211	C ₂ H ₅ +HO ₂ =C ₂ H ₆ +O ₂	3.00E+12	0	0	c
212	C ₂ H ₅ +HO ₂ =CH ₃ +CH ₂ O+OH	3.00E+13	0	0	c
213	C ₂ H ₅ +O ₂ =C ₂ H ₄ +HO ₂	2.89E+28	-5.4	7585	c
214	C ₂ H ₅ +O ₂ =CH ₃ CHO+OH	4.90E+11	-0.5	8357	c
215	C ₂ H ₄ +OH=C ₂ H ₄ OH	1.29E+12	0	-817	c
216	C ₂ H ₄ OH+O ₂ =HOC ₂ H ₄ OO	1.00E+12	0	-1100	c
217	HOC ₂ H ₄ OO=CH ₂ O+CH ₂ O+OH	6.00E+10	0	24500	c
218	C ₂ H ₄ +H=C ₂ H ₃ +H ₂	3.36E-07	6	1692	c
219	C ₂ H ₄ +OH=C ₂ H ₃ +H ₂ O	2.02E+13	0	5936	c
220	C ₂ H ₄ +O=CH ₃ +HCO	1.02E+07	1.9	179	c
221	C ₂ H ₄ +O=CH ₂ CHO+H	3.39E+06	1.9	179	c
222	C ₂ H ₄ +CH ₃ =C ₂ H ₃ +CH ₄	6.62E+00	3.7	9500	c
223	C ₂ H ₄ +H(+M)=C ₂ H ₅ (+M)	1.08E+12	0.5	1822	c
	Low pressure limit:	1.11E+34	-5	4448	
	TROE centering: 1 1E-15 95 200				
	Enhancement factor: H ₂ 2.0/CO 2.0/CO ₂ 3.0/H ₂ O 5.0				
224	C ₂ H ₄ (+M)=C ₂ H ₂ +H ₂ (+M)	1.80E+14	0	87000	c
	Low pressure limit:	1.50E+15	0	55443	
225	C ₂ H ₃ +H(+M)=C ₂ H ₄ (+M)	6.10E+12	0.3	280	c
	Low pressure limit:	9.80E+29	-3.86	3320	
	TROE centering: .782 208 2660 6100				
	Enhancement factor: H ₂ O 5.0				
226	C ₂ H ₃ +H=C ₂ H ₂ +H ₂	9.00E+13	0	0	c
227	C ₂ H ₃ +O=CH ₂ CO+H	3.00E+13	0	0	c
228	C ₂ H ₃ +O ₂ =CH ₂ O+HCO	1.70E+29	-5.3	6500	c
229	C ₂ H ₃ +O ₂ =CH ₂ CHO+O	5.50E+14	-0.6	5260	c
230	C ₂ H ₃ +O ₂ =C ₂ H ₂ +HO ₂	2.12E-06	6	9484	c

#	Reaction	A	n	E _a	Ref.
231	$C_2H_3+OH=C_2H_2+H_2O$	2.00E+13	0	0	c
232	$C_2H_3+C_2H=C_2H_2+C_2H_2$	3.00E+13	0	0	c
233	$C_2H_3+CH_3=C_2H_2+CH_4$	2.00E+13	0	0	c
234	$C_2H_2+OH=C_2H+H_2O$	3.37E+07	2	14000	c
235	$C_2H_2+OH=HCCOH+H$	5.04E+05	2.3	13500	c
236	$C_2H_2+OH=CH_2CO+H$	2.18E-04	4.5	-1000	c
237	Duplicate	2.00E+11	0	0	c
238	$C_2H_2+OH=CH_3+CO$	4.83E-04	4	-2000	c
239	$HCCOH+H=CH_2CO+H$	1.00E+13	0	0	c
240	$C_2H_2+O=CH_2+CO$	6.12E+06	2	1900	c
241	$C_2H_2+O=HCCO+H$	1.43E+07	2	1900	c
242	$C_2H_2+O=C_2H+OH$	3.16E+15	-0.6	15000	c
243	$C_2H_2+CH_3=C_2H+CH_4$	1.81E+11	0	17289	c
244	$C_2H_2+O_2=HCCO+OH$	4.00E+07	1.5	30100	c
245	$C_2H_2+M=C_2H+H+M$	4.20E+16	0	107000	c
246	$C_2H_2+H(+M)=C_2H_3(+M)$	3.11E+11	0.6	2589	c
	Low pressure limit:	2.25E+40	-7.27	6577	
	TROE centering: 1 1E-15 675 1E+15				
	Enhancement factor: H ₂ 2.0/CO 2.0/CO ₂ 3.0/H ₂ O 5.0				
247	$CHOCHO(+M)=CH_2O+CO(+M)$	4.27E+12	0	50600	c
	Low pressure limit:	8.91E+16	0	49200	
248	$CHOCHO=CO+CO+H_2$	4.07E+42	-8.5	69278	c
249	$CHOCHO+OH=HCO+CO+H_2O$	1.00E+13	0	0	c
250	$CHOCHO+O=HCO+CO+OH$	7.24E+12	0	1970	c
251	$CHOCHO+H=CH_2O+HCO$	1.00E+12	0	0	c
252	$CHOCHO+HO_2=HCO+CO+H_2O_2$	1.70E+12	0	10700	c
253	$CHOCHO+CH_3=HCO+CO+CH_4$	1.74E+12	0	8440	c
254	$CHOCHO+O_2=HCO+CO+HO_2$	1.00E+14	0	37000	c
255	$CH_3CO(+M)=CH_3+CO(+M)$	3.00E+12	0	16722	c
	Low pressure limit:	1.20E+15	0	12518	c
256	$CH_2CO+O=CO_2+CH_2$	1.75E+12	0	1350	c
257	$CH_2CO+H=CH_3+CO$	2.71E+04	2.8	714	c
258	$CH_2CO+H=HCCO+H_2$	2.00E+14	0	8000	c
259	$CH_2CO+O=HCCO+OH$	1.00E+13	0	8000	c
260	$CH_2CO+OH=HCCO+H_2O$	1.00E+13	0	2000	c
261	$CH_2CO+OH=CH_2OH+CO$	3.73E+12	0	-1013	c
262	$CH_2CO(+M)=CH_2+CO(+M)$	3.00E+14	0	70980	c
	Low pressure limit:	3.60E+15	0	59270	c
263	$C_2H+H_2=C_2H_2+H$	4.09E+05	2.4	864	c
264	$C_2H+OH=HCCO+H$	2.00E+13	0	0	c
265	$C_2H+O_2=CO+CO+H$	9.04E+12	0	-457	c
266	$HCCO+H=CH_2(S)+CO$	1.00E+14	0	0	c
267	$HCCO+O=H+CO+CO$	8.00E+13	0	0	c
268	$HCCO+O_2=HCO+CO+O$	2.50E+08	1	0	c
269	$HCCO+O_2=CO_2+HCO$	2.40E+11	0	-854	c
270	$HCCO+HCCO=C_2H_2+CO+CO$	1.00E+13	0	0	c
271	$HCCO+OH=C_2O+H_2O$	3.00E+13	0	0	c
272	$C_2O+O=CO+CO$	5.00E+13	0	0	c
273	$C_2O+OH=CO+CO+H$	2.00E+13	0	0	c

#	Reaction	A	n	E _a	Ref.
274	C ₂ O+O ₂ =CO+CO+O	2.00E+13	0	0	c
275	CH ₃ OO+CH ₃ OO=CH ₃ O+CH ₃ O+O ₂	5.48E+10	0	-835	d
276	CH ₃ OO+CH ₃ OO=CH ₃ OH+CH ₂ O+O ₂	2.19E+09	0	-3580	d
277	CH ₃ CO ₃ +CH ₃ CHO=>CH ₃ CO ₃ H+CH ₃ CO	1.20E+11	0	4900	d
278	CH ₃ CO ₃ H+CH ₃ CO=>CH ₃ CO ₃ +CH ₃ CHO	1.99E+10	0	10000	d
279	CH ₃ CHO+CH ₃ O=>CH ₃ CO+CH ₃ OH	1.15E+11	0	1280	d
280	CH ₃ CO+CH ₃ OH=>CH ₃ CHO+CH ₃ O	3.02E+11	0	18160	d
281	CH ₃ CHO+CH ₃ OO=>CH ₃ CO+CH ₃ OOH	3.55E+09	0	5050	d
282	CH ₃ CO+CH ₃ OOH=>CH ₃ CHO+CH ₃ OO	5.02E+09	0	10100	d
283	CH ₃ CO+O ₂ =>CH ₃ CO ₃	1.00E+10	0	-2700	d
284	CH ₃ CO ₃ =>CH ₃ CO+O ₂	2.88E+16	-1	37300	d
285	CH ₃ CO ₃ +HO ₂ =>CH ₃ CO ₃ H+O ₂	1.00E+12	0	0	d
286	CH ₃ CO ₃ H+O ₂ =>CH ₃ CO ₃ +HO ₂	3.98E+15	0	40000	d
287	CH ₃ CO ₃ H=>CH ₃ +CO ₂ +OH	2.00E+14	0	40150	d
288	CH ₃ CO ₃ +CH ₃ OO=>CH ₃ CO ₂ +CH ₃ O+O ₂	1.81E+12	0	0	d
289	CH ₃ CO ₃ +HO ₂ =>CH ₃ CO ₂ +OH+O ₂	1.00E+12	0	0	d
290	CH ₃ CO ₃ +CH ₃ CO ₃ =>CH ₃ CO ₂ +CH ₃ CO ₂ +O ₂	4.78E+12	0	0	d
291	CH ₃ CO ₂ (+M)=>CH ₃ +CO ₂ (+M)	3.00E+12	0	16722	d
	Low pressure limit:	1.20E+15	0	12518	
292	CH ₃ OO+HO ₂ =>CH ₃ O+OH+O ₂	1.00E+12	0	0	d
293	CH ₃ OOH+OH=>CH ₂ OOH+H ₂ O	2.51E+13	0	1000	d
294	CH ₂ OOH+H ₂ O=>CH ₃ OOH+OH	3.01E+13	0	32800	d
295	CH ₃ OOH+CH ₃ O=>CH ₃ OO+CH ₃ OH	7.07E+11	0	4000	d
296	CH ₃ OO+CH ₃ OH=>CH ₃ OOH+CH ₃ O	3.01E+13	0	32800	d
297	CH ₃ OOH+CH ₃ O=>CH ₂ OOH+CH ₃ OH	7.07E+11	0	4000	d
298	CH ₂ OOH+CH ₃ OH=>CH ₃ OOH+CH ₃ O	3.01E+13	0	32800	d
299	HOCO+O ₂ =CO ₂ +HO ₂	8.73E+11	0	0	d
300	HOCO+HO ₂ =CO ₂ +H ₂ O ₂	1.00E+12	0	0	d
301	HOCO+CH ₃ OO=CO ₂ +CH ₃ OOH	1.00E+12	0	0	d
302	CO+OH(+M)=HOCO(+M)	1.20E+07	1.8	-236	e
	Low pressure limit:	7.24E+25	-3.85	1550	
	TROE centering: 0.6 1E-15 1E+15				
303	OH+CO(+M)=H+CO ₂ (+M)	9.54E+04	2	-1484	e
	High pressure limit:	3.80E-138	51.93	-75965	
	TROE centering: 0.6 1E-15 1E+15				

a) Sullivan et al. (2004a); c) Marinov (1999); d) Rice and Croiset (2001); e) Senosiain et al. (2003).

Table 11-3: Organophosphorus SCWO submechanism. Units are in kcal, cm, mol, s.

#	Reaction	A	b	E _a	Ref
304	PO(OH) ₂ CH ₃ =PO ₂ CH ₃ +H ₂ O	2.20E+12	0	41900	a
305	PO(OH) ₂ CH ₃ =PO ₂ OH+CH ₄	6.40E+11	0.4	64100	a
306	PO(OH) ₂ CH ₃ =POOHCH ₂ +H ₂ O	2.56E+09	1.3	73000	a
307	PO(OH) ₂ CH ₃ =POOH+CH ₃ OH	5.09E+11	0.7	105130	a
308	PO ₂ CH ₃ +OH=PO ₂ OH+CH ₃	1.00E+12	0	2000	a
309	PO(OH) ₂ CH ₃ +OH=PO(OH) ₂ CH ₂ +H ₂ O	1.04E+06	2.4	-1137	a
310	PO(OH) ₂ CH ₃ +OH=PO ₂ (OH)CH ₃ +H ₂ O	2.13E+04	2.4	198	a

#	Reaction	A	b	E_a	Ref
311	$\text{PO(OH)}_2\text{CH}_3 + \text{OH} = \text{PO(OH)}_3\text{CH}_3$	5.32E+03	2	837	a
312	$\text{PO(OH)}_2\text{CH}_2 + \text{H} = \text{PO(OH)}_2\text{CH}_3$	1.00E+14	0	0	a
313	$\text{PO}_2(\text{OH})\text{CH}_3 + \text{H} = \text{PO(OH)}_2\text{CH}_3$	1.00E+14	0	0	a
314	$\text{PO(OH)}_2\text{CH}_3 + \text{H} = \text{PO(OH)}_2\text{CH}_2 + \text{H}_2$	2.80E+07	2	7700	a
315	$\text{PO(OH)}_2\text{CH}_3 + \text{O} = \text{PO(OH)}_2\text{CH}_2 + \text{OH}$	2.20E+06	2.4	5500	a
316	$\text{PO(OH)}_2\text{CH}_3 + \text{CH}_3 = \text{PO(OH)}_2\text{CH}_2 + \text{CH}_4$	6.51E+11	0	11600	a
317	$\text{PO(OH)}_2\text{CH}_3 + \text{CH}_3\text{O} = \text{PO(OH)}_2\text{CH}_2 + \text{CH}_3\text{OH}$	1.58E+11	0	7000	a
318	$\text{PO(OH)}_2\text{CH}_2 + \text{HO}_2 = \text{PO(OH)}_2\text{CH}_3 + \text{O}_2$	1.50E+11	0	0	a
319	$\text{PO(OH)}_2\text{CH}_3 + \text{CH}_3\text{OO} = \text{PO(OH)}_2\text{CH}_2 + \text{CH}_3\text{OOH}$	6.06E+12	0	20430	a
320	$\text{PO(OH)}_2\text{CH}_2\text{OO} + \text{PO(OH)}_2\text{CH}_3$ $= \text{PO(OH)}_2\text{CH}_2\text{OOH} + \text{PO(OH)}_2\text{CH}_2$	6.06E+12	0	20430	a
321	$\text{PO(OH)}_2\text{CH}_3 + \text{HO}_2 = \text{PO(OH)}_2\text{CH}_2 + \text{H}_2\text{O}_2$	4.02E+12	0	19400	a
322	$\text{PO(OH)}_3\text{CH}_3 = \text{PO(OH)}_3 + \text{CH}_3$	7.35E+11	0.1	2932	a
323	$\text{PO(OH)}_2\text{CH}_2 + \text{O}_2 = \text{PO(OH)}_2\text{CH}_2\text{OO}$	2.94E+13	-0.4	0	a
324	$\text{PO(OH)}_2\text{CH}_2 + \text{CH}_3\text{OO} = \text{PO(OH)}_2\text{CH}_2\text{O} + \text{CH}_3\text{O}$	1.90E+12	0	-1200	a
325	$\text{PO(OH)}_2\text{CH}_2 + \text{PO(OH)}_2\text{CH}_2\text{OO}$ $= \text{PO(OH)}_2\text{CH}_2\text{O} + \text{PO(OH)}_2\text{CH}_2\text{O}$	1.90E+12	0	-1200	a
326	$\text{PO(OH)}_2\text{CH}_2 + \text{HO}_2 = \text{PO(OH)}_2\text{CH}_2\text{O} + \text{OH}$	3.00E+13	0	0	a
327	$\text{PO(OH)}_2\text{CH}_2 + \text{O}_2 = \text{PO(OH)}_2\text{CH}_2\text{O} + \text{O}$	1.00E+13	-0.2	27902	a
328	$\text{PO(OH)}_2\text{CH}_2\text{O} = \text{PO(OH)}_2 + \text{CH}_2\text{O}$	1.10E+13	0	16700	a
329	$\text{PO(OH)}_2\text{CH}_2\text{O} + \text{O}_2 = \text{PO(OH)}_2\text{CHO} + \text{HO}_2$	3.60E+10	0	1090	a
330	$\text{PO(OH)}_2\text{CH}_2\text{O} + \text{CO} = \text{PO(OH)}_2\text{CH}_2 + \text{CO}_2$	4.68E+02	3.2	5380	a
331	$\text{PO(OH)}_2\text{CH}_2\text{O} + \text{OH} = \text{PO(OH)}_2\text{CHO} + \text{H}_2\text{O}$	1.00E+13	0	0	a
332	$\text{PO(OH)}_2\text{CH}_2\text{OH} = \text{PO(OH)}_2 + \text{CH}_2\text{OH}$	5.94E+23	-1.7	91163	a
333	$\text{PO(OH)}_2\text{CH}_2\text{OH} = \text{PO(OH)}_2\text{CH}_2 + \text{OH}$	1.25E+23	-1.5	96005	a
334	$\text{PO(OH)}_2\text{CH}_2\text{OH} = \text{PO(OH)}_2\text{CHO} + \text{H}_2$	7.24E+11	0.1	91010	a
335	$\text{PO(OH)}_2\text{CH}_2\text{OH} + \text{HO}_2 = \text{PO(OH)}_2\text{CH}_2\text{O} + \text{H}_2\text{O}_2$	2.50E+12	0	24000	a
336	$\text{PO(OH)}_2\text{CH}_2\text{OH} + \text{OH} = \text{PO(OH)}_2\text{CH}_2\text{O} + \text{H}_2\text{O}$	7.46E+11	0.3	1634	a
337	$\text{PO(OH)}_2\text{CH}_2\text{OH} + \text{H} = \text{PO(OH)}_2\text{CH}_2\text{O} + \text{H}_2$	1.50E+07	1.6	3038	a
338	$\text{PO(OH)}_2\text{CH}_2\text{OH} + \text{O} = \text{PO(OH)}_2\text{CH}_2\text{O} + \text{OH}$	1.58E+07	2	4448	a
339	$\text{PO(OH)}_2\text{CH}_2\text{OH} + \text{CH}_3 = \text{PO(OH)}_2\text{CH}_2\text{O} + \text{CH}_4$	1.45E+02	3	7649	a
340	$\text{PO(OH)}_2\text{CH}_2\text{OH} + \text{HO}_2 = \text{PO(OH)}_2\text{CHOH} + \text{H}_2\text{O}_2$	8.20E+03	2.5	10750	a
341	$\text{PO(OH)}_2\text{CH}_2\text{OH} + \text{OH} = \text{PO(OH)}_2\text{CHOH} + \text{H}_2\text{O}$	4.64E+11	0.1	0	a
342	$\text{PO(OH)}_2\text{CH}_2\text{OH} + \text{H} = \text{PO(OH)}_2\text{CHOH} + \text{H}_2$	2.58E+07	1.6	2827	a
343	$\text{PO(OH)}_2\text{CH}_2\text{OH} + \text{O} = \text{PO(OH)}_2\text{CHOH} + \text{OH}$	1.88E+07	1.9	1824	a
344	$\text{PO(OH)}_2\text{CH}_2\text{OH} + \text{CH}_3 = \text{PO(OH)}_2\text{CHOH} + \text{CH}_4$	7.28E+02	3	7948	a
345	$\text{PO(OH)}_2\text{CH}_2\text{OH} + \text{PO(OH)}_2\text{CH}_2$ $= \text{PO(OH)}_2\text{CHOH} + \text{PO(OH)}_2\text{CH}_3$	5.00E+10	0	10400	a
346	$\text{PO(OH)}_2\text{CH}_2\text{OH} + \text{O}_2 = \text{PO(OH)}_2\text{CHOH} + \text{HO}_2$	1.50E+13	0	50150	a
347	$\text{PO(OH)}_2\text{CHOH} + \text{O}_2 = \text{PO(OH)}_2\text{CHO} + \text{HO}_2$	8.43E+15	-1.2	0	a
348	Duplicate	4.82E+14	0	5017	a
349	$\text{PO(OH)}_2\text{CHOH} + \text{O} = \text{PO(OH)}_2\text{CHO} + \text{OH}$	1.00E+14	0	0	a
350	$\text{PO(OH)}_2\text{CHOH} + \text{HO}_2 = \text{PO(OH)}_2\text{CHO} + \text{H}_2\text{O}_2$	4.00E+13	0	0	a
351	$\text{PO(OH)}_2\text{CHOH} + \text{OH} = \text{PO(OH)}_2\text{CHO} + \text{H}_2\text{O}$	5.00E+12	0	0	a
352	$\text{PO(OH)}_2\text{CHO} = \text{PO(OH)}_2 + \text{HCO}$	2.61E+15	0.1	80550	a
353	$\text{PO(OH)}_2\text{CHO} + \text{HO}_2 = \text{PO(OH)}_2\text{CO} + \text{H}_2\text{O}_2$	3.01E+12	0	11930	a
354	$\text{PO(OH)}_2\text{CHO} + \text{OH} = \text{PO(OH)}_2\text{CO} + \text{H}_2\text{O}$	2.34E+10	0.7	-1113	a
355	$\text{PO(OH)}_2\text{CHO} + \text{H} = \text{PO(OH)}_2\text{CO} + \text{H}_2$	1.34E+13	0	3300	a
356	$\text{PO(OH)}_2\text{CHO} + \text{O} = \text{PO(OH)}_2\text{CO} + \text{OH}$	5.94E+12	0	1868	a

#	Reaction	A	b	E_a	Ref
357	$\text{PO}(\text{OH})_2\text{CHO} + \text{CH}_3 = \text{PO}(\text{OH})_2\text{CO} + \text{CH}_4$	2.61E+06	1.8	5911	a
358	$\text{PO}(\text{OH})_2\text{CHO} + \text{O}_2 = \text{PO}(\text{OH})_2\text{CO} + \text{HO}_2$	3.01E+13	0	39150	a
359	$\text{PO}(\text{OH})_2\text{CHO} + \text{CH}_3\text{OO} = \text{PO}(\text{OH})_2\text{CO} + \text{CH}_3\text{OOH}$	3.01E+12	0	11930	a
360	$\text{PO}(\text{OH})_2\text{CH}_2\text{OO} = \text{PO}(\text{OH})_2\text{CHO} + \text{OH}$	1.32E+09	1.4	41590	a
361	$\text{PO}(\text{OH})_2\text{CO} = \text{PO}(\text{OH})_2 + \text{CO}$	3.00E+12	0	16720	a
362	$\text{PO}(\text{OH})_2\text{CO} + \text{O} = \text{PO}(\text{OH})_2 + \text{CO}_2$	2.00E+13	0	0	a
363	$\text{PO}(\text{OH})_2\text{CO} + \text{CH}_3\text{OO} = \text{PO}(\text{OH})_2 + \text{CO}_2 + \text{CH}_3\text{O}$	2.40E+13	0	0	a
364	$\text{PO}(\text{OH})_2\text{CO} + \text{PO}(\text{OH})_2\text{CH}_2\text{OO}$ $= \text{PO}(\text{OH})_2 + \text{CO}_2 + \text{PO}(\text{OH})_2\text{CH}_2\text{O}$	2.40E+13	0	0	a
365	$\text{PO}(\text{OH})_2\text{CH}_2\text{OO} + \text{HO}_2 = \text{PO}(\text{OH})_2\text{CH}_2\text{OOH} + \text{O}_2$	1.62E+11	0	-1987	a
366	$\text{PO}(\text{OH})_2\text{CH}_2\text{OO} + \text{H}_2\text{O}_2 = \text{PO}(\text{OH})_2\text{CH}_2\text{OOH} + \text{HO}_2$	2.40E+12	0	9935	a
367	$\text{PO}(\text{OH})_2\text{CH}_2\text{OO} + \text{CH}_3 = \text{PO}(\text{OH})_2\text{CH}_2\text{O} + \text{CH}_3\text{O}$	3.80E+12	0	-1200	a
368	$\text{PO}(\text{OH})_2\text{CH}_2\text{OO} + \text{CH}_3\text{OO} = \text{PO}(\text{OH})_2\text{CH}_2\text{O} + \text{CH}_3\text{O} + \text{O}_2$	1.00E+11	0	0	a
369	$\text{PO}(\text{OH})_2\text{CH}_2\text{OO} + \text{PO}(\text{OH})_2\text{CH}_2\text{OO}$ $= \text{PO}(\text{OH})_2\text{CH}_2\text{O} + \text{PO}(\text{OH})_2\text{CH}_2\text{O} + \text{O}_2$	3.23E+10	0	248	a
370	$\text{PO}(\text{OH})_2\text{CH}_2\text{OO} + \text{PO}(\text{OH})_2\text{CH}_2\text{OO}$ $= \text{PO}(\text{OH})_2\text{CHO} + \text{PO}(\text{OH})_2\text{CH}_2\text{OH} + \text{O}_2$	1.64E+10	0	248	a
371	$\text{PO}(\text{OH})_2\text{CH}_2\text{OO} + \text{CH}_4 = \text{PO}(\text{OH})_2\text{CH}_2\text{OOH} + \text{CH}_3$	1.81E+11	0	18480	a
372	$\text{PO}(\text{OH})_2\text{CH}_2\text{OO} + \text{CH}_2\text{O} = \text{PO}(\text{OH})_2\text{CH}_2\text{OOH} + \text{HCO}$	1.99E+12	0	11660	a
373	$\text{PO}(\text{OH})_2\text{CH}_2\text{OO} + \text{H}_2 = \text{PO}(\text{OH})_2\text{CH}_2\text{OOH} + \text{H}$	3.00E+13	0	26030	a
374	$\text{PO}(\text{OH})_2\text{CH}_2\text{OO} + \text{H} = \text{PO}(\text{OH})_2\text{CH}_2\text{O} + \text{OH}$	9.64E+13	0	0	a
375	$\text{PO}(\text{OH})_2\text{CH}_2\text{OO} + \text{HCO} = \text{PO}(\text{OH})_2\text{CH}_2\text{O} + \text{H} + \text{CO}_2$	3.01E+13	0	0	a
376	$\text{PO}(\text{OH})_2\text{CH}_2\text{OO} + \text{CH}_3\text{O} = \text{PO}(\text{OH})_2\text{CH}_2\text{OOH} + \text{CH}_2\text{O}$	3.00E+11	0	0	a
377	$\text{PO}(\text{OH})_2\text{CH}_2\text{OO} + \text{CH}_2\text{OH} = \text{PO}(\text{OH})_2\text{CH}_2\text{OOH} + \text{CH}_2\text{O}$	1.21E+13	0	0	a
378	$\text{PO}(\text{OH})_2\text{CH}_2\text{OO} + \text{CH}_3\text{OH} = \text{PO}(\text{OH})_2\text{CH}_2\text{OOH} + \text{CH}_2\text{OH}$	1.81E+11	0	13712	a
379	$\text{PO}(\text{OH})_2\text{CH}_2\text{OO} + \text{O} = \text{PO}(\text{OH})_2\text{CH}_2\text{O} + \text{O}_2$	3.61E+13	0	0	a
380	$\text{PO}(\text{OH})_2\text{CH}_2\text{OO} + \text{CH}_2 = \text{PO}(\text{OH})_2\text{CH}_2\text{O} + \text{CH}_2\text{O}$	1.81E+13	0	0	a
381	$\text{PO}(\text{OH})_2\text{CH}_2\text{OO} = \text{PO}_2(\text{OH})\text{CH}_2\text{OOH}$	1.00E+10	0	35250	a
382	$\text{PO}(\text{OH})_2\text{CH}_2\text{O} = \text{PO}_2(\text{OH})\text{CH}_2\text{OH}$	1.00E+10	0	32100	a
383	$\text{PO}_2(\text{OH})\text{CH}_2\text{OH} = \text{PO}_2\text{OH} + \text{CH}_2\text{OH}$	3.50E+13	0	7910	a
384	$\text{PO}(\text{OH})_2\text{CH}_2\text{OOH} = \text{PO}(\text{OH})_2\text{CH}_2\text{O} + \text{OH}$	6.31E+14	0	42300	a
385	$\text{PO}(\text{OH})_2\text{CH}_2\text{OOH} + \text{OH} = \text{PO}(\text{OH})_2\text{CH}_2\text{OO} + \text{H}_2\text{O}$	7.23E+11	0	-258	a
386	$\text{PO}(\text{OH})_2\text{CH}_2\text{OOH} + \text{H} = \text{PO}(\text{OH})_2\text{CH}_2\text{O} + \text{H}_2\text{O}$	7.27E+10	0	1860	a
387	$\text{PO}_2(\text{OH})\text{CH}_2\text{OOH} = \text{PO}_2\text{OH} + \text{CH}_2\text{O} + \text{OH}$	3.50E+13	0	7910	a
388	$\text{PO}(\text{OH})_2\text{CH}_2\text{OOH} + \text{OH} = \text{PO}_2(\text{OH})\text{CH}_2\text{OOH} + \text{H}_2\text{O}$	2.13E+04	2.4	198	a
389	$\text{PO}_2(\text{OH})\text{CH}_3 = \text{PO}_2\text{OH} + \text{CH}_3$	1.10E+13	0	16700	a
390	$\text{PO}(\text{OH})_3 = \text{PO}_2\text{OH} + \text{H}_2\text{O}$	2.09E+07	1.5	42118	a
391	$\text{PO}_2\text{OH} + \text{H} = \text{PO}(\text{OH})_2$	3.20E+08	1.6	6190	a
392	$\text{PO}(\text{OH})_2 + \text{H} = \text{PO}_2\text{OH} + \text{H}_2$	4.00E+13	0	0	a
393	$\text{PO}(\text{OH})_3 = \text{PO}(\text{OH})_2 + \text{OH}$	3.63E+15	0	120000	a
394	$\text{PO}(\text{OH})_3 + \text{H} = \text{PO}(\text{OH})_2 + \text{H}_2\text{O}$	3.09E+06	2.6	37721	a
395	$\text{PO}(\text{OH})_2 + \text{O}_2 = \text{PO}_2\text{OH} + \text{HO}_2$	1.30E+02	2.4	420	a
396	$\text{PO}(\text{OH})_3 + \text{H} = \text{H}_4\text{PO}_4$	4.94E+06	2.1	21771	a
397	$\text{H}_4\text{PO}_4 = \text{PO}(\text{OH})_2 + \text{H}_2\text{O}$	1.58E+09	0.9	26893	a

a) Sullivan et al. (2004a)

Table 11-4: Ammonia SCWO submechanism. Units are in kcal, cm, mol, s.

#	Reaction	A	n	E _a	Ref.
398	NH ₃ +OH=NH ₂ +H ₂ O	5.00E+07	1.6	954	f
399	NH ₃ +HO ₂ =NH ₂ +H ₂ O ₂	2.51E+12	0	23845	g
400	NH ₃ +H=NH ₂ +H ₂	5.42E+05	2.4	9916	f
401	NH ₃ +O=>NH ₂ +OH	9.64E+12	0	7292	g
402	NH ₃ +NH ₂ =>N ₂ H ₃ +H ₂	7.94E+11	0.5	21560	f
403	NH ₃ (+M)=NH ₂ +H(+M)	8.30E+15	0	109622	g
	Enhancement factor: O ₂ 0.4/N ₂ 0.4/CO 0.75/CO ₂ 1.5/H ₂ O 6.5/CH ₄ 3.0				
	Low pressure limit:	1.27E+16	0	1	
	TROE centering: 0.42 4581 102				
404	NH ₃ +M=NH+H ₂ +M	1.80E+15	0	93392	g
	Enhancement factor: O ₂ 0.4/N ₂ 0.4/CO 0.75/CO ₂ 1.5/H ₂ O 6.5/CH ₄ 3.0				
405	O+NH ₂ =NH+OH	6.90E+11	0.3	-201	g
406	O+NH ₂ =HNO+H	8.93E+14	-0.5	325	g
407	OH+NH ₂ =>NH+H ₂ O	2.40E+06	2	50	f
408	OH+NH ₂ =>O+NH ₃	1.99E+10	0.4	497	g
409	NH ₂ +OH=NH ₂ OH	1.00E+12	0	0	k
410	NH ₂ OH+NO ₂ =H ₂ NO+HNO ₂	1.60E+02	2.97	10609	k
411	NH ₂ OH+OH=>H ₂ NO+H ₂ O	1.00E+13	0	0	k
412	NH ₂ OH+HO ₂ =>H ₂ NO+H ₂ O ₂	2.82E-01	3.71	3577	k
413	NH ₂ OH+HO ₂ =>HNOH+H ₂ O ₂	3.48E-02	4.0	6711	k
414	NH ₂ OH+NH ₂ =>HNOH+NH ₃	1.80E+06	1.94	3229	f
415	NH ₂ OH+NH ₂ =>H ₂ NO+NH ₃	9.20E+05	1.94	1888	f
416	HNOH+M=>H+HNO+M	2.00E+24	-2.84	58934	f
417	HNOH+OH=>HNO+H ₂ O	2.40E+06	2	-1192	f
418	HNOH+NH ₂ =>HNO+NH ₃	1.80E+06	1.94	-1152	f
419	HNOH+HO ₂ =>HNO+H ₂ O ₂	2.90E+04	2.69	-1600	f
420	NH+NH ₂ =>N ₂ H ₂ +H	1.50E+15	-0.5	0	f
421	NH+NH ₂ =>NH ₃ +N	9.20E+05	1.9	2444	f
422	NH ₂ +NH ₂ =>N ₂ H ₂ +H ₂	2.30E+19	-2.5	4183	f
423	NH ₂ +NH ₂ =>N ₂ H ₃ +H	4.70E+12	-0.2	10621	f
424	NH ₂ +NH ₂ =>NH ₃ +NH	5.00E+13	0	9935	f
425	NH ₂ +M=NH+H+M	7.91E+23	-2	91392	g
	Enhancement factor: O ₂ 0.4/N ₂ 0.4/CO 0.75/CO ₂ 1.5/H ₂ O 6.5/CH ₄ 3.0				
426	NH ₂ +NNH=>N ₂ +NH ₃	9.20E+05	1.9	-1152	f
427	NH ₂ +HNO=NH ₃ +NO	5.01E+11	0.5	994	g
428	NH ₂ +NO=H ₂ NNO	1.00E+13	0	0	k
429	H ₂ NNO=HNNOHtc	1.40E+15	-0.8	31116	k
430	HNNOHtc=HNNOHtt	1.56E+12	0.3	9079	k
431	HNNOHtt=HNNOHct	2.76E+10	1	33084	k
432	HNNOHct=N ₂ +H ₂ O	1.61E+10	1.1	20587	k
433	HNNOHtc=HNNOHcc	2.60E+10	1	36883	k
434	HNNOHcc=HNNOHct	2.66E+12	0.2	2988	k
435	HNNOHcc=N ₂ O+H ₂	1.69E+10	0.9	38480	k
436	H ₂ NNO=N ₂ O+H ₂	2.01E+12	0.2	71731	k
437	H ₂ NNO=OHNNHc	9.09E+14	-0.7	59467	k
438	OHNNHc=OHNNHt	7.09E+10	0.8	36253	k
439	OHNNHt=N ₂ O+H ₂	1.50E+10	1.2	95108	k

#	Reaction	A	n	E _a	Ref.
440	HNNOHtt=OHNNHt	4.97E+11	0.5	54398	k
441	HNNOHct=OHNNHc	5.91E+11	0.5	53162	k
442	NNH+OH=HNNOHtc	1.00E+13	0	0	k
443	NNH+OH=HNNOHtt	1.00E+13	0	0	k
444	NNH+OH=HNNOHct	1.00E+13	0	0	k
445	NNH+OH=HNNOHcc	1.00E+13	0	0	k
446	NNH+OH=OHNNHt	1.00E+13	0	0	k
447	NNH+OH=OHNNHc	1.00E+13	0	0	k
448	HNNOt=HNNOc	3.07E+11	0.6	16029	k
449	H ₂ NNO ₂ =HNN(OH)Otc	2.75E+13	0	37348	k
450	HNN(OH)Otc=HNN(OH)Ott	8.37E+11	0.5	5722	k
451	HNN(OH)Ott=HNN(OH)Otc	8.70E+11	0.3	25026	k
452	HNN(OH)Otc=N ₂ O+H ₂ O	1.34E+08	1.7	28696	k
453	HNN(OH)Otc=H ₂ NONO	4.30E+13	0.1	33576	k
454	NH ₂ +NO ₂ =H ₂ NNO ₂	1.00E+13	0	0	k
455	NH ₂ +NO ₂ =H ₂ NONO	1.00E+13	0	0	k
456	H ₂ NO+NO=H ₂ NONO	1.00E+13	0	0	k
457	HNNO ₂ =NN(O)OH	3.96E+13	-0.6	15553	k
458	HNONO=HNO+NO	1.18E+12	0.4	-4355	k
459	NN(O)OH=N ₂ O+OH	1.24E+11	0.7	1502	k
460	H ₂ NNO ₂ +OH=HNNO ₂ +H ₂ O	1.00E+13	0	0	k
461	H ₂ NNO ₂ +HO ₂ =HNNO ₂ +H ₂ O ₂	1.00E+13	0	3656	k
462	H ₂ NNO ₂ +O ₂ =HNNO ₂ +HO ₂	1.00E+13	0	24418	k
463	H ₂ NNO ₂ +NO ₂ =HNNO ₂ +HNO ₂	1.00E+13	0	6671	k
464	HNN(OH)Otc+OH=HNNO ₂ +H ₂ O	1.00E+13	0	2310	k
465	HNN(OH)Otc+HO ₂ =HNNO ₂ +H ₂ O ₂	1.00E+13	0	15397	k
466	HNN(OH)Otc+O ₂ =HNNO ₂ +HO ₂	1.00E+13	0	48036	k
467	HNN(OH)Otc+NO ₂ =HNNO ₂ +HNO ₂	1.00E+13	0	21449	k
468	HNN(OH)Ott+OH=HNNO ₂ +H ₂ O	1.00E+13	0	2310	k
469	HNN(OH)Ott+HO ₂ =HNNO ₂ +H ₂ O ₂	1.00E+13	0	15397	k
470	HNN(OH)Ott+O ₂ =HNNO ₂ +HO ₂	1.00E+13	0	48036	k
471	HNN(OH)Ott+NO ₂ =HNNO ₂ +HNO ₂	1.00E+13	0	21449	k
472	HNN(OH)Otc+OH=HNNO ₂ +H ₂ O	1.00E+13	0	2310	k
473	HNN(OH)Otc+HO ₂ =HNNO ₂ +H ₂ O ₂	1.00E+13	0	15397	k
474	HNN(OH)Otc+O ₂ =HNNO ₂ +HO ₂	1.00E+13	0	48036	k
475	HNN(OH)Otc+NO ₂ =HNNO ₂ +HNO ₂	1.00E+13	0	21449	k
476	HNN(OH)Otc+OH=NN(O)OH+H ₂ O	1.00E+13	0	2551	k
477	HNN(OH)Otc+HO ₂ =NN(O)OH+H ₂ O ₂	1.00E+13	0	16075	k
478	HNN(OH)Otc+O ₂ =NN(O)OH+HO ₂	1.00E+13	0	49103	k
479	HNN(OH)Otc+NO ₂ =NN(O)OH+HNO ₂	1.00E+13	0	22247	k
480	HNN(OH)Ott+OH=NN(O)OH+H ₂ O	1.00E+13	0	2551	k
481	HNN(OH)Ott+HO ₂ =NN(O)OH+H ₂ O ₂	1.00E+13	0	16075	k
482	HNN(OH)Ott+O ₂ =NN(O)OH+HO ₂	1.00E+13	0	49103	k
483	HNN(OH)Ott+NO ₂ =NN(O)OH+HNO ₂	1.00E+13	0	22247	k
484	HNN(OH)Otc+OH=NN(O)OH+H ₂ O	1.00E+13	0	2551	k
485	HNN(OH)Otc+HO ₂ =NN(O)OH+H ₂ O ₂	1.00E+13	0	16075	k
486	HNN(OH)Otc+O ₂ =NN(O)OH+HO ₂	1.00E+13	0	49103	k
487	HNN(OH)Otc+NO ₂ =NN(O)OH+HNO ₂	1.00E+13	0	22247	k
488	H ₂ NONO+OH=HNONO+H ₂ O	1.00E+13	0	2720	k

#	Reaction	A	n	E_a	Ref.
489	$H_2NONO+HO_2=HNONO+H_2O_2$	1.00E+13	0	16537	k
490	$H_2NONO+O_2=HNONO+HO_2$	1.00E+13	0	49816	k
491	$H_2NONO+NO_2=HNONO+HNO_2$	1.00E+13	0	22788	k
492	$H_2NNO+OH=HNNOc+H_2O$	1.00E+13	0	763	k
493	$H_2NNO+HO_2=HNNOc+H_2O_2$	1.00E+13	0	10172	k
494	$H_2NNO+O_2=HNNOc+HO_2$	1.00E+13	0	38942	k
495	$H_2NNO+NO_2=HNNOc+HNO_2$	1.00E+13	0	15151	k
496	$H_2NNO+OH=HNNOt+H_2O$	1.00E+13	0	218	k
497	$H_2NNO+HO_2=HNNOt+H_2O_2$	1.00E+13	0	7324	k
498	$H_2NNO+O_2=HNNOt+HO_2$	1.00E+13	0	33226	k
499	$H_2NNO+NO_2=HNNOt+HNO_2$	1.00E+13	0	11567	k
500	$HNNOHtc+OH=HNNOt+H_2O$	1.00E+13	0	162	k
501	$HNNOHtc+HO_2=HNNOt+H_2O_2$	1.00E+13	0	6907	k
502	$HNNOHtc+O_2=HNNOt+HO_2$	1.00E+13	0	32325	k
503	$HNNOHtc+NO_2=HNNOt+HNO_2$	1.00E+13	0	11029	k
504	$HNNOHtc+OH=N_2+OH+H_2O$	1.00E+13	0	295	k
505	$HNNOHtc+HO_2=N_2+OH+H_2O_2$	1.00E+13	0	7829	k
506	$HNNOHtc+O_2=N_2+OH+HO_2$	1.00E+13	0	34293	k
507	$HNNOHtc+NO_2=N_2+OH+HNO_2$	1.00E+13	0	12213	k
508	$HNNOHtt+OH=HNNOt+H_2O$	1.00E+13	0	129	k
509	$HNNOHtt+HO_2=HNNOt+H_2O_2$	1.00E+13	0	6635	k
510	$HNNOHtt+O_2=HNNOt+HO_2$	1.00E+13	0	31726	k
511	$HNNOHtt+NO_2=HNNOt+HNO_2$	1.00E+13	0	10676	k
512	$HNNOHtt+OH=N_2+OH+H_2O$	1.00E+13	0	249	k
513	$HNNOHtt+HO_2=N_2+OH+H_2O_2$	1.00E+13	0	7537	k
514	$HNNOHtt+O_2=N_2+OH+HO_2$	1.00E+13	0	33680	k
515	$HNNOHtt+NO_2=N_2+OH+HNO_2$	1.00E+13	0	11840	k
516	$HNNOHct+OH=HNNOc+H_2O$	1.00E+13	0	619	k
517	$HNNOHct+HO_2=HNNOc+H_2O_2$	1.00E+13	0	9535	k
518	$HNNOHct+O_2=HNNOc+HO_2$	1.00E+13	0	37720	k
519	$HNNOHct+NO_2=HNNOc+HNO_2$	1.00E+13	0	14360	k
520	$HNNOHct+OH=N_2+OH+H_2O$	1.00E+13	0	275	k
521	$HNNOHct+HO_2=N_2+OH+H_2O_2$	1.00E+13	0	7708	k
522	$HNNOHct+O_2=N_2+OH+HO_2$	1.00E+13	0	34039	k
523	$HNNOHct+NO_2=N_2+OH+HNO_2$	1.00E+13	0	12058	k
524	$HNNOHcc+OH=HNNOc+H_2O$	1.00E+13	0	142	k
525	$HNNOHcc+HO_2=HNNOc+H_2O_2$	1.00E+13	0	6747	k
526	$HNNOHcc+O_2=HNNOc+HO_2$	1.00E+13	0	31975	k
527	$HNNOHcc+NO_2=HNNOc+HNO_2$	1.00E+13	0	10822	k
528	$HNNOHcc+OH=N_2+OH+H_2O$	1.00E+13	0	0	k
529	$HNNOHcc+HO_2=N_2+OH+H_2O_2$	1.00E+13	0	5255	k
530	$HNNOHcc+O_2=N_2+OH+HO_2$	1.00E+13	0	28537	k
531	$HNNOHcc+NO_2=N_2+OH+HNO_2$	1.00E+13	0	8858	k
532	$OHNNHc+OH=HNNOc+H_2O$	1.00E+13	0	0	k
533	$OHNNHc+HO_2=HNNOc+H_2O_2$	1.00E+13	0	5998	k
534	$OHNNHc+O_2=HNNOc+HO_2$	1.00E+13	0	30289	k
535	$OHNNHc+NO_2=HNNOc+HNO_2$	1.00E+13	0	9844	k
536	$OHNNHt+OH=HNNOt+H_2O$	1.00E+13	0	0	k
537	$OHNNHt+HO_2=HNNOt+H_2O_2$	1.00E+13	0	2534	k

#	Reaction	A	n	E _a	Ref.
538	OHNNHt+O ₂ =HNNOt+HO ₂	1.00E+13	0	21102	k
539	OHNNHt+NO ₂ =HNNOt+HNO ₂	1.00E+13	0	5058	k
540	HNNOt+OH=N ₂ O+H ₂ O	1.00E+13	0	0	k
541	HNNOt+HO ₂ =N ₂ O+H ₂ O ₂	1.00E+13	0	0	k
542	HNNOt+O ₂ =N ₂ O+HO ₂	1.00E+13	0	1926	k
543	HNNOt+NO ₂ =N ₂ O+HNO ₂	1.00E+13	0	0	k
544	HNNOc+OH=N ₂ O+H ₂ O	1.00E+13	0	0	k
545	HNNOc+HO ₂ =N ₂ O+H ₂ O ₂	1.00E+13	0	0	k
546	HNNOc+O ₂ =N ₂ O+HO ₂	1.00E+13	0	916	k
547	HNNOc+NO ₂ =N ₂ O+HNO ₂	1.00E+13	0	0	k
548	O ₂ +NH ₂ =HNO+OH	1.51E+12	-0.4	36098	g
549	O ₂ +NH ₂ =H ₂ NO+O	1.10E+18	-1.3	33598	g
550	N ₂ H ₂ +NH ₂ =NH+N ₂ H ₃	1.00E+11	0.5	33770	g
551	N ₂ H ₂ +NH ₂ =NH ₃ +NNH	1.00E+13	0	3975	g
552	H+NH ₂ =NH+H ₂	6.02E+12	0	0	g
553	HO ₂ +NH ₂ =>H ₂ NO+OH	2.50E+13	0	0	f
554	HO ₂ +NH ₂ =>NH ₃ +O ₂	9.20E+05	1.9	-1152	f
555	N+NH ₂ =>N ₂ +H+H	7.10E+13	0	0	f
556	NH+NO=>N ₂ +OH	1.40E+17	-1.5	1311	f
557	NH+NO=>N ₂ O+H	3.00E+18	-1.6	1430	f
558	NH+NO=>NNH+O	1.70E+14	-0.2	12200	f
559	NH+NO ₂ =HNO+NO	1.00E+11	0.5	3975	g
560	NH+NO ₂ =N ₂ O+OH	9.71E+12	0	0	g
561	N ₂ O+NH=HNO+N ₂	2.00E+12	0	5961	g
562	O+NH=N+OH	3.72E+13	0	0	g
563	O+NH=NO+H	5.50E+13	0	0	g
564	OH+NH=>HNO+H	2.00E+13	0	0	f
565	OH+NH=>N+H ₂ O	1.20E+06	2	-487	f
566	O ₂ +NH=>NO+OH	7.60E+10	0	1530	f
567	NH+O ₂ =>H+NO ₂	2.30E+10	0	2484	f
568	NH+O ₂ =>HNO+O	4.60E+05	2	6497	f
569	NH+N=>N ₂ +H	1.50E+13	0	0	f
570	NH+NH=>N ₂ + ₂ H	5.10E+13	0	0	f
571	NH+H=>N+H ₂	3.50E+13	0	1729	f
572	NH+NNH=N ₂ +NH ₂	2.00E+11	0.5	1986	g
573	NH+M=N+H+M	7.57E+14	0	75506	g
	Enhancement factor: O ₂ 0.4/N ₂ 0.4/CO 0.75/CO ₂ 1.5/H ₂ O 6.5/CH ₄ 3.0				
574	CH ₄ +N=NH+CH ₃	1.00E+13	0	23995	g
575	O ₂ +N=>NO+O	9.00E+09	1	6497	f
576	N+OH=>NO+H	1.10E+14	0	1123	f
577	N ₂ H ₃ +H=>N ₂ H ₂ +H ₂	2.40E+08	1.5	0	f
578	H+N ₂ H ₃ =NH+NH ₃	1.00E+11	0	0	g
579	N ₂ H ₃ +M=N ₂ H ₂ +H+M	2.50E+16	0	49675	g
	Enhancement factor: O ₂ 0.4/N ₂ 0.4/CO 0.75/CO ₂ 1.5/H ₂ O 6.5/CH ₄ 3.0				
580	N ₂ H ₃ +M=NH ₂ +NH+M	2.50E+16	0	41728	g
	Enhancement factor: O ₂ 0.4/N ₂ 0.4/CO 0.75/CO ₂ 1.5/H ₂ O 6.5/CH ₄ 3.0				
581	N ₂ H ₃ +OH=>N ₂ H ₂ +H ₂ O	1.20E+06	2	-1192	f
582	N ₂ H ₃ +CH ₃ =>N ₂ H ₂ +CH ₄	8.20E+05	1.9	1818	f
583	N ₂ H ₃ +NH ₂ =>N ₂ H ₂ +NH ₃	9.20E+05	1.9	-1153	f

#	Reaction	A	n	E _a	Ref.
584	$N_2H_3+HO_2 \Rightarrow N_2H_2+H_2O_2$	2.90E+04	2.7	-1600	f
585	$N_2H_2+M=NNH+H+M$	2.50E+16	0	49663	g
	Enhancement factor: O ₂ 0.4/N ₂ 0.4/CO 0.75/CO ₂ 1.5/H ₂ O 6.5/CH ₄ 3.0				
586	$N_2H_2+M=NH+NH+M$	7.91E+16	0	99350	g
	Enhancement factor: O ₂ 0.4/N ₂ 0.4/CO 0.75/CO ₂ 1.5/H ₂ O 6.5/CH ₄ 3.0				
587	$N_2H_2+O=NH_2+NO$	1.00E+13	0	0	g
588	$N_2H_2+O=NNH+OH$	1.00E+11	0.5	0	g
589	$N_2H_2+NH \Rightarrow NNH+NH_2$	2.40E+06	2	-1192	f
590	$N_2H_2+NO \Rightarrow N_2O+NH_2$	4.00E+12	0	11922	f
591	$N_2H_2+OH \Rightarrow NNH+H_2O$	2.40E+06	2	-1192	f
592	$N_2H_2+H=NNH+H_2$	1.00E+13	0	994	g
593	$N_2H_2 \Rightarrow NNH+H$	1.30E+44	-9.2	77076	f
594	$NNH \Rightarrow N_2+H$	3.00E+08	0.5	3060	f
595	$NNH+M \Rightarrow N_2+H+M$	1.00E+13	0.5	3060	f
596	$NNH+O_2 \Rightarrow N_2+HO_2$	1.20E+12	-0.3	149	f
597	$NNH+O_2 \Rightarrow N_2O+OH$	2.90E+11	-0.3	149	f
598	$N+NNH=NH+N_2$	3.16E+13	0	1987	g
599	$OH+NNH \Rightarrow N_2+H_2O$	2.40E+22	-2.9	2454	f
600	$O+NNH=N_2+OH$	1.00E+13	0	4969	g
601	$O+NNH \Rightarrow N_2O+H$	1.00E+13	0	2980	g
602	$H+NNH \Rightarrow N_2+H_2$	2.40E+08	1.5	-894	f
603	$NO+NNH \Rightarrow N_2+HNO$	1.20E+06	2	-1192	f
604	$NNH+HO_2 \Rightarrow N_2+H_2O_2$	1.40E+04	2.7	-1600	f
605	$H_2NO+M \Rightarrow HNO+H+M$	2.80E+24	-2.8	64915	f
606	$H_2NO+H \Rightarrow NH_2+OH$	4.00E+13	0	0	f
607	$H_2NO+H \Rightarrow HNO+H_2$	4.80E+08	1.5	1560	f
608	$H_2NO+O \Rightarrow HNO+OH$	3.30E+08	1.5	487	f
609	$H_2NO+OH \Rightarrow HNO+H_2O$	2.40E+06	2	-1192	f
610	$H_2NO+CH_3 \Rightarrow CH_3O+NH_2$	2.00E+13	0	0	f
611	$H_2NO+CH_3 \Rightarrow CH_4+HNO$	1.60E+06	1.9	2961	f
612	$H_2NO+NH_2 \Rightarrow HNO+NH_3$	1.80E+06	1.9	-1152	f
613	$H_2NO+HO_2 \Rightarrow HNO+H_2O_2$	2.90E+04	2.7	-1600	f
614	$H+HNO \Rightarrow H_2+NO$	4.50E+11	0.7	656	f
615	$O+HNO \Rightarrow OH+NO$	4.50E+11	0.7	656	f
616	$HNO+O_2 \Rightarrow NO+HO_2$	2.00E+13	0	15896	f
617	$HNO+CH_3 \Rightarrow NO+CH_4$	8.20E+05	1.9	954	f
618	$OH+HNO \Rightarrow NO+H_2O$	1.30E+07	1.9	-954	f
619	$HNO+M=H+NO+M$	5.09E+16	0	48681	g
	Enhancement factor: O ₂ 0.4/N ₂ 0.4/CO 0.75/CO ₂ 1.5/H ₂ O 6.5/CH ₄ 3.0				
620	$HNO+HNO \Rightarrow N_2O+H_2O$	8.50E+08	0	3080	f
621	$NO+HNO \Rightarrow N_2O+OH$	8.50E+12	0	29586	f
622	$NO+CH_2(S)=HCN+OH$	9.64E+13	0	0	g
623	$NO+CH_3=HCN+H_2O$	9.28E+11	0	16709	g
624	$NO+CH_3=H_2CN+OH$	9.28E+11	0	16709	g
625	$NO+HO_2 \Rightarrow NO_2+OH$	2.20E+12	0	-476	f
626	$NO+N \Rightarrow N_2+O$	4.28E+13	0	1570	g
627	$NO+NCO=N_2O+CO$	1.39E+18	-1.7	755	g
628	$NO+M=N+O+M$	3.62E+15	0	148327	g
	Enhancement factor: O ₂ 0.4/N ₂ 0.4/CO 0.75/CO ₂ 1.5/H ₂ O 6.5/CH ₄ 3.0				

#	Reaction	A	n	E _a	Ref.
629	CO ₂ +N=NO+CO	1.90E+11	0	3398	g
630	NO+N ₂ O=N ₂ +NO ₂	1.00E+14	0	49675	g
631	NO+H=>N+OH	2.17E+14	0	49496	g
632	NO ₂ +NO ₂ =NO+NO+O ₂	2.00E+12	0	26825	g
633	NO ₂ +H=>NO+OH	1.30E+14	0	358	f
634	NO ₂ +O=>NO+O ₂	3.90E+12	0	-238	f
635	NO ₂ +N=NO+NO	8.07E+11	0	0	g
636	NO ₂ +N=N ₂ O+O	1.00E+12	0	0	g
637	NO ₂ +CN=NCO+NO	3.00E+13	0	0	g
638	NO ₂ +M=NO+O+M	3.13E+16	0	65571	g
	Enhancement factor: O ₂ 0.4/N ₂ 0.4/CO 0.75/CO ₂ 1.5/H ₂ O 6.5/CH ₄ 3.0				
639	NO ₂ +CH ₃ =>NO+CH ₃ O	1.40E+13	0	0	f
640	NO ₂ +CO=NO+CO ₂	9.03E+13	0	33800	i
641	HNO ₂ +M=>OH+NO+M	2.00E+31	-4.6	51175	f
642	HNO ₂ +H=>H ₂ +NO ₂	2.00E+08	1.6	6617	f
643	HNO ₂ +H=>H ₂ O+NO	8.10E+06	1.9	3845	f
644	HNO ₂ +OH=H ₂ O+NO ₂	1.20E+06	2	-596	f
645	HNO ₂ +CH ₃ =>NO ₂ +CH ₄	8.10E+05	1.9	4838	f
646	HNO ₂ +NH ₂ =>NO ₂ +NH ₃	9.20E+05	1.9	874	f
647	NO ₂ +O(+M)=NO ₃ (+M)	1.30E+13	0	0	h
	Low pressure limit:	1.00E+28	-4.08	2470	
648	NO ₃ +OH=NO ₂ +HO ₂	1.00E+13	0	0	h
649	NO ₂ +NO ₂ =NO ₃ +NO	9.60E+09	0.7	20900	h
650	NO ₃ +H=NO ₂ +OH	6.00E+13	0	0	h
651	HNO ₃ +OH=NO ₃ +H ₂ O	8.50E+09	0	-1240	h
652	OH+NO ₂ (+M)=HNO ₃ (+M)	2.40E+13	0	0	h
	Enhancement factor: O ₂ 0.4/N ₂ 0.4/CO 0.75/CO ₂ 1.5/H ₂ O 6.5/CH ₄ 3.0				
	Low pressure limit:	6.40E+32	-5.49	2350	
653	N ₂ O+H=>N ₂ +OH	2.20E+14	0	16750	f
654	N ₂ O+H=>NH+NO	8.50E+20	-1.6	35368	f
655	N ₂ O+H=>NNH+O	2.40E+19	-1.3	47092	f
656	N ₂ O+O=>N ₂ +O ₂	1.40E+12	0	10809	f
657	N ₂ O+O=>NO+NO	2.90E+13	0	22970	f
658	N ₂ O+OH=>N ₂ +HO ₂	1.30E-02	4.7	36560	f
659	N ₂ O+N=N ₂ +NO	1.00E+13	0	19870	g
660	N ₂ O=N ₂ +O	1.26E+12	0	62600	j
661	CO+N ₂ O=CO ₂ +N ₂	5.01E+13	0	44000	i
662	N+N+M=N ₂ +M	6.52E+15	0	0	g
	Enhancement factor: O ₂ 0.4/N ₂ 0.4/CO 0.75/CO ₂ 1.5/H ₂ O 6.5/CH ₄ 3.0				
663	N ₂ +O=>NO+N	1.81E+14	0	76103	g
664	H ₂ +CN=HCN+H	1.93E+04	2.9	1629	g
665	CH ₄ +CN=HCN+CH ₃	9.03E+04	2.6	-298	g
666	O ₂ +CN=NCO+O	7.23E+12	0	-417	g
667	O ₂ +NCO=NO+CO ₂	1.72E+07	0	-734	g
668	N ₂ +CH ₂ =HCN+NH	1.00E+13	0	73997	g
669	C ₂ N ₂ +O=NCO+CN	1.29E+14	0	14168	g
670	C ₂ N ₂ +OH=HOCN+CN	1.87E+11	0	2877	g
671	HCN+O=NCO+H	8.45E+05	2.1	6111	g
672	HCN+O=NH+CO	3.19E+05	2.1	6111	g

#	Reaction	A	n	E _a	Ref.
673	HCN+O=CN+OH	2.22E+05	2.1	6111	g
674	HCN+OH=CN+H ₂ O	9.03E+12	0	10731	g
675	HCN+OH=HOCN+H	5.85E+04	2.4	12500	g
676	HCN+OH=HNCO+H	1.98E-03	4	1000	g
677	HCN+CN=C ₂ N ₂ +H	3.80E+07	1.6	100	g
678	HOCN+H=H ₂ O+CN	1.00E+12	0	0	g
679	HOCN+H=H ₂ +NCO	1.00E+12	0	0	g
680	HOCN+H=HNCO+H	1.00E+13	0	0	g
681	HNCO+H=NCO+H ₂	2.05E+14	-0.3	20250	g
682	HNCO+H=NH ₂ +CO	1.10E+14	0	12715	g
683	HNCO+O=NH+CO ₂	2.00E+13	0	13016	g
684	HNCO+O=HNO+CO	1.90E+12	0	10301	g
685	HNCO+O=OH+NCO	2.00E+14	0	23049	g
686	HNCO+OH=NCO+H ₂ O	1.99E+12	0	5540	g
687	HNCO+OH=NH ₂ +CO ₂	6.62E+11	0	5540	g
688	HNCO+HO ₂ =NCO+H ₂ O ₂	3.00E+13	0	29000	g
689	HNCO+N=NH+NCO	3.98E+13	0	35766	g
690	HNCO+NH=NH ₂ +NCO	3.00E+13	0	23700	g
691	HNCO+NH ₂ =NH ₃ +NCO	1.00E+12	0	6955	g
692	HNCO+M=NH+CO+M	2.40E+16	0	84728	g
	Enhancement factor: O ₂ 0.4/N ₂ 0.4/CO 0.75/CO ₂ 1.5/H ₂ O 6.5/CH ₄ 3.0				
693	HNCO+M=H+NCO+M	2.86E+17	0	112072	g
	Enhancement factor: O ₂ 0.4/N ₂ 0.4/CO 0.75/CO ₂ 1.5/H ₂ O 6.5/CH ₄ 3.0				
694	H+NCO=NH+CO	5.24E+13	0	0	g
695	CH ₂ +N=HCN+H	5.00E+13	0	0	g
696	CH ₂ +NH=HCN+H+H	3.00E+13	0	0	g
697	CH ₃ +N=H ₂ CN+H	2.59E+14	0	834	g
698	C ₂ H ₃ +N=HCN+CH ₂	2.00E+13	0	0	g
699	O+CN=CO+N	1.02E+13	0	0	g
700	O+NCO=NO+CO	3.16E+13	0	0	g
701	OH+CN=NCO+H	6.02E+13	0	0	g
702	OH+NCO=NO+HCO	5.00E+12	0	15000	g
703	OH+NCO=NO+CO+H	1.00E+13	0	0	g
704	HCCO+N=HCN+CO	5.00E+13	0	0	g
705	N+H ₂ CN=N ₂ +CH ₂	2.00E+13	0	0	g
706	N+NCO=NO+CN	2.77E+18	-1	17267	g
707	N+NCO=N ₂ +CO	1.99E+13	0	0	g
708	H ₂ CN+M=HCN+H+M	7.50E+14	0	22000	g
	Enhancement factor: O ₂ 0.4/N ₂ 0.4/CO 0.75/CO ₂ 1.5/H ₂ O 6.5/CH ₄ 3.0				
709	NCO+M=N+CO+M	2.91E+15	0	46695	g
	Enhancement factor: O ₂ 0.4/N ₂ 0.4/CO 0.75/CO ₂ 1.5/H ₂ O 6.5/CH ₄ 3.0				
710	NH ₂ +NO=N ₂ +H ₂ O	4.70E+12	-0.25	-1202	f, l
711	NH ₂ +NO=NNH+OH	3.50E+10	0.34	-765	f, l
712	NH ₂ +NO ₂ =H ₂ NO+NO	6.60E+16	-1.44	268	f, l
713	NH ₂ +NO ₂ =N ₂ O+H ₂ O	1.50E+16	-1.44	268	f, l

f) Dean and Bozzelli (2000); g) Hughes et al. (2001); h) Glarborg et al. (1995); i) Allen et al. (1997); j) Rörhig et al. (1996); k) this study; l) rates replaced by H₂NNO_x submechanism.

Table 11-5: Thermodynamic values for SCWO mechanisms.

ΔH_f^o values in kcal/mol, S^o and C_p^o values in cal/mol K for the ideal gas reference state conditions at the temperatures indicated and 1.01 bar.

Compound	ΔH_f^o (298K)	S^o (298K)	C_p^o (300K)	C_p^o (400K)	C_p^o (500K)	C_p^o (600K)	C_p^o (800K)	C_p^o (1000K)	C_p^o (1500K)	Ref.
OH	8.91	43.91	7.14	7.07	7.05	7.06	7.15	7.34	7.88	m
HO ₂	3.00	54.75	8.35	8.89	9.46	9.99	10.77	11.38	12.48	m
H ₂ O ₂	-32.48	56.04	10.15	11.08	11.98	12.78	13.98	14.93	16.58	m
H ₂	0.00	31.23	6.89	7.00	7.00	6.99	7.08	7.21	7.73	m
H	52.10	27.41	4.97	4.97	4.97	4.97	4.97	4.97	4.97	m
O ₂	0.00	49.02	7.02	7.20	7.43	7.67	8.07	8.34	8.72	m
O	59.55	38.49	5.23	5.13	5.08	5.05	5.02	5.00	4.98	m
H ₂ O	-57.79	45.12	8.03	8.19	8.42	8.68	9.26	9.87	11.31	m
CH ₄	-17.83	44.53	8.55	9.69	11.11	12.60	15.29	17.59	21.51	m
CO	-26.42	47.23	6.96	7.02	7.12	7.27	7.62	7.93	8.40	m
CO ₂	-94.04	51.09	8.89	9.86	10.66	11.32	12.29	12.98	13.91	m
CH ₂ O	-25.95	52.28	8.47	9.36	10.44	11.52	13.37	14.82	16.93	m
HCOOH	-90.20	59.39	10.86	12.86	14.58	16.05	18.36	20.00	22.24	m
HOCO	-43.61	59.12	12.01	12.86	13.62	14.30	15.44	16.34	29.33	o
CH ₂	93.49	46.46	8.37	8.73	9.07	9.39	9.97	10.59	11.77	m
CH ₃	35.06	46.36	9.20	9.98	10.75	11.50	12.86	14.09	16.25	m
CH ₂ (S)	102.47	45.22	8.08	8.33	8.66	9.04	9.83	10.57	11.91	m
HCO	10.11	53.59	8.29	8.75	9.29	9.84	10.85	11.66	12.94	m
CH ₂ OH	-4.11	58.35	11.35	12.79	14.16	15.36	17.08	18.44	20.59	m
CH ₃ O	5.04	55.98	10.20	12.05	13.86	15.47	17.86	19.70	22.25	m
CH ₃ OH	-48.04	57.51	10.28	12.07	14.07	15.98	19.00	21.38	25.07	m
CH ₃ OO	2.15	65.27	12.51	14.78	16.81	18.62	21.58	23.77	27.11	m
CH ₃ OOH	-33.40	66.09	14.44	17.12	19.61	21.79	25.10	27.52	30.96	m
CH ₂ OOH	33.34	59.54	13.56	16.00	18.24	20.16	22.99	24.98	39.06	m
C ₂ H ₅ OH	-56.20	67.09	15.46	19.23	22.54	25.44	30.17	33.75	39.36	m
C ₂ H ₄ OH	-7.20	70.50	14.69	17.86	20.63	23.06	27.02	30.02	34.73	m
HOC ₂ H ₄ OO	-41.29	86.94	21.80	25.33	28.43	31.17	35.67	39.14	44.68	m
CH ₃ CHOH	-9.85	71.53	13.93	16.89	19.61	22.08	26.25	29.46	34.24	m
CH ₃ CH ₂ O	-4.10	62.21	14.08	17.72	20.85	23.53	27.75	30.80	35.81	p
CH ₃ CHO	-39.51	63.04	13.25	15.87	18.31	20.52	24.17	26.88	30.87	m
CH ₂ CHO	6.00	63.99	13.18	15.15	16.96	18.60	21.30	23.34	26.35	m
CH ₃ CO	-5.40	63.73	12.42	14.44	16.33	18.06	20.94	23.07	26.19	m
CH ₃ CO ₃	-28.58	78.01	19.21	22.53	25.33	27.67	31.23	33.69	37.15	m
CH ₃ CO ₃ H	-80.48	77.22	20.55	24.40	27.64	30.35	34.52	37.42	41.51	m
CH ₃ CO ₂	-51.38	63.55	14.78	17.74	20.26	22.41	25.78	28.20	31.77	m
CH ₂ CO	-12.40	57.78	12.43	14.17	15.67	16.91	18.79	20.24	22.44	m
HCCO	42.44	60.73	12.65	13.47	14.23	14.92	16.07	16.83	17.98	m
HCCOH	22.27	59.53	13.75	15.41	16.65	17.62	19.18	20.39	22.43	m
CHOCHO	-50.60	68.16	14.90	17.51	19.69	21.48	24.15	25.89	27.10	p
C ₂ H ₆	-20.04	54.72	12.58	15.69	18.62	21.30	25.82	29.30	34.61	m
C ₂ H ₅	28.01	60.13	11.32	13.60	15.95	18.29	22.58	25.50	29.56	m
C ₂ H ₄	12.54	52.37	10.23	12.79	14.94	16.83	20.05	22.51	26.22	m
C ₂ H ₃	68.41	55.32	9.57	11.19	12.78	14.31	16.98	18.75	21.26	m

C ₂ H ₂	54.19	48.01	10.62	11.99	13.08	13.95	15.27	16.31	18.27	m
C ₂ H	135.00	49.55	8.90	9.63	10.22	10.72	11.54	12.18	13.31	m
C ₂ O	69.55	55.82	10.32	11.12	11.73	12.23	13.06	13.66	14.62	m
PO(OH) ₂ CH ₃	-217.47	79.85	25.93	30.47	33.87	36.44	40.00	42.46	46.40	n
PO(OH) ₃	-271.71	80.55	21.92	25.06	27.41	29.16	31.53	33.15	35.86	n
PO(OH) ₂ CH ₂	-164.97	83.16	25.48	29.56	32.36	34.32	36.87	38.63	41.59	n
PO ₂ (OH)CH ₃	-150.68	78.80	23.69	27.75	30.96	33.48	37.03	39.37	42.78	n
PO(OH) ₃ CH ₃	-212.22	88.53	31.77	37.62	41.96	45.23	49.87	53.20	58.65	n
PO ₂ OH	-168.45	66.57	14.42	16.62	18.27	19.50	21.15	22.19	23.68	n
PO(OH) ₂ CH ₂ OO	-198.47	94.42	32.91	37.78	41.40	44.13	47.88	50.33	49.38	n
PO(OH) ₂ CH ₂ OOH	-233.11	97.90	35.12	40.55	44.49	47.35	51.10	53.46	56.99	n
PO(OH) ₂ CH ₂ O	-190.50	88.63	28.28	32.62	35.90	38.37	41.74	44.00	47.45	n
PO ₂ (OH)CH ₂ OOH	-166.30	96.85	32.87	37.82	41.57	44.39	48.13	50.37	53.38	n
PO(OH) ₂	-157.03	74.39	17.31	19.66	21.33	22.52	24.07	25.09	26.78	n
PO(OH) ₂ CH ₂ OH	-247.76	89.79	30.91	35.58	39.03	41.60	45.06	47.42	51.23	n
PO(OH) ₂ CHO	-220.13	88.11	26.08	29.67	32.28	34.21	36.93	38.84	41.88	n
PO(OH) ₂ CO	-185.33	89.40	26.28	28.87	30.69	32.00	33.80	35.07	37.17	n
PO(OH) ₂ CHOH	-210.76	90.01	29.07	34.11	37.60	39.97	42.72	44.34	46.90	n
PO ₂ (OH)CH ₂ OH	-163.35	84.32	26.53	31.20	34.88	37.78	41.91	44.76	49.12	n
PO ₂ CH ₃	-118.43	71.21	15.94	18.79	21.23	23.31	26.48	28.75	32.17	n
POOHCH ₂	-90.64	71.09	18.44	21.68	24.10	25.93	28.53	30.36	33.27	n
POOH	-111.07	62.39	11.64	13.17	14.30	15.14	16.25	16.97	18.08	n
H ₄ PO ₄	-217.64	81.24	26.04	30.28	33.15	35.13	37.70	39.49	42.65	n
NH ₃	-10.97	46.03	8.48	9.33	10.08	10.80	12.21	13.53	15.90	m
NH ₂	45.50	46.50	8.01	8.25	8.50	8.79	9.49	10.21	11.54	m
NH	85.20	43.29	6.96	6.98	7.00	7.04	7.21	7.48	8.06	m
N	112.95	36.61	4.97	4.97	4.97	4.97	4.97	4.97	4.97	m
N ₂	0.00	45.76	6.95	7.01	7.08	7.19	7.50	7.83	8.32	m
N ₂ O	19.61	52.55	9.27	10.18	10.94	11.56	12.51	13.12	13.94	m
NO	21.58	50.34	7.11	7.19	7.31	7.45	7.82	8.14	8.54	m
NO ₂	7.91	57.33	8.83	9.64	10.33	10.93	11.89	12.49	13.17	m
NO ₃	17.00	60.37	11.26	13.28	14.93	16.16	17.51	18.31	19.09	m
HNO ₃	-32.00	63.77	12.98	15.31	17.21	18.71	20.71	21.94	23.33	m
NH ₂ OH	-11.95	56.44	11.14	12.77	14.24	15.51	17.47	19.12	22.07	m
H ₂ NO	15.82	55.68	9.29	10.39	11.36	12.22	13.67	14.84	16.78	m
HNOH	-32.00	63.77	12.98	15.31	17.21	18.71	20.71	21.94	23.33	m
HNO	23.80	52.72	8.26	8.84	9.36	9.84	10.76	11.48	12.49	m
N ₂ H ₃	36.78	54.61	10.60	12.24	13.79	15.17	17.34	18.94	21.57	m
N ₂ H ₂	50.90	52.20	8.70	9.87	10.90	11.84	13.54	14.88	16.85	m
NNH	58.57	53.62	8.32	8.83	9.36	9.88	10.85	11.52	12.44	m
HNO ₂	-18.75	60.71	11.10	12.41	13.52	14.43	15.69	16.58	17.88	m
H ₂ NNO ₂	-2.91	62.65	14.45	17.41	19.68	21.42	23.82	25.43	27.97	q
HNN(OH)Otc	7.29	63.47	13.07	15.95	18.29	20.18	22.97	24.85	27.67	q
HNN(OH)Ott	6.93	63.64	13.18	16.02	18.33	20.20	22.97	24.85	27.67	q
HNN(OH)Oct	7.12	63.70	13.33	16.18	18.48	20.34	23.07	24.92	27.70	q
H ₂ NONO	17.58	68.52	14.69	16.69	18.43	19.95	22.38	24.16	26.86	q
H ₂ NNO	16.35	61.93	12.58	14.87	16.78	18.36	20.67	22.15	24.00	q
HNNOHtc	17.35	60.43	10.71	12.68	14.36	15.78	18.00	19.60	22.08	q
HNNOHct	17.63	60.95	11.20	13.07	14.67	16.03	18.16	19.71	22.12	q
HNNOHtt	18.03	60.73	11.10	12.99	14.59	15.96	18.09	19.64	22.06	q

HNNOHcc	23.90	60.94	11.12	13.02	14.65	16.03	18.21	19.78	22.22	q
OHNNHc	25.82	59.98	9.78	11.67	13.38	14.91	17.41	19.25	21.97	q
OHNNHt	31.11	59.89	9.87	11.78	13.49	15.00	17.48	19.29	22.00	q
HNNO ₂	52.17	70.21	14.01	16.60	18.69	20.33	22.60	23.89	25.20	q
NN(O)OH	53.23	67.97	15.33	16.94	18.18	19.12	20.42	21.29	22.69	q
HNONO	64.39	66.37	14.12	16.08	17.64	18.89	20.68	21.87	23.58	q
HNNOt	46.02	60.39	10.62	11.95	13.09	14.04	15.49	16.48	17.90	q
HNNOc	52.17	59.98	10.39	11.78	12.95	13.93	15.42	16.44	17.91	q
CN	104.00	48.40	6.97	7.03	7.15	7.32	7.71	8.02	8.49	m
HCN	31.89	48.21	8.60	9.36	9.97	10.48	11.31	12.00	13.22	m
NCO	31.51	54.14	9.65	10.50	11.25	11.90	12.90	13.53	14.15	m
HOCN	-3.53	59.25	10.56	11.45	12.27	13.02	14.26	15.19	16.55	m
H ₂ CN	59.11	53.59	9.16	10.32	11.42	12.47	14.24	15.42	17.13	m
C ₂ N ₂	73.87	57.72	13.63	14.71	15.59	16.32	17.45	18.24	19.41	m
HNCO	-28.22	57.05	11.23	12.26	13.19	14.02	15.37	16.32	17.63	m

m) Burcat (2003); n) Sullivan et al. (2004b); o) Janoshek and Rossi (2002); p) Marinov (1999); q) this study.